TECHNICAL REPORTS SERIES

Handbook for calculations of nuclear reaction data, RIPL-2

Reference Input Parameter Library-2

Final report of a coordinated research project

INTERNATIONAL ATOMIC ENERGY AGENCY
VIENNA, 2006

Reference Input Parameter Library-2
(RIPL-2)
IAEA, Vienna, 2006
ISBN ..-..-.....-.

FOREWORD

Nuclear data for applications constitute an integral part of the IAEA programme of activities. When considering low-energy nuclear reactions induced with light particles, such as neutrons, protons, deuterons, alphas and photons, a broad range of applications are addressed, from nuclear power reactors and shielding design through cyclotron production of medical radioisotopes and radiotherapy to transmutation of nuclear waste. All these and many other applications require a detailed knowledge of production cross sections, spectra of emitted particles and their angular distributions.

A long-standing problem of how to meet the nuclear data needs of the future with limited experimental resources puts a considerable demand upon nuclear model computation capabilities. Originally, almost all nuclear data were provided by measurement programmes. Over time, theoretical understanding of nuclear phenomena has reached a high degree of reliability, and nuclear modeling has become standard practice in nuclear data evaluations (with measurements remaining critical for data testing and benchmarking). Thus, theoretical calculations are instrumental in obtaining complete and internally consistent nuclear data files.

The practical use of nuclear model codes requires a considerable numerical input that describes the properties of the nuclei and the interactions involved. Experts have used a variety of different input sets, often developed over years in their own laboratories. Many of these partial input databases were poorly documented or not documented at all, and were not always available for other users. With the trend of reduced funds for nuclear data evaluations, there is a real threat that the immense accumulated knowledge of input parameters and associated calculations may be compromised or even lost for future applications. Therefore, the IAEA has undertaken an extensive co-ordinated effort to develop a library of evaluated and tested nuclear-model input parameters.

Considering that such a task is so immense, it was decided to proceed in two major steps. First, to summarize the present knowledge on input parameters and to develop a single Starter File of input model parameters, and then to focus on testing, validating and improving the Starter File. The first step was addressed through the IAEA Co-ordinated Research Project (CRP) entitled *"Development of Reference Input Parameter Library for Nuclear Model Calculations of Nuclear Data (Phase I: Starter File)"*, initiated in 1994 and completed successfully in 1997. The electronic Starter File (known as RIPL-1) was developed and made available to users throughout the world. The second step followed immediately afterwards within the CRP entitled *"Nuclear Model Parameter Testing for Nuclear Data Evaluation (Reference Input Parameter Library: Phase II)"*, initiated in 1998 and completed in 2002. This later CRP resulted in the revision and extension of the original RIPL-1 Starter File to produce a consistent RIPL-2 library containing recommended input parameters, a large amount of theoretical results suitable for nuclear reaction calculations, and a number of computer codes for parameter retrieval, determination and use. The new library will be of immediate practical value for a number of users and should represent a firm basis for future improvements.

Initial objectives of the RIPL-2 CRP were:

- Test and improve nuclear model parameters for theoretical calculations of nuclear reaction cross sections at incident energies below 100 MeV.
- Produce a well-tested Reference Input Parameter Library for calculations of nuclear reactions using nuclear reaction codes.
- Develop user-oriented retrieval tools and interfaces to established codes for nuclear reaction calculations.

- Publish Technical Report and make the library and tools available on-line and on CD-ROM.

The CRP participants (T. Belgya (Hungary), O. Bersillon (France), R. Capote Noy (Cuba), T. Fukahori (Japan), Ge Zhigang (China), S. Goriely (Belgium), M. Herman (IAEA), A. V. Ignatyuk (Russian Federation), S. Kailas (India), A. J. Koning (Netherlands), P. Obložinský (USA), V. Plujko (Ukraine) and P. G. Young (USA)) convened at three Research Co-ordination Meetings held at:

- Vienna, Austria, 25-27 November 1998 (see INDC(NDS)-389, February 1999)
- Varenna, Italy, 12-16 June 2000 (see INDC(NDS)-416, September 2000)
- Vienna, Austria, 3-7 December 2001 (see INDC(NDS)-431, April 2002)

to discuss progress and agree on the contents and form of the new library. In the course of work, the original scope of the CRP has been substantially extended by inclusion of new quantities and results of microscopic calculations for about 8000 nuclei. Extensive efforts have also been dedicated to the testing of the RIPL-2 data.

RIPL-2 is targeted at users of nuclear reaction codes interested in low-energy nuclear applications. Incident and outgoing particles include neutrons, protons, deuterons, tritons, ^{3}He, ^{4}He and γ, with energies up to approximately 100 MeV. The numerical data and computer codes included in the library are arranged in seven segments/directories:

No	Directory	Contents
1	MASSES	Atomic Masses and Deformations
2	LEVELS	Discrete Level Schemes
3	RESONANCES	Average Neutron Resonance Parameters
4	OPTICAL	Optical Model Parameters
5	DENSITIES	Level Densities (Total, Partial)
6	GAMMA	Gamma-Ray Strength Functions
7	FISSION	Fission Barriers and Level Densities

The RIPL-2 library is physically located at a Web server operated by the IAEA, and can be conveniently accessed by pointing any Web browser at:

http://www-nds.iaea.org/RIPL-2/

This Web site provides for downloading entire RIPL-2 segments, individual files, and retrieval of selected data. In addition, some basic calculations and graphical comparisons of parameters are also available. A CD-ROM with the complete RIPL-2 library can be requested cost-free from the IAEA. This Handbook contains a full description of the library including the physics involved, with an introductory and seven technical chapters, plus related Annexes that describe the library structure as defined above.

During the development of RIPL-2, several important issues could not be addressed within the current CRP. Therefore, a third phase of the RIPL project has been initiated in 2002 in order to extend the applicability of the library to cross sections for reactions on nuclei far from the stability line, incident energies beyond 100 MeV, and reactions induced by charged particles. This phase is planned for completion in 2006-07.

The IAEA wishes to thank all participants of the CRP for their diligent work that has lead to the creation of the Reference Input Parameter Library, and for their valuable contributions to the present Technical Report. Finally, M. Herman was the IAEA responsible officer for the CRP, this publication and the resulting database.

Contents

1 INTRODUCTION

An important trend in the evaluation of neutron and charged-particle nuclear data is the increased use of nuclear reaction theory codes to compute cross sections, spectra and angular distributions required for a large variety of applications. As a matter of principle, the use of model codes offers many advantages such as preservation of the energy balance and coherence of partial cross sections with total and/or reaction cross sections. These features are essential for consistent and reliable transport calculations. In addition, the theoretical approach permits the prediction of data for unstable nuclei and fills gaps in the experimental data. Nuclear reaction theory is believed to be in a position to meet many of the requirements for practical applications. The major sources of uncertainty are the input parameters needed to perform theoretical calculations.

For any nuclear reaction calculation, nuclear masses are the basic data for obtaining binding energies and Q-values. These data are presented in **Chapter 2**, together with other useful information such as ground state deformations.

Discrete level schemes, including spins, parities, γ-transition branchings and conversion coefficients are important for the determination of low-energy nuclear level densities and for cross-section calculations. Most of the related experimental information is contained in the ENSDF library. However, the format of the ENSDF library is not appropriate for reaction calculations. In addition, a lack of unique spin and/or parity assignments for many levels, and missing conversion coefficients for most of the electromagnetic transitions prevent direct use of the ENSDF library by the reaction model codes. To overcome these deficiencies, a dedicated RIPL-2 library of discrete levels has been created. **Chapter 3** describes the contents, along with the procedures used to retrieve the necessary data and fill gaps.

As is well known, neutron cross sections at low incident energies exhibit resonant behavior, and a careful statistical analysis of the experimental results leads to the average neutron resonance parameters, as described in **Chapter 4**. These average quantities are not directly used in the model calculations, but are important data for constraining the parameters of different models:

- average spacing of resonances is the only measure of the level density near the neutron binding energy,
- neutron strength functions have to be reproduced by the optical model at low energies, and
- average radiative width is used to normalize γ-ray strength functions.

Above the resonance energy region, the nuclear reaction models can only reproduce the smooth behavior of the cross sections, and the evaluation of nuclear data is generally divided into two major steps. By using the optical model in the first step, the elastic channel and the direct inelastic channels for deformed nuclei are explicitly calculated, whereas all other channels are lumped together in the reaction cross section. **Chapter 5** gives an extensive compilation of optical model parameters for different types of incident

particles, from the neutron to ^{4}He. A consistent evaluation can be achieved for each interacting system by using a unique parameterization which reproduces the relevant observables (total or reaction cross sections, elastic angular distributions, analyzing powers) over an energy range as broad as possible, including, the low energy region in the case of neutron interaction, where the calculated neutron strength function and scattering radius should match the experimental values. Furthermore, the parameters should have a smooth energy dependence.

The second step consists in sharing the reaction cross section among all possible individual channels. For incident energies lower than about 10 MeV, this is done by using the statistical decay of the compound nucleus, a formalism often referred to as the Hauser-Feshbach theory. Written in a compact form, the Hauser-Feshbach formula that gives the cross section for the A(a,b)B reaction is represented by the expression:

$$\sigma_{a\to b} = \sum_{J^\pi} \frac{T_a\, T_b}{\sum_i \sum_c T_{ic}}$$

where the index i stands for the different types of outgoing particles[1] (or the fission channel, if any), and the Ts are the transmission coefficients calculated by the optical model for this particle. The index c represents all accessible final states which are either discrete excited levels of the residual nucleus or a continuum of levels described by the level density.

In the case of discrete levels, one should only take into account the low-lying levels of known excitation energy, spin, parity, and decay branchings (if γ production is required). Above the energy of the last level for which one of the previous quantities is missing or uncertain, one has to consider a continuum of levels described by the total level density. At low excitation energy, the level density should match the cumulative number of discrete levels and reproduce the average spacing of neutron resonances at the neutron binding energy. Different theoretical approaches to this longstanding problem are presented in **Section 6.1**.

For incident energies higher than approximately 10 MeV, the pre-equilibrium reaction mechanism constitutes the bridge between fast (direct) processes and slow (compound) processes providing for the high-energy tails in spectra and the smoothly forward peaked angular distributions. Methods for calculating partial (or particle-hole) level densities used in the pre-equilibrium model calculations are given in **Section 6.2**.

Gamma-ray emission is an almost universal reaction channel since γ rays, in general, accompany any nuclear reaction. Modeling of the γ cascade provides γ spectra and allows calculation of isomeric cross sections. The basic quantity is the γ-ray strength function derived typically from the Giant Resonance parameters, as discussed in **Chapter 7**.

The fission cross-section calculations depend on two key ingredients: (i) fission level density (level density of the fissioning nucleus at the saddle point deformation), and (ii) fission barriers. These two strongly interdependent parameters are discussed in **Chapter 8**.

[1] Outgoing particles considered are normally p, n, d, t, ^{3}He, α and γ.

Many of the parameters are model dependent, and should therefore be used strictly within the frame of their definitions. Although the parameters reported in RIPL-2 are ready to be used in reaction calculations, some of them may still need improvements or adjustments. The reaction models are particularly sensitive to optical model potentials and total level densities, which have to reproduce consistently different pieces of information. Therefore, utmost care should be applied when selecting an adequate set of parameters.

Due to the extensive testing and additions, the RIPL-2 database has been substantially improved compared to the original RIPL-1 database. Nevertheless, RIPL-2 does not fully supersede the original RIPL-1 library since only the recommended files were considered in the RIPL-2 exercise. So called 'other' files of RIPL-1 were not incorporated in the new database. Although these do not match the level of testing typical for RIPL-2, they still might be of practical use in nuclear data evaluations or basic research, and therefore RIPL-1 information and data continue to be fully tracable through:

(a) Handbook for Calculations of Nuclear Reaction Data - Reference Input Parameter Library, IAEA-TECDOC-1034, IAEA, Vienna (1998);

(b) Web site address: http://www-nds.iaea.org/ripl/;

(c) CD-ROM: RIPL-1.

RIPL-2 contains numerical values for most of the parameters needed to model nuclear reactions and a number of computer codes. For nuclei close to the stability line, the parameters were derived from the available experimental data. For a certain nucleus, these are usually sets of a few numbers used by the reaction codes to calculate derived quantities such as Q-values, transmission coefficients, level densities or γ-ray strength functions. Often, these parameters are supplemented with closed-form systematics to fill gaps in the experimental data. Since these systematics were obtained by fitting existing data, their extrapolation to the nuclei far from the stability line is doubtful. Therefore, RIPL-2 also contains parameters and some derived quantities provided by the large-scale calculations within microscopic models adjusted to the existing experimental data. These results are tabulated for practically all nuclei between drip lines and can be directly used by nuclear reaction codes. All RIPL-2 data are stored in a unified format to facilitate their use. In addition to the model parameters, RIPL-2 includes a number of utility codes, which are intended for calculating derived quantities from the RIPL-2 parameters, data retrieval and library maintenance. The internet address for the RIPL-2 database is http://www-nds.iaea.org/RIPL-2/.

2 ATOMIC MASSES

Coordinator: S. Goriely

Summary

Nuclear ground state properties are fundamental quantities in many different fields of physics. The present chapter considers the available experimental data concerning the atomic masses (Audi and Wapstra 1995 [2.1]), as well as the deformation parameters (Raman et al. 2001 [2.13]) extracted from the experimental reduced electric quadrupole transition probability. When no experimental data exist, ground-state properties can be derived from local or global theoretical approaches. RIPL-2 provides ground-state properties predicted by three global models: the Finite-Range Droplet Model (Möller et al. 1995 [2.3]), the Hartree-Fock-Bogoliubov Model (Goriely et al. 2002 [2.6]) and the approximation to the Shell Model by Duflo and Zuker (1995 [2.8]). In addition to nuclear masses, the FRDM model also provides microscopic corrections and deformation parameters, while the HFB model provides density distributions and deformation parameters. Relative isotopic abundances for all stable nuclei found naturally on earth are also provided as supplementary information.

2.1 Atomic masses

Nuclear ground state properties, and more particularly nuclear masses, are fundamental quantities in many different fields of physics. The mass $M_{nuc}(N,Z)$ of a nucleus with N neutrons (of mass M_n) and Z protons (of mass M_p) is measurably different from the sum of the masses of the free nucleons, and provides a direct determination of the internal energy E_{nuc} (negative of the binding energy) of the nucleus:

$$E_{nuc} = \{M_{nuc}(N,Z) - NM_n - ZM_p\}c^2 \tag{2.1}$$

The atomic mass can be calculated from the nuclear mass from the relationship:

$$M_{at} = M_{nuc}(N,Z) + ZM_e - B_e(Z) \tag{2.2}$$

where M_e is the electron mass, and B_e is the total atomic binding energy of all electrons.

Most of the nuclear masses for nuclei close to the stability line were measured with high accuracy. However, many applications involve nuclear species for which no experimental data are available. In these cases, they have to be estimated on a theoretical basis. Many different mass formulae are available nowadays. We will consider here only global approaches, which provide predictions of nuclear masses for all nuclei lying between the proton and the neutron drip lines up to the super-heavy region $Z \lesssim 120$.

2.1.1 Experimental masses

The latest compilation of experimental atomic masses at the time was the 1995 work of Audi and Wapstra [2.1], which includes 1964 nuclei. In addition, these authors also estimated a set of additional 967 masses from trends in systematics based on the regularity of the mass surface. This final set of Audi and Wapstra *best recommended* masses included 2931 nuclei.

2.1.2 Finite-Range-Droplet-Model mass table

Attempts to develop formula or algorithms representing the variation in E_{nuc} from one nucleus to another go back to the 1935 "semi-empirical mass formula" of von Weizsäcker [2.2]. This approach corresponds to the widely used liquid-drop model of the nucleus, i.e., the macroscopic mass formula which accounts for all but a small part of the variation in the binding energy. Improvements have been gradually made to the original liquid-drop mass formula, leading to the development of macroscopic-microscopic mass formulae, where microscopic corrections accounting for the shell and pairing correlation effects are added to the liquid drop part. Thus, the macroscopic and microscopic features are treated independently, both parts being connected exclusively by a parameter fit to experimental masses. Later developments included modifications to the macroscopic properties of the infinite and semi-infinite nuclear matter and the finite range character of the nuclear forces. The most sophisticated version of this macroscopic-microscopic mass formula is the "finite-range droplet model" (FRDM) [2.3]. The atomic mass excesses and nuclear ground-state deformations are tabulated for 8979 nuclei ranging from ^{16}O to A=339. The calculations are based on the finite-range droplet macroscopic model and the folded-Yukawa single-particle microscopic correction. Relative to the 1981 version, improvements are mainly found in the macroscopic model, pairing model with a new form for the effective-interaction pairing gap, and minimization of the ground-state energy with respect to the additional shape degrees of freedom. The parameters are determined directly from a least-squares adjustment to the ground-state masses of 1654 nuclei ranging from ^{16}O to ^{106}Sg. The error of this mass model is 0.689 MeV for the 1888 $Z, N \geq 8$ nuclei with experimental masses. Data file **mass-frdm95.dat** includes the Audi and Wapstra (1995) experimental and *best recommended* masses when available, along with the FRDM calculated masses, microscopic corrections and deformation parameters in the β-parameterization. The microscopic correction E_{mic} corresponds to the difference between the total binding energy and the spherical macroscopic energy (see below).

2.1.3 Hartree-Fock-Bogoliubov mass table

As well as the liquid-drop approach, there are microscopic theories based on the nucleonic interactions providing estimates of the binding energies. The most promising approach nowadays is the non-relativistic Hartree-Fock (HF) method based on an effective nucleon-nucleon interaction of Skyrme type. It was demonstrated that HF calculations in which the Skyrme force is fitted essentially to all mass data are not only feasible, but can also compete with the most accurate droplet-like formulae available nowadays [2.4].

Recently, a new Skyrme force has been derived on the basis of HF calculations with pairing correlations taken into account in the Bogoliubov approach, using a δ-function pairing force [2.5, 2.6]. Pairing correlations are often described within the BCS framework. However, the BCS procedure neglects the fact that the scattering of nucleon pairs between different single-particle states under the influence of the pairing interaction will actually modify the single-particle states, a difficulty that becomes particularly serious close to the neutron-drip line where nucleon pairs are scattered into the continuum. For such nuclei, this problem is avoided in the HF-Bogoliubov (HFB) method.

The Skyrme and pairing parameters of the HFB-2 mass table are determined by fitting to all Audi and Wapstra (1995) experimental masses for 1888 $Z, N \geq 8$ nuclei, both spherical and deformed. A Wigner correction term of the form $E_W = V_W \exp(-\lambda(N - Z)^2/A^2) - V'_W|N - Z| \exp(-A^2/A_0^2)$ is also included to account for the over-binding in the $Z \simeq N$ nuclei. The latest force (BSk2) is a standard Skyrme which gives an rms error of 0.680 MeV with respect to the 1888 known masses. The quality of the HFB predictions is identical to the one obtained with the FRDM (the same rms of about 0.680 MeV on the same set of masses). The BSk2 force is characterized by the following nuclear matter properties: energy per nucleon at equilibrium in symmetric nuclear matter $a_v = -15.794$ MeV, the corresponding density $\rho_0 = 0.1575$ fm^{-3}, the isoscalar effective mass $M_s^*/M = 1.04$, the isovector effective mass $M_v^*/M = 0.86$ and the symmetry coefficient $J = 28$ MeV. Details regarding the BSk2 force can be found in Ref. [2.6] and those regarding the HFB model in Ref. [2.5]. The HFB model was also found to give reliable predictions of nuclear radii. A comparison with the measured radii of the 523 nuclei in the 1994 data compilation of Nadjakov et al. [2.7] shows an rms error of 0.028 fm.

The complete HFB-2 mass table is available in the **mass-hfb02.dat** file. In addition to the Audi and Wapstra (1995) experimental and *best recommended* masses when available, this mass table includes the HFB masses, deformation parameters in the β-parameterization and the parameters of the nucleon density distribution for all 9200 nuclei lying between the two drip lines over the range $Z, N \geq 8$ and $Z \leq 120$. The density distribution amplitude $\rho_{q,0}$, radius r_q and diffuseness a_q are determined by fitting the HFB distribution by a simple spherical Fermi function $\rho_q(r) = \rho_{q,0}/[1 + \exp(-(r - r_q)/a_q)]$. Note that the amplitude $\rho_{q,0}$ is determined so that the nucleon number is conserved in the spherical approximation. Exact HFB density distributions (assuming spherical symmetry) are also tabulated in the **matter-density-hfb02** subdirectory for nuclear radii up to 15 fm in steps of 0.1 fm. The tabulated nucleon densities do not take into account the finite size of the proton.

2.1.4 Duflo-Zuker approximation to the Shell Model

Another microscopic approach worth considering is the development by Duflo and Zuker [2.8] of a mass formula based on the shell model. In this approach, the nuclear Hamiltonian is separated into a monopole term and a residual multipole term. The monopole term is responsible for saturation and single-particle properties, and is fitted phenomenologically, while the multipole part is derived from realistic interactions. The latest version of the mass formula made of 10 free parameters reproduces the 1888 $Z, N \geq 8$ experimental masses with an rms error of 0.553 MeV. A simple 120-lines FORTRAN subroutine in the **masses/duflo-zuker96.for** file makes the computation of any mass straightforward, and

is especially useful when the nucleus is not available in the previously mentioned tables.

2.2 Shell corrections

The microscopic correction to the binding energy is a quantity of fundamental importance in the derivation of many physical properties affected by the shell, pairing and deformation effects. However, there is a lot of confusion in the literature about what is referred to as the shell correction energy; different definitions exist. The most common one defines the various microscopic corrections (e.g., [2.3]) as follows:

The total nuclear binding energy is written as

$$E_{tot}(Z, A, \beta) = E_{mac}(Z, A, \beta) + E_{s+p}(Z, A, \beta) \tag{2.3}$$

where β characterizes the nuclear shape at equilibrium, i.e., the shape which minimizes the total binding energy. $E_{s+p} = E_{shell} + E_{pair}$ is the shell-plus-pairing correction energy[1]. Defining a macroscopic deformation energy by the difference in the macroscopic energy between the equilibrium and spherical shape:

$$E_{def}(Z, A, \beta) = E_{mac}(Z, A, \beta) - E_{mac}(Z, A, \beta = 0), \tag{2.4}$$

the total nuclear binding energy can now be expressed as

$$E_{tot}(Z, A, \beta) = E_{mac}(Z, A, \beta = 0) + E_{mic}(Z, A, \beta) \tag{2.5}$$

with the microscopic correction

$$E_{mic}(Z, A, \beta) = E_{shell}(Z, A, \beta) + E_{pair}(Z, A, \beta) + E_{def}(Z, A, \beta) \tag{2.6}$$

including all shell, pairing and deformation effects. Another frequent definition of the microscopic energy considers the experimental energy $E_{exp}(Z, A)$, when available, instead of the total theoretical binding energy E_{tot} and is given by the equation:

$$\begin{aligned} E_{mic}^{exp} &= E_{exp}(Z, A) - E_{mac}(Z, A, \beta) && (2.7) \\ &\simeq E_{shell}(Z, A, \beta) + E_{pair}(Z, A, \beta) = E_{s+p}(Z, A, \beta) && (2.8) \end{aligned}$$

Should the mass formula be exact, $E_{mic}^{exp} = E_{s+p}(Z, A, \beta)$. Although E_{mic}^{exp} is often referred to as an "experimental" microscopic correction, this terminology is incorrect, since the parameter remains model-dependent through the use of the model-dependent E_{mac} quantity. Each mass model calls for specific theoretical backgrounds to estimate the macroscopic part, as well as the shell, pairing and deformation energies. The most common approaches to derive the macroscopic part are the Finite-Range Droplet or Liquid Drop model [2.3], the Thomas-Fermi approach [2.9] or the Extended-Thomas-Fermi approach [2.10]. Depending on the approach followed to derive the smooth macroscopic part of the binding energy and the parameter set adopted for the macroscopic part, the microscopic corrections can take different values. The FRDM microscopic correction E_{mic} can be found in the **mass-frdm95.dat** file. This dataset also contains the deformation corrections calculated for the deformation parameters β_2 and β_4 estimated from the FRDM mass formula.

[1]Note that we define the pairing correction for even-even nuclei, and do not consider the odd-even effect also attributed to the pairing interaction.

Therefore, these corrections can also be used for transforming the FRDM microscopic corrections into the corresponding FRDM shell corrections. The shell corrections calculated according to the liquid drop model of Myers-Swiatecki [2.11] are included in the "Nuclear Level Densities" segment (**shellcor-ms.dat** file).

When shell, pairing and deformation corrections are introduced to a given quantity (for example the nuclear level density) using the corresponding energy correction, special attention should be paid to the prescription adopted. In particular, depending on the level density formula considered, the "microscopic" correction to the level density a-parameter can include very different effects, so that different energy corrections should be considered (see [2.12] for more details).

2.3 Deformations

In addition to the theoretical deformation parameters derived from the FRDM and HFB ground-state predictions, information can also be extracted from the experimental reduced electric quadrupole transition probabilities $B(E2)$. Assuming a uniform charge distribution to distance R and zero charge beyond, the model-dependent deformation parameter β is related to $B(E2)$ by [2.13]:

$$\beta = \frac{4\pi}{3ZR_0^2}\,[B(E2)/e^2]^2 \tag{2.9}$$

where $R_0 = 1.2\ A^{1/3}$. The final compilation of 328 experimental deformation parameters β (and corresponding uncertainties) is included in the **gs-deformations-exp.dat** file. Note that a similar parameter β_2 is widely used in the theory of the direct-interaction excitation of collective states to describe the deformation of the average potential. While the β values given here provide a useful guide to the values to be expected for this nuclear potential deformation parameter, the β and β_2 values can differ somewhat.

2.4 Relative isotopic abundances

For practical applications, the relative isotopic abundances (expressed in percent) for each stable nucleus found naturally on earth is given in the **abundance.dat** file. The data originate from the Nuclear Wallet Cards, as retrieved from Brookhaven National Laboratory [2.14].

2.5 Summary of codes and data files

The programs and data files included in the directory are:

abundance.dat - Natural abundances of stable isotopes.

abundance.readme - Description of the abundance.dat file.

duflo-zuker96.for - Code to estimate nuclear masses with the 10 parameter formula of Duflo and Zuker.

duflo-zuker96.readme - Description of the duflo-zuker96.for file.

gs-deformations-exp.dat - Compilations of experimental deformation parameters beta2.

gs-deformations-exp.readme - Description of the gs-deformations-exp.dat. file.

mass-frdm95.dat - Ground state properties based on the FRDM model.

mass-frdm95.readme - Description of the mass-frdm95.dat file.

mass-hfb02.dat - Ground state properties based on the HFB model.

mass-hfb02.readme - Description of the mass-hfb02.dat file.

matter-density-hfb02/zxxx.dat - Neutron and proton density distributions based on the HFB model.

matter-density-hfb02.readme - Description of the matter-density-hfb02/zxxx.dat files.

REFERENCES

[2.1] AUDI, G., WAPSTRA, A.H., Nucl. Phys. **A595** (1995) 409.

[2.2] VON WEIZSÄCKER, C.F., Z. Phys. **99** (1935) 431.

[2.3] MÖLLER, P., NIX, J.R., MYERS, W.D., SWIATECKI, W.J., At. Data Nucl. Data Tables **59** (1995) 185.

[2.4] GORIELY, S., TONDEUR, F., PEARSON, J.M., At. Data Nucl. Data Tables **77** (2001) 311.

[2.5] SAMYN, M., GORIELY, S., HEENEN, P.-H., PEARSON, J.M., TONDEUR, F., Nucl. Phys. **A700** (2002) 142.

[2.6] GORIELY, S., SAMYN, M., HEENEN, P.-H., PEARSON, J.M., TONDEUR, F., Phys. Rev. **C66** (2002) 024326.

[2.7] NADJAKOV, E., MARINOVA, K., GANGRSKY, Y., At. Data Nucl. Data Tables **56** (1994) 134.

[2.8] DUFLO, J., ZUCKER, A., Phys. Rev. **C52** (1995) R23.

[2.9] MYERS, W.D., SWIATECKI, W.J., Nucl. Phys. **A601** (1996) 141.

[2.10] ABOUSSIR, Y., PEARSON, J.M., DUTTA, A.K., TONDEUR, F., At. Data Nucl. Data Tables **61** (1995) 127.

[2.11] MYERS, W.D., SWIATECKI, W.J., Nucl. Phys. **A80** (1966) 1.

[2.12] GORIELY, S., Proc. Research Co-ordination Meeting on Nuclear Model Parameter Testing for Nuclear Data Evaluation, Varenna, Italy, June 2000, INDC(NDS)-416, IAEA, Vienna (2000) 87.

[2.13] RAMAN, S., NESTOR, Jr., C.W., TIKKANEN, P., At. Data Nucl. Data Tables **78** (2001) 1.

[2.14] TULI, J.K., Nuclear Wallet Cards, NNDC, Brookhaven National Laboratory, 2001.

3 DISCRETE LEVELS

Coordinator: T. Belgya

Summary

Discrete levels and their decay characteristics are required as input for nuclear reaction calculations, which replace the statistical level densities and strength functions below a certain energy E_{max}. Most of the data were extracted from the ENSDF library. However, many missing data such as unique spins and parities were inferred using statistical methods, while missing internal conversion coefficients (ICC) and electromagnetic decay probabilities were calculated. For each element the data have been stored in a file containing all isotopes in increasing mass order.

In addition, cutoff energies E_{max} for completeness of level schemes and spin cutoff parameters have been determined for a large number of nuclei. The latter data have been collected in a separate data file, together with the results obtained from a constant temperature fit to the nuclear level schemes.

Nuclear reaction and statistical model calculations require complete knowledge of the nuclear level schemes in order to specify all possible outgoing reaction channels and to calculate partial (isomeric) cross sections. Knowledge of discrete levels is also important for adjusting level densities, which replace unknown discrete level schemes at higher excitation energies. For this purpose completeness of the level scheme is of crucial importance. The term "completeness" means that up to a certain excitation energy all discrete levels in a given nucleus are observed and are characterized by unique energy, spin and parity values. Knowledge of particle and gamma-ray decay branches is also required, especially when the population of isomeric states is of interest.

Complete level schemes can only be obtained from comprehensive spectroscopic studies of non-selective reactions. Statistical reactions, such as $(n, n'\gamma)$ and averaged resonance capture, are particularly suitable due to their non-selective excitation mechanism and completeness of information obtained by means of gamma-ray spectroscopy [3.1]. For practical reasons the vast majority of nuclei cannot be studied by such means; hence the degree of knowledge of the experimentally determined discrete level schemes varies widely throughout the nuclear chart. While this knowledge is compiled for the Evaluated Nuclear Structure Data File (ENSDF) [3.2], the format is too involved for use in reaction calculations. The original purpose of the ENSDF is to serve as a typographical input for the preparation of Nuclear Data Sheets, and extracting data is by no means simple. ENSDF contains a great deal of information in a format that can not be easily decoded by the computer codes. Therefore, the data have to be extracted and reformatted for

practical applications.

The first attempt to create a suitable library of discrete levels was undertaken in the RIPL-1 project [3.3, 3.4, 3.5]. However, the RIPL-1 starter file suffered from a number of deficiencies related to the use of the retrieval code NUDAT and a format that was too restrictive. Therefore, a new extended Discrete Level Schemes Library has been created and formatted according to the recommendations of the RIPL-2 co-ordination meetings [3.6, 3.7].

3.1 Discrete Level Scheme Library (DLSL)

The RIPL-2 Discrete Level Scheme Library (DLSL) has been created by the Budapest group using the ENSDF-II data set of 1998 as a source [3.2, 3.8]. This data set is a slightly modified version of the original ENSDF library [3.2], and contains explicit final states for gamma transitions. In the new version of the DLSL, there are no limitations to the number of levels or transitions, which were identified as deficiencies in the RIPL-1 file [3.5].

The 1998 ENSDF II CD-ROM contains 2637 data sets of nuclear decay schemes (606254 rows of data). There are 2546 nuclear decay schemes with at least 1 known level, that cover the range $A = 1-266$, $Z = 0-109$. These 2546 level schemes, have been called the basic set, and were processed to obtain the DLSL files. The basic set contains 113346 levels out of which 8554 have unknown level energies. These are marked with +X, +Y..., an ENSDF notation also used in the RIPL-2 DLSL files. A total of 12956 spins are unique; for the additional 8708 levels, spin and/or parity assignment is considered uncertain (parenthesis around a single spin or parity value). These spin-parity values were adopted and extracted from the ENSDF file. The basic set also reports 159323 γ transitions between the levels.

Some of the data such as level spins, parities and electron conversion coefficients were found to be missing in the basic data set. Since these data are crucial for model calculations, they have been calculated or inferred from other available data using statistical assumptions. Table 3.1 shows the number of spins that has been inferred under different assumptions.

Table 3.1: Type and number of spin estimates.

Type of method	Number
Spin ranges from gamma transitions	3560
Spins from spin distribution	3551
Spins chosen from a list using spin distribution	6280

One of the most difficult tasks was the determination of the maximum level number (N_{max}), and the corresponding energy (E_{max}) up to which a level scheme is supposed to be complete. A new fitting method that eliminates the deficiencies of the earlier fitting procedure [3.5, 3.9] has been developed, and is outlined in Ref. [3.7] and detailed in ANNEX 3.A. The temperature as a function of the mass number A was obtained from

a global least-squares fit for 625 nuclei. An additional 503 nuclei that were not used in the global fit have been fitted using the above $T(A)$ function in order to estimate N_{max} values. The results for the 2546 nuclei are reported in the file **level-param.dat**.

In order to calculate γ-ray emission intensities from nuclear reactions, the ICCs must be known for all electromagnetic transitions from a given level. Since only some of them are available in ENSDF, the missing values have been calculated and included in the RIPL-2 file. This brings the number of ICCs in RIPL-2 to 92634 compared to 21595 in ENSDF.

Data uncertainties have generally been disregarded since they are not used in the reaction calculations.

The major steps in the construction of the Discrete Level Scheme Library are outlined below:

- Adopted or available discrete nuclear levels and γ-ray transitions have been retrieved and converted into RIPL-2 format using FORTRAN programs developed within the CRP.

- Cut-off energies (E_{max}) and the corresponding cumulative numbers of levels (N_{max}) below these energies have been determined from constant-temperature fits to the staircase plots for nuclei with at least 20 known levels.

- Additional energy cut-offs (E_c), corresponding to the energy of the highest level with unique spin and parity assignment, have been determined for all nuclei on the basis of the ENSDF data alone.

- Data retrieved from ENSDF have been extended in order to obtain unique data values as required for reaction calculations. Thus, unique spin and parity values have been generated from known data up to the cut-off energy E_{max}. Internal conversion coefficients (ICC) for electromagnetic transitions have been calculated using unique spin and parity values if they were not given in ENSDF.

  The extension has included the complete (γ-ray and particle emission) decay behavior of the levels if known from experiments.

- Data have been tested for internal inconsistencies that may arise from misprints, logical errors, or use of improper algorithms.

- For nuclei that have at least 10 levels with spin assignment below E_{max}, the spin cut-off factors have been calculated from the spin assignments provided in ENSDF.

- Missing spins and parities were inferred up to N_{max} because up to this energy one relies on spin/parity distributions derived from known data.

It should be stressed, that the data in the RIPL-2 DLSL files are intended only for nuclear reaction calculations and not for nuclear structure studies. This warning refers particularly to inferred spins and calculated quantities such as ICCs.

3.1.1 Format of the Discrete Level Schemes Library

The library is located in the RIPL-2/levels/levels directory and is arranged in separate elemental files. The file names are **zxxx.dat** where xxx stands for the charge number of an element preceded with zeros if necessary to form three digits. The charge number runs from 0 to 109. Each file contains decay data for all isotopes of an element ordered by increasing mass number.

There are three kinds of records. Data for each isotope begin with an identification record. An example is given below for Nb-89. The upper lines with labels are not part of the actual file and serve only to facilitate explanation of the format:

```
SYMB     A     Z   Nol   Nog Nmax    Nc      Sn[MeV]      Sp[MeV]

89Nb    89    41    25    24   16     1   12.270000     4.286000
```

The corresponding FORTRAN format is (a5,6i5,2f12.6), and the labels mean:

SYMB: mass number with elemental symbol

A: mass number

Z: charge number

Nol: number of levels in decay scheme

Nog: number of gamma rays in decay scheme

Nmax: maximum number of levels up to which the level-scheme is complete; the corresponding level energy is E_{max}

Nc: level number up to which the experimental spins and parities are unique

Sn: neutron separation energy in MeV

Sp: proton separation energy in MeV

The identification record is followed by level records shown below for the first three levels in Nb-89:

```
 Nl    El[MeV]     J  p    T1/2[s] Ng s unc          spin info  nd m    percent    mode

  1   0.000000   4.5  1   6.84E+03  0 u +X              (9/2+)  1 =    100.0000 %EC+%B+
  2   0.000000   0.5 -1   4.25E+03  0 u +Y              (1/2)-  1 =    100.0000 %EC+%B+
  3   0.658600   3.5 -1   4.00E-09  1 c          (7/2,9/2,11/2)  0
```

The corresponding FORTRAN format is:

(i3,1x,f10.6,1x,f5.1,i3,1x,(e10.2),i3,1x,a1,1x,a4,1x,a18,i3,10(1x,a2,1x,f10.4,1x,a7)),

and the labels mean:

Nl: serial number of level

El: level energy in (MeV)

J: Assigned unique spin, determined from spin information; details are given in ANNEX 3.B

p: calculated unique parity determined from parity information; details are given below

T1/2: half-life of level if known; details are given below

Ng: number of gamma rays de-exciting the level

s: method of selection of J and p; details are given in ANNEX 3.B

unc: uncertain level energy; details are given below

spin info: original spin information from ENSDF file; can be used to adjust spin-parity values by hand

nd: number of decay mode of a level if known (values up to 10); value 0 means that decay may occur by gamma-ray emissions, but other decay modes are not known

m: modifier of percentage; details are given below

percent: percent of the decay mode; details are given below

mode: ENSDF notation of decay modes; details are given below

The third kind of record is a gamma record, which immediately follows a corresponding level record. Number of gamma records is given in the level record. The sample gamma records below correspond to the decay of the 5^{th} level in Nb-94 (level record is also shown):

```
5   0.113401  5.0  1   5.00E-09  2 u                    (5)+  0
                                      Nf    Eg[MeV]     Pg        Pe        ICC
                                      3      0.055  4.267E-02  1.301E-00 2.050E+00
                                      1      0.113  7.499E-01  8.699E-01 1.600E-01
```

The corresponding FORTRAN format is (39x,i4,1x,f10.3,3(1x,e10.3)), and the labels are:

Nf: serial number of the final state

Eg: gamma-ray energy in (MeV)

Pg: probability of decay with gamma ray; details are given below

Pe: probability of decay with electromagnetic transition; details are given in ANNEX 3.D

ICC: internal conversion coefficient; details are given below

3.1.2 Conventions and methods

This section contains detailed description of the conventions used to represent physical quantities and methods of their determination. Formulas for estimating certain quantities are given if not trivial.

J: Spin of a level. Unknown spin values have been determined according to the procedure described in ANNEX 3.B. Possible values are -1.0 for unknown spin, otherwise 0.0, 0.5, 1.0 ...

p: Parity of a level. If parity was not known, positive or negative values were chosen with equal probability for levels up to E_{max}. The method used for the parity determination is not indicated in the file. Possible values are 1 for positive parity, -1 for negative parity, and 0 for unknown parity.

T1/2: Half-life of a level. All known half-lives or level widths have been converted into seconds. Half-lives of stable nuclei are represented as -1.0E+0.

unc: Flag indicating uncertain energy of a level. Under certain cases, such as an unobserved low energy transition out of a band head or decays to a large number of levels from a super-deformed band, the energy of a corresponding band may be impossible to determine. This field provides the means of introducing a note about this problem in the level scheme. ENSDF evaluators set the energy of such band heads to 0.0 keV or, if the level order is known, to the preceding level energy, and they place a note that one should add an unknown energy X to this value. In such cases, a decay scheme is not suitable for level density determination. Usually, the super-deformed levels are inadequate for calculation of the level density anyway. Therefore, the nuclei with more then two uncertain levels have been excluded from level density calculations. Two uncertain levels have been accepted, because in some cases they correspond to important isomeric states.

m: The decay percentage modifier informs a user about major uncertainties in the decay pattern of a level. Modifiers have been copied from ENSDF without any modifications. They can have the following values: $=, <, >, ?$ (unknown, but expected), AP (approximate), GE (greater than or equal), LE (less than or equal), LT (less than), and SY (value from systematics).

percent: Probability of different decay modes of a level. As a general rule, probabilities of various decay modes add up to 100% except: (i) when a small probability is present, the sum may be slightly more then 100% due to rounding, (ii) when β-decay is followed by heavier particle emission, probability of the β-delayed particle emission is also included as a portion of the β-decay and the sum can be substantially larger then 100%. When the modifier is '?', the sum is indefinite.

mode: Short notation for decay modes of a level (see Table 3.2 for details). Some minor channels, such as decay through emission of ^{20}Ne, have been ignored.

Pg: Probability that a level decays through γ-ray emission (ratio of the total electromagnetic decay of the level to the intensity of the γ ray). If no branching ratio was provided in ENSDF file, Pg is set to zero.

Table 3.2: Decay mode codes.

Code	Explanation
%B−	β^- decay
%EC	electron capture
%EC+%B+	electron capture and β^+ decay
%N	neutron decay
%A	α decay
%IT	isomeric transition
%P	proton decay
%3HE	^3He decay
%B+P	β^+ delayed proton decay
%B−N	β^- delayed neutron decay
%SF	spontaneous fission
%ECP	electron capture delayed proton decay
%ECA	electron capture delayed α decay
%G	γ decay
%B+2P	β^+ delayed double proton decay
%B−2N	β^- delayed double neutron decay

Pe: Probability that a level decays with the given electromagnetic transition (ratio of the intensity of a given electromagnetic transition and the total electromagnetic decays of the level). The sum of the electromagnetic decays has been normalized to %IT or %G (see ANNEX 3.D). If no branching ratio was provided in ENSDF, Pe is set to zero.

ICC: Internal conversion coefficient for a transition. An improved version of the NNDC program HSICC.FOR [3.10] has been used to calculate the ICC values if not provided in ENSDF (see ANNEX 3.C for details). When calculating the ICCs, the first multipole mixing ratio given in ENSDF has been used. If there was no multipole mixing ratio given, E2 has been assumed for the mixed E2+M1 transitions of even-even nuclei, and M1 for the others. No attempt has been made to include possible E0 decays. For other mixing possibilities the lowest multipole order has been used unless the mixing ratio was found in ENSDF. The mass of the nucleus and energy of the transition also limits the ICC calculations. Below A=10, ICCs have only been calculated for Li and C. ICCs have been set to zero if the transition energy exceeds a certain (mass dependent) energy.

3.1.3 Format of the file with constant-temperature fit parameters

The parameters resulting from the constant-temperature fits to the discrete levels have been tabulated in a separate file **(level-param.dat)**. An excerpt from this file is given below:

```
#          Results of constant temperature fits to discrete levels
#  Z   A El       T        dT        U0        dU0 Nlev Nmax NO  Nc    Emax       Ec     Chi Fit Flag NoX  Xm  EX    sigma
#               [MeV]     [MeV]     [MeV]     [MeV]                    [MeV]     [MeV]                          [MeV]
#-------------------------------------------------------------------------------------------------------------------------------

  24  46 Cr   1.15020   0.11901   0.00000   0.00000   1   1   1   1  0.00000  0.00000                 0            0.000
  24  47 Cr   1.13140   0.11924  -0.89872   0.24665  31   9   7   1  1.54100  0.00000  3.291E-02      0            0.000
  24  49 Cr   1.10760   0.11815   0.28855   0.35758 159  46   7  13  5.05800  2.61320  2.419E-02 *    0            2.899
  24  50 Cr   1.10170   0.11543   0.71883   0.34984 146  41   7   7  4.80100  3.32457  1.706E-02 *    0            2.711
  24  51 Cr   1.09890   0.11131  -0.51774   0.39928 270  93   7  13  4.45100  2.38540  5.770E-03 *    0            3.010
  24  52 Cr   1.09810   0.10624   1.11616   0.28719 272  27   7  12  4.83730  3.77172  1.467E-02 *    0            2.993
  24  53 Cr   1.09860   0.10091  -0.18601   0.31142 167  31  15   9  3.61651  2.32071  6.920E-03 *    0            2.856
  24  54 Cr   1.09950   0.09625   0.71942   0.28388 121  38   7   7  4.68052  3.15956  1.097E-02 *    0            2.475
  24  55 Cr   1.09960   0.09324  -0.68804   0.25704 105  33   7   5  3.35100  0.88071  1.789E-02 *    0            2.554
  24  56 Cr   1.09800   0.09261   0.91710   0.22630  36  18   7   3  4.01400  1.83160  8.940E-03 *    0            2.082
  24  57 Cr   1.09340   0.09437   0.00000   0.00000   1   1   1   1  0.00000  0.00000                 0            0.000
  24  58 Cr   1.08490   0.09767   0.00000   0.00000   1   1   1   1  0.00000  0.00000                 0            0.000
```

where:

Z: charge number

A: mass number

El: elemental symbol

T: temperature in the CT model

dT: uncertainty of T

U0: back-shift in CT model

dU0: uncertainty of U0

Nlev: number of levels in the ENSDF data set

Nmax: level up to which the level scheme is complete (from CT fit)

Nmin: first level considered in the fit

Nc: last level with unique spin assignment

Emax: energy corresponding to N_{max}

Ec: energy corresponding to Nc

Chi: measure of the fit quality (see ANNEX 3.A)

Fit: 'star' if the record comes from the global fit of pre-selected nuclei used to determine the $T(A)$ function

Flag: 'F' if Chi > 0.05, i.e., bad fit

NoX: number of levels with +X, +Y, +Z ... notation (X, Y, Z... are unknown energy values)

Xm: level at which the first +X, +Y, +Z ... notation appears

Ex: level energy at which the first +X, +Y, +Z ... notation appears

sigma: spin-cutoff parameter deduced from experimental spins (see ANNEX 3.B for details)

The corresponding FORTRAN format statement is:
(2i4,1x,a2,4(1x,f9.5),4i4,1x,f8.5,1x,f8.5,(1x,e10.3),1x,a1,a2,i4,i4,f7.3,1x,f6.3)

No constant-temperature fits have been carried out for nuclei with less then 20 known levels or more then 2 uncertain levels. In such cases, the Chi value is left blank and $U0 = 0, dU0 = 0, Nmax = 1, Nmin = 1, Emax = 0$.

3.2 Applied procedures

This section contains a detailed description of the procedure applied in the construction of the DLSL, and should possibly facilitate future updates of the library.

3.2.1 Construction of Discrete Level Scheme Library

Several FORTRAN codes have been developed and used in the preparation of the Discrete Level Scheme Library (see flowchart in ANNEX 3.F). The available data sets were collected from the individual ENSDF-II data files [3.8] and transferred into a single data file (my.enx) using a simple FORTRAN code ensdf2read.f90. The order of data sets in the single file has been determined by the order of file names in the input file (file.ENSDF).

FORTRAN code (discretels.f90) has been used to provide a simplified level scheme file for drawing and fitting, or to create a more complete intermediate file. The simplified level scheme file (levdens.dat) was used as an input for the global constant-temperature level-density fitting code (levglobal.f90), which is described in ANNEX 3.A. Output of the levglobal.f90 code is par30_20_-4_4.dat, which contains the results of global level density fitting. The numbers in the file name indicate nuclei that have been included in the global fit (actually those with a minimum of 30 levels and lying within -4 to +4 mass units around the stability valley). Number 20 indicates the number of nodes of the Cardinal spline used to describe temperature as a function of A ($T(A)$). The total number of nuclei included in the fit was 625. Several combinations of the above input parameters had been studied before the best combination was found. Program levglobal.f90 provides the graphic interface [3.11] to visualize the development of the $T(A)$ function during the iterative fitting procedure. In each iteration, the program changes N_{max} and the N_{min} level numbers for each nucleus independently, in such a way that the fit approaches that part of the level scheme that can be well described by a constant temperature formula. Ten iterations were generally enough to minimize the global χ^2 and determine the N_{max} and N_{min} values. Resulting N_{max} values have been identified as the cut-off point at which the level schemes can be considered complete. The final nuclear temperature function $T(A)$ is shown in Fig. 3.1. A comparison of this function with the temperatures obtained from the Gilbert-Cameron fits by the Bombay group is favorable [3.6], although there are differences at shell closures and in the transitional regions (see Ref. [3.7]).

Values of the corresponding shift parameters U_0 as a function of mass are shown in Fig. 3.2. It is important to note that for the first time reliable uncertainty estimates could be determined for the temperature and the shift parameter values.

The FORTRAN code cumcomp.f90 was used to visualize the results of global fitting.

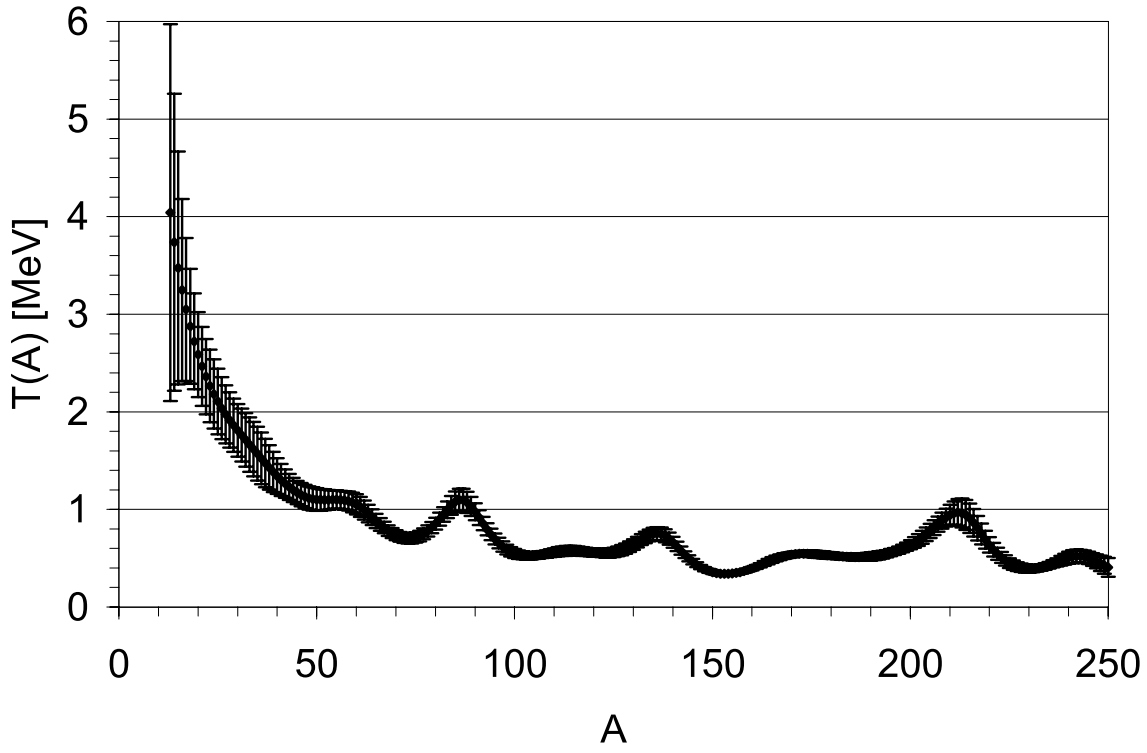

Figure 3.1: Nuclear temperature T as a function of the mass number A for nuclei near the valley of stability.

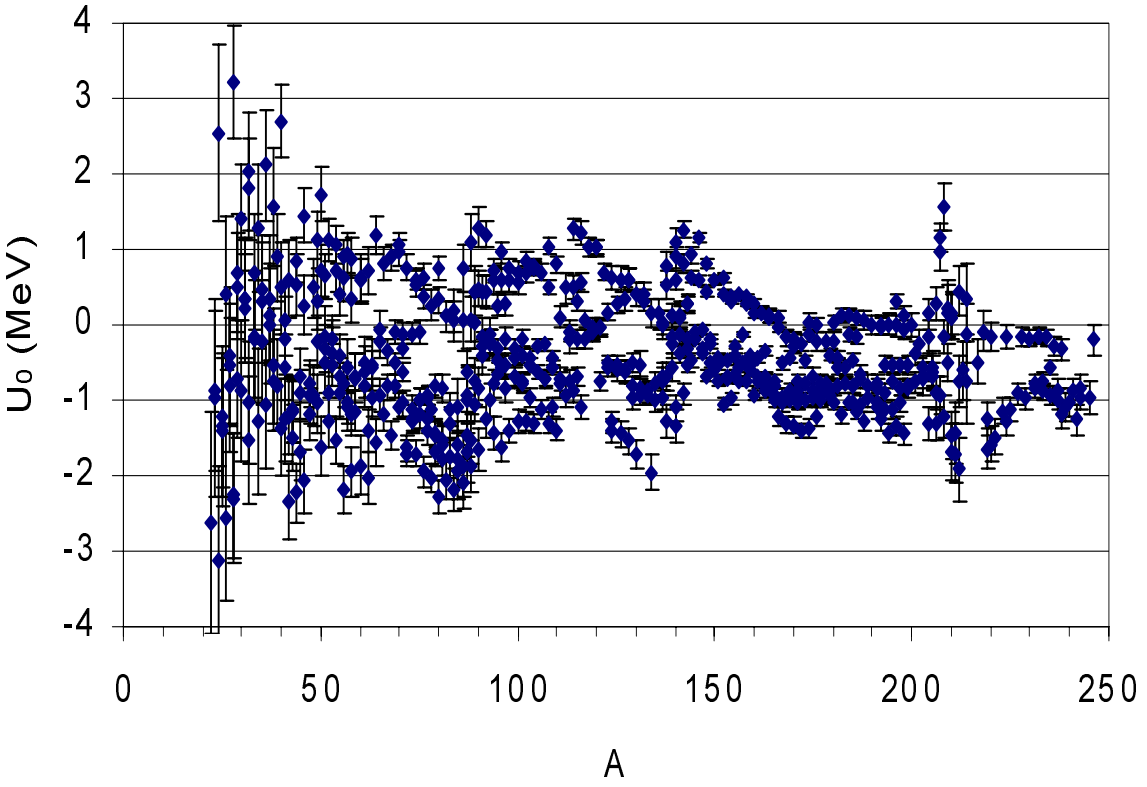

Figure 3.2: Shift parameter U_0 as a function of mass number A.

For each nucleus, the constant-temperature formula with fitted parameters was compared to the actual staircase plot of cumulative level numbers, providing a visual test of the fit quality.

In a subsequent run of the discretels.f90 code a complete intermediate file (dls.dat) was created using files my.enx and par30_20_-4_4.dat as input. This exercise constituted the actual retrieval of ENDSF data and included the decoding of all relevant information from the ENSDF data file. Fixed temperature fits were also performed for those nuclei that have more then 20 levels and no more than 2 with uncertain energies, but had not been not included in the global fit. The code assigned N_{max} to each nucleus, based on the agreement of the constant-temperature fit with the staircase diagram for this nucleus. Also unique spins and parities for levels up to N_{max} were assigned using the available data and algorithms described in ANNEX 3.B. In addition, the level-param.dat file containing the results of the constant temperature fits was created.

The last step in DLSL construction is the final formatting and testing. Calculations of the ICCs and transition probabilities were also performed during this step, using the code dtest.f90 to read the intermediate dls.dat file as input. Missing ICCs for the electromagnetic transitions were calculated by means of a FORTRAN subroutine developed from the ENSDF HISCC code and input files Icctbl.dat and Iccndx.dat (see ANNEX 3.C for details). The code dtest.f90 was used for calculating decay probabilities (formula are given in ANNEX 3.D) and for testing the internal consistency of the data stored in dls.dat file. The outputs of the code dtest.f90 are zxxx.dat files with nuclear decay schemes that constitute the Discrete Level Scheme Library and several additional files with the results of the tests.

3.2.2 Consistency tests

The following tests have been performed with the code dtest.f90.

- The difference between the initial and final level energies has been compared with the de-exciting γ-ray energy corrected for the nucleus recoil. Cases with energy differences larger then 5 keV are listed in Table 3.3. While small differences might well be within the quoted uncertainties, the larger values indicate internal inconsistencies in the ENSDF library. Therefore, these observations have been collected together and communicated to the ENSDF manager at the National Nuclear Data Center in Brookhaven National Laboratory. As a result, some of these problems have been corrected in the ENSDF data set.

- Sums of the decay probabilities have been tested by printing deviations of the sum from 100% if they exceeded 0.1%. There are cases in which the decay probabilities sum up to much less then 100%. Typically, they correspond to one known partial width and known total width for a level at which the evaluators were unable to distribute the difference among other possible decay modes such as neutron or alpha. On the other hand, when β delayed-neutron or proton decay occurs, the sum of decay probabilities given in ENSDF is substantially larger than 100%, because the percentage given for the heavy particle is a portion of the β-decay followed by the heavier particle (or particles) emission.

Table 3.3: Statistics of energy differences

No. Cases	Range $[keV]$
289	$5 \leq E < 10$
116	$10 \leq E < 20$
50	$20 \leq E < 50$
21	$50 \leq E < 100$
33	$100 \leq E$
Sum 509	

- Errors in the ICC calculation occurred when a γ decay of unknown energy occurs between two levels with energies E and E+X, where X is unknown.
- Multiple orders of γ-ray transitions have been checked yielding 19 cases with unusually high multipolarities. Some of them are actually real, while others result from deficiencies in the original ENSDF file or from the spin assignment of the present work since the unique spin selection (see ANNEX 3.B) makes use of only the final state spin. Cases in which a γ cascade between two states with known spins involves an intermediate state of unknown spin were not considered. Fortunately, there are not too many such cases and they can be treated individually (see Table 3.4). Also note that the 1998 version of the ENSDF-II does not contain the corresponding spin limitation.

Table 3.4: Cases of very large multipole order

Symbol	$E_i\,[keV]$	J_i	J_f	Comment
^{58}Mn	728.060	1.0	6.0	Spin selection should be improved
^{53}Fe	3040.400	-9.5	-4.5	Known M5 transition from isomer level
^{53}Fe	3040.400	-9.5	-3.5	Known E6 transition from isomer level
^{67}Zn	2434.930	-5.5	-0.5	M5 non-isomer (transition rate must be too high)
^{90}Y	682.030	7.0	-2.0	Known E5 transition from isomer level
^{113}Cd	263.590	-5.5	0.5	Known E5 transition from isomer level
^{117}Sn	314.580	-5.5	0.5	Known E5 transition from isomer level
^{123}Te	247.550	-5.5	0.5	Known E5 transition from isomer level
^{125}Te	144.795	-5.5	0.5	Known E5 transition from isomer level
^{133}Ba	288.247	-5.5	0.5	Known E5 transition from isomer level
^{184}Re	188.010	8.0	-3.0	Known E5 transition from isomer level
^{192}Ir	155.160	9.0	4.0	Known E5 transition from isomer level[1]
^{206}Tl	2643.110	-12.0	6.0	Exists in ENSDF; no multipolarity stated
^{207}Tl	1348.100	-5.5	0.5	Known E5 transition from isomer level
^{202}Pb	2169.830	-9.0	4.0	Known E5 transition from isomer level
^{202}Pb	2169.830	-9.0	4.0	Known E5 transition from isomer level
^{204}Pb	2185.790	-9.0	4.0	Known E5 transition from isomer level
^{211}Po	1462.000	12.5	-3.5	Spin selection should be improved[2]

[1]Level energy has changed in the recent evaluation.
[2]Final spin is given in a recent evaluation as $17/2^+$ to give an E4 isomeric transition.

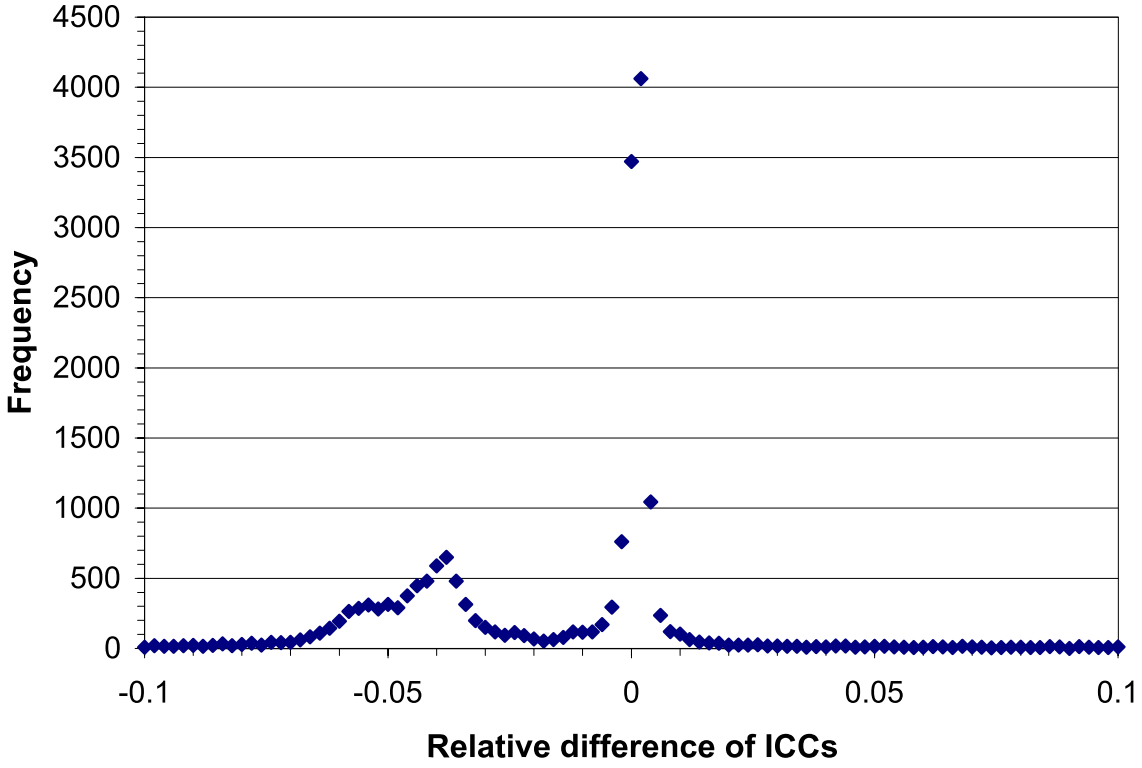

Figure 3.3: Distribution of relative differences between calculated ICCs, and ICCs from ENSDF.

- A total of 21595 calculated ICC values were compared with those given in the ENSDF file. The distribution of relative differences $((ICC_{cal} - ICC_{exp})/ICC_{exp})$ is shown in Fig. 3.3. Out of 21595 relative differences, about half (10493) are within 1% and approximate to a normal distribution resulting partly from rounding errors. About 6000 relative differences form a double peak structure; the reason for these differences was far from trivial. When analyzing absolute and relative differences, part of this structure arose from rounding effects and there were other unclear reasons for the small ICC values. To make the above statements clear, Fig. 3.4 presents the absolute value of small differences of ICCs as a function of the calculated ICC values. By scanning the horizontal axis one can see similar patterns as in fractals. The origin of the grouping can be traced back to rounding or perhaps to the differences in the ICC theory and/or measured values. The remaining 5000 values show very large differences due to various reasons. For example, an arbitrary rule is used to calculate ICCs in the case of unknown mixing ratios: the present ICC values for M1+E2 mixed transitions were calculated assuming pure E2 in even-even nuclei and pure M1 otherwise, while in ENSDF the ICC values were calculated assuming 50% mixing. In summary, the applied subroutine can be concluded to provide satisfactory ICC values for the current purpose, although the origin of the differences between the present calculations and ENSDF values should be investigated further.

- Electromagnetic transition rates have been successfully tested - all of the calculated rates satisfy the Recommended Upper Limit (RUL) [3.12].

- Formal correctness of the zxxx.dat files has been tested with the code zread.f90 and

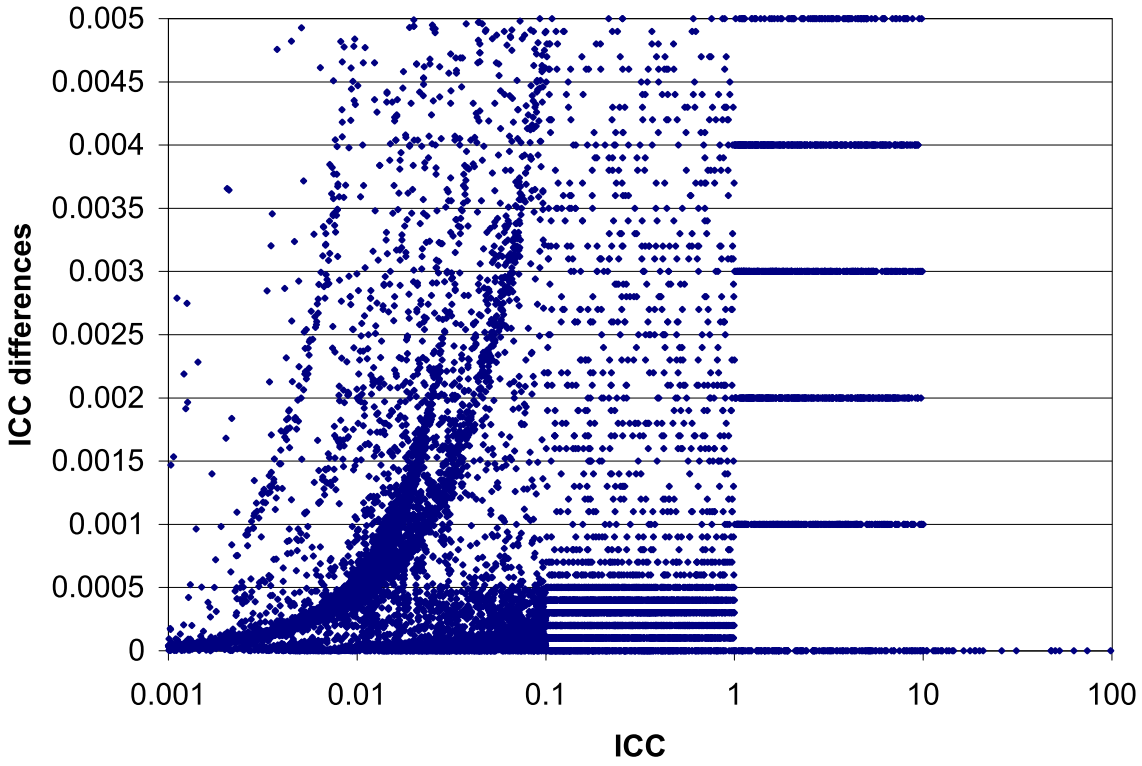

Figure 3.4: Absolute differences between calculated and ENSDF ICC values as a function of ICC.

no formatting problems have been encountered. The zread.f90 code includes the getza subroutine which can also be used to retrieve level schemes from the library.

- A new method to extract nuclear temperature T has been developed (see ANNEX 3.E). The temperatures provided by this procedure have been compared to the $T(A)$ function obtained in the global fit (see Fig. 3.5). Most of the T values obtained with the method described in ANNEX 3.E are close to the $T(A)$ curve. Only a small percentage of cases are discrepant due to bad fits and/or low number of available levels.

3.2.3 Physical validation of the files

The Discrete Level Scheme Library was tested in reaction calculations using three statistical model codes (EMPIRE, TALYS and UNF). These tests helped to disclose and correct some deficiencies (such as negative internal conversion coefficients and zero branching ratios assigned to a single transition depopulating a level) that had escaped previous checks.

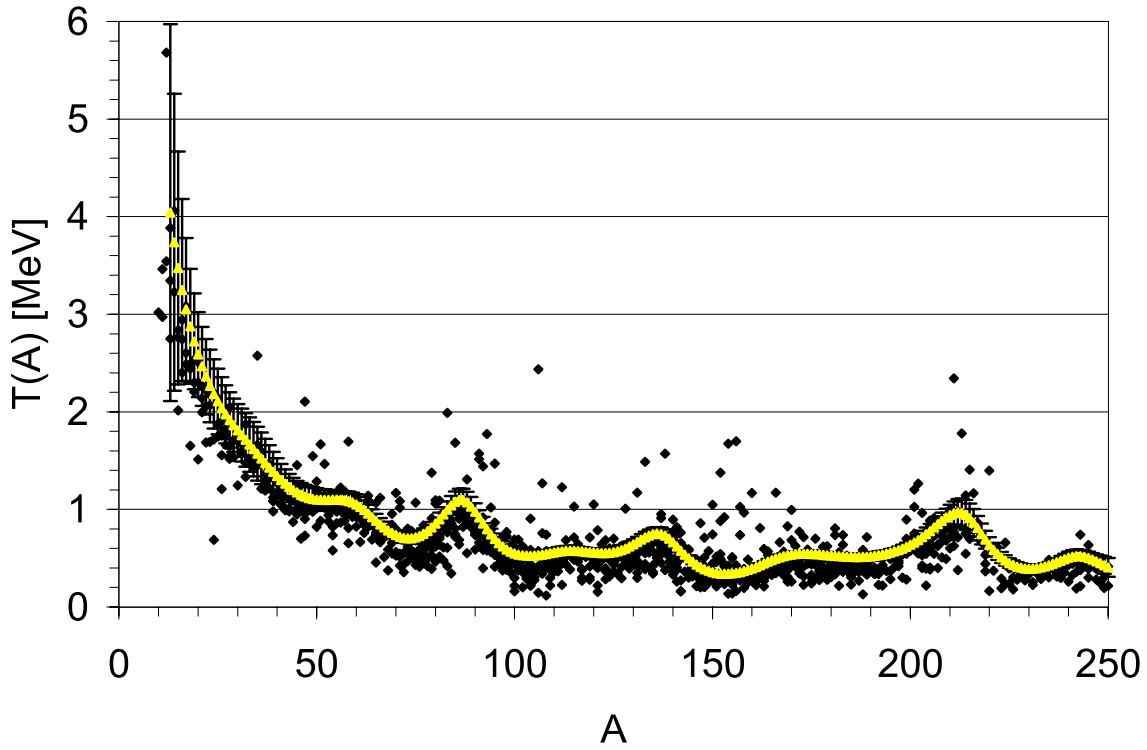

Figure 3.5: Comparison of temperature values obtained from two independent methods. Points with no uncertainty bars are obtained using the method described in ANNEX 3.E, while points with error bars originate from the global fit procedure (see Fig. 3.1).

REFERENCES

[3.1] MOLNÁR, G., BELGYA, T., FAZEKAS, B., "Complete Spectroscopy of Discrete Nuclear Level", Proc. First Research Co-ordination Meeting on Development of Reference Input Parameter Library for Nuclear Model Calculations of Nuclear Data, Cervia (Ravenna), Italy, September 1994, INDC(NDS)-335, IAEA, Vienna (1995) 97.

[3.2] Evaluated Nuclear Structure Data File (ENSDF) - produced by members of the International Nuclear Structure and Decay Data Network, and maintained by the National Nuclear Data Center, BNL, USA. Also available online from IAEA Nuclear Data Section, Vienna.

[3.3] Proc. First Research Co-ordination Meeting on Development of Reference Input Parameter Library for Nuclear Model Calculations of Nuclear Data, Cervia (Ravenna), Italy, September 1994, INDC(NDS)-312, IAEA, Vienna (1994).

[3.4] Proc. Second Research Co-ordination Meeting on Development of Reference Input Parameter Library for Nuclear Model Calculations of Nuclear Data, IAEA, Vienna, November 1995, INDC(NDS)-350, IAEA, Vienna (1996).

[3.5] INTERNATIONAL ATOMIC ENERGY AGENCY, Handbook for Calculations of Nuclear Reaction Data - Reference Input Parameter Library, Final Report of a Co-ordinated Research Project, IAEA-TECDOC-1034, Vienna (1998) 11-24.

[3.6] Proc. First Research Co-ordination Meeting on Nuclear Model Parameter Testing for Nuclear Data Evaluation (Reference Input Parameter Library: Phase II),

IAEA, Vienna, November 1998, INDC(NDS)-389, IAEA, Vienna (1998).

[3.7] Proc. Second Research Co-ordination Meeting on Nuclear Model Parameter Testing for Nuclear Data Evaluation (Reference Input Parameter Library: Phase II), Varenna, Italy, June 2000, INDC(NDS)-416, IAEA, Vienna (2000).

[3.8] Table of Isotopes CD-ROM, Eighth Edition: 1998 Update, FIRESTONE, R.B., SHIRLEY, V.S., CHU, S.Y.F., BAGLIN, C.M., ZIPKIN, J., Eds., Lawrence Berkeley National Laboratory, University of California, Wiley-Interscience (1998).

[3.9] BELGYA, T., MOLNÁR, G.L., FAZEKAS, B., ÖSTÖR, J., Histogram Plots and Cutoff Energies for Nuclear Discrete Levels, INDC(NDS)-367, IAEA, Vienna (1997).

[3.10] EWBANK, W.B., modified by EWBANK, W.B., BELL, J., ORNL-NDP HSICC program for ENSDF data sets (1976).

[3.11] PGPLOT FORTRAN Graphics Subroutine Library was used, as obtained with FTP from the California Institute of Technology.

[3.12] ENDT, P.M., Strengths of Gamma-ray Transitions in A = 91-150 Nuclei, At. Data Nucl. Data Tables **26** (1981) 47.

ANNEX 3.A

PROCEDURE FOR CONSTANT TEMPERATURE FITTING OF CUMULATIVE NUMBER OF LEVELS

The nuclear temperature is a smooth function of mass number A [A3.1, A3.2]. This observation supports the possibility of simultaneously fitting the temperature T as a function of mass number for a large number of nuclei. Furthermore, the work of the CRP has demonstrated that nuclei around the valley of stability can be fitted in this way. A natural requirement is that there must be a certain minimum number (N_0) of known levels in each nucleus.

The nuclei suitable for fitting were selected and the following method has been applied. First, the fit which was used in the RIPL-1 project [A3.1] has been repeated for a set of selected nuclei. This approach provided initial values for N_{max}, while the initial minimum numbers of levels (N_{min}) were set to 14 for odd-odd, and to 7 for other nuclei. A temperature function $T(A)$ has been subsequently fitted to the cummulative number of levels for all these nuclei and was represented by a Cardinal spline. The formulas used in the fitting procedure are listed below.

Let $N(E_{mi})$ denote the cumulative number of levels at level i in the m_{th} nucleus and $Y_{im} = ln(N(E_{im}))$ denote the associated natural logarithm. The constant temperature formula can be written as

$$N(E) = exp\left(\frac{E - U_0}{T}\right), \tag{3.1}$$

and the natural logarithm is

$$ln(N(E)) = \frac{E - U_0}{T} = aE + b \tag{3.2}$$

with

$$T = \frac{1}{a} \quad \text{and} \quad U_0 = -\frac{b}{a} \tag{3.3}$$

The dependence of $a(A)$ as a function of mass number A can be expressed using the following linear equation

$$a(A) = A\sum_{k=1}^{20} \beta_k C_k(A) \tag{3.4}$$

In Eq. 3.4, $C_k(A)$ is the k^{th} Cardinal spline [A3.3]. Multiplying the spline with the mass number A transforms the approximate linear dependence of $a(A)$ into dependence on A. We are now ready to set up the least square function for the problem:

$$\chi^2 = \sum_{i,m} \frac{(Y_{i,m} - a(A_m)E_{i,m} - b_m)^2}{E_{i,m}} \tag{3.5}$$

The index i runs from N_{min} to N_{max} in each nucleus. N_{min} and N_{max} are independent for each nucleus and were changed during this fitting process in such a way that the fit approached the linear part of Y_{im}. Limits were applied for the N_{min} and N_{max} values. If $N_{max} - N_{min} > 15$, the new N_{max} and N_{min} values have been set. For non even-even nuclei, the N_{min} values were limited to the 7-20 region.

Energy weighting ($E_{i,m}$) has been chosen to decrease the weight of the potentially poorly-known high energy levels. By solving Eq. 3.5, a universal $T(A)$ function for all nuclei and U_0 values for individual nuclei have been obtained. 10 iterations were sufficient to achieve convergence. Since the χ^2 values provided by the procedure were unconventional, the final χ^2 values have been calculated for each individual nucleus using the corresponding partial sum in Eq. 3.5, normalized to the difference between N_{max} and N_{min}.

ANNEX 3.B

DETERMINATION OF UNIQUE SPINS

When determining the unique spin for a level, a check was made as to whether a range of spin values could be assigned with the help of γ transitions to final levels of known spin. Otherwise, if there were more than 10 levels with known spins (not necessarily unique), a continuous spin distribution was determined from the existing spin assignments up to E_{max}, and all missing spins up to E_{max} were randomly extracted from the resulting spin distribution. If there were less than 10 known spins, a reliable spin distribution could not be estimated and no spins were inferred.

For the continuous spin distribution, the usual formula has been used [A3.4, A3.5]

$$\rho(J) = \frac{(2J+1)exp\left(-(J+1/2)^2/(2\sigma^2)\right)}{2\sqrt{2\pi}\sigma^3}, \tag{3.6}$$

where J is the spin and σ is the spin cut-off parameter. The normalization factor N can be obtained by integration

$$N = \int_0^{+\infty} \rho(J)dJ = \frac{\sqrt{2}exp\left(-1/(8\sigma^2)\right)}{2\sqrt{\pi}\sigma}. \tag{3.7}$$

The normalized spin distribution is

$$\rho_N(J) = \frac{\rho(J)}{N} = \frac{2J+1}{2\sigma^2}exp\left(-\frac{(J+1/2)^2}{(2\sigma^2)} - \frac{1}{8\sigma^2}\right). \tag{3.8}$$

The spin cut-off parameter was obtained from the following formula

$$\int_0^{+\infty} (J+1/2)^2\rho_N(J)dJ = 2\sigma^2 + 1/4. \tag{3.9}$$

The experimental spin cut-off was calculated with the discrete representation of Eq. 3.9.

$$\sigma^2_{exp} = \frac{\sum_{i=1}^{N_{max}} \sum_{k=1}^{N_i} (J_{i,k}+1/2)^2/N_i}{2N} - \frac{1}{8}, \tag{3.10}$$

where N_i is the number of known possible spins (e.g., for $1/2, 3/2, 5/2; N_i = 3$) given for the i^{th} level and $k = 1, 2, ...N_i$. N is the number of levels for which $N_i > 0$, while the level index i extends to the cut-off number N_{max}.

The continuous normalized spin distribution with the experimental spin cut-off parameter has been used to determine unique spin values for levels up to energy E_{max} using a Monte Carlo procedure. Five cases can be distinguished:

1. $N_i = 0$. When there was no experimental information on the spin, J has been chosen randomly with a probability modeled by the spin distribution. In such cases, the type of selection 's' has been coded as 'n'.

2. $N_i = 1$. Despite uncertainties (such as $(1)^+$), the spin has been considered to be "unique" and selection type 's' has been coded as 'u'. We note that N_c is not consistent with the 'u' sign and is meant to give the highest level number with unique (i.e., single and unequivocal) experimental spin and parity values.

3. $N_i > 1$. The spin has been chosen using the probabilities obtained from the spin distribution, but constrained to spin values of a given set (e.g., $(1, 3, 4)^-$). The sum of these probabilities was normalized to 1 before a spin was chosen in a Monte Carlo procedure using the normalized weights. In such cases, the type of selection 's' has been coded as 'c'.

4. If a set of possible spins was inferred from the spins of final states after γ transitions, 's' has been coded as 'g'. Method 2 or 3 was then used for selection depending on the number of possible spins.

5. Above E_{max} or if unique spins could not be determined due to the lack of experimental spin distribution, the 's' field has been coded as 'blank'. If there were levels with unique experimental spin above E_{max}, the corresponding 's' fields have been coded as 'u'. The possible spin values are: 0.0, 0.5, 1.0 ... and -1.0 for an unknown spin.

ANNEX 3.C

DETERMINATION OF MISSING INTERNAL CONVERSION COEFFICIENTS

The National Nuclear Data Center provides the HSICC Program Package for calculating Internal Conversion Coefficients (ICC). One component (hsicc.for) calculates internal conversion coefficients by cubic spline interpolation of the values tabulated by Hager and Seltzer for the K, L, and M shells and by Dragoun, Plajner, and Schmetzler for the N + O + ... shells. However, this program was designed as a stand-alone code and involves a large number of instructions for handling ENSDF input files. Therefore, the code was transformed into a subroutine that uses the original Iccndx.dat and Icctbl.dat files containing tabulated ICC values as input. The spline interpolation has been replaced with Cardinal cubic splines [A3.3], which are suitable for interpolation because they guarantee mutual orthogonality of the splines at node points. Let $S(x)$ be a linear combination of Cardinal splines

$$S(x) = \sum_{k=1}^{n} \beta_k C_k(x). \tag{3.11}$$

$C_k(x)$ Cardinal splines satisfy the following orthogonal relations

$$C_k(x_j) = \delta_{k,j}. \tag{3.12}$$

Due to the orthogonality of the Cardinal splines, the value of $S(x)$ at the node point x_j is β_j.

The binary index file Iccndx.dat contains the record number corresponding to a certain charge in the table Icctlb.dat. Icctlb.dat contains ICC values as a function of transition energy for four electric and four magnetic multipolarities. The natural logarithm of the tabulated ICC values in Icctlb.dat multiplied by some power of the γ-ray energies (in the same way as in hsicc.for) have been interpolated as a function of the natural logarithm of transition energies at node points. The interpolation for a given Z is done only once by using multiple-spline or hyper-spline interpolation for all sub-shells and multipoles. Let us denote the sub-shells by l and the multipoles by m. Since the Cardinal splines are completely defined by their node points, for different multipoles only the $\beta_{k,l,m}$ values of the multiple-spline $S_{l,m}(x)$ vary. Accordingly, the ICC calculations were very fast to perform.

ANNEX 3.D

CALCULATION OF DECAY PROBABILITIES

Calculations of total decay probabilities were based on the following rules: (i) if no decay mode was given for a level, but there were de-exciting γ transitions, 100% electromagnetic decay was assigned to the level (%IT=100%); (ii) if other decay modes beside the electromagnetic were given, the percentage of electromagnetic decay mode was obtained from the decay mode information. This procedure was identified by the notation %IT or %G in the decay record in the ENSDF files. First, the total relative electromagnetic decay probability was calculated

$$P_{tot\_rel} = \sum_{k=1}^{No_\gamma} I_k(1+\alpha_k), \tag{3.13}$$

where I_k is the relative γ intensity and α_k is the ICC. The absolute electromagnetic decay probability of the k^{th} branch is

$$P_{electromagnetic,k} = \frac{I_k(1+\alpha_k)}{P_{tot\_rel}} \cdot 0.01 \cdot \%IT(\%G), \tag{3.14}$$

while the absolute γ-decay probability is

$$P_{\gamma,k} = \frac{I_k}{P_{tot\_rel}} \cdot 0.01 \cdot \%IT(\%G). \tag{3.15}$$

Other decay probabilities (particle) are given in the information on decay modes for a level.

ANNEX 3.E

SIMPLE METHOD FOR DETERMINATION OF APPROXIMATE NUCLEAR TEMPERATURE

A simple method of determining approximate nuclear temperature was developed and applied to DLSL. Assuming that the constant temperature model describes level densities at low energies with some confidence, a useful expression was derived to determine the temperature T. If one calculates the average level energy in continuous approximation with the constant-temperature level density, the following expression is obtained:

$$E_{average}(E_{max}) = \frac{\frac{1}{T}\int_{-\infty}^{E_{max}} E exp\Big(\frac{E-U_0}{T}\Big)dE}{exp\Big(\frac{E_{max}-U_0}{T}\Big)} = E_{max} - T, \tag{3.16}$$

which is replaced by the following sum in discrete representation:

$$E_{average}(E_{max}) = \frac{\sum_{i=1}^{N_{max}} E_i}{N_{max}} \approx E_{max} - T \tag{3.17}$$

T can easily be obtained from Eq 3.17. This equation can be used to calculate the nuclear temperature by using the E_{max} obtained from the least-square fits (as compared with the $T(A)$ function of Fig. 3.5). This new method is independent of the global fitting method because any functional dependence of the temperature on the mass number is not assumed, although the usage of E_{max} may introduce some correlation between the two methods.

ANNEX 3.F

FLOWCHART OF DLSL CONSTRUCTION

Sequence of codes together with respective input and output files are listed below, as used in the preparation of the Discrete Leval Scheme Library.

- **ensdf2read.f90**

  input: *file.ENSDF* (list of 2637 nuclei to be retrieved form ENSDF II)

  output: *my.enx* (data for the 2637 nuclei retrieved from ENSDF II)

- **discretels.f90**

  input (in step 1): *my.enx* (output of ensdf2read.f90)

  output (in step 1): *levdens.dat* (first run contains only levels to be used for fitting and plotting)

- **levglobal.f90**

  inputs: *levdens.dat* (output of discretels.f90), and *stable1.txt* (list of isotopes located in the valley of stability).

  output: *par30_20_-4_4.dat* (results of the constant temperature fit (T and U_0) for 625 nuclei)

- **cumcomp.f90**

  inputs: *levdens.dat* (output of discretels.f90) and *par30_20_-4_4.dat* (output of levglobal.f90)

  output: plots of cumulative number of levels for visual check of fits

- **discretels.f90**

  inputs (in step 2): *my.enx* (output of ensdf2read.f90) and *par30_20_-4_4.dat* (output of levglobal.f90)

  outputs (in step 2): *dls.dat* (intermediate file containing level schemes of nuclei) and *level-param.dat* (results of the constant temprature fit for all nuclei that have enough levels but were not considered in the global fit with levglobal.f90)

- **dtest.f90**

  inputs: dls.dat, parall.dat, Icctbl.dat and Iccndx.dat

  outputs: *zxxx.dat* (discrete level files), *decay_list.txt, Decayprob_error.txt, Energydiff_error.txt, Multipol_errot.txt* (diagnostic files)

REFERENCES TO ANNEXES

[A3.1] BELGYA, T., MOLNÁR, G., FAZEKAS, B., ÖSTÖR, J., Histogram plots and cutoff energies for nuclear discrete levels, INDC(NDS)-367, IAEA, Vienna (1997).

[A3.2] INTERNATIONAL ATOMIC ENERGY AGENCY, Handbook for Calculations of Nuclear Reaction Data - Reference Input Parameter Library, IAEA-TECDOC-1034 (1998).

[A3.3] WINTERBON, K.B., Nucl. Phys. **A246** (1975) 293.

[A3.4] ERICSON, T., Adv. Phys. **9** (1960) 425.

[A3.5] GILBERT, A., CAMERON, A.G.W., Can J. Phys. **43** (1965) 1446.

4 AVERAGE NEUTRON RESONANCE PARAMETERS

Coordinator: A. Ignatyuk

Summary

Average resonance parameters included in the recommended RIPL-1 file were tested and revised during RIPL-2. The differences between the recommended and alternative files were analyzed on the basis of the last compilation of the resolved resonance parameters. Recommended data were corrected for some nuclei, and the number of nuclei has been extended to 297. Along with the data for the s-wave neutron resonances, the evaluations of the average parameters for the p-wave resonances have been added to the RIPL-2 library. The file formats are explained in the corresponding readme file.

Parameters required for statistical model calculations are neutron strength functions, average radiative widths and the average spacing of resonances. These parameters are generally obtained from the analysis of parameter sets for the resolved resonances. Experimental resolution and sensitivity limits create incomplete (missing resonances) or distorted (errors in width determination) information on the resonance parameters. Therefore, the average widths and resonance spacings cannot be directly deduced from available resonance sequences, and should always be estimated while taking into account missing resonances. Various methods for statistical analysis of missing resonances have been developed, and most of them were applied to evaluate average resonance parameters during the RIPL project. Advantages and shortcomings of such methods are briefly discussed below in order to obtain some objective estimation of the accuracy of the recommended parameters. Before describing the statistical methods for resonance analysis, one should be aware that statistical methods of resonance analysis work only when applied to pure resonance samples - results become less and less accurate with sample deficiencies.

Sample cases of pure resonances are rare. Such difficulties are overcome by adopting different statistical analysis methods as well as sampling criteria to identify a reduced sample in which missing resonances and/or distortions are reduced. Thus, determinig average resonance parameters is an iterative procedure in which one tries to reach convergence of results from different methods of analysis. The spread of values from different statistical procedures indicates that the uncertainties are affecting the results. However, in many cases such an iterative procedure is not sufficient to guarantee the correctness of the parameters. Whenever possible, they should be validated by use of supplementary information such as capture cross sections and radiative widths.

4.1 Evaluation methods

The neutron strength functions for a given orbital angular momentum l are defined by the relationship

$$S_l = \frac{< g\Gamma_n^l >}{(2l+1)D_l} = \frac{1}{(2l+1)\Delta E}\sum_r g_r \Gamma_{nr}^l, \tag{4.1}$$

where the summation is performed over N resonances in the energy interval ΔE; $g_r = (2J_r + 1)/2(2I_0 + 1)$ is the statistical weight factor that depends on the angular momentum J_r of a resonance and the spin I_0 of the target nucleus; Γ_{nr}^l are the reduced neutron widths of resonances, and D_l is the average resonance spacing defined as

$$D_l = \Delta E/(N-1). \tag{4.2}$$

The reliable identification of s- and p-wave resonances is most important for an accurate evaluation of the average parameters. If such an identification can be made, the neutron strength functions can be simply evaluated from the linear approximation of the cumulative sum of the products $g_r\Gamma_{nr}^l$. Departure from linearity may indicate missing resonances. The relative error of the evaluation can be defined from the equation

$$\frac{\delta S_l}{S_l} = \sqrt{2/N}, \tag{4.3}$$

which is based on an asymptotic estimate for the variance of the sum of neutron widths distributed in accordance with the Porter-Thomas law [4.1].

Dominant contributions to the sum in Eq. (4.1) for s-neutrons are given by resonances with large neutron widths; missing weak resonances or admixture of p-wave resonances have a rather small effect on the evaluation of the strength functions. The situation is not so favorable for p-neutrons, for which the strength function can be strongly distorted by any admixture of incorrectly identified s-wave resonances. This is the main reason that the relative accuracies of p-wave strength functions for many nuclei are much lower than for the s-waves.

For a rather full set of resonances the relative statistical error of the resonance spacing can be determined by the relationship

$$\frac{\delta D_l}{D_l} = \frac{0.45\sqrt{\ln N + 2.18}}{N} \approx \frac{1}{N}, \tag{4.4}$$

which was obtained by Dayson and Mehta for the Gaussian orthogonal ensemble [4.2]. Obviously, missing resonances in the analyzed set result in an error that essentially exceeds the statistical error. Thus, an estimation of the missing resonances is crucial for an accurate evaluation of the average resonance spacings.

Three approaches were developed to account statistically for the missing or erroneously identified resonances: (i) methods that exploit the statistics of level spacings, (ii) methods based on the fit of the reduced neutron width distribution by the Porter-Thomas law, (iii) methods that use combined simulation of the level and width statistics. Both the advantages and weaknesses of these various methods have been broadly discussed in Refs. [4.3–4.8]. Some new developments related to the third type of method were proposed recently [4.9–4.12].

The simplest method of resonance analysis is the staircase plot of the cumulative number $N(E)$ of resonances as a function of energy. It is usually assumed that at low energies there are no missing resonances, and a linear approximation of this part of the plot gives a direct estimation of D_l. A variation of this method is the approach based on Δ_3 statistics given by Dayson and Mehta [4.2]. The best fit of $N(E)$ is determined through a least-squares study of the parameter

$$\Delta = \min\left[\frac{1}{\Delta E}\int_0^{\Delta E}[N(E) - AE - B]^2 \mathrm{d}E\right]. \tag{4.5}$$

For a complete set of levels, the value and the variance of this parameter are defined by the relationships:

$$\Delta_3 =< \Delta >= \frac{1}{\pi^2}(\ln N - 0.0687), \qquad \sigma = \frac{1}{\pi^2}\sqrt{\frac{4\pi^2}{45} + \frac{7}{24}} = 0.11. \tag{4.6}$$

Obviously, absence of levels or presence of spurious levels from another sequences increases Δ_3. Therefore, if the fitted value of Δ satisfies the condition $\Delta_3 - \sigma < \Delta < \Delta_3 + \sigma$, the analyzed set of resonances may be considered as a pure and complete set. Unfortunately, Δ_3 statistics provide no means of correcting an inadequate set of resonance parameters. Besides, one finds in practice that the Δ_3 test criteria are often satisfied for samples that are known to be neither pure nor complete [4.6, 4.8].

In contrast to the spacing distribution, the neutron width distribution is only slightly affected by missing or spurious weak resonances. The upper part of the Porter-Thomas distribution, corresponding to strong resonances, can be regarded as virtually unperturbed. A number of resonances that have the reduced neutron width above a given value are described by the function

$$N(\Gamma) = N_0 \int_{\Gamma/\overline{\Gamma}}^{\infty} \frac{\exp(-x/2)\mathrm{d}x}{\sqrt{2\pi x}} = N_0\left[1 - \mathrm{erf}\sqrt{\Gamma/2\overline{\Gamma}}\right]. \tag{4.7}$$

Thus, by fitting the corresponding distribution of neutron widths with a maximum likelihood approach, we can find both the average reduced neutron width and total number of resonances N_0 at the considered energy interval. Various versions of this method were developed to take into account energy variations of the measurement threshold and other experimental conditions [4.8, 4.9].

The third class of methods attempts to account simultaneously for limitations imposed on estimations of a mean width and resonance spacing by the Wigner and Porter-Thomas laws. Simulations of the neutron cross section by the Monte-Carlo methods that include experimental resolution and other conditions are applied in most cases. Some analytical treatments that could replace the Monte-Carlo simulation for some calculations were discussed in Ref. [4.9].

The conclusion that can be formulated on the basis of the resonance parameter analyses performed by different groups is that none of the methods guarantees an unambiguous identification of missed or spurious resonances. Critical analyses of the experimental conditions and approaches used to obtain individual resonance parameters are very important in many cases. Priority in average parameter evaluations should be given to the quality of the selected resonance set rather than to the total number of resonances considered

[4.9, 4.13]. Only for a rather small number of nuclei is the accuracy of the evaluated resonance spacings better than 10%. The best examples of such nuclei are U-235 and U-238 for which the relative errors of the recommended D_0 are better than 2%, and Pu-239, Pu-240 and Pu-242 for which such errors are about 5% [4.9, 4.11].

4.2 Files of average neutron resonance parameters

Complete tables of average resonance parameters provided by Beijing, Bologna and Obninsk groups were collected during the course of the RIPL-1 project. All these parameters are mainly based on the analysis of the resolved resonance parameters presented in the well-known BNL compilation [4.14, 4.15]. Despite the common base, many discrepancies were found between the average parameter estimations. These discrepancies were rather large when compared to the parameter uncertainties, especially for cases with less than 20 resonances.

After consideration of the existing discrepancies, the Beijing and Obninsk groups reanalyzed some of their previous evaluations, and prepared updated versions of the average resonance parameters. Agreement between the updated parameters has been significantly improved for most of the nuclei, although the uncertainties quoted for the Obninsk evaluations were systematically higher than the uncertainties given in the original BNL evaluations [4.14, 4.15] and the revised Beijing data. This difference was shown to be mainly concerned with the reduction of the energy interval that the Obninsk group used to improve the quality of the analyzed sets of resonances in accord with the statistical methods described above. Taking into account substantial differences between the uncertainties obtained by the various methods, those of the Obninsk group seem more reliable than others. Accordingly, the Obninsk evaluation of the average resonance parameters was included in RIPL-1 as the recommended file, and the Beijing evaluation as the alternative [4.16]. The Minsk evaluation of the average resonance parameters for the actinides was also included as an alternative file, and the additional compilations of the average resonance spacings (*mengoni_gc.dat* and *iljinov_gc.dat* files) were included in Segment 5 of the RIPL-1 Starter File [4.16], because of their relevance to nuclear level densities.

The recommended data sets have been extended under the RIPL-2 project to include the average parameters for p-wave neutron resonances along with the s-wave resonance parameters considered previously. Although the accuracy of the data for p-wave resonances is certainly not as good as for s-wave resonances, such improved data are important in the optical and statistical models. Another task of the RIPL-2 project was to test and revise the previously recommended parameters.

A reliable separation of p-wave resonances from the background of stronger s-wave resonances plays a crucial role in estimating the average resonance parameters. Thus, trustworthy results for the p-wave resonance parameters can only be obtained under the simultaneous analysis of the resolved resonance data for both s- and p-wave neutrons. Such an analysis for nuclei included in the RIPL-1 list of recommended parameters was performed by the Obninsk group [4.17], and the corresponding resonance spacings D_1, the neutron strength functions S_1, and the average radiative widths of p-wave resonances were added to the RIPL-2 database.

Another problem is to produce a complete list of recommended parameters. In the original BNL compilation [4.14, 4.15], the average resonance parameters were obtained for about 230 nuclei; Iljinov et al. [4.18] compiled the resonance spacings for 284 nuclei; the Beijing compilation reports data for 344 nuclei [4.19]; however, the recommended RIPL-1 file is limited to only 281 nuclei. A careful review of the Beijing compilation shows that 35 out of 344 nuclei contain no data quantifying the neutron strength functions and a number of resonances are set to zero. This observation indicates that the resonance spacings for these nuclei were not obtained from the analysis of experimental data, but rather from the systematics of neighboring nuclei. Such systematics could be useful for many applications, but the results should not be mixed with the direct experimental data, and therefore have been removed from the RIPL-2 database. All issues related to the resonance spacing systematics that are connected with nuclear level densities are considered in Chapter 6.

Some skepticism can arise with respect to the recommended parameters of nuclei for which data are available for a rather small number of resonances, particularly for about 45 nuclei in RIPL-1 in which the number of resonances are equal or less than five. Any statistical analysis of such data is doubtful. Nevertheless, we decided to include such cases in the recommended file to provide an estimate that is certainly better than nothing. So all nuclei available in the alternative files of RIPL-1 but not in the recommended file were re-analyzed on the basis of the last compilation of the resolved resonance parameters [4.20]. As a result, 16 nuclei were added to the list of average resonance parameters included in the RIPL-2 file. This file was tested by the Brussels group in their microscopic calculations of nuclear level densities, and some misprints were corrected in the final version of the RIPL-2 file.

Independent analyses of the resonance parameters for about 20 nuclei have been performed by the BNL group [4.21]. They re-evaluated the resonance spacings, the neutron strength functions and the radiative widths for the most important fission products. In most cases, the new BNL results overlap with the RIPL-1 recommended parameters within the bounds of the accepted uncertainties.

The s-wave resonance spacings included in RIPL-2 are shown in Fig. 4.1, along with the Beijing evaluation [4.16] and BNL data. Uncertainties for most of the data do not exceed the sizes of the symbols, showing that the results of all the evaluations agree rather well for nuclei with more than 30 known resonances. For other nuclei, the data included in the RIPL-2 file seem preferable for two reasons: (i) more accurate selection of the energy interval used for the average parameter evaluations and (ii) more reliable estimations of the quoted uncertainties.

The resonance spacings of the p-wave resonances are shown in Fig. 4.2. These data were obtained for a substantially smaller number of nuclei than for the s-wave resonances. Nevertheless, the p-resonance spacing data are very important in testing the consistency of the results. Based on the general statistical properties of nuclear levels, the spacings of the s- and p-wave resonances should be related ($D_1 = D_0/3$) at least for nuclei far from the magic numbers. This relationship is also useful for a coarse estimation of the s-resonance spacing when only p-resonance data are available. Data included in RIPL-2 for the s-wave neutron strength functions are shown in Fig. 4.3, and compared with BNL data [4.14, 4.15] corrected in a new evaluation [4.21]. For most cases, there are no significant differences between the two evaluations. As explained above, the

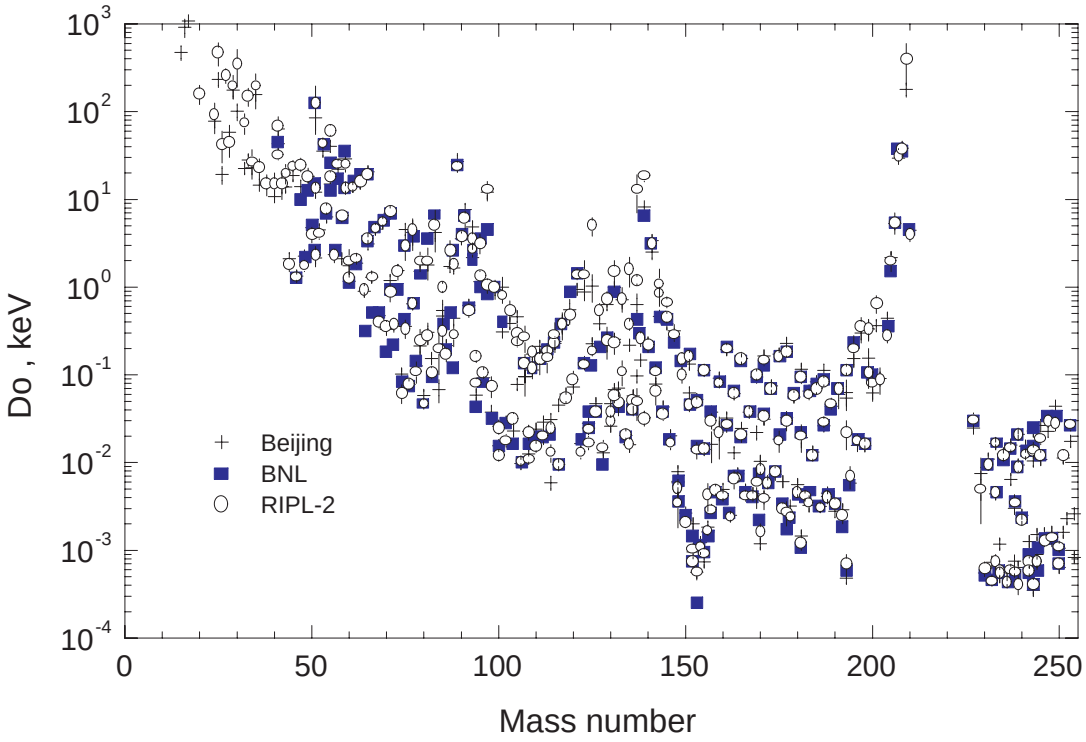

Figure 4.1: Average resonance spacings for the s-wave neutron resonances included in the BNL [4.14, 4.15, 4.21], Beijing [4.16, 4.19] and RIPL-2 evaluations.

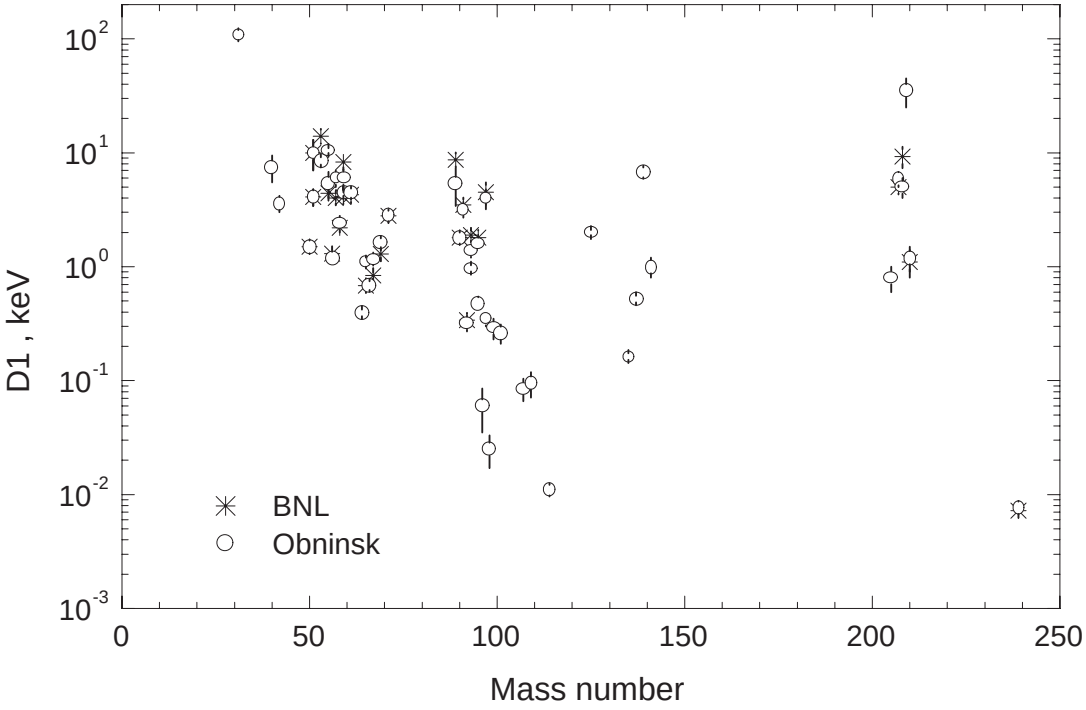

Figure 4.2: Average resonance spacings for the p-wave neutron resonances included in the BNL [4.14, 4.15] and RIPL-2 evaluations.

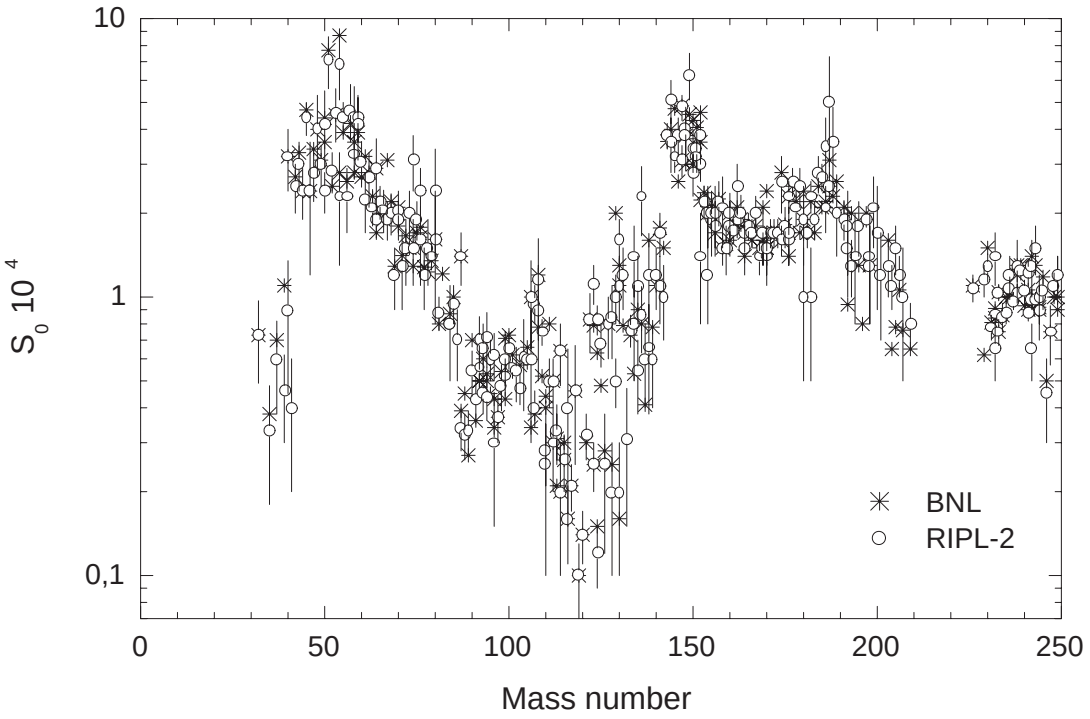

Figure 4.3: The *s*-wave neutron strength functions included in the BNL [4.14, 4.15, 4.21] and RIPL-2 evaluations. Uncertainties are shown for the RIPL-2 evaluations only.

uncertainties quoted in the RIPL-2 file are slightly higher than those in the BNL evaluation, partially because they take into account sample quality in addition to statistical errors.

Similar results for the *p*-wave neutron strength functions are presented in Fig. 4.4. The BNL compilation includes some additional data on the *p*-wave strength functions that were obtained from neutron cross-section analyses in the unresolved resonance region. However, such analyses require some additional, model-dependent approximations, and therefore we decided to limit the RIPL-2 resonance files to the data based on the resolved resonance parameters observed directly.

Average radiative widths included in the RIPL-2 files are shown in Figs. 4.5 and 4.6 for the *s*- and *p*-wave resonances, respectively. The recommended values obtained by different groups agree with each other in general [4.16]. However, we note that for many nuclei the average widths are given without any uncertainties in the BNL and Beijing evaluations. Under such circumstances, the uncertainties provided in the RIPL-2 file should be adopted.

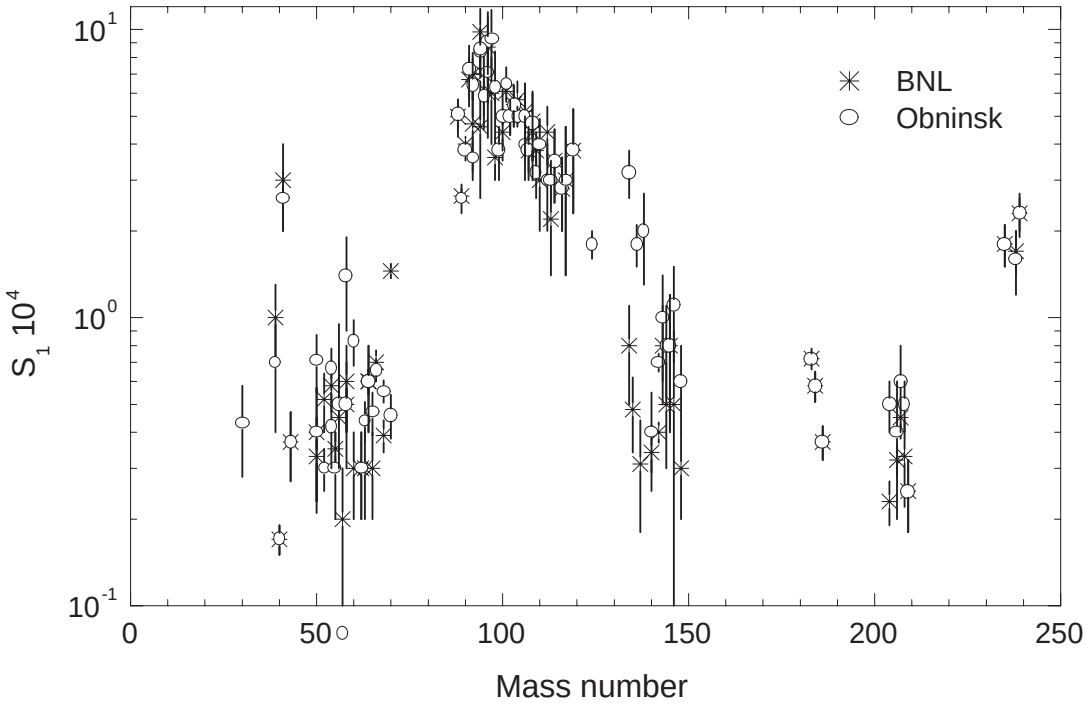

Figure 4.4: The p-wave neutron strength functions included in the BNL [4.14, 4.15] and RIPL-2 evaluations.

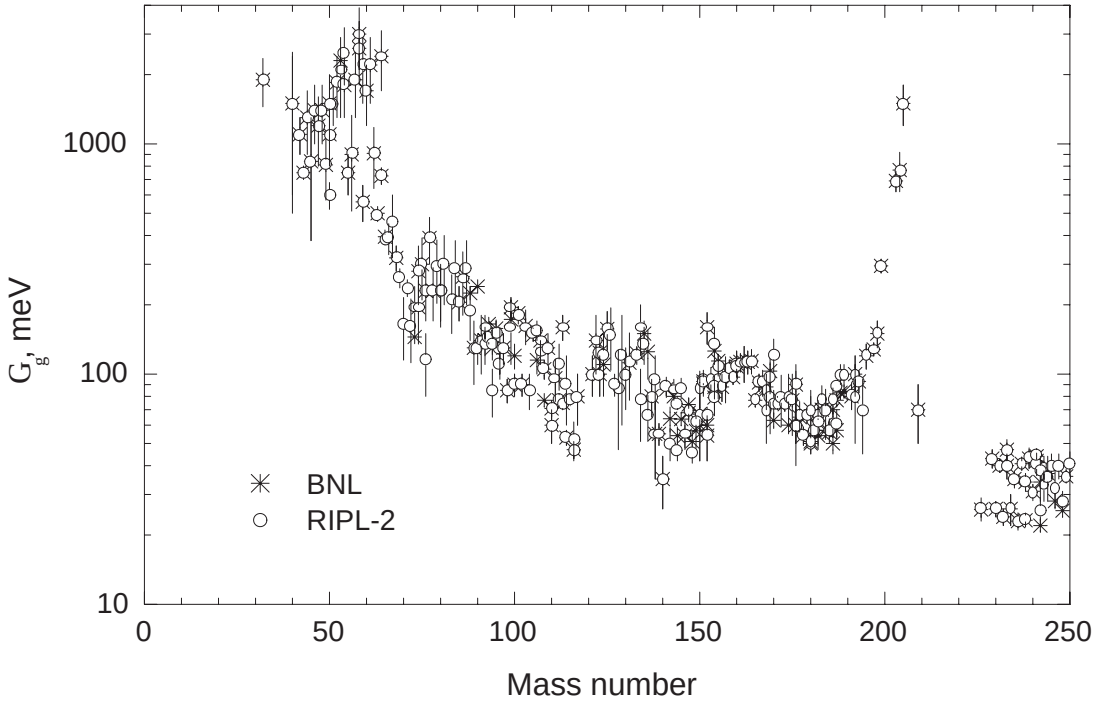

Figure 4.5: Average radiative widths for the s-wave neutron resonances included in the BNL and RIPL-2 evaluations.

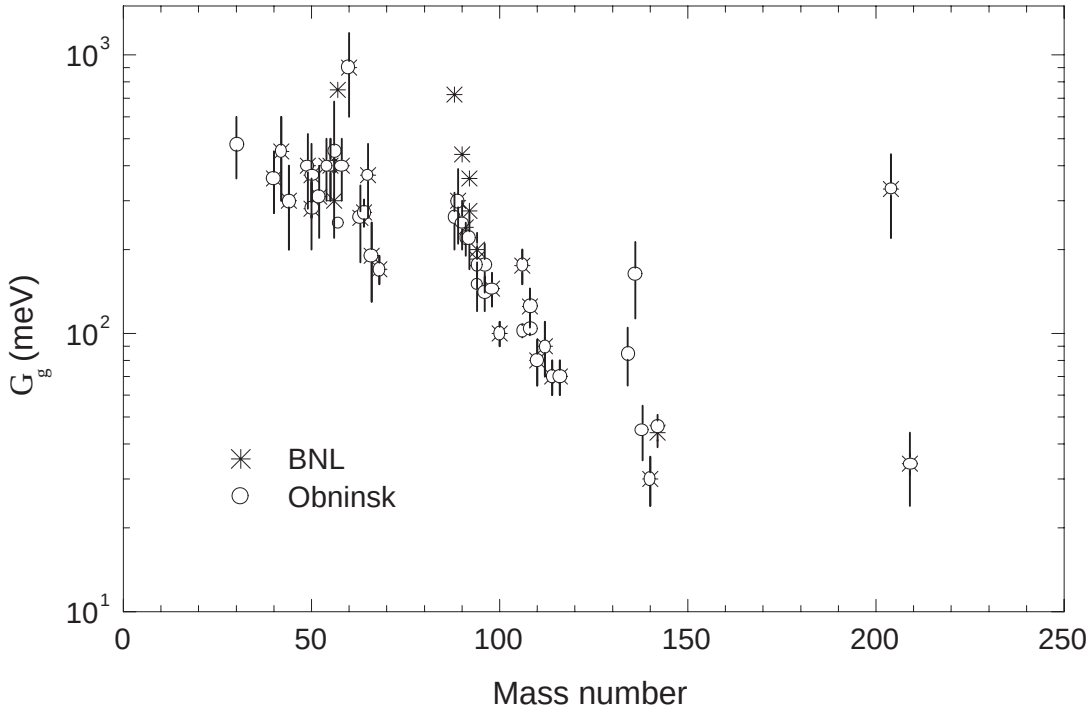

Figure 4.6: Average radiative widths for the p-wave neutron resonances included in the BNL [4.14, 4.15] and RIPL-2 evaluations.

4.3 Conclusions and recommendations

All recent evaluations by the Beijing, Minsk, Obninsk, and Troitsk groups have been included in the RIPL-1 database, and the recommended RIPL-1 data were tested and revised during the RIPL-2 project. Previous data were corrected and extended by taking into account recent experimental data. In addition to the data for the s-wave neutron resonances, new evaluations of the average parameters for the p-wave resonances have been included in the RIPL-2 library.

REFERENCES

[4.1] PORTER, C.E., THOMAS, R.G., Phys. Rev. **104** (1956) 483.

[4.2] PORTER, C.E. (Ed.), Statistical Theories of Spectra, Academic Press, New York (1965).

[4.3] MEHTA, M.L., Random Matrices, Academic Press, New York (1967).

[4.4] LYNN, J.E., Theory of Neutron Resonance Reactions, Clarendon Press, Oxford (1968).

[4.5] CAMARDA, H.S., et al., in Statistical Properties of Nuclei, CARD., J.B., (Ed.), Plenum Press, New York (1972) 285.

[4.6] LIOU, H.I., CAMARDA, H.S., WYNCHANK, S., SLAGOWITZ, M., HACKEN, G., RAHN, F., RAINWATER, J., Phys. Rev. **C5** (1972) 974.

[4.7] DELFINI, G., GRUPPELLAAR, H., in Proc. Meeting on Neutron Cross Sections of Fission Product Nuclei, COCEVA, C., PANINI, G.C., (Eds.), NEANDC(E)-209, Bologna (1979) 169.

[4.8] FORT, E., DERRIEN, H., LAFOND, O. in Proc. Meeting on Neutron Cross Sections of Fission Product Nuclei, COCEVA, C., PANINI, G.C., (Eds.), NEANDC(E) 209, Bologna (1979) 121.

[4.9] FRÖHNER, F.H., in IAEA Advisory Group Meeting on Basic and Applied Problems of Nuclear Level Densities, BHAT, M.R., (Ed.), BNL-NCS-51694, Brookhaven (1983) 219.

[4.10] RIBON, P., *ibid.*, 245.

[4.11] ZONGDI SU, et al., in Proc. Meeting on Nuclear Data Evaluation Methods, DUNFORD, C., (Ed.), New York (1992).

[4.12] PORODZINSKI, Yu.V., SUKHOVITSKI, E.Sh., in Proc. ISTC Workshop on Nuclear Data for Minor Actinides, JAERI-97-001, Tokai (May 1996) 34.

[4.13] BELANOVA, T.S., IGNATYUK, A.V., PASHCHENKO, A.B., PLYASKIN, V.I., Radiative Neutron Capture - Handbook (in Russian), Energoatomizdat, Moscow (1986).

[4.14] MUGHABGHAB, S.F., DIVADEENAM, M., HOLDEN, N.E., Neutron Cross Sections, Vol. 1, part A, Academic Press, New York and London (1981).

[4.15] MUGHABGHAB, S.F., Neutron Cross Sections, Vol. 1, part B, Academic Press, New York and London (1985).

[4.16] INTERNATIONAL ATOMIC ENERGY AGENCY, Handbook for Calculations of Nuclear Reaction Data - Reference Input Parameter Library, IAEA-TECDOC-1034, Vienna (1998).

[4.17] IGNATYUK, A.V., Low Energy Neutron Physics, Landolt-Boernstein Series **16A**, part 2, Springer, Berlin (2000) 1.

[4.18] ILJINOV, A.S., MEBEL, M.V., BIANCHI, N., DE SANCTIS, E., GUARALDO, C., LUCHERINI, V., MUCCIFORA, V., POLLI, E., REOLON, A.R., ROSSI, P., Nucl. Phys. **A543** (1992) 517.

[4.19] ZONGDI SU, et al., Contribution to Third CRP Meeting on RIPL, Trieste, May 1997.

[4.20] SUKHORUCHKIN, S.M., et al., Low Energy Neutron Physics, Landolt-Boernstein Series **16B**, Springer, Berlin (2000).

[4.21] OH, SOO-YOUL, CHANG, J., MUGHABGHAB, S.F., Neutron Cross Section Evaluations of Fission Products Below the Fast Energy Region, BNL-NCS-67469 (ENDF-362) (2000).

5 OPTICAL MODEL PARAMETERS

Coordinators: O. Bersillon and P.G. Young

Summary

The optical model segment of the Reference Input Parameter Library is described. Available files include a library of phenomenological optical model potentials (OMP) for incident neutrons, protons, deuterons, tritons, ^{3}He and ^{4}He particles; a microscopic optical model code for incident nucleons; several retrieval and utility codes for accessing the OMP library; definition of the format of the OMP library; and user information for the various codes. Global as well as nuclide-specific potentials are included that utilize spherical, vibrational, dispersive and rotational models. The optical model parameterizations in the library are given in a general format that allows for easy expansion. Recommendations for the use of the library are given, together with user instructions for the various computer codes.

The optical model provides the basis for many theoretical analyzes and/or evaluations of nuclear cross sections that are used in providing nuclear data for applied purposes. As well as offering a convenient means for the calculation of reaction, shape elastic and (neutron) total cross sections, optical model potentials are widely used in quantum-mechanical pre-equilibrium and direct-reaction theory calculations, and (most importantly) in supplying particle transmission coefficients for Hauser-Feshbach statistical-theory as used in nuclear data evaluations.

The importance of optical model parameterizations is made even more apparent by the worldwide diminution of experimental facilities for low-energy nuclear physics measurements and the consequent increased reliance on theoretical methods for providing nuclear data for applications. Therefore, the preservation of past work aimed at describing experimental results with optical model potentials is vital for the future development of nuclear databases. Additionally, the availability and use of microscopic optical model codes is important for predicting data for target nuclei far from the line of stability, where phenomenological models might not be valid.

The optical model segment of RIPL-2 is aimed at extending the library of optical model parameterizations developed under the RIPL-1 project [5.1], and providing access to a microscopic optical model code. The product of this activity for phenomenological optical potentials is an optical model potential (OMP) library that contains reliable, state-of-the-art parameterizations for the conventional optical model codes used in calculations of nuclear data for applications. In addition to preserving optical model parameterizations for future activities, the library offers a convenient means for evaluators to access a wide

body of information on the optical model. Subroutines have been developed for reading and writing the data library and for creating convenient summaries of the library. Processing codes are provided that permit direct interfacing of the library with the selected optical model codes.

The OMP library is organized in two parts: an archival file and a user file. The archival file contains all potentials compiled so far, totaling some 533 entries; the user file is a subset of the archival file and contains 406 potentials. The focus of the RIPL-2 studies was the user library, which contains the most useful optical potentials for calculating data for applications. The format of the archival library is identical to the user library, and the various retrieval and utility codes that are provided work equally well with either library. Details of the phenomenological library and supporting codes are given below.

In addition to the OMP library, a semi-microscopic optical model code is also supplied and described in Section 5.2. This model should mainly be used when experimental data are missing.

5.1 Phenomenological parameterizations

5.1.1 Description of the potential

One of the primary goals of the optical model segment is to provide a format for optical model parameterizations that is general enough to cover all commonly used phenomenological potential representations and that is easily expanded for additional types of optical potentials. We have focused on standard Schrödinger-type forms of optical model potentials, and have included spherical, coupled-channel rotational, vibrational and dispersive optical models.

As presently formulated, potentials of the form

$$\begin{aligned} V(r) &= -V_R\, f_R(r) - iW_V\, f_V(r) + 4a_{VD}\, V_D \frac{d}{dr} f_{VD}(r) + 4ia_{WD}\, W_D \frac{d}{dr} f_{WD}(r) + \\ &\quad \frac{\lambda_\pi^2}{r} \left[V_{SO} \frac{d}{dr} f_{VSO}(r) + iW_{SO} \frac{d}{dr} f_{WSO}(r) \right] \sigma \cdot l \end{aligned} \tag{5.1}$$

are allowed, in which V_R and W_V are the real and imaginary volume potential well depths, V_D and W_D are the real and imaginary well depths for the surface derivative term, V_{SO} and W_{SO} are the real and imaginary well depths for the spin-orbit potential, and λ_π^2 is the pion Compton wavelength squared ($\simeq 2$ fm^2). The quantity $\sigma \cdot l$ is the scalar product of the intrinsic and orbital angular momentum operators and is given by

$$\begin{aligned} \sigma \cdot l &= l \qquad\qquad \text{for } j = l + \frac{1}{2} \\ &= -(l+1) \qquad \text{for } j = l - \frac{1}{2} \end{aligned} \tag{5.2}$$

where $f_i(r)$ are radial-dependent form factors and are defined below (Section 5.1.5).

Any incident particle is permitted by the format, but we have limited our initial library to incident neutrons, protons, deuterons, tritons, ^{3}He and ^{4}He particles. Our

approach is to supply a general form for optical model potentials that is an extension of the representation implemented in the **SCAT2000** optical model code [5.2] and that describes most of the parameterizations that have been commonly used in the past. Additionally, three specialized formats are formulated that describe particular less common forms of potentials, but which offer promise as being important for applied purposes.

Many high energy potentials are obtained with the use of the relativistic kinematics (see Annex 5.D). It should be noted here that the relativistic OMPs given in the library *include* the γ relativistic factor [5.3].

5.1.2 Dispersive relations

The dispersive optical model is a natural result of the causality principle: a scattered wave cannot be emitted before the arrival of the incident wave. This introduces an integral relationship [5.4] which links the real and imaginary parts of the nuclear potential

$$\Delta V(E) = \frac{1}{\pi}\mathcal{P}\int_{-\infty}^{\infty}\frac{W(E')}{E'-E}\,dE'\,.$$

where W is either the volume or the surface absorption potential. This addition provides a more realistic description of the energy dependence of the optical potential and enables the prediction of single-particle, bound-state quantities (such as binding energies, occupation probabilities and spectroscopic factors). There are few analyses that include dispersive relationships. One reason is that the integrals are analytical for only a very restricted number of absorption potential energy dependences (piecewise linear [5.2] or Brown and Rho form [5.5, 5.6]). Precise numerical calculation of these integrals might make the use of the dispersion approach easier [5.7].

An example is given in Ref. [5.8] of the extension of the dispersive optical model approach to permanently deformed nuclei.

5.1.3 Nucleon-nucleus potentials

Individual Nucleus Potentials

The bulk of the nucleon-nucleus potentials in the OMP library is for single target nuclei (or perhaps for a very narrow range of neighboring targets) and cover a range of incident energies. These potentials are usually the most accurate for specific targets and should be considered whenever accuracy is imperative. There is one important series of potentials that, while given for specific targets, were derived as part of a comprehensive analysis covering targets from ^{24}Mg to ^{209}Bi. These are the spherical optical model potentials by Koning and Delaroche [5.9]. Other significant individual nuclide potentials are those by Arthur [5.10] and the extensive lists of potentials used in PR China [5.11] and Japan [5.12] for fission products. All of the rotational model potentials described below are in the form of individual nucleus potentials with relatively small ranges of validity in Z and A.

Global potentials

The use of the term "global" refers to optical model potentials that cover a wide range of incident energy and target nuclei. The most important potentials that are global for both incident neutrons and protons are those of

- Koning and Delaroche [5.9] (Z=12-83, A=27-209, E=0.001-200 MeV), and
- Madland [5.3] (Z=6-82, A=12-208, E=50-400 MeV).

In addition to incorporating improved methodology, these potentials are the most recently developed global potentials and, as such, their analyses have drawn upon a wider range of experimental data than the older potentials.

Other older global potentials that cover both incident neutrons and protons are those of

- Becchetti and Greenlees [5.13] (Z=20-92, A=40-238, E=10-50 MeV),
- Walter and Guss [5.14] (Z=26-82, A=54-208, E=10-80 MeV), and
- Varner *et al.* [5.15] (Z=20-83, A=40-209, E=16-65 MeV).

Older global potentials developed exclusively for incident *neutrons* are those of

- Moldauer [5.16] (Z=20-83, A=40-209, E=0.001-5 MeV),
- Wilmore and Hodgson [5.17] (Z=20-92, A=40-238, E=0.01-25 MeV),
- Engelbrecht and Fiedeldey [5.18] (Z=20-83, A=40-210, E=0.001-155 MeV),
- Strohmaier *et al.* [5.19] (Z=23-41, A=50-95, E=0.001-30 MeV).

For incident *protons* alone, there are the potentials of

- Menet *et al.* [5.20] (Z=6-82, A=12-208, E=30-60 MeV),
- Perey [5.21] (Z=16-49, A=30-100, E=0.01-22 MeV), and
- Patterson *et al.* [5.22] (Z=20-82, A=48-208, E=25-45 MeV).

Coupled-channels potentials

The RIPL-2 OMP library contains 33 neutron and 8 proton coupled-channels potentials for ground-state rotational bands. These potentials have been necessarily developed for more limited target Z and A ranges, as they are dependent upon the structure of each target nucleus. For incident neutrons, the targets include $^{151-153}$Eu, ^{165}Ho, ^{169}Tm,

$^{182-186}$W, ^{185,187}Re, ^{197}Au and a number of actinides between ^{232}Th and ^{252}Cf. In each case, the structure information is provided in the OMP library for the target nuclei for which the potential was determined. It is possible for the user to use these potentials over a broader range of target nuclei, most probably with reduced accuracy, although the user must provide the required structure information.

Coupled-channels potentials for incident protons are provided for the same target nuclei, except that only one potential is included for actinides. These potentials were determined with the neutron potentials using the Lane model [5.23].

5.1.4 Complex-particle potentials

A limited number of spherical potentials are included for complex particles.

For incident deuterons, there are global potentials from

- Bojowald *et al.* [5.24] (Z=6-82, A=12-208, E=20-100 MeV),
- Lohr and Haeberli [5.25] (Z=20-83, A=40-209, E=8-13 MeV), and
- Perey and Perey [5.26] (Z=20-82, A=40-208, E=11-27 MeV).

Additionally, there are individual target potentials for 5 nuclei between ^{40}Ca and ^{208}Pb by Daehnick *et al.* [5.27], each covering the incident deuteron energy range from 11.8 to 90 MeV.

For incident tritons and ^{3}He particles, the global potentials of Becchetti and Greenlees [5.28] (Z=20-82, A=40-208, E=1-40 MeV) are included. The energy dependence of the triton potential is based on the ^{3}He potential, which covers the same energy range for the same target charge and mass range.

In the case of incident alpha particles, the OMP library includes global potentials from

- McFadden and Satchler [5.29] (Z=8-82, A=16-208, E=1-25 MeV),
- Avrigeanu *et al.* [5.30] (Z=8-96, A=16-250, E=1-73 MeV),
- Huizenga and Igo [5.31] (Z=10-92, A=20-235, E=1-46 MeV), and
- Strohmaier *et al.* [5.19] (Z=20-45, A=40-100, E=1-30 MeV).

Also included in the RIPL-2 optical file space is a code that can be used to obtain phenomenological alpha-particle potentials *(om-alpha.f)*. This code was developed by Kumar and Kailas [5.32] for the RIPL-2 co-ordinated research project, and utilizes systematics of the nuclear radius and slope as well as real potential microscopic volume integrals from earlier analyzes of alpha optical model potentials. The new global potential is valid for incident alpha energies near the Coulomb barrier up to 150 MeV and for target nuclei over the mass range A = 16 to 208. The elastic and reaction cross sections calculated with this

model show satisfactory agreement with experimental data for the limited cases checked so far. At energies below the Coulomb barrier, the potential has not been thoroughly tested.

5.1.5 Format of OMP library

A complete description of the format of the OMP library is given in Annex 5.A, so only a summary is given here. The format allows parameterizations for spherical, coupled-channels rotational, vibrational and non-axial deformed optical models. Potentials may be relativistic or non-relativistic, dispersive or non-dispersive. The format allows for inclusion of structure data for coupled-channels rotational, vibrational and non-axial deformed models.

The general form of the optical model potential is the following:

$$\begin{aligned} V_i(E) &= \alpha_1 + \alpha_7\eta + \alpha_8\Delta_c + \alpha_9 A + \alpha_{10}A^{1/3} + \alpha_{11}A^{-2/3} + \alpha_{12}\Delta_{c'} + \\ &\quad (\alpha_2 + \alpha_{13}\eta + \alpha_{14}A)E + \alpha_3 E^2 + \alpha_4 E^3 + \alpha_6\sqrt{E} + \\ &\quad (\alpha_5 + \alpha_{15}\eta + \alpha_{16}E)\ln(E) + \alpha_{17}\Delta_c E^{-2} \end{aligned} \tag{5.3}$$

where $V_i(E)$ designates the ith term of the potential (for example, V_R, W_D, V_{SO}, etc.) at incident laboratory energy E, $\eta = (N - Z)/A$, N and Z are the neutron and proton numbers of the target nucleus, and A is the integer atomic mass of the target, i.e., $A = N + Z$. Two different forms of correction terms for Coulomb repulsion with incident protons are provided:

$$\Delta_c = \frac{0.4\ Z}{A^{1/3}} \quad \text{and} \quad \Delta_{c'} = \frac{1.73\ Z}{R_c} \tag{5.4}$$

where R_c is the Coulomb radius. The coefficients that multiply Δ_c and $\Delta_{c'}$ are usually zero for incident neutrons.

Each of the potential terms in Eq. 5.1 can be represented over any number of defined energy ranges using as many of the terms given in Eq. 5.3 as required, with the coefficients of the unused terms set to zero.

Either Woods-Saxon or Gaussian form factors are permitted for the $f_i(r)$ terms in Eq. 5.1:

$$f_i(r) = \left[1 + \exp\left(\frac{r - R_i}{a_i}\right)\right]^{-1} \qquad \text{(Woods-Saxon form)} \tag{5.5}$$

or

$$f_i(r) = \exp\left[\frac{-(r - R_i)^2}{a_i^2}\right] \qquad \text{(Gaussian form).} \tag{5.6}$$

The nuclear radius is given by $R_i = r_i\, A^{1/3}$, where r_i is given by

$$\begin{aligned} r_i(E) &= \beta_1 + \beta_2 E + \beta_3\eta + \beta_4 A^{-1} + \beta_5 A^{-1/2} + \beta_6 A^{2/3} + \beta_7 A + \beta_8 A^2 + \\ &\quad \beta_9 A^3 + \beta_{10}A^{1/3} + \beta_{11}A^{-1/3}, \end{aligned} \tag{5.7}$$

and a similar form is used for the diffuseness (a_i):

$$\begin{aligned} a_i(E) &= \delta_1 + \delta_2 E + \delta_3 \eta + \delta_4 A^{-1} + \delta_5 A^{-1/2} + \delta_6 A^{2/3} + \delta_7 A + \delta_8 A^2 + \\ &\quad \delta_9 A^3 + \delta_{10} A^{1/3} + \delta_{11} A^{-1/3}. \end{aligned} \tag{5.8}$$

β_i and δ_i are constants that are given in the OMP library. Note that the $\beta_{11} A^{-1/3}$ term in Eq. 5.7 permits the inclusion of a constant (A-independent) quantity to the radius that is $R_i = r_o + r_i' A^{1/3} = \beta_{11} + r_i' A^{1/3}$.

In addition to the general formula given in Eq. 5.7, three specialized formats are provided for inclusion of potentials by Smith *et al.* [5.33], Engelbrecht and Fiedeldey [5.18], Varner *et al.* [5.15], and Koning and Delaroche [5.9]. The first two special forms are described in the RIPL-1 report [5.1]; whereas the third is used with potentials from Koning and Delaroche, has changed since RIPL-1, and is summarized below.

The format used for the Koning and Delaroche potentials, as well as that of Koning *el al.* [5.34], is given by the following expression:

$$\begin{aligned} V_i &= b_1[1 - b_2(E - E_f) + b_3(E - E_f)2 - b_4(E - E_f)3] + b_5 + \\ &\quad b_6(E - E_f)^n/[(E - E_f)^n + b_7^n] + b_{11} \exp[-b_{12}(E - E_f)] + \\ &\quad b_8 \exp[-b_9(E - E_f)](E - E_f)^n/[(E - E_f)^n + b_{10}^n] \end{aligned} \tag{5.9}$$

where E_f is the Fermi energy and is provided in the library. Likewise, the various b_i are determined from parameters in the library. The format and relationships are fully defined in Annex 5.A.

5.1.6 Contents of OMP library

The OMP library is given in two parts: an archival file and a user file. The archival file contains all potentials compiled so far and totaling 533, of which 287 are potentials for incident neutrons, 146 potentials for protons, 11 for deuterons, 26 for tritons, 53 for ^{3}He particles, and 10 for incident alpha particles. The user file is a subset of the archival file with all single-energy potentials eliminated, and contains 406 entries.

Each potential included in RIPL is given a unique reference number, according to a system that is described in Annex 5.B. This numbering system was adopted in order to separate the potentials for different incident particles into different reference number regions, and to provide approximate information on the sources of the various potentials by geographical region. For example, the latter information might be used if only potentials from a particular source are adopted for a given set of calculations.

An example of a complete entry for one reference in the library is given in Annex 5.C, following the format given in Annex 5.A. The reference number (5003) indicates that the incident particle is a proton, and that the source of the potential is a laboratory in the United States of America.

Summary information on all the potentials compiled to date is given in Annex 5.D, together with references for each potential. The user library to date includes:

- 283 optical model parameterizations for incident neutrons,
- 101 parameterizations for incident protons,
- 8 parameterizations for incident deuterons,
- 1 parameterization for incident tritons,
- 3 parameterizations for ^{3}He particles, and
- 10 parameterizations for incident alpha particles.

5.2 Microscopic optical model

The phenomenological parameterizations described in the previous section are suitable if there are sufficient experimental data to constrain the optical model parameters. If these data are too sparse or totally lacking, one has to move to global parameterizations or, in a more physical way, to a semi-microscopic approach as described in Ref. [5.35].

The potentials in this model are *calculated* by folding the target radial matter density with an optical potential in nuclear matter based on the Brückner-Hartree-Fock work of Jeukenne *et al.* [5.36]. Parameterization of this potential in nuclear matter was revised by unifying the low and high energy components [5.35, 5.37], and thus making the semi-microscopic model applicable in the nucleon energy range from 1 keV to 200 MeV and for spherical nuclei with mass number A $>$ 30.

The semi-Microscopic Optical Model is implemented in the **MOM** package which is included in the optical directory.

5.3 Validation

Validation of the potentials in the library has been carried out at several levels. In addition to considerable proof reading, several of the potentials contained in the RIPL-2 library have been tested by Kumar *et al.* [5.38] against experimental data. In every case where local potentials were compared to global potentials, the local parameterizations produced better agreement with the experimental data than did the global potentials. Additionally, volume integrals from several well-known global potentials were compared to "best-fit" potentials for the ^{208}Pb + n system [5.1], which indirectly involved experimental data.

The testing of the present RIPL-2 OMP library has focused on verifying that the potentials in the library are accurately entered and that they produce reasonable results when used in optical model calculations. To this end, every potential in the library has been processed with the **OM-RETRIEVE** code to make inputs for the **ECIS96** code. **ECIS96** calculations were performed at one or more incident energies, and the resulting reaction cross sections were compared to check for obvious errors. Additionally, inputs were made for the **SCAT2000** code from every spherical potential and the resulting reaction cross sections were compared against one another and with the **ECIS96** results.

Table 5.1: Comparison of total (σ_t) and reaction (σ_r) cross sections calculated for 14 MeV neutrons on ^{27}Al with the **SCAT2000** and **ECIS96** codes from spherical potentials in the RIPL-2 library. The *om-retrieve.f* code was used to generate inputs for the codes.

RIPL number	First author	σ_t (mb) **SCAT2000**	σ_t (mb) **ECIS96**	σ_r (mb) **SCAT2000**	σ_r (mb) **ECIS96**
18	Harper	1670.9	1672.0	919.0	919.1
117	Petler	1709.1	1709.1	954.0	953.2
419	Molina*	1688.1	1688.1	907.8	906.9
1402	Koning	1722.8	1722.5	987.4	992.3
2405	Koning	1780.7	1780.6	1051.9	1051.4
242	Lee	1749.0	1747.9	1029.4	1028.4
418	Molina*	1697.9	1698.0	932.1	931.4
101	Ferrer	1774.6	1774.8	1099.0	1099.0

* Dispersive potentials.

No consideration was given to the Z and A ranges of validity of the potentials, as the test was merely intended to check for library data input errors.

The global potential of Madland [5.3], as processed from the RIPL-2 library with **OM-RETRIEVE**, has been checked in detail against Madland's calculations with the **SNOOPY** code used in his original analysis. Additionally, the global and individual-nucleus potentials of Koning and Delaroche [5.9] have been checked in detail by comparison with parameter values supplied by Koning. The results of **SCAT2000** and **ECIS96** calculations with these potentials have been compared with some of the older potentials for particular targets and incident energies.

Table 5.1 compares reaction cross sections calculated with **SCAT2000** and **ECIS96** for 14 MeV neutrons on ^{27}Al and a variety of RIPL-2 potentials. All the potentials are spherical, and two of the potentials are dispersive. **SCAT2000** and **ECIS96** results are in excellent agreement, typically within a few tenths of a percent. These small differences can be attributed to the differences in the target masses adopted in the two codes. The

Table 5.2: Comparison of total (σ_t), elastic scattering (σ_e), reaction (σ_r), first (σ_1) and second (σ_2) excited state cross sections calculated for 10 MeV neutrons on ^{238}U with the **ECIS96** code from coupled-channels rotational potentials in the RIPL-2 library. The *om-retrieve.f* code was used to generate inputs for the codes.

RIPL number	First author	σ_t (mb)	σ_e (mb)	σ_r (mb)	σ_1 (mb)	σ_2 (mb)	Type of potential
600	Vladuca	5745.0	2592.0	3153.0	248.6	39.0	Coupled-channels
410	Lagrange	5774.1	2609.2	3164.9	238.5	54.1	Coupled-channels
416	Haouat	5774.1	2609.2	3164.9	238.5	54.1	Coupled-channels
5	Young	5780.1	2628.3	3151.7	259.6	60.7	Coupled-channels
2006	Young	5760.3	2620.7	3139.5	263.8	61.6	Coupled-channels

Table 5.3: Comparison of reaction cross sections (σ_r) calculated for 50 and 90 MeV protons on ^{208}Pb with the **SCAT2000** and **ECIS96** codes from spherical potentials in the RIPL-2 library. The *om-retrieve.f* code was used to generate inputs for the codes.

		50 MeV		90 MeV	
RIPL	First	σ_r (mb)	σ_r (mb)	σ_r (mb)	σ_r (mb)
number	author	**SCAT2000**	**ECIS96**	**SCAT2000**	**ECIS96**
4101	Becchetti	2049.5	2049.4	-	-
4102	Menet	2122.6	2122.5	-	-
4131	Schwandt	1998.8	1991.2	1919.5	1913.3
4428	Koning	2028.3	2020.7	1956.3	1949.5
5405	Koning	2033.0	2025.4	1950.5	1943.8
5001	Madland	1974.8	1967.2	1894.1	1888.0
5100	Varner	2103.2	2103.2	-	-
5101	Walter	2029.1	2029.1	-	-

total cross sections from the various potentials show a total spread of roughly 6 percent, whereas the spread in the reaction cross sections is almost 20 percent.

Similar comparisons are given in Table 5.2 for 10 MeV neutrons on ^{238}U, limited to the **ECIS96** code because the potentials use a coupled-channels rotational model. The agreement in this case is much better for the total, reaction and elastic cross sections, and is reasonably good for the (n, n′) cross sections.

Proton potentials for ^{208}Pb are compared at 50 and 90 MeV in Table 5.3. Again, the **SCAT2000** and **ECIS96** results are in good agreement, and the spread in the reaction cross sections is small. Note that calculations are only included over the energy range of validity of the various potentials.

5.4 Recommendations and conclusions

5.4.1 Recommendations

Ultimately, it is the responsibility of the users of the RIPL-2 data files to choose potentials that are most appropriate for the particular applications they are addressing. However, on the basis of our testing of these data, some general recommendations can be made.

Nucleus-specific potentials can be expected to give better results than global potentials, provided the potential has been carefully derived under physical constraints, and users apply only the potentials in the Z, A and energy ranges where the potentials were derived. This conclusion is supported by the work of Kumar *et al.* [5.38] who found that in every case where local potentials were compared to global potentials, the local parameterizations produced better agreement with experimental data.

A common situation is that nucleus-specific potentials may not exist or be so limited as to be useless for a particular problem. Under such circumstances, one must resort to

other options. Additionally, even if nucleus-specific potentials are available for a problem, the choice always exists as to which nucleus-specific potential to choose for a particular problem. Accordingly, we have made suggestions or recommendations for an initial choice of potentials that can be adopted for most problems.

Actinide and rare earth targets

1. In the case of strongly deformed nuclei, we recommend that coupled-channels rotational potentials be used for the individual nucleus involved if such are available. These potentials can be chosen from those listed in Annex 5.D.

Incident neutrons - targets with Z $\leq$ 90

1. We recommend the individual-nucleus potentials of Koning and Delaroche (RIPL 1400 - 1467).
2. For cases where option 1 is not possible but the target is still close to the line of stability, we recommend the global potential of Koning and Delaroche (RIPL 2405). For 50 $\leq$ E $\leq$ 400 MeV, a possible alternative is the potential of Madland (RIPL 2001).
3. If the target lies far from the line of stability, we recommend use of the microscopic optical model code **MOM**.

Incident protons - targets with Z $\leq$ 90

1. We recommend the individual-nucleus potentials of Koning and Delaroche (RIPL 4416 - 4429).
2. For cases where option 1 is not possible but the target is still close to the line of stability, we recommend the global potential of Koning and Delaroche (RIPL 5405). For 50 $\leq$ E $\leq$ 400 MeV, a possible alternative is the potential of Madland (RIPL 5001).
3. If the target lies far from the line of stability, we recommend use of the microscopic optical model code **MOM**.

Incident deuterons

1. We recommend the individual-nucleus potentials of Daehnick (RIPL 6112 - 6116), where applicable.
2. If option 1 not possible, we recommend the global potential of Bojowald *et al.* (RIPL 6400).

Incident tritons

1. We recommend the global potential of Becchetti and Greenlees (RIPL 7100); this is the only choice available in the RIPL-2 library.

Incident ^{3}He

1. We recommend the global potential of Becchetti and Greenlees (RIPL 7100).

Incident alpha particles

1. We recommend the individual-nucleus potentials from Annex 5.D, where possible.

2. If option 1 is not possible, we recommend the global potential of Strohmaier (RIPL 9400: Z = 20 - 45, E = 1 - 30 MeV) or Avrigeanu *et al.* (RIPL 9600: Z = 8 - 96, E = 1 - 73 MeV).

5.4.2 Conclusions

Improved phenomenological optical model potentials have been developed in recent years that can enhance significantly the quality of optical model calculations for applied problems. These include Koning and Delaroche's extensive set of optical model potentials for individual target nuclei covering the nucleon energy range E=1-200 MeV and the target range Z=12-83, A=24-209, with accompanying global potentials covering the same energy and target ranges [5.9]. These potentials not only span very broad ranges in energy, Z and A, but are also based upon a modern analysis approach that utilizes an extensive experimental data base [5.34]. Additionally, the use of microscopic optical model calculations has advanced to a state where routine use of such potentials as a supplement to phenomenological models is not only feasible but also very desirable.

A primary aim of the RIPL-2 optical segment has been to accumulate a large body of information that will be useful in optical model calculations and to provide computer codes for processing the information into inputs for commonly used optical model codes. The RIPL-2 optical model potential library includes a wide collection of older, traditional potentials as well as many of the newer ones. The data base and codes in the RIPL-2 library should permit users to perform a wide range of optical model calculations of high quality. Considerable testing of the OMP library has been performed, and the reliability of the data base is judged to be high. While it is recognized that the information base is by no means exhaustive, these data have been formulated in a manner that permits easy expansion as new information becomes available or as gaps are filled in older data.

5.5 Summary of codes and data files

The structure of the optical directory in RIPL-2 is as follows:

```
optical/

     om.readme
     om-utility.readme
     om-utility.tgz
          om-summary.f
          om-modify.f
          om-utility.cmb

     om-data/
          om-parameter.readme
          om-parameter-a.dat
          om-parameter-u.dat
          om-deformations.readme
          om-deformations.dat

     om-get/
          om-retrieve.readme
          om-retrieve.tgz
               om-retrieve.f
               om-retrieve.cmb
               gs-mass-sp.dat
          kd-global.readme
          kd-global.f
          om-alpha.readme
          om-alpha.tgz

     om-microscopic/
          mom.readme
          mom.tgz
          mom-manual.ps
```

Programs and data files are included in the directory:

om.readme - short description of the overall content of the OPTICAL directory.

om-utility.readme - description of the *om-summary.f* and *om-modify.f* codes.

om-utility.tgz - tarred and zipped (gzip) file containing the *om-summary.f*, *om-modify.f*, and *om-utility.cmb* files.

om-summary.f - code that provides summary information about the *om-parameter-a.dat* or *om-parameter-u.dat* libraries. The only input required is the OMP library file, plus a terminal input specifying whether the outputs are sorted on RIPL reference number or on target Z, A, E_{min} for each projectile type. The code creates three output files: (*i*) a concise table of potentials with a description of each, one line per RIPL reference; (*ii*) publication references for each entry in the table: (*iii*) a summary for each RIPL entry giving RIPL reference, authors, publication reference, and a brief summary of the work. See Annex 5.D for the table and references file that result from the *om-parameter-u.dat* file.

om-modify.f - code that allows addition or deletion of potentials from the OMP library. Contains a simple option for creating a user OMP file from an inputted archival OMP file.

om-utility.cmb - common-block file required by both the *om-summary.f* and *om-modify.f* code.

om-parameter.readme - description of the optical model parameter library files, including complete details of the format of the library.

om-parameter-a.dat - archival version of the OMP library.

om-parameter-u.dat - user version of the OMP library.

om-deformations.readme - description of the *om-deformations.dat* file.

om-deformations.dat - file of deformation parameters that can be accessed by the *om-retrieve.f* code for distorted-wave Born-approximation calculations; described below.

om-retrieve.readme - description of the input options and files required for the *om-retrieve.dat* code. A summary is given of the output files, together with instructions for compiling the code.

om-retrieve.tgz - tarred and zipped (gzip) file containing the *om-retrieve.f*, *om-retrieve.cmb* and *gs-mass-sp.dat* files.

om-retrieve.f - FORTRAN-77 code that allows retrieval of potential parameters from the OMP library and formatting into inputs for the **SCAT2000** [5.2] spherical or the **ECIS96** [5.6] coupled-channels optical model codes. Inputs for spherical, coupled-channels rotational, vibrational, or DWBA calculations can be made, with **SCAT2000** limited to spherical models only.

Summary of the code:

1. The three basic options are to produce (*i*) **SCAT2000** input, (*ii*) **ECIS96** inputs, or (*iii*) **ECIS96** inputs for DWBA calculations. If option (*ii*) is chosen, the form of the **ECIS96** input is determined by whether the OMP potential is spherical, rotational, or vibrational. Any required structure information is provided by the OMP library.
2. The input to the *om-retrieve.f* code includes the RIPL potential reference number, incident particle, target nucleus and energies at which **SCAT2000** or **ECIS96** inputs are required.
3. Using a built-in energy grid, a table of potential values can be made as a function of energy using option (*ii*) above.
4. A simple input exists that allows **ECIS** or **SCAT** inputs to be made for a given target Z, A and a given incident particle at a given energy from every spherical potential in the library - useful for checking purposes.
5. If the option is chosen to make DWBA inputs for **ECIS96**, deformation information is taken from an external file, either user-provided or from the *om-deformations.dat* file, as described above.

The code contains certain protections for misuse of the potentials. For example, only **ECIS96** inputs can be made from coupled-channels or vibrational potentials, and the DWBA option only works for **ECIS96** inputs. However, only a screen message is given if the user attempts to utilize a potential in a Z or A or energy range outside the range of validity of a particular potential, because there can be valid reasons for highlighting such a situation.

om-retrieve.cmb - common-block file required by the *om-retrieve.f* code.

gs-mass-sp.dat - file of nuclear masses (and ground-state spins and parities) required by the *om-retrieve.f* code. The mass values in the file are entirely consistent with those provided in the RIPL-2 file mass/*mass-frdm95.dat*.

om-kd02.readme - description of the *kd-global.f* code.

om-kd02.tgz - simple stand-alone code for calculating optical parameters from the Koning-Delaroche global neutron and proton potential (RIPL reference numbers 2405 and 5405). The code requires a simple input that specifies whether the incident particle is a neutron or proton, the energy of the incident particle, and the Z and A of the target nucleus.

om-alpha.readme - description of the *alphaop.f* code, including instructions for the input and a summary of the output quantities.

om-alpha.tgz - tarred and zipped (gzip) file containing a stand-alone code for calculating phenomenological optical model potentials. Instructions for using the code are included in the *om-alpha.readme* file.

mom.readme - description of the microscopic optical model code and supplementary files.

mom.tgz - tarred and zipped (gzip) file containing files required for microscopic optical model calculations.

mom-manual.ps - postscript file containing the manual for the **mom.f** code. The manual contains a description of the physics in the code and instructions for use.

REFERENCES

[5.1] INTERNATIONAL ATOMIC ENERGY AGENCY, Handbook for Calculations of Nuclear Reaction Data - Reference Input Parameter Library, IAEA-TECDOC-1034, Vienna (1998).

[5.2] BERSILLON, O., **SCAT2000** - Un programme de modèle optique sphérique, to be published, 2002; see also **SCAT2** - Un programme de modèleoptique sphérique, Commissariat à l'Énergie Atomique report CEA-N-2227 (1978), Proc. ICTP Workshop on Computation and Analysis of Nuclear Data Relevant to Nuclear Energy and Safety, 10 February - 13 March 1992, Trieste, Italy.

[5.3] MADLAND, D.G.,"Progress in the Development of Global Medium-Energy Nucleon-Nucleus Optical-Model Potential", Proc. OECD/NEA Specialists Meeting on Nucleon-Nucleus Optical Model to 200 MeV, Bruyères-le-Châtel, France (1997) 129.

[5.4] MAHAUX, C., SARTOR, R., Adv. Nucl. Phys. **20** (1991) 1.

[5.5] BROWN, G.E., RHO, M., Nucl. Phys. **A372** (1981) 397.

[5.6] RAYNAL, J., ECIS96, Proc. OECD/NEA Specialists Meeting on Nucleon-Nucleus Optical Model to 200 MeV, Bruyères-le-Châtel, France (1997) 159.

[5.7] CAPOTE, R., MOLINA, A., QUESADA, J.M., J. Phys. G: Nucl. Phys. **27** B15 (2001).

[5.8] ROMAIN, P., DELAROCHE, J.P., in Proc. OECD/NEA Specialists Meeting on Nucleon-Nucleus Optical Model to 200 MeV, Bruyères-le-Châtel, France (1997) 167.

[5.9] KONING, A.J., DELAROCHE, J.P., Nucl. Phys. **A713** (2003) 231.

[5.10] For example, see ARTHUR, E.D., Nucl. Sci. Eng. **76** (1980) 137 and other references in Annex 5.D.

[5.11] For example, see GE ZHIGANG, China Nuclear Data Center, Communication of Nuclear Data Progress, No. 21 (1999) 35 and other references in Annex 5.D.

[5.12] For example, see IGARASI, S., JAERI-M 5752 (1974) and other references in Annex 5.D.

[5.13] BECHETTI Jr., F.D., GREENLEES, G.W., Phys. Rev. **182** (1969) 1190.

[5.14] WALTER, R.L., GUSS, P.P., Rad. Effects **95** (1986) 73.

[5.15] VARNER, R.L., THOMPSON, W.J., MCABEE, T.L., LUDWIG, E.J., CLEGG, T.B., Phys. Repts. **201** (1991) 57.

[5.16] MOLDAUER, P.A., Nucl. Phys. **47** (1963) 65.

[5.17] WILMORE, D., HODGSON, P.E., Nucl. Phys. **55** (1964) 673.

[5.18] ENGELBRECHT, C.A., FRIEDELDEY, H., Ann. Phys. **42** (1967) 262.

[5.19] STROHMAIER, B., UHL, M., REITER, W., "Neutron Cross Section Calculations for ^{52}Cr, ^{55}Mn, ^{56}Fe, and ^{58,60}Ni", IAEA Advisory Group Meeting on Nuclear Data for Radiation Damage Assessment and Related Safety Aspects, Vienna, Austria, October 1981, INDC(NDS)-128, IAEA Vienna (1982).

[5.20] MENET, J.J.H., GROSS, E.E., MALANIFY, J.J., ZUCKER, A., Phys. Rev. **C4** (1971) 1114.

[5.21] PEREY, F.G., Phys. Rev. **131** (1963) 745.

[5.22] PATTERSON, D.M., DOERING, R.R., GALONSKY, A., Nucl. Phys. **A263** (1976) 261.

[5.23] LANE, A.M., Nucl. Phys. **35** (1962) 676.

[5.24] BOJOWALD, J., MACHNER, H., NANN, H., OELERT, W., ROGGE, M., TUREK, P., Phys. Rev. **C38** (1988) 1153.

[5.25] LOHR, J.M., HAEBERLI, W., Nucl. Phys. **A232** (1974) 381.

[5.26] PEREY, C.M., PEREY, F.G., At. Data Nucl. Data Tables **17** (1976) 1.

[5.27] DAEHNICK, W.W., CHILDS, J.D., VRCELJ, Z., Phys. Rev. **C21** (1980) 2253.

[5.28] BECCETTI Jr., F.D., GREENLEES, G.W., Annual Report, J.H. Williams Laboratory, University of Minnesota (1969).

[5.29] MCFADDEN, L., SATCHLER, G.R., Nucl. Phys. **84** (1966) 177.

[5.30] AVRIGEANU, V., HODGSON, P.E., AVRIGEANU, M., Phys. Rev. **C49** (1994) 2136; see also AVRIGEANU, M., AVRIGEANU, V., Development of a Computerized System for the Storage, Retrieval, and Optimization of Optical Model Parameters for Nuclear Data Computations, Institute of Atomic Physics, Bucharest, NP-83-1994 (1994).

[5.31] HUIZENGA, J.R., IGO, G., Nucl. Phys. **29** (1962) 462.

[5.32] KUMAR, A., KAILAS, S., Bhabha Atomic Research Centre, personal communication (2002).

[5.33] SMITH, A.B., GUENTHER, P.T., WHALEN, J.F., Nucl. Phys. **A415** (1984) 1.

[5.34] KONING, A.J., VAN WIJK, J.J., DELAROCHE, J.P., "ECISVIEW: An Interactive Toolbox for Optical Model Development", Proc. OECD/NEA Specialists Meeting on Nucleon-Nucleus Optical Model to 200 MeV, Bruyères-le-Châtel, France (1997) 111.

[5.35] BAUGE, E., DELAROCHE, J.P., GIROD, M., Phys. Rev. **C63** (2001) 024607.

[5.36] JEUKENNE, J.P., LEJEUNE, A., MAHAUX, C., Phys. Rev. **C14**, 1391 (1974); Phys. Rev. **C15** (1977) 10; Phys. Rev. **C16** (1976) 80; Phys. Rep. **25C** (1976) 83.

[5.37] BAUGE, E., DELAROCHE, J.P., GIROD, M., Phys. Rev. **C58** (1998) 1118.

[5.38] KUMAR, A., YOUNG, P.G., CHADWICK, M.B., Assessment of Some Optical Model Potentials in Predicting Neutron Cross Sections, LA-UR-97-0289 (1997).

ANNEX 5.A

OPTICAL MODEL PARAMETER FORMAT FOR RIPL LIBRARY

Structure of the format

```
[ALL INPUT PARAMETERS ARE READ IN FREE FORMAT READ STATEMENTS]

iref
author      [1 line of author names]
reference   [1 line of reference information]
summary     [4 lines of descriptive information]
emin,emax
izmin,izmax
iamin,iamax
imodel,izproj,iaproj,irel,idr

       *****LOOP: i=1,6
jrange(i)
       *****LOOP j=1,jrange
epot(i,j)
(rco(i,j,k), k=1,11)
(aco(i,j,k), k=1,11)
(pot(i,j,k), k=1,25)
       *****END i AND j LOOPS

jcoul
       *****LOOP j=1,jcoul
ecoul(j),rcoul0(j),rcoul(j),rcoul1(j),rcoul2(j),beta(j)
       *****END j LOOP

    (1)*****SKIP TO (2)***** IF IMODEL NOT EQUAL TO 1

nisotopes
       *****LOOP n=1,nisotopes
iz(n),ia(n),ncoll(n),lmax(n),idef(n),bandk(n),[def(j,n),
                                              j=2,idef(n),2]
       *****LOOP k=1,ncoll(n)
ex(k,n),spin(k,n),ipar(k,n)
       *****END k AND n LOOPS

    (2)*****SKIP TO (3)***** IF IMODEL NOT EQUAL TO 2

nisotopes
       *****LOOP n=1,nisotopes
iz(n),ia(n),nvib(n)
       *****LOOP k=1,nvib(n)
exv(k,n),spinv(k,n),iparv(k,n),nph(k,n),defv(k,n),thetm(k,n)
       *****END k LOOP
       *****END n LOOP

    (3)*****SKIP REMAINING LINES IF IMODEL NOT EQUAL TO 3

nisotopes
       *****LOOP n=1,nisotopes
iz(n),ia(n),beta0(n),gamma0(n),xmubeta(n)
       *****END n LOOP
```

Definitions

```
      iref  = unique fixed point reference number for this potential
    author  = authors for this potential (up to 80 characters, 1 line)
 reference  = reference for this potential (up to 80 characters, 1 line)
   summary = short description of the potential (320 characters, 4 lines)
 emin,emax  = minimum and maximum energies for validity of this potential
izmin,izmax = minimum and maximum Z values for this potential, where
              Z is the number of protons in the target nucleus.
iamin,iamax = minimum and maximum A values for this potential, where
              A = Z + N and N is the number of neutrons in the target.
    imodel  = 0 for spherical potential
            = 1 for coupled-channel, rotational model
            = 2 for vibrational model
            = 3 for non-axial deformed model
    izproj  = Z for incident projectile
    iaproj  = A for incident projectile
    irel    = 0 for non-relativistic parameterization
            = 1 for relativistic parameterization
    idr     = 0 dispersion relations not used
            = 1 dispersion relations with equivalent volume real
              potential used
            = 2 exact dispersion relations used, i.e., volume +
              surface real potential used. In this case the real surface
              potential is entered in the library as zero and must be
              supplied by a processing code.  This calculation is done
              in the om-retrieve code.
    index i = 1 real volume potential (Woods-Saxon)
            = 2 imaginary volume potential (Woods-Saxon)
            = 3 real surface derivative potential
            = 4 imaginary surface derivative potential
            = 5 real spin-orbit potential
            = 6 imaginary spin-orbit potential
    jrange  = number of energy ranges over which the potential is specified
            = positive for potential strengths
            = negative for volume integrals
            = 0 if potential of type i not used
  epot(i,j) = upper energy limit for jth energy range for potential i
  rco(i,j,k)= coefficients for multiplying A**(1/3) for
              specification of radius R in fm where:
     R(i,j) = {abs[rco(i,j,1)] + rco(i,j,2)*E + rco(i,j,3)*eta
             + rco(i,j,4)/A + rco(i,j,5)/sqrt(A)
             + rco(i,j,6)*A**(2/3) + rco(i,j,7)*A
             + rco(i,j,8)*A**2  + rco(i,j,9)*A**3
             + rco(i,j,10)*A**(1/3)
             + rco(i,j,11)*A**(-1/3)} * [A**(1/3)]
```

and

if rco(4,j,1) > 0.0: Woods-Saxon derivative surface potential
if rco(4,j,1) < 0.0: Gaussian surface potential.

[Note that the A dependence of rco(i,j,11) cancels out so that
rco(i,j,11) is equivalent to adding a constant of that magnitude
to the radius R(i,j)].

```
 aco(i,j,k) = coefficients for specification of diffuseness a in fm
              where:

     a(i,j) = abs(aco(i,j,1)) + aco(i,j,2)*E + aco(i,j,3)*eta
                + aco(i,j,4)/A + aco(i,j,5)/sqrt(A)
                + aco(i,j,6)*A**(2/3) + aco(i,j,7)*A
                + aco(i,j,8)*A**2 + aco(i,j,9)*A**3
```

```
               + aco(i,j,10)*A**(1/3) + aco(i,j,11)*A**(-1/3)

 pot(i,j,k) = strength parameters in MeV when aco(i,j,1)>0.
            = volume integral of strength in MeV-fm**3 when
              aco(i,j,1) < 0., and are given as follows:

if pot(i,j,k>21) .eq. 0, then    [standard form]

V(i,j) = pot(i,j,1) + pot(i,j,7)*eta + pot(i,j,8)*Ecoul1
       + pot(i,j,9)*A + pot(i,j,10)*A**(1/3)
       + pot(i,j,11)*A**(-2/3) + pot(i,j,12)*Ecoul2
       + [pot(i,j,2) + pot(i,j,13)*eta + pot(i,j,14)*A]*E
       + pot(i,j,3)*E*E + pot(i,j,4)*E*E*E + pot(i,j,6)*sqrt(E)
       + [pot(i,j,5) + pot(i,j,15)*eta + pot(i,j,16)*E]*ln(E)
       + pot(i,j,17)*Ecoul1/E**2

if pot(i,j,22) .ne. 0, then      [Smith form]

V(i,j) = pot(i,j,1) + pot(i,j,2)*eta
       + pot(i,j,3)*cos[2*pi*(A - pot(i,j,4))/pot(i,j,5)]
       + pot(i,j,6)*exp[pot(i,j,7)*E + pot(i,j,8)*E*E]
       + pot(i,j,9)*E*exp[pot(i,j,10)*E**pot(i,j,11)]

if pot(i,j,23) .ne. 0, then      [Varner form]

V(i,j) = [pot(i,j,1) + pot(i,j,2)*eta]/
       {1 + exp[(pot(i,j,3) - E + pot(i,j,4)*Ecoul2)/pot(i,j,5)]}
       + pot(i,j,6)*exp[(pot(i,j,7)*E - pot(i,j,8))/pot(i,j,6)]

if pot(i,j,24) .ne. 0, then      [Koning form]

V(i,j) =  b(i,j,1)*(1.- b(i,j,2)*(E-EF) + b(i,j,3)*(E-EF)**2
        - b(i,j,4)*(E-EF)**3) + b(i,j,5)
        + b(i,j,6)*((E-EF)**n(i,j)/((E-EF)**n(i,j) + b(i,j,7)**n(i,j)))
        + b(i,j,8)*exp(-b(i,j,9)*(E-EF))*((E-EF)**n(i,j)/
        ((E-EF)**n(i,j) + b(i,j,10)**n(i,j)))
        + b(i,j,11)*exp(-b(i,j,12)*(E-EF))

where
     E      = projectile laboratory energy in MeV
     eta    = (N-Z)/A
     Ecoul1 = 0.4Z/A**(1/3)
     Ecoul2 = 1.73*Z/RC
     EF     = Fermi energy in MeV [for above case when
              pot(i,j,24).ne.0. or when idr=2].
            = pot(i,j,18) + pot(i,j,19)*A

If pot(i,j,18) and pot(i,j,19) = 0., then
     EF     = -0.5*[SN(Z,A) + SN(Z,A+1)]   (for incident neutrons)
            = -0.5*[SP(Z,A) + SP(Z+1,A+1)] (for incident protons)

where
    SN(Z,A) = the neutron separation energy for nucleus (Z,A)
    SP(Z,A) = the proton separation energy for nucleus (Z,A).

For cases where idr=2:
     EP     = pot(i,j,20)
            = average energy of particle states.
              If pot(i,j,20)=0., then use default value of EP=EF.
     EA     = pot(i,j,21)
            = energy above which nonlocality of the absorptive potential
              will be assumed.
              If pot(i,j,21)=0., then use default value of EA=1000.

For pot(i,j,24).ne.0., the b(i,j,m) are defined as:
```

```
      b(i,j,m)  =  0 for i=1,6, j=1,jrange(i), m=1,12, except for
                   the following:
      b(1,j,1)  =  pot(1,j,1) + pot(1,j,2)*A + pot(1,j,8)*eta
      b(1,j,2)  =  pot(1,j,3) + pot(1,j,4)*A
      b(1,j,3)  =  pot(1,j,5) + pot(1,j,6)*A
      b(1,j,4)  =  pot(1,j,7)
      b(1,j,5)  =  pot(1,j,9)
      b(1,j,11) =  pot(1,j,10) + pot(1,j,11)*A
      b(1,j,12) =  pot(1,j,12)
      b(2,j,6)  =  pot(2,j,1) + pot(2,j,2)*A
      b(2,j,7)  =  pot(2,j,3) + pot(2,j,4)*A
      b(4,j,8)  =  pot(4,j,1) + pot(4,j,8)*eta
      b(4,j,9)  =  pot(4,j,2)
                  + pot(4,j,3)/(1. + exp((A-pot(4,j,4))/pot(4,j,5)))
      b(4,j,10) =  pot(4,j,6)
      b(5,j,11) =  pot(5,j,10) + pot(5,j,11)*A
      b(5,j,12) =  pot(5,j,12)
      b(6,j,6)  =  pot(6,j,1)
      b(6,j,7)  =  pot(6,j,3)
      n(i,j)    =  int(pot(i,j,13))
```

And, continuing the definitions:

```
    jcoul    = number of energy ranges for specifying coulomb
               radius and nonlocality range
   ecoul(j)  = maximum energy of coulomb energy range j
   rcoul0(j),rcoul(j),rcoul1(j),rcoul2(j) =
               coefficients to determine the coulomb radius, RC,
               from the expression
      RC     = [rcoul0(j)*A**(-1/3) + rcoul(j) + rcoul1(j)*A**(-2/3) +
                rcoul2(j)*A**(-5/3)] * A**(1/3)
    beta(j)  = nonlocality range.  Note that when beta(j).ne.0.,
               then the imaginary potential is pure derivative
               Woods-Saxon for energy range j.
  nisotopes  = number of isotopes for which deformation parameters
               and discrete levels are given
     iz,ia   = Z and A of the target associated with the deformation
               parameters and discrete levels that follow
     ncoll   = number of collective states in the coupled-channel
               rotational model for this iz, ia
       lmax  = maximum l value for multipole expansion
       idef  = largest order of deformation
      bandk  = k for the rotational band
        def  = deformation parameters, l=2,4,6,...through lmax
         ex  = rotational level excitation energy (MeV)
       spin  = rotational level spin
       ipar  = rotational level parity (+1 or -1)
       nvib  = number of vibrational states in the model for this
               iz, ia (first level must be ground state)
        exv  = vibrational level excitation energy (MeV)
      spinv  = vibrational level spin
      iparv  = vibrational level parity (+1 or -1)
        nph  = 1 for pure 1-phonon state
             = 2 for pure 2-phonon state
             = 3 for mixture of 1- and 2-phonon states
       defv  = vibrational model deformation parameter
      thetm  = mixing parameter (degrees) for nph=3
      beta0  = beta deformability parameter
     gamma0  = gamma deformability parameter
    xmubeta  = non-axiality parameter
```

ANNEX 5.B

REFERENCE NUMBERING SYSTEM FOR RIPL OPTICAL MODEL POTENTIALS

DEFINITION: IREF = 1000*I + JREF

Table 5.4: Incident Particles (leading digit, I).

IREF			I			Particle
1	-	3999	0	-	3	Neutrons
4000	-	5999	4	-	5	Protons
6000	-	6999		6		Deuterons
7000	-	7999		7		Tritons
8000	-	8999		8		He-3
9000	-	9999		9		He-4

Table 5.5: Geographic Indicators (trailing 3 digits, JREF).

JREF			Region
1	-	99	Los Alamos National Laboratory (LANL)
100	-	199	Other U.S. laboratories, universities
200	-	299	Japan, JAERI
300	-	399	Russia
400	-	499	Western Europe, JEF community
500	-	599	China
600	-	649	Former Soviet Union and Eastern Europe
650	-	699	India, Pakistan
700	-	799	Others
800	-	999	Reserved

ANNEX 5.C

EXAMPLE OF A POTENTIAL IN THE OPTICAL PARAMETER LIBRARY

```
5003
E.D.Arthur and C.Philis
Report LA-8630-PR, p.2 (1980)
Parameters are based on fits to 169Tm low-energy resonance data and total
cross sections, plus fits to 11-MeV neutron scattering on 165Ho. Lane
model used to relate n and p potentials.

     0.001  100.0000
   67   69
  165  169
    1    1    1    0    0
    1
   100.000
     1.26000  0.00000+0  0.00000+0  0.00000+0  0.00000+0  0.00000+0  0.00000+0
              0.00000+0  0.00000+0  0.00000+0  0.00000+0
     0.63000  0.00000+0  0.00000+0  0.00000+0  0.00000+0  0.00000+0  0.00000+0
              0.00000+0  0.00000+0  0.00000+0  0.00000+0
    49.80000 -2.50000-1  0.00000+0  0.00000+0  0.00000+0  0.00000+0  1.60000+1
              1.00000+0  0.00000+0  0.00000+0  0.00000+0  0.00000+0  0.00000+0
              0.00000+0  0.00000+0  0.00000+0  0.00000+0  0.00000+0  0.00000+0
              0.00000+0  0.00000+0  0.00000+0  0.00000+0  0.00000+0  0.00000+0
    2
     8.300
     1.26000  0.00000+0  0.00000+0  0.00000+0  0.00000+0  0.00000+0  0.00000+0
              0.00000+0  0.00000+0  0.00000+0  0.00000+0
     0.63000  0.00000+0  0.00000+0  0.00000+0  0.00000+0  0.00000+0  0.00000+0
              0.00000+0  0.00000+0  0.00000+0  0.00000+0
     0.00000  0.00000+0  0.00000+0  0.00000+0  0.00000+0  0.00000+0  0.00000+0
              0.00000+0  0.00000+0  0.00000+0  0.00000+0  0.00000+0  0.00000+0
              0.00000+0  0.00000+0  0.00000+0  0.00000+0  0.00000+0  0.00000+0
              0.00000+0  0.00000+0  0.00000+0  0.00000+0  0.00000+0  0.00000+0
   100.000
     1.26000  0.00000+0  0.00000+0  0.00000+0  0.00000+0  0.00000+0  0.00000+0
              0.00000+0  0.00000+0  0.00000+0  0.00000+0
     0.63000  0.00000+0  0.00000+0  0.00000+0  0.00000+0  0.00000+0  0.00000+0
              0.00000+0  0.00000+0  0.00000+0  0.00000+0
    -1.00000  1.20000-1  0.00000+0  0.00000+0  0.00000+0  0.00000+0  0.00000+0
              0.00000+0  0.00000+0  0.00000+0  0.00000+0  0.00000+0  0.00000+0
              0.00000+0  0.00000+0  0.00000+0  0.00000+0  0.00000+0  0.00000+0
              0.00000+0  0.00000+0  0.00000+0  0.00000+0  0.00000+0  0.00000+0
    0
    2
     6.500
     1.26000  0.00000+0  0.00000+0  0.00000+0  0.00000+0  0.00000+0  0.00000+0
              0.00000+0  0.00000+0  0.00000+0  0.00000+0
     0.48000  0.00000+0  0.00000+0  0.00000+0  0.00000+0  0.00000+0  0.00000+0
              0.00000+0  0.00000+0  0.00000+0  0.00000+0
     5.02000  5.10000-1  0.00000+0  0.00000+0  0.00000+0  0.00000+0  8.00000+0
              0.00000+0  0.00000+0  0.00000+0  0.00000+0  0.00000+0  0.00000+0
              0.00000+0  0.00000+0  0.00000+0  0.00000+0  0.00000+0  0.00000+0
              0.00000+0  0.00000+0  0.00000+0  0.00000+0  0.00000+0  0.00000+0
   100.000
     1.26000  0.00000+0  0.00000+0  0.00000+0  0.00000+0  0.00000+0  0.00000+0
              0.00000+0  0.00000+0  0.00000+0  0.00000+0
     0.48000  0.00000+0  0.00000+0  0.00000+0  0.00000+0  0.00000+0  0.00000+0
              0.00000+0  0.00000+0  0.00000+0  0.00000+0
     8.93300 -9.20000-2  0.00000+0  0.00000+0  0.00000+0  0.00000+0  8.00000+0
              0.00000+0  0.00000+0  0.00000+0  0.00000+0  0.00000+0  0.00000+0
              0.00000+0  0.00000+0  0.00000+0  0.00000+0  0.00000+0  0.00000+0
              0.00000+0  0.00000+0  0.00000+0  0.00000+0  0.00000+0  0.00000+0
    1
```

```
  100.000
    1.26000  0.00000+0  0.00000+0  0.00000+0  0.00000+0  0.00000+0  0.00000+0
             0.00000+0  0.00000+0  0.00000+0  0.00000+0
    0.63000  0.00000+0  0.00000+0  0.00000+0  0.00000+0  0.00000+0  0.00000+0
             0.00000+0  0.00000+0  0.00000+0  0.00000+0
    6.00000  0.00000+0  0.00000+0  0.00000+0  0.00000+0  0.00000+0  0.00000+0
             0.00000+0  0.00000+0  0.00000+0  0.00000+0  0.00000+0  0.00000+0
             0.00000+0  0.00000+0  0.00000+0  0.00000+0  0.00000+0  0.00000+0
             0.00000+0  0.00000+0  0.00000+0  0.00000+0  0.00000+0  0.00000+0
     0
     1
   100.000    0.0000    1.2500    0.0000    0.0000    0.0000
     2
    67  165    3    4    4  3.5  3.000E-01 -2.000E-02
  0.00000000    3.5  -1
  0.09470000    4.5  -1
  0.20980000    5.5  -1
    69  169    5    4    4  0.5  2.900E-01 -1.000E-02
  0.00000000    0.5   1
  0.00842000    1.5   1
  0.11810000    2.5   1
  0.13890000    3.5   1
  0.33190000    4.5   1
++++++++++++++++++++++++++++++++++++++++++++++++++++++++++++++++++++++++++++++++++++
```

ANNEX 5.D

SUMMARY OF ENTRIES AND REFERENCES INCLUDED IN THE RIPL-2 OPTICAL MODEL POTENTIAL LIBRARY

This annex contains a summary of the optical model parameterizations that are included in the user version of the RIPL-2 optical model potential ibrary. The results are given in tabular form, with each entry summarized in a single line and with a complete list of the references included in the library (as defined by Ref. No.). The table and reference list were obtained using the **om-summary.f** computer code, which is included in the *RIPL-2/optical/om-get* directory.

Lib. No.	Inc. Part.	Model Type	Disp Pot	Rel Pot	Z-Range	A-Range	E-Range (MeV)	Ref. No.	First Author
15	n	spher.	no	no	6- 6	12- 12	0.0- 65.0	1	M.B.Chadwick
2001	n	spher.	no	yes	6-82	12-208	50.0-400.0	2	D.G.Madland
16	n	spher.	no	no	7- 7	14- 14	0.0- 60.0	1	M.B.Chadwick
136	n	spher.	no	no	7- 7	14- 14	18.0- 60.0	3	M.S.Islam
17	n	spher.	no	no	8- 8	16- 16	0.0- 50.0	1	M.B.Chadwick
137	n	spher.	no	no	8- 8	16- 16	18.0- 60.0	3	M.S.Islam
101	n	spher.	no	no	12-83	24-209	11.0- 11.0	4	J.C.Ferrer
1400	n	spher.	no	yes	12-12	24- 24	0.0-200.0	5	A.J.Koning
1401	n	spher.	no	yes	12-12	26- 26	0.0-200.0	5	A.J.Koning
18	n	spher.	no	no	13-13	27- 27	0.0- 20.0	6	R.C.Harper
430	n	spher.	no	no	13-82	27-208	0.1- 24.0	7	O.Bersillon
117	n	spher.	no	no	13-13	27- 27	0.0- 60.0	8	J.Petler
243	n	spher.	no	no	13-47	27-109	0.0- 80.0	9	N.Yamamuro
419	n	spher.	yes	no	13-13	27- 27	0.0-150.0	10	A. Molina
1402	n	spher.	no	yes	13-13	27- 27	0.0-200.0	5	A.J.Koning
2405	n	spher.	no	yes	13-83	27-209	0.0-200.0	11	A.J.Koning
242	n	spher.	no	no	13-13	27- 27	0.0-250.0	12	Lee
418	n	spher.	yes	yes	13-13	27- 27	0.0-250.0	10	A. Molina
1403	n	spher.	no	yes	14-14	28- 28	0.0-200.0	5	A.J.Koning
1404	n	spher.	no	yes	15-15	31- 31	0.0-200.0	5	A.J.Koning
1405	n	spher.	no	yes	16-16	32- 32	0.0-200.0	5	A.J.Koning
1406	n	spher.	no	yes	17-17	35- 35	0.0-200.0	5	A.J.Koning
1408	n	spher.	no	yes	18-18	40- 40	0.0-200.0	5	A.J.Koning
1407	n	spher.	no	yes	19-19	39- 39	0.0-200.0	5	A.J.Koning
116	n	spher.	no	no	20-83	40-209	0.0- 5.0	13	P.A.Moldauer
401	n	spher.	no	no	20-92	40-238	0.0- 25.0	14	D.Wilmore
2100	n	spher.	no	no	20-83	40-209	10.0- 26.0	15	R.L.Varner
100	n	spher.	no	no	20-92	40-238	10.0- 50.0	16	F.D.Becchetti
138	n	spher.	no	no	20-20	40- 40	18.0- 60.0	3	M.S.Islam
800	n	spher.	no	no	20-83	40-210	0.0-155.0	17	C.A.Engelbrecht
1409	n	spher.	no	yes	20-20	40- 40	0.0-200.0	5	A.J.Koning
1410	n	spher.	no	yes	21-21	45- 45	0.0-200.0	5	A.J.Koning
133	n	spher.	no	no	22-22	44- 50	0.1- 20.0	18	D.W.Muir
1411	n	spher.	no	yes	22-22	48- 48	0.0-200.0	5	A.J.Koning
134	n	spher.	no	no	23-23	50- 51	0.1- 20.0	18	D.W.Muir
404	n	spher.	no	no	23-41	50- 95	0.0- 30.0	19	B.Strohmaier

1412	n	spher.	no	yes	23-23	51- 51	0.0-200.0	5	A.J.Koning
112	n	spher.	no	no	24-24	50- 50	0.0-100.0	20	A.Prince
114	n	spher.	no	no	24-24	52- 52	0.0-100.0	20	A.Prince
1413	n	spher.	no	yes	24-24	52- 52	0.0-200.0	5	A.J.Koning
113	n	spher.	no	no	24-24	53- 53	0.0-100.0	20	A.Prince
115	n	spher.	no	no	24-24	54- 54	0.0-100.0	20	A.Prince
1415	n	spher.	no	yes	25-25	55- 55	0.0-200.0	5	A.J.Koning
125	n	spher.	no	no	26-26	54- 54	8.0- 14.0	21	S.M.El-Kadi
428	n	vibra.	no	no	26-26	54- 56	0.1- 14.0	22	J.P.Delaroche
129	n	spher.	no	no	26-29	54- 65	8.0- 30.0	21	S.M.El-Kadi
130	n	spher.	no	no	26-29	54- 65	8.0- 30.0	21	S.M.El-Kadi
10	n	spher.	no	no	26-26	54- 56	0.0- 52.0	23	E.D.Arthur
2101	n	spher.	no	no	26-82	54-208	10.0- 80.0	24	R.L.Walter
104	n	spher.	no	no	26-26	54- 54	0.0-100.0	20	A.Prince
1414	n	spher.	no	yes	26-26	54- 54	0.0-200.0	5	A.J.Koning
126	n	spher.	no	no	26-26	56- 56	8.0- 14.0	21	S.M.El-Kadi
103	n	spher.	no	no	26-26	56- 56	0.0-100.0	20	A.Prince
1416	n	spher.	no	yes	26-26	56- 56	0.0-200.0	5	A.J.Koning
105	n	spher.	no	no	26-26	57- 57	0.0-100.0	20	A.Prince
106	n	spher.	no	no	26-26	58- 58	0.0-100.0	20	A.Prince
11	n	spher.	no	no	27-27	59- 59	0.0- 27.5	25	E.D.Arthur
1419	n	spher.	no	yes	27-27	59- 59	0.0-200.0	5	A.J.Koning
19	n	spher.	no	no	28-28	58- 58	0.0- 20.0	6	R.C.Harper
131	n	vibra.	no	no	28-28	58- 60	0.0- 80.0	26	P.P.Guss
132	n	spher.	no	no	28-28	58- 60	0.0- 80.0	26	P.P.Guss
107	n	spher.	no	no	28-28	58- 58	0.0-100.0	20	A.Prince
1417	n	spher.	no	yes	28-28	58- 58	0.0-200.0	5	A.J.Koning
108	n	spher.	no	no	28-28	60- 60	0.0-100.0	20	A.Prince
1418	n	spher.	no	yes	28-28	60- 60	0.0-200.0	5	A.J.Koning
109	n	spher.	no	no	28-28	61- 61	0.0-100.0	20	A.Prince
110	n	spher.	no	no	28-28	62- 62	0.0-100.0	20	A.Prince
111	n	spher.	no	no	28-28	64- 64	0.0-100.0	20	A.Prince
127	n	spher.	no	no	29-29	63- 63	8.0- 14.0	21	S.M.El-Kadi
429	n	vibra.	no	no	29-29	63- 65	0.1- 14.0	22	J.P.Delaroche
1420	n	spher.	no	yes	29-29	63- 63	0.0-200.0	5	A.J.Koning
128	n	spher.	no	no	29-29	65- 65	8.0- 14.0	21	S.M.El-Kadi
1421	n	spher.	no	yes	29-29	65- 65	0.0-200.0	5	A.J.Koning
12	n	spher.	no	no	30-30	57- 81	0.0- 20.0	27	P.G.Young
200	n	spher.	no	no	31-69	69-146	0.0- 20.0	28	S.Igarasi
240	n	spher.	no	no	31-69	69-146	0.0- 20.0	29	S.Igarasi
500	n	spher.	no	no	31-31	69- 69	0.1- 20.0	30	Zhang
1422	n	spher.	no	yes	31-31	69- 69	0.0-200.0	5	A.J.Koning
1423	n	spher.	no	yes	32-32	74- 74	0.0-200.0	5	A.J.Koning
202	n	spher.	no	no	33-37	61-107	0.0- 20.0	31	Japan
1424	n	spher.	no	yes	33-33	75- 75	0.0-200.0	5	A.J.Koning
1425	n	spher.	no	yes	33-33	79- 79	0.0-200.0	5	A.J.Koning
1426	n	spher.	no	yes	34-34	80- 80	0.0-200.0	5	A.J.Koning
501	n	spher.	no	no	36-36	83- 83	0.1- 20.0	32	Cai
502	n	spher.	no	no	36-36	86- 86	0.1- 20.0	33	Cai
503	n	spher.	no	no	37-37	85- 85	0.1- 20.0	32	Cai
1427	n	spher.	no	yes	37-37	85- 85	0.0-200.0	5	A.J.Koning
203	n	spher.	no	no	38-42	69-116	0.0- 20.0	31	Japan
504	n	spher.	no	no	38-38	88- 88	0.1- 20.0	32	Cai
1428	n	spher.	no	yes	38-38	88- 88	0.0-200.0	5	A.J.Koning
118	n	spher.	no	no	39-51	85-125	0.0- 5.0	34	A.B.Smith
505	n	spher.	no	no	39-39	89- 89	0.1- 20.0	32	Cai
13	n	spher.	no	no	39-39	89- 89	0.0- 21.0	35	E.D.Arthur
1429	n	spher.	no	yes	39-39	89- 89	0.0-200.0	5	A.J.Koning
506	n	spher.	no	no	39-39	91- 91	0.1- 20.0	36	Cai
14	n	spher.	no	no	40-40	90- 90	0.0- 20.0	37	E.D.Arthur
1430	n	spher.	no	yes	40-40	90- 90	0.0-200.0	5	A.J.Koning
2404	n	spher.	no	no	40-40	90- 90	0.0-200.0	38	A.J.Koning
1431	n	spher.	no	yes	40-40	91- 91	0.0-200.0	5	A.J.Koning
1432	n	spher.	no	yes	40-40	92- 92	0.0-200.0	5	A.J.Koning
1435	n	spher.	no	yes	40-40	94- 94	0.0-200.0	5	A.J.Koning

20	n	spher.	no	no	41-41	93- 93	0.0- 20.0	6	R.C.Harper
507	n	spher.	no	no	41-41	93- 93	0.1- 20.0	39	Rong
1434	n	spher.	no	yes	41-41	93- 93	0.0-200.0	5	A.J.Koning
508	n	spher.	no	no	41-41	95- 95	0.1- 20.0	39	Rong
422	n	spher.	no	no	42-42	92-100	0.0- 20.0	40	Ch.Lagrange
1433	n	spher.	no	yes	42-42	92- 92	0.0-200.0	5	A.J.Koning
1436	n	spher.	no	yes	42-42	94- 94	0.0-200.0	5	A.J.Koning
509	n	spher.	no	no	42-42	95- 95	0.1- 20.0	41	Cai
1437	n	spher.	no	yes	42-42	96- 96	0.0-200.0	5	A.J.Koning
510	n	spher.	no	no	42-42	97- 97	0.1- 20.0	42	Cai
511	n	spher.	no	no	42-42	98- 98	0.1- 20.0	42	Cai
1438	n	spher.	no	yes	42-42	98- 98	0.0-200.0	5	A.J.Koning
512	n	spher.	no	no	42-42	100-100	0.1- 20.0	33	Cai
1440	n	spher.	no	yes	42-42	100-100	0.0-200.0	5	A.J.Koning
204	n	spher.	no	no	43-45	80-125	0.0- 20.0	31	Japan
513	n	spher.	no	no	43-43	99- 99	0.1- 20.0	36	Cai
1439	n	spher.	no	yes	43-43	99- 99	0.0-200.0	5	A.J.Koning
514	n	spher.	no	no	44-44	99- 99	0.1- 20.0	43	Zhang
515	n	spher.	no	no	44-44	100-100	0.1- 20.0	43	Zhang
516	n	spher.	no	no	44-44	101-101	0.1- 20.0	44	Zhang
517	n	spher.	no	no	44-44	102-102	0.1- 20.0	43	Zhang
518	n	spher.	no	no	44-44	103-103	0.1- 20.0	44	Zhang
519	n	spher.	no	no	44-44	104-104	0.1- 20.0	43	Zhang
520	n	spher.	no	no	44-44	105-105	0.1- 20.0	43	Zhang
521	n	spher.	no	no	45-45	103-103	0.1- 20.0	43	Zhang
1441	n	spher.	no	yes	45-45	103-103	0.0-200.0	5	A.J.Koning
522	n	spher.	no	no	45-45	105-105	0.1- 20.0	43	Zhang
205	n	spher.	no	no	46-48	89-134	0.0- 20.0	31	Japan
523	n	spher.	no	no	46-46	105-105	0.1- 20.0	45	Zhang
1442	n	spher.	no	yes	46-46	106-106	0.0-200.0	5	A.J.Koning
524	n	spher.	no	no	46-46	108-108	0.1- 20.0	45	Zhang
1443	n	spher.	no	yes	47-47	107-107	0.0-200.0	5	A.J.Koning
525	n	spher.	no	no	48-48	113-113	0.1- 20.0	46	Zhang
1444	n	spher.	no	yes	48-48	114-114	0.0-200.0	5	A.J.Koning
206	n	spher.	no	no	49-51	97-141	0.0- 20.0	31	Japan
526	n	spher.	no	no	49-49	115-115	0.1- 20.0	46	Zhang
1445	n	spher.	no	yes	49-49	115-115	0.0-200.0	5	A.J.Koning
1446	n	spher.	no	yes	50-50	116-116	0.0-200.0	5	A.J.Koning
1447	n	spher.	no	yes	50-50	118-118	0.0-200.0	5	A.J.Koning
1448	n	spher.	no	yes	50-50	120-120	0.0-200.0	5	A.J.Koning
1450	n	spher.	no	yes	50-50	122-122	0.0-200.0	5	A.J.Koning
1452	n	spher.	no	yes	50-50	124-124	0.0-200.0	5	A.J.Koning
527	n	spher.	no	no	51-51	121-121	0.1- 20.0	46	Zhang
1449	n	spher.	no	yes	51-51	121-121	0.0-200.0	5	A.J.Koning
528	n	spher.	no	no	51-51	123-123	0.1- 20.0	46	Zhang
1451	n	spher.	no	yes	51-51	123-123	0.0-200.0	5	A.J.Koning
207	n	spher.	no	no	52-54	103-150	0.0- 20.0	31	Japan
1454	n	spher.	no	yes	52-52	128-128	0.0-200.0	5	A.J.Koning
529	n	spher.	no	no	52-52	130-130	0.1- 20.0	45	Zhang
530	n	spher.	no	no	53-53	127-127	0.1- 20.0	45	Zhang
1453	n	spher.	no	yes	53-53	127-127	0.0-200.0	5	A.J.Koning
531	n	spher.	no	no	53-53	135-135	0.1- 20.0	45	Zhang
532	n	spher.	no	no	54-54	123-123	0.1- 20.0	47	Shen
533	n	spher.	no	no	54-54	124-124	0.1- 20.0	47	Shen
534	n	spher.	no	no	54-54	129-129	0.1- 20.0	48	Shen
535	n	spher.	no	no	54-54	131-131	0.1- 20.0	48	Shen
536	n	spher.	no	no	54-54	132-132	0.1- 20.0	48	Shen
537	n	spher.	no	no	54-54	134-134	0.1- 20.0	48	Shen
538	n	spher.	no	no	54-54	135-135	0.1- 20.0	48	Shen
539	n	spher.	no	no	54-54	136-136	0.1- 20.0	48	Shen
208	n	spher.	no	no	55-55	111-153	0.0- 20.0	31	Japan
540	n	spher.	no	no	55-55	133-133	0.1- 20.0	43	Zhang
1455	n	spher.	no	yes	55-55	133-133	0.0-200.0	5	A.J.Koning
541	n	spher.	no	no	55-55	134-134	0.1- 20.0	43	Zhang
542	n	spher.	no	no	55-55	135-135	0.1- 20.0	43	Zhang

543	n	spher.	no	no	55-55	137-137	0.1- 20.0	43	Zhang
209	n	spher.	no	no	56-56	112-154	0.0- 20.0	31	Japan
544	n	spher.	no	no	56-56	135-135	0.1- 20.0	43	Zhang
545	n	spher.	no	no	56-56	136-136	0.1- 20.0	43	Zhang
546	n	spher.	no	no	56-56	137-137	0.1- 20.0	43	Zhang
547	n	spher.	no	no	56-56	138-138	0.1- 20.0	43	Zhang
1456	n	spher.	no	yes	56-56	138-138	0.0-200.0	5	A.J.Koning
210	n	spher.	no	no	57-58	117-156	0.0- 20.0	31	Japan
548	n	spher.	no	no	57-57	139-139	0.1- 20.0	43	Zhang
1457	n	spher.	no	yes	57-57	139-139	0.0-200.0	5	A.J.Koning
549	n	spher.	no	no	58-58	140-140	0.1- 20.0	43	Zhang
1458	n	spher.	no	yes	58-58	140-140	0.0-200.0	5	A.J.Koning
550	n	spher.	no	no	58-58	141-141	0.1- 20.0	43	Zhang
551	n	spher.	no	no	58-58	142-142	0.1- 20.0	43	Zhang
552	n	spher.	no	no	58-58	144-144	0.1- 20.0	43	Zhang
211	n	spher.	no	no	59-59	119-160	0.0- 20.0	31	Japan
553	n	spher.	no	no	59-59	141-141	0.1- 20.0	47	Shen
1459	n	spher.	no	yes	59-59	141-141	0.0-200.0	5	A.J.Koning
212	n	spher.	no	no	60-60	141-143	0.0- 20.0	31	Japan
420	n	vibra.	no	no	60-60	142-148	0.0- 15.0	49	G.Haouat
554	n	spher.	no	no	60-60	142-142	0.1- 20.0	47	Shen
1460	n	spher.	no	yes	60-60	142-142	0.0-200.0	5	A.J.Koning
555	n	spher.	no	no	60-60	143-143	0.1- 20.0	47	Shen
213	n	spher.	no	no	60-60	144-148	0.0- 20.0	31	Japan
556	n	spher.	no	no	60-60	144-144	0.1- 20.0	47	Shen
1461	n	spher.	no	yes	60-60	144-144	0.0-200.0	5	A.J.Koning
557	n	spher.	no	no	60-60	145-145	0.1- 20.0	47	Shen
558	n	spher.	no	no	60-60	146-146	0.1- 20.0	47	Shen
559	n	spher.	no	no	60-60	147-147	0.1- 20.0	47	Shen
421	n	CC rot.	no	no	60-60	148-150	0.0- 15.0	49	G.Haouat
560	n	spher.	no	no	60-60	148-148	0.1- 20.0	47	Shen
214	n	spher.	no	no	60-60	150-999	0.0- 20.0	31	Japan
561	n	spher.	no	no	60-60	150-150	0.1- 20.0	47	Shen
215	n	spher.	no	no	61-61	147-999	0.0- 20.0	31	Japan
562	n	spher.	no	no	61-61	147-147	0.1- 20.0	47	Shen
563	n	spher.	no	no	61-61	148-148	0.1- 20.0	47	Shen
564	n	spher.	no	no	61-61	149-149	0.1- 20.0	47	Shen
216	n	spher.	no	no	62-62	144-144	0.0- 20.0	31	Japan
565	n	spher.	no	no	62-62	144-144	0.1- 20.0	47	Shen
217	n	spher.	no	no	62-62	147-147	0.0- 20.0	31	Japan
566	n	spher.	no	no	62-62	147-147	0.1- 20.0	47	Shen
123	n	vibra.	no	no	62-62	148-150	0.0- 15.0	50	M.T.McEllistrem
218	n	spher.	no	no	62-62	148-148	0.0- 20.0	31	Japan
567	n	spher.	no	no	62-62	148-148	0.1- 20.0	47	Shen
1462	n	spher.	no	yes	62-62	148-148	0.0-200.0	5	A.J.Koning
219	n	spher.	no	no	62-62	149-149	0.0- 20.0	31	Japan
568	n	spher.	no	no	62-62	149-149	0.1- 20.0	47	Shen
124	n	CC rot.	no	no	62-62	150-152	0.0- 15.0	50	M.T.McEllistrem
220	n	spher.	no	no	62-62	150-150	0.0- 20.0	31	Japan
569	n	spher.	no	no	62-62	150-150	0.1- 20.0	47	Shen
570	n	spher.	no	no	62-62	151-151	0.1- 20.0	47	Shen
571	n	spher.	no	no	62-62	152-152	0.1- 20.0	47	Shen
572	n	spher.	no	no	62-62	154-154	0.1- 20.0	47	Shen
221	n	spher.	no	no	63-63	151-999	0.0- 20.0	31	Japan
573	n	spher.	no	no	63-63	151-151	0.1- 20.0	51	Ge
2004	n	CC rot.	no	no	63-63	151-153	0.0- 20.0	52	R.Macklin
574	n	spher.	no	no	63-63	153-153	0.1- 20.0	51	Ge
575	n	spher.	no	no	63-63	154-154	0.1- 20.0	51	Ge
576	n	spher.	no	no	63-63	155-155	0.1- 20.0	51	Ge
222	n	spher.	no	no	64-64	133-171	0.0- 20.0	31	Japan
577	n	spher.	no	no	64-64	152-152	0.1- 20.0	47	Shen
578	n	spher.	no	no	64-64	154-154	0.1- 20.0	47	Shen
579	n	spher.	no	no	64-64	155-155	0.1- 20.0	47	Shen
580	n	spher.	no	no	64-64	156-156	0.1- 20.0	47	Shen
581	n	spher.	no	no	64-64	157-157	0.1- 20.0	47	Shen

582	n	spher.	no	no	64-64	158-158	0.1- 20.0	47	Shen
583	n	spher.	no	no	64-64	160-160	0.1- 20.0	47	Shen
223	n	spher.	no	no	65-65	138-175	0.0- 20.0	31	Japan
584	n	spher.	no	no	66-66	164-164	0.1- 20.0	53	Ge
119	n	CC rot.	no	no	67-67	165-165	0.0- 30.0	54	A.B.Smith
120	n	CC rot.	yes	no	67-67	165-165	0.0- 30.0	54	A.B.Smith
2007	n	CC rot.	no	no	67-69	165-169	0.0- 30.0	55	P.G.Young
2003	n	CC rot.	no	no	67-69	165-169	0.0-100.0	56	E.D.Arthur
201	n	spher.	no	no	69-74	147-186	0.0- 20.0	28	S.Igarasi
241	n	spher.	no	no	69-74	147-186	0.0- 20.0	29	S.Igarasi
585	n	spher.	no	no	69-69	169-169	0.1- 20.0	53	Ge
586	n	spher.	no	no	71-71	174-174	0.1- 20.0	57	Han
587	n	spher.	no	no	71-71	175-175	0.1- 20.0	57	Han
423	n	CC rot.	no	no	74-74	182-186	0.0- 9.0	58	J.P.Delaroche
2406	n	CC rot.	no	no	74-74	182-186	0.0- 16.0	58	J.P.Delaroche
403	n	spher.	no	no	74-74	182-186	0.0- 30.0	59	J.P.Delaroche
2002	n	CC rot.	no	no	74-74	182-186	0.0-100.0	60	P.G.Young
2005	n	CC rot.	no	no	75-75	185-187	0.0- 20.0	61	R.Macklin
1463	n	spher.	no	yes	78-78	194-194	0.0-200.0	5	A.J.Koning
21	n	spher.	no	no	79-79	197-197	0.0- 20.0	6	R.C.Harper
400	n	CC rot.	no	no	79-79	197-197	0.0- 57.0	62	J.P.Delaroche
1464	n	spher.	no	yes	79-79	197-197	0.0-200.0	5	A.J.Koning
1465	n	spher.	no	yes	80-80	202-202	0.0-200.0	5	A.J.Koning
102	n	spher.	no	no	82-82	206-208	5.0- 50.0	63	R.W.Finlay
121	n	spher.	yes	yes	82-82	208-208	0.0- 80.0	64	Weisel
2	n	vibra.	no	no	82-82	208-208	0.0-200.0	65	H.Vonach
1466	n	spher.	no	yes	82-82	208-208	0.0-200.0	5	A.J.Koning
402	n	spher.	no	no	83-83	209-209	0.0- 30.0	66	O.Bersillon
122	n	spher.	yes	yes	83-83	209-209	0.0- 80.0	64	Weisel
1467	n	spher.	no	yes	83-83	209-209	0.0-200.0	5	A.J.Koning
9	n	spher.	no	no	90-95	230-250	0.0- 10.0	67	D.G.Madland
408	n	CC rot.	no	no	90-90	230-232	0.0- 20.0	68	Ch.Lagrange
414	n	CC rot.	no	no	90-90	232-232	0.0- 20.0	69	G.Haouat
600	n	CC rot.	no	no	90-95	232-242	0.0- 20.0	70	G.Vladuca
409	n	CC rot.	no	no	92-92	234-234	0.0- 20.0	68	Ch.Lagrange
415	n	CC rot.	no	no	92-92	235-235	0.0- 20.0	69	G.Haouat
3	n	CC rot.	no	no	92-92	235-235	0.0- 30.0	71	P.G.Young
4	n	CC rot.	no	no	92-92	237-237	0.0- 30.0	72	P.G.Young
410	n	CC rot.	no	no	92-92	238-238	0.0- 20.0	68	Ch.Lagrange
416	n	CC rot.	no	no	92-94	238-239	0.0- 20.0	69	G.Haouat
5	n	CC rot.	no	no	92-92	238-238	0.0- 30.0	72	P.G.Young
2006	n	CC rot.	no	no	92-92	238-238	0.0-200.0	73	P.G.Young
2300	n	CC rot.	no	yes	92-92	238-238	0.0-200.0	74	A.V.Ignatyuk
1	n	CC rot.	no	no	93-93	237-237	0.0- 30.0	71	P.G.Young
406	n	CC rot.	no	no	94-94	236-244	0.0- 20.0	75	Ch.Lagrange
7	n	CC rot.	no	no	94-94	239-239	0.0- 30.0	72	P.G.Young
6	n	CC rot.	no	no	94-94	242-242	0.0- 20.0	76	D.G.Madland
411	n	CC rot.	no	no	94-94	242-242	0.0- 20.0	68	Ch.Lagrange
417	n	CC rot.	no	no	94-94	242-242	0.0- 20.0	69	G.Haouat
8	n	CC rot.	no	no	95-95	241-243	0.0- 30.0	77	P.G.Young
412	n	CC rot.	no	no	96-96	246-246	0.0- 20.0	68	Ch.Lagrange
413	n	CC rot.	no	no	98-98	252-252	0.0- 20.0	68	Ch.Lagrange
4102	p	spher.	no	no	6-82	12-208	30.0- 60.0	78	J.J.H.Menet
4015	p	spher.	no	no	6- 6	12- 12	0.0- 65.0	79	M.B.Chadwick
5001	p	spher.	no	yes	6-82	12-208	50.0-400.0	2	D.G.Madland
4016	p	spher.	no	no	7- 7	14- 14	0.0- 70.0	79	M.B.Chadwick
4017	p	spher.	no	no	8- 8	16- 16	0.0- 50.0	79	M.B.Chadwick
4131	p	spher.	no	yes	12-82	24-208	80.0-180.0	80	P.Schwandt
4018	p	spher.	no	no	13-13	27- 27	0.1- 20.0	6	R.C.Harper
4416	p	spher.	no	yes	13-13	27- 27	0.0-200.0	5	A.J.Koning
5405	p	spher.	no	yes	13-83	27-209	0.0-200.0	11	A.J.Koning
4417	p	spher.	no	yes	14-14	28- 28	0.0-200.0	5	A.J.Koning
4100	p	spher.	no	no	16-49	30-100	0.0- 22.0	81	F.G.Perey
4660	p	spher.	no	no	19-19	41- 41	1.0- 7.0	82	Y.P.Viyogi

4101	p	spher.	no	no	20-83	40-209	10.0- 50.0	83	F.D.Becchetti
5100	p	spher.	no	no	20-83	40-209	16.0- 65.0	15	R.L.Varner
4418	p	spher.	no	yes	20-20	40- 40	0.0-200.0	5	A.J.Koning
4651	p	spher.	no	no	20-20	48- 48	3.0- 5.0	84	S.Kailas
4662	p	spher.	no	no	20-20	48- 48	1.0- 7.0	82	Y.P.Viyogi
4108	p	spher.	no	no	20-82	48-208	25.0- 45.0	85	D.M.Patterson
4650	p	spher.	no	no	21-21	45- 45	3.0- 5.0	84	S.Kailas
4661	p	spher.	no	no	21-21	45- 45	1.0- 7.0	82	Y.P.Viyogi
4663	p	spher.	no	no	22-22	49- 49	1.0- 7.0	82	Y.P.Viyogi
4652	p	spher.	no	no	23-23	51- 51	3.0- 5.0	84	S.Kailas
4664	p	spher.	no	no	23-23	51- 51	1.0- 7.0	82	Y.P.Viyogi
4653	p	spher.	no	no	24-24	54- 54	3.0- 5.0	84	S.Kailas
4000	p	spher.	no	no	25-26	54- 56	0.0- 28.0	23	E.D.Arthur
4665	p	spher.	no	no	25-25	55- 55	1.0- 7.0	82	Y.P.Viyogi
5101	p	spher.	no	no	26-82	54-208	10.0- 80.0	86	R.L.Walter
4419	p	spher.	no	yes	26-26	54- 54	0.0-200.0	5	A.J.Koning
4420	p	spher.	no	yes	26-26	56- 56	0.0-200.0	5	A.J.Koning
4001	p	spher.	no	no	26-27	59- 59	0.0- 23.0	87	E.D.Arthur
4654	p	spher.	no	no	27-27	59- 59	3.0- 5.0	84	S.Kailas
4666	p	spher.	no	no	27-27	59- 59	1.0- 7.0	82	Y.P.Viyogi
4019	p	spher.	no	no	28-28	58- 58	0.1- 20.0	6	R.C.Harper
4421	p	spher.	no	yes	28-28	58- 58	0.0-200.0	5	A.J.Koning
4422	p	spher.	no	yes	28-28	60- 60	0.0-200.0	5	A.J.Koning
4655	p	spher.	no	no	28-28	61- 61	3.0- 5.0	84	S.Kailas
4667	p	spher.	no	no	28-28	61- 61	1.0- 7.0	82	Y.P.Viyogi
4423	p	spher.	no	yes	28-28	62- 62	0.0-200.0	5	A.J.Koning
4425	p	spher.	no	yes	28-28	64- 64	0.0-200.0	5	A.J.Koning
4424	p	spher.	no	yes	29-29	63- 63	0.0-200.0	5	A.J.Koning
4656	p	spher.	no	no	29-29	65- 65	3.0- 5.0	84	S.Kailas
4668	p	spher.	no	no	29-29	65- 65	1.0- 7.0	82	Y.P.Viyogi
4669	p	spher.	no	no	30-30	68- 68	1.0- 7.0	82	Y.P.Viyogi
4657	p	spher.	no	no	31-31	71- 71	3.0- 5.0	84	S.Kailas
4670	p	spher.	no	no	31-31	71- 71	1.0- 7.0	82	Y.P.Viyogi
4658	p	spher.	no	no	33-33	75- 75	3.0- 5.0	84	S.Kailas
4671	p	spher.	no	no	33-33	75- 75	1.0- 7.0	82	Y.P.Viyogi
4659	p	spher.	no	no	34-34	80- 80	3.0- 5.0	84	S.Kailas
4672	p	spher.	no	no	34-34	80- 80	1.0- 7.0	82	Y.P.Viyogi
4002	p	spher.	no	no	38-38	88- 89	0.0- 21.0	35	E.D.Arthur
4109	p	spher.	no	no	39-39	89- 89	1.0- 7.0	88	C.H.Johnson
4673	p	spher.	no	no	39-39	89- 89	1.0- 7.0	82	Y.P.Viyogi
4003	p	spher.	no	no	39-39	89- 89	0.0- 21.0	35	E.D.Arthur
4426	p	spher.	no	yes	40-40	90- 90	0.0-200.0	5	A.J.Koning
5404	p	spher.	no	no	40-40	90- 90	0.0-200.0	38	A.J.Koning
4125	p	spher.	no	no	40-40	92- 92	2.0- 7.0	89	D.S.Flynn
4126	p	spher.	no	no	40-40	94- 94	2.0- 7.0	89	D.S.Flynn
4127	p	spher.	no	no	40-40	96- 96	2.0- 7.0	89	D.S.Flynn
4110	p	spher.	no	no	41-41	93- 93	1.0- 7.0	88	C.H.Johnson
4674	p	spher.	no	no	41-41	93- 93	1.0- 7.0	82	Y.P.Viyogi
4020	p	spher.	no	no	41-41	93- 93	0.1- 20.0	6	R.C.Harper
4128	p	spher.	no	no	42-42	95- 95	2.0- 7.0	89	D.S.Flynn
4675	p	spher.	no	no	42-42	96- 96	1.0- 7.0	82	Y.P.Viyogi
4129	p	spher.	no	no	42-42	98- 98	2.0- 7.0	89	D.S.Flynn
4676	p	spher.	no	no	42-42	98- 98	1.0- 7.0	82	Y.P.Viyogi
4130	p	spher.	no	no	42-42	100-100	2.0- 7.0	89	D.S.Flynn
4111	p	spher.	no	no	45-45	103-103	1.0- 7.0	88	C.H.Johnson
4677	p	spher.	no	no	45-45	103-103	1.0- 7.0	82	Y.P.Viyogi
4112	p	spher.	no	no	46-46	105-105	1.0- 7.0	88	C.H.Johnson
4678	p	spher.	no	no	46-46	105-105	1.0- 7.0	82	Y.P.Viyogi
4113	p	spher.	no	no	47-47	107-107	1.0- 7.0	88	C.H.Johnson
4679	p	spher.	no	no	47-47	107-107	1.0- 7.0	82	Y.P.Viyogi
4114	p	spher.	no	no	47-47	109-109	1.0- 7.0	88	C.H.Johnson
4680	p	spher.	no	no	47-47	109-109	1.0- 7.0	82	Y.P.Viyogi
4115	p	spher.	no	no	48-48	110-110	1.0- 7.0	88	C.H.Johnson
4681	p	spher.	no	no	48-48	110-110	1.0- 7.0	82	Y.P.Viyogi
4116	p	spher.	no	no	48-48	111-111	1.0- 7.0	88	C.H.Johnson

4117	p	spher.	no	no	48-48	113-113	1.0- 7.0	88	C.H.Johnson
4118	p	spher.	no	no	48-48	114-114	1.0- 7.0	88	C.H.Johnson
4119	p	spher.	no	no	49-49	115-115	1.0- 7.0	88	C.H.Johnson
4682	p	spher.	no	no	49-49	115-115	1.0- 7.0	82	Y.P.Viyogi
4120	p	spher.	no	no	50-50	116-116	1.0- 7.0	88	C.H.Johnson
4683	p	spher.	no	no	50-50	120-120	1.0- 7.0	82	Y.P.Viyogi
4427	p	spher.	no	yes	50-50	120-120	0.0-200.0	5	A.J.Koning
4121	p	spher.	no	no	50-50	122-122	1.0- 7.0	88	C.H.Johnson
4122	p	spher.	no	no	50-50	124-124	1.0- 7.0	88	C.H.Johnson
4684	p	spher.	no	no	50-50	124-124	1.0- 7.0	82	Y.P.Viyogi
4123	p	spher.	no	no	52-52	128-128	1.0- 7.0	88	C.H.Johnson
4685	p	spher.	no	no	52-52	128-128	1.0- 7.0	82	Y.P.Viyogi
4124	p	spher.	no	no	52-52	130-130	1.0- 7.0	88	C.H.Johnson
4686	p	spher.	no	no	52-52	130-130	1.0- 7.0	82	Y.P.Viyogi
5004	p	CC rot.	no	no	63-63	151-153	0.0- 20.0	52	R.Macklin
5003	p	CC rot.	no	no	67-69	165-169	0.0-100.0	56	E.D.Arthur
5406	p	CC rot.	no	no	74-74	182-186	0.0- 16.0	58	J.P.Delaroche
5002	p	CC rot.	no	no	74-74	182-186	0.0-100.0	60	P.G.Young
5005	p	CC rot.	no	no	75-75	185-187	0.0- 20.0	61	R.Macklin
4004	p	CC rot.	no	no	79-79	197-197	0.0- 57.0	90	P.G.Young
4428	p	spher.	no	yes	82-82	208-208	0.0-200.0	5	A.J.Koning
4429	p	spher.	no	yes	83-83	209-209	0.0-200.0	5	A.J.Koning
5006	p	CC rot.	no	no	92-92	238-238	0.0-200.0	73	P.G.Young
5300	p	CC rot.	no	yes	92-92	238-238	0.0-200.0	74	A.V.Ignatyuk
6400	d	spher.	no	no	6-82	12-208	20.0-100.0	91	J.Bojowald
6100	d	spher.	no	no	20-83	40-209	8.0- 13.0	92	J.M.Lohr
6101	d	spher.	no	no	20-82	40-208	11.0- 27.0	93	C.M.Perey
6112	d	spher.	no	no	20-20	40- 40	11.8- 90.0	94	W.W.Daehnick
6113	d	spher.	no	no	28-28	58- 58	11.8- 90.0	94	W.W.Daehnick
6114	d	spher.	no	no	40-40	90- 90	11.8- 90.0	94	W.W.Daehnick
6115	d	spher.	no	no	50-50	120-120	11.8- 90.0	94	W.W.Daehnick
6116	d	spher.	no	no	82-82	208-208	11.8- 90.0	94	W.W.Daehnick
7100	t	spher.	no	no	20-82	40-208	1.0- 40.0	95	F.D.Becchetti
8100	3He	spher.	no	no	20-82	40-208	1.0- 40.0	95	F.D.Becchetti
8101	3He	spher.	no	no	20-20	40- 40	21.0- 84.0	96	H.H.Chang
8102	3He	spher.	no	no	28-28	58- 58	22.0- 84.0	96	H.H.Chang
9100	4He	spher.	no	no	8-82	16-208	1.0- 25.0	97	L.McFadden
9600	4He	spher.	no	no	8-96	16-250	1.0- 73.0	98	V.Avrigeanu
9101	4He	spher.	no	no	10-92	20-235	1.0- 46.0	99	J.R.Huizenga
9018	4He	spher.	no	no	13-13	27- 27	0.1- 20.0	6	R.C.Harper
9000	4He	spher.	no	no	13-26	27- 56	1.0-100.0	100	E.D.Arthur
9400	4He	spher.	no	no	20-45	40-100	1.0- 30.0	19	B.Strohmaier
9401	4He	spher.	no	no	22-30	37- 86	20.0- 30.0	101	O.F.Lemos
9001	4He	spher.	no	no	27-27	59- 59	1.0-100.0	102	E.D.Arthur
9019	4He	spher.	no	no	28-28	58- 58	0.1- 20.0	6	R.C.Harper
9020	4He	spher.	no	no	41-41	93- 93	0.1- 20.0	6	R.C.Harper

REFERENCES TO ANNEX 5.D

[1] CHADWICK, M.B., YOUNG, P.G., Nucl. Sci. Eng. **123** (1996) 17.

[2] MADLAND, D.G., OECD/NEA Specialists' Meeting Nucleon-Nucleus Optical Model to 200 MeV, Paris (1997) 129.

[3] ISLAM, M.S., FINLAY, R.W., PETLER, J.S., RAPAPORT, J., ALARCON, R., Phys. Med. Biol. **33** (1988) 315.

[4] FERRER, J.C., CARLSON, J.D., RAPAPORT, J., Nucl. Phys. **A275** (1977) 325.

[5] KONING, A.J., DELAROCHE, J.P., Nucl. Phys. **A713** (2003) 231.

[6] HARPER, R.C., ALFORD, W.L., J. Phys. G: Nucl. Phys. **8** (1982) 153.

[7] BERSILLON, O., CINDRO, Fifth Int. Sym. Interactions of Fast Neutrons with Nuclei, Gaussig (1975).

[8] PETLER, J., ISLAM, M.S., FINLAY, R.W., Phys. Rev. **C32** (1985) 673.

[9] YAMAMURO, N., Int. Conf. Nucl. Data for Science and Technol., Mito (1988) 489.

[10] MOLINA, A., CAPOTE, R., QUESADA, J.M., LOZANO, M., Phys. Rev. **C65** (2002) 034616.

[11] KONING, A.J., DELAROCHE, J.P., Nucl. Phys. **A713** (2003) 231.

[12] LEE, Y-O., CHANK, J., FUKAHORI, T., CHIBA, S., J. Nucl. Sci. Technol. **36** (1999) 1125.

[13] MOLDAUER, P.A., Nucl. Phys. **47** (1963) 65.

[14] WILMORE, D., HODGSON, P.E., Nucl. Phys. **55** (1964) 673.

[15] VARNER, R.L., THOMPSON, W.J., MCABEE, T.L., LUDWIG, E.J., CLEGG, T.B., Phys. Rep. **201** (1991) 57.

[16] BECCETTI Jr., F.D., GREENLEES, G.W., Phys. Rev. **182** (1969) 1190.

[17] ENGELBRECHT, C.A., FIEDELDEY, H., Ann. Phys. **42** (1967) 262.

[18] MUIR, D.W., ARTHUR, E.D., J. Nucl. Mat. **122/123** (1984) 1058.

[19] STROHMAIER, B., UHL, M., REITER, W., "Neutron Cross Section Calculations for ^{52}Cr, ^{55}Mn, ^{56}Fe, and ^{58,60}Ni", IAEA Advisory Group Meeting on Nuclear Data for Radiation Damage Assessment and Related Safety Aspects, Vienna, Austria, October 1981, INDC(NDS)-128, IAEA Vienna (1982).

[20] PRINCE, A., Int. Conf. Nucl. Data, Antwerp (1982).

[21] EL-KADI, S.M., NELSON, C.E., PURSER, F.O., WALTER, R.L., BEYERLE, A., GOULD, C.R. SEAGONDOLLA, L.W., Nucl. Phys. **A390** (1982) 509.

[22] DELAROCHE, J.P., EL-KADI, S.M., GUSS, P.P., FLOYD, C.E., WALTER, R.L., Nucl. Phys. **A390** (1982) 541.

[23] ARTHUR, E.D., YOUND, P.G., LA-UR-95-3654 (1995), BNL-NCS-51245 (1980) 731, LA-8626-MS (1980).

[24] WALTER, R.L., GUSS, P.P., Rad. Effects **95** (1986) 73.

[25] ARTHUR, E.D., YOUNG, P.G., MATTHES, W., BNL-51245 (1980) 751; Nucl. Sci. Eng. **124** (1996) 271.

[26] GUSS, P.P., BYRD, R.C., FLOYD, C.E., HOWELL, C.R., MURPHY, K., TUNGATE, G., DELAROCHE, J.P., Nucl. Phys. **A438** (1985) 187.

[27] YOUNG, P.G., RUTHERFORD, D., IAEA-TECDOC-483 (1988) 167.

[28] IGARASI, S., Japan Atomic Energy Research Institute, JAERI **1228** (1973) 41.

[29] IGARASI, S., JAERI-M 5752 (1974).

[30] ZHANG SONGBAI, China Nuclear Data Center, Communication of Nuclear Data Progress, No. 21 (1999) 52.

[31] Japan Atomic Energy Research Institute (JAERI), JNDC FP Nucl. Data WG.

[32] CAI CHONGHAI, Nankai University, Tianjin, P.R. China, Communication of Nuclear Data Progress, No. 21 (1999) 40.

[33] CAI CHONGHAI, Nankai University, Tainjin, P.R. China, private communication.

[34] SMITH, A.B., GUENTHER, P.T., WHALEN, J.F., Nucl. Phys. **A415** (1984) 1.

[35] ARTHUR, E.D., Nucl. Sci. Eng. **76** (1980) 137.

[36] CAI CHONGHAI, Nankai University, Tianjin, P.R. China, private communication.

[37] ARTHUR, E.D., Nucl. Sci. Eng. **76** (1980) 137; LA-UR-94-3104 (1994).

[38] KONING, A.J., VAN WIJK, J.J., DELAROCHE, J.P., OECD/NEA Specialist Mtg. Nucleon-Nucleus Opt. Mod. to 200 MeV, Paris (1997) 111.

[39] RONG JIAN, ZHANG ZHENGJUN, China Nuclear Data Center, private communication.

[40] LAGRANGE, Ch., Specialist Meeting Neutron Data for Structural Materials, Geel (1977).

[41] CAI CHONGHAI, Nankai University, Tainjin, P.R. China, private communication.

[42] CAI CHONGHAI, GE ZHIGANG, China Nuclear Data Center, private communication.

[43] ZHANG ZHENGJUN, Phys. Dept. of Northwest University, Xian, private communication.

[44] ZHANG ZHENGJUN, GE ZHIGANG, China Nuclear Data Center, private communication.

[45] ZHANG ZHENGJUN, GE ZHIGANG, China Nuclear Data Center, private communication.

[46] ZHANG ZHENGJUN, et al., Communication of Nuclear Data Progress, No. 20 (1998) 77.

[47] SHEN QINGBIAO, China Nuclear Data Center, private communication.

[48] SHEN QINGBIAO, ZHANG ZHENGJUN, China Nuclear Data Center, private communication.

[49] HAOUAT, G., LACHKAR, J., LAGRANGE, Ch., MCELLISTREM, M.T., PATIN, Y., SHAMU, R.E., SIGAUD, J., Phys. Rev. **C20** (1979) 78.

[50] McELLISTREM, M.T., SHAMU, R.E., LACHKAR, J., HAOUAT, G., LAGRANGE, Ch., PATIN, Y., SIGAUD, J., COCU, F., Phys. Rev. **C15** (1977) 927.

[51] GE ZHIAGANG, China Nuclear Data Center, Communication of Nuclear Data Progress, No. 21 (1999) 35.

[52] MACKLIN, R., YOUNG, P.G., Nucl. Sci. Eng. **95** (1987) 189.

[53] GE ZHIAGANG, China Nuclear Data Center, private communication.

[54] SMITH, A.B., ANL/NDM-151 (December 2000).

[55] YOUNG, P.G., LA-UR (1997).

[56] ARTHUR, E.D., PHILIS, C., LA-8630-PR (1980) 2.

[57] HAN YINLU, China Nuclear Data Center, private communication.

[58] DELAROCHE, J.P., HAOUAT, G., LACHKAR, J., PATIN, Y., SIGAUD, J., CHARDINE, J., Phys. Rev. **C23** (1981) 136.

[59] DELAROCHE, J.P., et al., Int. Conf. Nucl. Data, Knoxville, TN (1978).

[60] YOUNG, P.G., ARTHUR, E.D., BOZIAN, M., ENGLAND, T.R., HALE, G.M., LABAUVE, R.J., LITTLE, R.C., et al., LA-11753-MS (1990); see also LA-8630-PR, (1980) 2.

[61] MACKLIN, R., YOUNG, P.G., Nucl. Sci. Eng. **97** (1987) 239.

[62] DELAROCHE, J.P., Proc. Int. Conf. Neut. Phys. for Reactors, Harwell, UK, 25-29 Sept. 1978.

[63] FINLAY, R.W., ANNAND, J.R.M., CHEEMA, T.S. RAPAPORT, J., DIETRICH, F.S., Phys. Rev. **C30** (1984) 796.

[64] WEISEL, G.J., TORNOW, W., HOWELL, C.R., FELSHER, P.D., ALOHALI, M., ROBERTS, M.L., DAS, R.K., WALTER, R.L., Phys. Rev. **C54** (1996) 2410.

[65] VONACH, H., PAVLIK, A., CHADWICK, M.B., HAIGHT, R.C., NELSON, R.O., WENDER, S.A., YOUNG, P.G., Phys. Rev. **C50** (1994) 1952.

[66] BERSILLON, O., CEA-N-2284 (1982) 130; see also NEANDC-222.

[67] MADLAND, D.G., YOUNG, P.G., Int. Conf. Neut. Phys. for Reactors, Harwell, UK, 25-29 Sept. 1978.

[68] LAGRANGE, Ch., NEANDC(E)228, INDC(FR)-56 (1982).

[69] HAOUAT, G., LACHKAR, J., LAGRANGE, Ch., Nucl. Sci. Eng. **81** (1982) 491.

[70] VLADUCA, G., TUDORA, A., SIN, M., Rom. J. Phys., **41**, no. 7-8 (1996) 515.

[71] YOUNG, P.G., ARTHUR, E.D., in Proc. Int. Conf. Nucl. Data Sci. Tech., Jülich (1992) 894.

[72] YOUNG, P.G., ARTHUR, E.D., LA-UR-91-1424, 894 (1992).

[73] YOUNG, P.G., LA-11972-PR (1990) 9.

[74] IGNATYUK, A.V., LUNEV, V.P., SHUBIN, Yu.N., GAI, E.V., TITARENKO, N.N., VENTURA, A., GUDOWSKI, W., Nucl. Sci. Eng. **136** (2000) 340.

[75] LAGRANGE, Ch., CEA-N-1970, NEANDC(E) 179, INDC(FR)-16 (1977).

[76] MADLAND, D.G., YOUNG, P.G., LA-7533-MS (1978).

[77] YOUNG, P.G., ARTHUR, E.D., LA-UR-95-3654, paper at CRP RIPL Meeting, Vienna, 30 Oct. - 3 Nov. 1995.

[78] MENET, J.J.H., GROSS, E.E., MALANIFY, J.J., ZUCKER, A., Phys. Rev. **C4** (1971) 1114.

[79] CHADWICK, M.B., YOUNG, P.G., Proc. Int. Particle Therapy Meeting and PTCOG XXIV, 24-26 April 1996, Detroit, Michigan, USA.

[80] SCHWANDT, P., MEYER, H.O., JACOBS, W.W., BACHER, A.D., VIGDOR, S.E., KAITCHUCK, M.D., et al., Phys. Rev. **C26** (1982) 55.

[81] PEREY, F.G., Phys. Rev. **131** (1963) 745.

[82] VIYOGI, Y.P., Ph.D Thesis, Calcutta University (1983).

[83] BECCHETTI Jr., F.D., GREENLEES, G.W., Phys. Rev. **182** (1969) 1190.

[84] KAILAS, S., MEHTA, M.K., GUPTA, S.K., VIYOGI, Y.P., GANGULY, N.K., Phys. Rev. **C20** (1979) 1272;
MEHTA, M.K., KAILAS, S., Pramana. J. Phys. **27** (1986) 139.

[85] PATTERSON, D.M., DOERING, R.R., GALONSKY, A., Nucl. Phys. **A263** (1976) 261.

[86] WALTER, R.L., GUSS, P.P., Rad. Effects **95** (1986) 73.

[87] ARTHUER, E.D., YOUNG, P.G., MATTHES, W., BNL-51245 (1980) 751; Nucl. Sci. Eng. **124** (1996) 271.

[88] JOHNSON, C.H., GALONSKY, A., KERNELL, R.L., Phys. Rev. Lett. **39** (1977) 1604; Phys. Rev. **C20** (1979) 2052.

[89] FLYNN, D.S., HERSHBERGER, R.L., GABBARD, F., Phys. Rev. **C31** (1985) 87.

[90] YOUNG, P.G., ARTHUR, E.D., LA-UR-84-2767 (1984); LA-UR-94-3104 (1994).

[91] BOJOWALD, J., MACHNER, H., NANN, H., OELERT, W., ROGGE, M., TUREK, P., Phys. Rev. **C38** (1988) 1153.

[92] LOHR, J.M., HAEBERLI, W., Nucl. Phys. **A232** (1974) 381.

[93] PEREY, C.M., PEREY, F.G., Phys. Rev. **132** (1963) 755.

[94] DAEHNICK, W.W., CHILDS, J.D., VRCELJ, Z., Phys. Rev. **C21** (1980) 2253.

[95] BECCHETTI Jr., F.D., GREENLEES, G.W., Annual Report, J.H. Williams Laboratory, University of Minnesota (1969).

[96] CHANG, H.H., RIDLEY, B.W., BRAID, T.H., CONLON, T.W., GIBSON, E.F., KING, N.S.P., Nucl. Phys. **A297** (1978) 105.

[97] MCFADDEN, L., SATCHLER, G.R., Nucl. Phys. **84** (1966) 177.

[98] AVRIGEANU, V., HODGSON, P.E., AVRIGEANU, M., OUNP-94-02 (1994); Phys. Rev. **C49** (1994) 2136.

[99] HUIZENGA, J.R., IGO, G., Nucl. Phys. **29** (1962) 462.

[100] ARTHUR, E.D., YOUNG, P.G., LA-8636-MS(ENDF-304) (1980).

[101] LEMOS, O.F., Orsay, Series A, No. 136 (1972).

[102] ARTHUR, E.D., YOUNG, P.G., MATTHES, W., BNL-51245, 751 (1980).

6 NUCLEAR LEVEL DENSITIES

Coordinators: A.V. Ignatyuk and R. Capote

Summary

Level densities are key ingredients of the statistical theory of nuclear reactions. Practical formalisms of nuclear level densities and their parameterization are considered in this chapter. The total level densities required for the statistical calculations of reaction cross sections at low and intermediate energies are described in Section 6.1. Then, the partial (particle-hole) level densities needed as input to the extremely useful pre-equilibrium model of nuclear reactions are discussed in Section 6.2. The fission level densities required for the statistical calculations of the fission cross sections are considered separately in Chapter 8, together with the corresponding fission barriers.

The RIPL-2 library includes a FORTRAN code written by Avrigeanu for various Fermi-gas single-particle models in the equidistant spacing approximation, including pairing and shell effects within the closed-form treatments. A FORTRAN code produced by Capote and Pedrosa has also been adopted which uses a microscopic theory based on a convolution of shell-model single-particle states with BCS pairing.

The statistical properties of excited nuclear levels have been a matter of concern and study for many years. One of the basic statistical properties of these levels is their density, for which the Fermi-gas and constant temperature models are frequently used with input parameters obtained from fitting certain experimental data. However, the physical assumptions underlying these models are not sufficiently sophisticated to account properly for variations of level densities over a wide energy interval from the ground state to well above the neutron separation energy. This is not surprising as these models were formulated more than fifty years ago, in the infancy of such concepts of nuclear physics.

Some of the most important concepts upon which our current understanding of the structure of low-lying nuclear levels is based include shell effects, pairing correlations and collective phenomena. All these concepts have been incorporated into the generalized super-fluid model developed by many authors over the last 30 years. The phenomenological versions of this model are convenient for the analysis of experimental data and have been developed intensively over recent years.

For practical applications of the statistical models, it is very important to obtain parameters of the level densities from reliable experimental data. The cumulative numbers of low-lying levels and the average distances between neutron resonances are usually

used for this purpose. The systematics of the level density parameters developed under the RIPL project are discussed below together with recommendations regarding their application to different tasks.

6.1 Total level densities

6.1.1 Composite Gilbert-Cameron model

Simple analytical expressions for the excited state density $\rho(U)$ of a nucleus with a given excitation energy U and level density $\rho(U,J)$ of a nucleus with a given angular momentum J were obtained by Bethe on the basis of the Fermi-gas model [6.1]:

$$\begin{aligned} \rho(U) &= \frac{\sqrt{\pi}}{12a^{1/4}U^{5/4}}\exp(2\sqrt{aU}), \\ \rho(U,J) &= \frac{2J+1}{2\sqrt{2\pi}\sigma^3}\rho(U)\exp\left[-\frac{(J+1/2)^2}{2\sigma^2}\right], \end{aligned} \tag{6.1}$$

in which $a=\pi^2 g/6$ is the level density parameter proportional to the single-particle state density g near the Fermi energy, and σ^2 is the spin cutoff parameter.

For the Fermi-gas model, the state equations determining the dependence of the excitation energy U, the entropy S and other thermodynamic functions of a nucleus on temperature t have simple forms:

$$U=at^2, \qquad S=2at, \qquad \sigma^2 =< m^2 > gt, \tag{6.2}$$

where $< m^2 >$ is the mean square value of the angular momentum projections for the single-particle states around the Fermi energy, which may also be associated with the moment of inertia of a heated nucleus $\mathcal{I} = g < m^2 >$. There are obvious connections between the thermodynamic functions (Eqs. 6.2) and the state and level densities (Eq. 6.1).

The main parameters of the Fermi-gas model may be estimated rather simply using the semi-classical approximation:

$$a = 2\left(\frac{\pi}{3}\right)^{4/3}\frac{m_0 r_0^2}{\hbar^2}A(1+\beta_s A^{-1/3}), \tag{6.3}$$

$$\mathcal{I}_0 = \frac{2}{5}\frac{m_0 r_0^2}{\hbar^2}A^{5/3}, \tag{6.4}$$

where m_0 is the nucleon mass, r_0 is the nuclear radius parameter, A is the mass number and β_s defines the surface component of the single-particle level density. Eq. 6.4 corresponds to the rigid-body value of the nuclear moment of inertia, and differences between various semi-classical determinations of the level density parameters (Eq. 6.3) are mainly due to the large uncertainties in the existing evaluations for β_s.

The most direct information on the level density of highly-excited nuclei is obtained from the average parameters of neutron resonances, which have been analyzed by many

authors [6.2–6.11]. For the majority of nuclei the observed resonances correspond to s-neutrons, and therefore the value of the average spacings D_0 is related to the level density of the compound nucleus by the relationships:

$$(D_0)^{-1} = \begin{cases} \frac{1}{2}\left[\rho(B_n + \Delta E/2, I_0 + 1/2) + \rho(B_n + \Delta E/2, I_0 - 1/2)\right] & \text{for } I_0 \neq 0, \\ \frac{1}{2}\rho(B_n + \Delta E/2, 1/2) & \text{for } I_0 = 0, \end{cases} \tag{6.5}$$

were B_n is the neutron binding energy, ΔE is the energy interval for which the resonances are being examined, I_0 is the target nucleus spin, and the coefficient 1/2 before the sum takes into account that s-neutrons form resonances only of a particular parity. If necessary, resonances for p-neutrons can be considered in a similar way.

The experimental values of D_0 are normally used as source data, from which the magnitude of the level density parameter can be derived by means of Eqs. 6.1 and 6.5. Many authors have carried out such an analysis [6.5, 6.7, 6.8]. The regular differences of the level densities for even-even, odd and odd-odd nuclei analogous to the even-odd differences of the nuclear masses have been already noted in the early systematics of the experimental data. The so-called effective excitation energy is normally introduced to take this effect into account:

$$U^* = U - \begin{cases} \delta_Z + \delta_N & \text{for even} - \text{even} \\ \delta_Z & \text{for even } Z \\ \delta_N & \text{for even } N \\ 0 & \text{for odd} - \text{odd} \end{cases} \tag{6.6}$$

where δ_I is the corresponding phenomenological correction for even-odd differences of nuclear binding energies.

Data on the cumulative numbers of low-lying nuclear levels are also very important for level density analyses. The observed energy dependence of the cumulative number of levels can be described rather well by the function [6.3, 6.5]:

$$N(U) = \exp[(U - U_0)/T], \tag{6.7}$$

where U_0 and T are free parameters determined by fitting corresponding data. $N(U)$ is related to the level density by the equation:

$$\rho_{lev}(U) = \frac{\mathrm{d}N}{\mathrm{d}U} = \frac{1}{T}\exp\left[(U - U_0)/T\right], \tag{6.8}$$

in which the parameter T corresponds simply to a nuclear temperature. Since the value of this parameter is assumed to be constant over the energy range considered, Eq. 6.8 is called the constant temperature model.

A description of the level density for the whole range of excitation energies is obtained by combining the low-energy dependent Eq. 6.8 with the high-energy dependence predicted by the Fermi-gas model. The link between the parameters of both models can be found by imposing the continuity of level density and the first derivative at some matching energy

$$U_x = U_0 + T\ln\rho_{fg}(U_x), \qquad \frac{1}{T} = \sqrt{\frac{a}{U_x^*}} - \frac{3}{2U_x^*}, \tag{6.9}$$

where U_x^* is the effective matching energy that includes the pairing corrections (Eq. 6.6).

Analysis of the experimental data within this phenomenological approach was carried out initially by Gilbert and Cameron [6.5], and the parameters obtained by different authors in the subsequent analyzes of experimental data are reported in the RIPL-1 Handbook [6.12]. A rather simple systematic relationship has been proposed for the level density parameter:

$$\frac{a}{A} = 0.0088\,(S(Z) + S(N)) + Q(Z,N), \tag{6.10}$$

where $S(I)$ are the shell corrections for protons and neutrons, respectively, and $Q(Z,N) = 0.12$ for deformed nuclei ($54 < Z < 78$, $86 < N < 122$, and $86 < Z < 122$, $130 < N < 182$), and $Q(Z,N) = 0.142$ for other nuclei considered as spherical. Tables of the shell corrections and the corresponding pairing contribution corrections are given in the RIPL-1 data files.

Values of the a-parameters depend to some extent on the determination of the spin cutoff parameter. Early systematics used a value of $< m^2 >= 0.146A^{2/3}$, which corresponds to mean-square averaging of the proton and neutron angular momenta projections over all single-particle levels occupied in the ground state of a nucleus [6.5, 6.7]. Later analyses used more correct values $< m^2 >= 0.24A^{2/3}$, or the rigid body values of the moment of inertia. These differences in the choice of the spin cutoff parameters, as well as some variations in the even-odd corrections to the excitation energies, should be borne in mind when comparing the a-parameters obtained by different authors.

Adjusted tables of the shell and pairing corrections were proposed in Refs. [6.13-6.15]. The systematics of the a-parameter differ from Eq. 6.10 only in the numerical values of the coefficients and a slightly different definition of the functions $Q(Z,N)$. Parameters derived by the Beijing group [6.15] are based on rather recent compilations of the neutron resonance densities, and were included in the *beijing_gc.dat* file of the RIPL-1 project as recommended data.

Revision of the low-lying data and the neutron resonance spacings described in Chapters 3 and 4 requires an updating of the level density parameters. Level density parameters obtained for the updated resonance spacings are shown in Fig. 6.1 in comparison with the results of previous analyses [6.11, 6.15]. We have used the pairing corrections $\delta = n12A^{-1/2}$ with $n = 2$ for even-even nuclei, $n = 1$ for odd nuclei and $n = 0$ for odd-odd nuclei. Such a definition of the pairing corrections is used in the Myers-Swiatecki mass formula, and reproduces the averaged behavior of the corrections reported in Refs. [6.5, 6.15]. The same corrections were also used in Ref. [6.11]. Agreement of the RIPL-2 results with the parameters obtained by Iljinov et al [6.11] is good for most nuclei, and their differences from the Beijing data arise from the slightly different pairing corrections and the updated values of the resonance spacings.

The level density parameters obtained from the resonance spacing analysis were matched with the level density of low-lying levels by solving Eqs. 6.7 and 6.9 for the cumulative numbers N_0 of low-lying levels and the corresponding excitation energies U_0 as defined in the recommendations of Chapter 3. Fig. 6.2 shows the nuclear temperatures T, the energy shifts U_0 , and the matching energies U_x. Generally, the present results are close to similar results of previous analyses considered in the RIPL-1 Handbook [6.12]. However, the matching equations for the level densities (Eqs. 6.9) set some limitations on the temperatures and the energy shifts, resulting in differences between the values derived from the matching conditions and the same parameters estimated from the analysis of low-lying

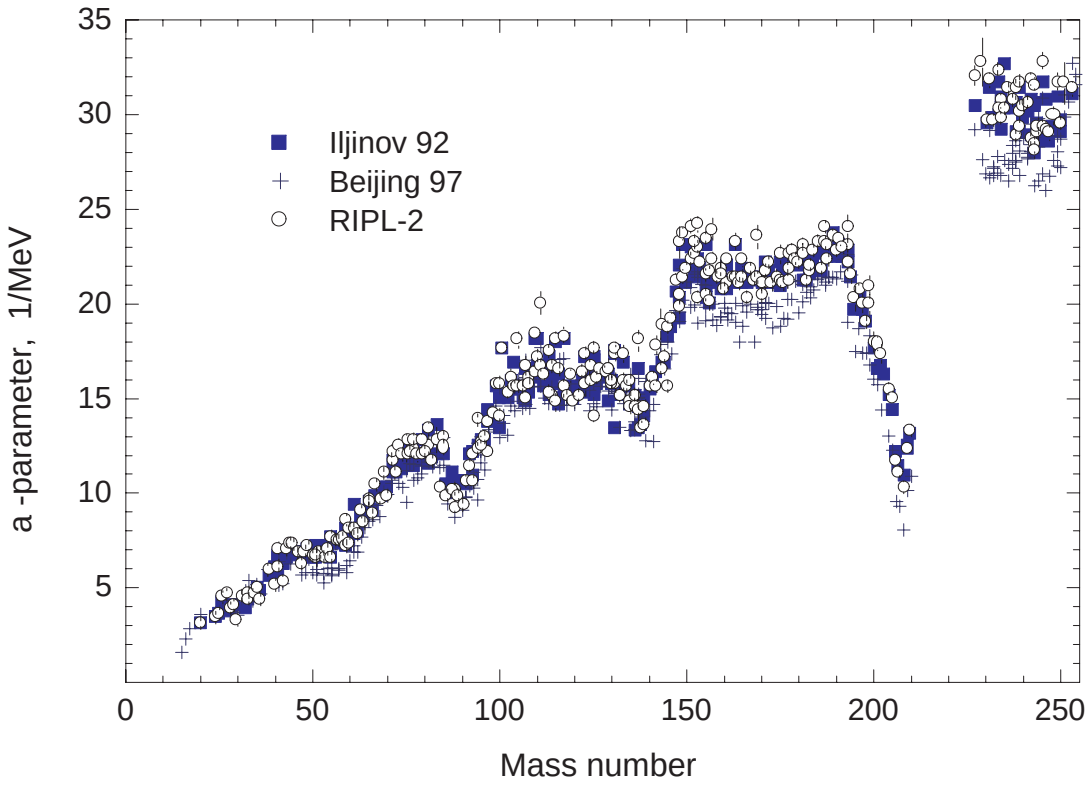

Figure 6.1: Level density parameters of the Fermi-gas model with normal shift.

levels only. These differences can be seen in Fig. 6.2 where both sets of parameters are shown for the same nuclei.

The complete set of level density parameters obtained for the composite Gilbert-Cameron model is given in the *level-density-gc.dat* file, and the format is described in the *level-density-gc.readme* file.

The parameters are evaluated when the experimental data for the neutron resonance spacings are available. Systematics for the parameters $a(Z,N)$ and $\delta(Z,N)$, that can be used for the remaining nuclei were developed in Refs. [6.5, 6.13, 6.15] and reported in the corresponding RIPL-1 files.

One of the serious deficiencies of systematics discussed so far is the energy independence of the a-parameters. The results of all consistent microscopic calculations of the nuclear level densities display damping of the shell effect at high excitation energies [6.16, 6.17, 6.19]. In order to account for the damping of the shell effects, the level density parameter a should become energy dependent, as approximated by the formula [6.20]

$$a(U,Z,A) = \tilde{a}(A)\left\{1 + \frac{\delta E_0}{U}\left[1 - \exp(-\gamma U)\right]\right\}, \qquad (6.11)$$

where $\tilde{a}$ is the asymptotic level density parameter to which $a(U)$ tends at high excitation energies, δE_0 is the shell correction energy, and γ is the damping parameter. Systematics

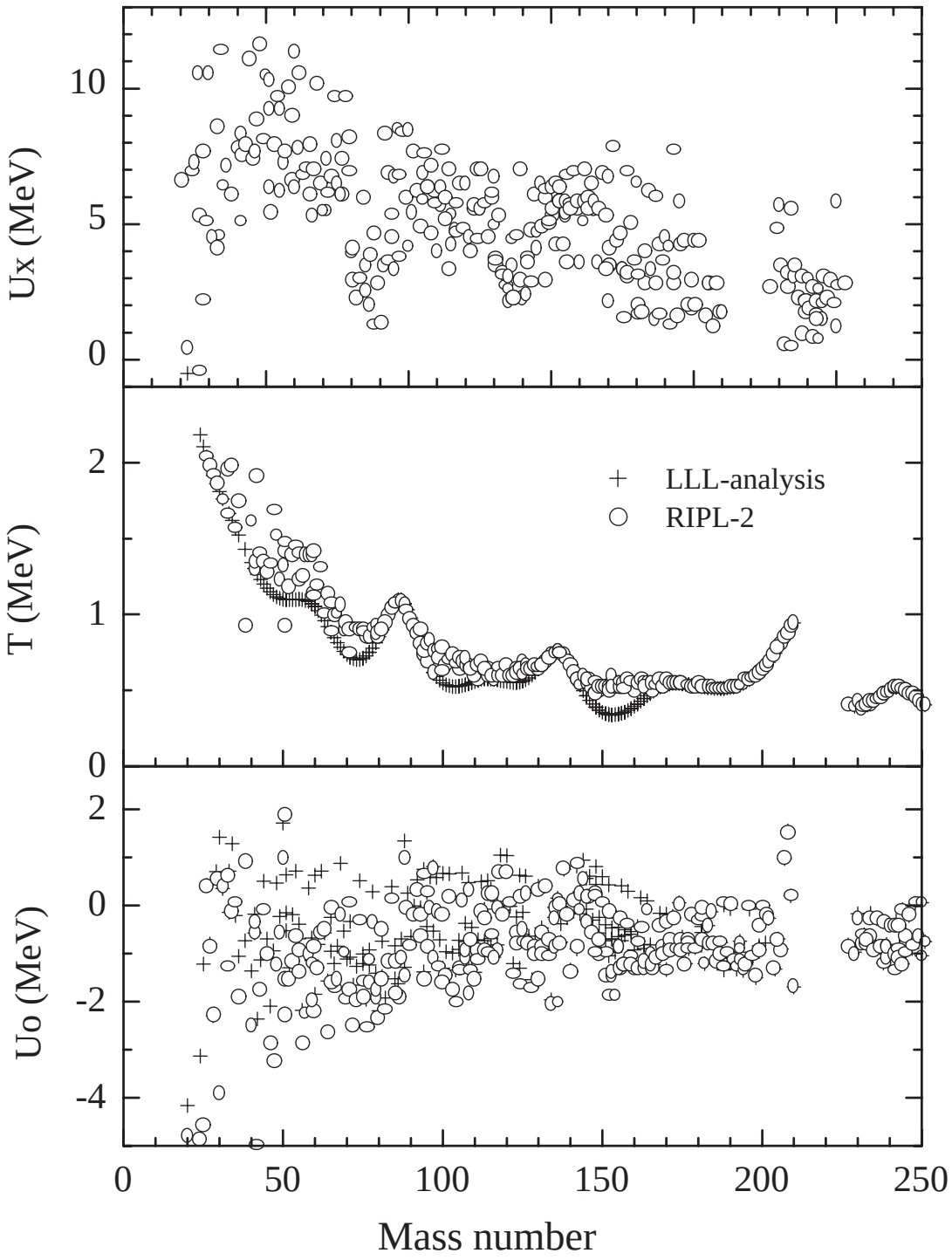

Figure 6.2: Level density parameters for the constant temperature model.

based on similar formula were proposed in Refs. [6.20, 6.21, 6.22, 6.35], and the differences between the corresponding level density parameters are mainly related to different shell corrections.

Shell corrections are usually determined as

$$\delta E_0 = M_{exp}(Z,A) - M_{ld}(Z,A,\beta), \tag{6.12}$$

where M_{exp} is the experimental value of the mass defect, and M_{ld} is the liquid-drop component of the mass formula [6.23]. Differences between the various approximations are mainly related to the liquid-drop component; if the liquid-drop model formula for spherical nuclei are adopted in Eq. 6.12, the shell corrections coincide with the microscopic energies considered in Chapter 2. However, some authors prefer to include the deformation energies within the liquid-drop component of Eq. 6.12 [6.23]. Such a consistent definition of the shell corrections is important for the analysis of equilibrium deformations of highly excited nuclei [6.18], but differences in the shell correction estimations are less essential for the systematics of the level density parameters.

Fig. 6.3 shows the shell corrections corresponding to the most widely used mass formula [6.5, 6.23, 6.24] for the nuclei considered above. If these corrections are taken together with the a-parameter values for the neutron binding energies (Fig. 6.1), the asymptotic level density parameters can be derived on the basis of Eq. 6.11. Using the semi-classical formula for the asymptotic and damping parameters

$$\tilde{a} = \alpha A + \beta A^{2/3}, \qquad \gamma = \gamma_0 / A^{1/3}, \tag{6.13}$$

and the Myers-Swiatecki shell corrections, the following coefficients (in units of MeV^{-1}) were obtained from a least-squares fit of the a-parameters:

$$\alpha = 0.0959 \pm 0.0005, \qquad \beta = 0.1468 \pm 0.0035, \qquad \gamma_0 = 0.325 \pm 0.015 \tag{6.14}$$

Another mass-dependence formula for the asymptotic level density parameter is preferable for the Möller-Nix shell corrections because of their large values for the actinides:

$$\tilde{a} = \alpha A + \beta A^2, \qquad [\text{with } \gamma = \gamma_0 / A^{1/3}] \tag{6.15}$$

with the corresponding coefficients:

$$\alpha = 0.1125 \pm 0.0005, \qquad \beta = (1.22 \pm 0.11) 10^{-4}, \qquad \gamma_0 = 0.325 \pm 0.015. \tag{6.16}$$

Deviations of the a-parameters included in the RIPL-2 *level-densities-gc.dat* file from the parameters calculated on the basis of systematics are shown in Fig. 6.4 for both sets of shell corrections. Standard deviations are equal to 0.0613 for the systematics using Myers-Swiatecki corrections, and 0.0649 for Möller-Nix corrections. These results show that both systematics have approximately equal accuracy, and can be used for the evaluation of unknown level density parameters with expected uncertainties of about 6.5%. The Myers-Swiatecki shell corrections for about 8000 nuclei are given in the *shellcor-ms.dat* file, while those of Möller-Nix are listed in the *masses/mass-frdm95.dat* file discussed in Chapter 2.

The systematics of the constant temperature model parameters were discussed in Ref. [6.25], in which the nuclear temperature used in Eq. 6.7 was approximated by the formula

$$T = 17.60 A^{-0.699} \sqrt{1 + \gamma \delta E_0}, \tag{6.17}$$

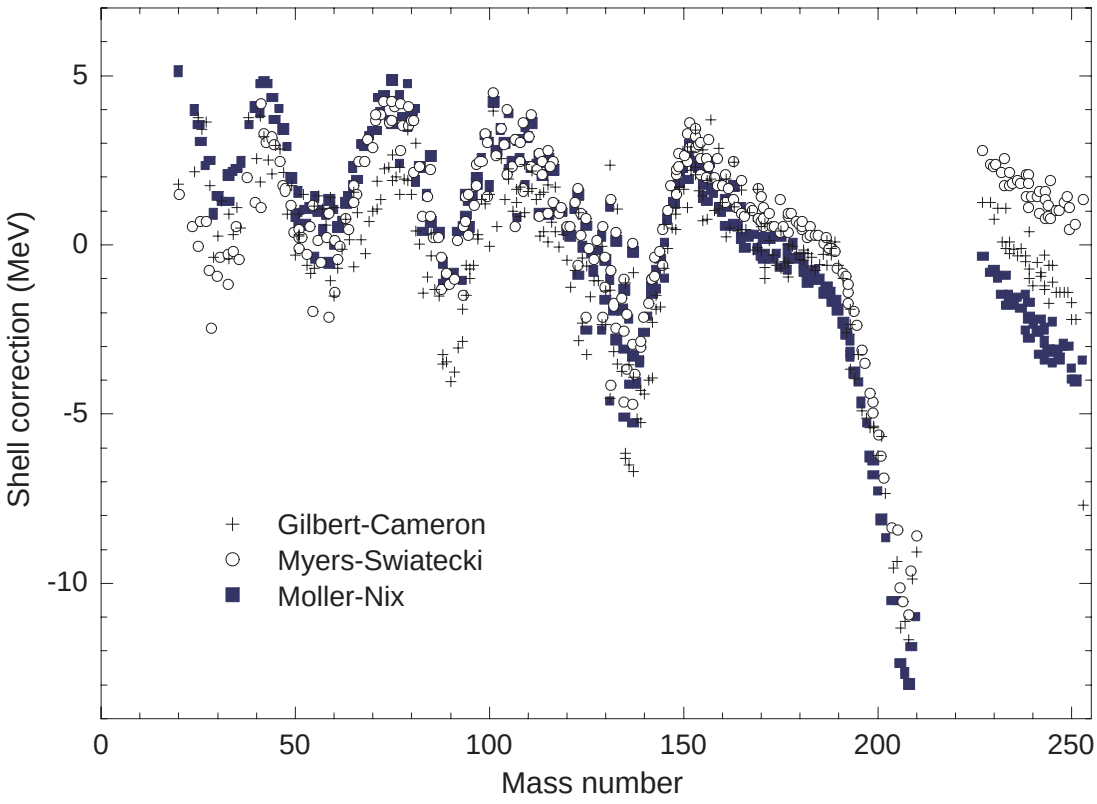

Figure 6.3: Shell corrections to the nuclear binding energies estimated by different authors.

where numerical coefficients are obtained by a least-squares fit of the data shown in Fig. 6.2. The same approach can be adopted for the energy shifts in which the following relationships were derived:

$$U_0 = \begin{cases} 11.17A^{-0.464} - 0.520 - 0.79\delta E_0 & \text{for even} - \text{even nuclei,} \\ -0.390 - 0.00058A - 0.79\delta E_0 & \text{for odd nuclei,} \\ -11.17A^{-0.464} + 0.285 - 0.79\delta E_0 & \text{for odd} - \text{odd nuclei.} \end{cases} \tag{6.18}$$

Both the nuclear temperatures and the energy shifts in Chapter 3 are evaluated for a much larger number of nuclei than included in the above list of a-parameters. When available, these parameters are certainly preferable for level density calculations at low excitation energies. However, for intermediate energies, values of T and U_0 should always be re-estimated in accordance with the matching conditions (Eqs. 6.9) and corresponding systematics of the a-parameters for highly excited nuclei.

6.1.2 Back-shifted Fermi-gas model

Another approach to the problem of a simultaneous description of neutron resonance densities and low-lying levels was proposed in Ref. [6.9]. Both sets of experimental data are assumed to be described on the basis of the Fermi-gas relationships if the level density

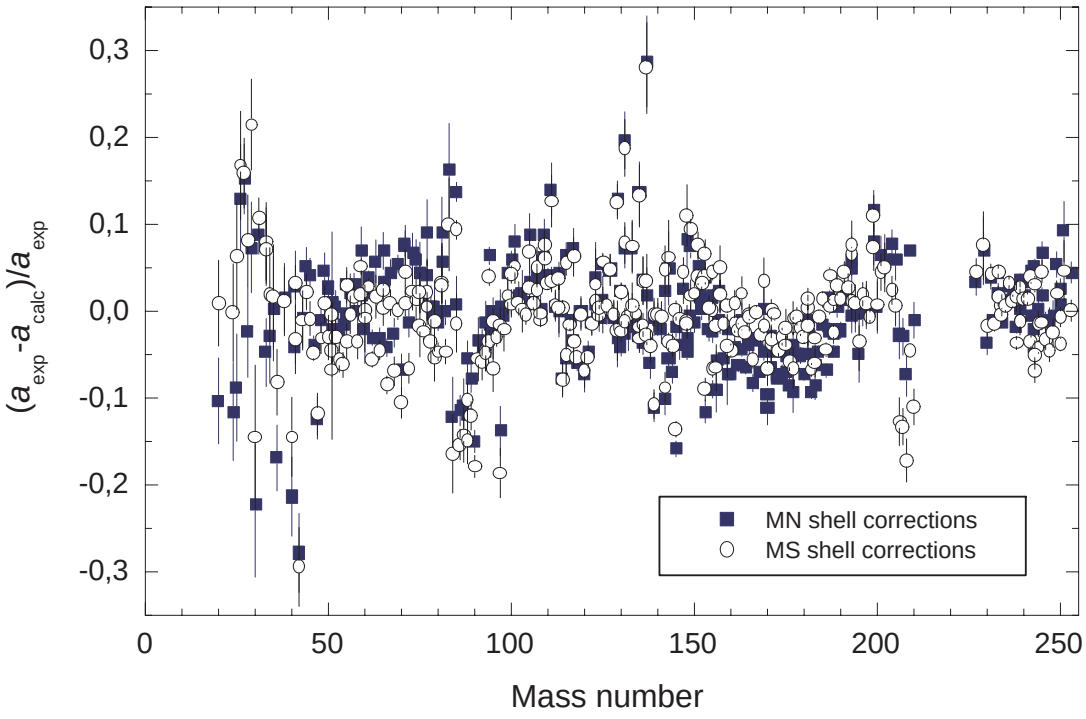

Figure 6.4: Deviations between the level density parameters derived from the resonance spacing analysis and the systematics based on the shell-correction formula (Möller-Nix (MN) and Myers-Swiatecki (MS)).

parameter a and the excitation energy shift δ_{eff} are considered as free parameters for each nucleus. Since for odd-odd nuclei the resulting displacement is negative, the above approach is known as the back-shifted Fermi-gas model. Since in this approach the Fermi-gas formula are applied to a rather low excitation energies, a more accurate estimation of temperature is used

$$U - \delta_{eff} = at^2 - t,$$

and the temperature is usually added to the excitation energy in the dominator of Eq. 6.1 [6.9].

Results of the corresponding analysis of the neutron resonance densities and low-lying nuclear levels are shown in Fig. 6.5. Due to the change in the determination of the effective excitation energies, the values obtained for the a-parameters are somewhat lower than those shown in Fig. 6.1. However, shell effects in the mass dependence of the a-parameter remain essentially the same. Differences between parameters obtained in RIPL-1 [6.12] and RIPL-2 reflect the improvements achieved for both sets of experimental data: neutron resonance spacings and cumulative numbers of low-lying levels.

Spin cutoff parameters are usually determined on the basis of the evaluation of the moment of inertia to give the rigid-body value and half this value. The results of the spin-distribution analysis of low-lying levels considered in Chapter 3 are shown in Fig. 6.6. The half-rigid-body value of the moment of inertia is in reasonable agreement with the

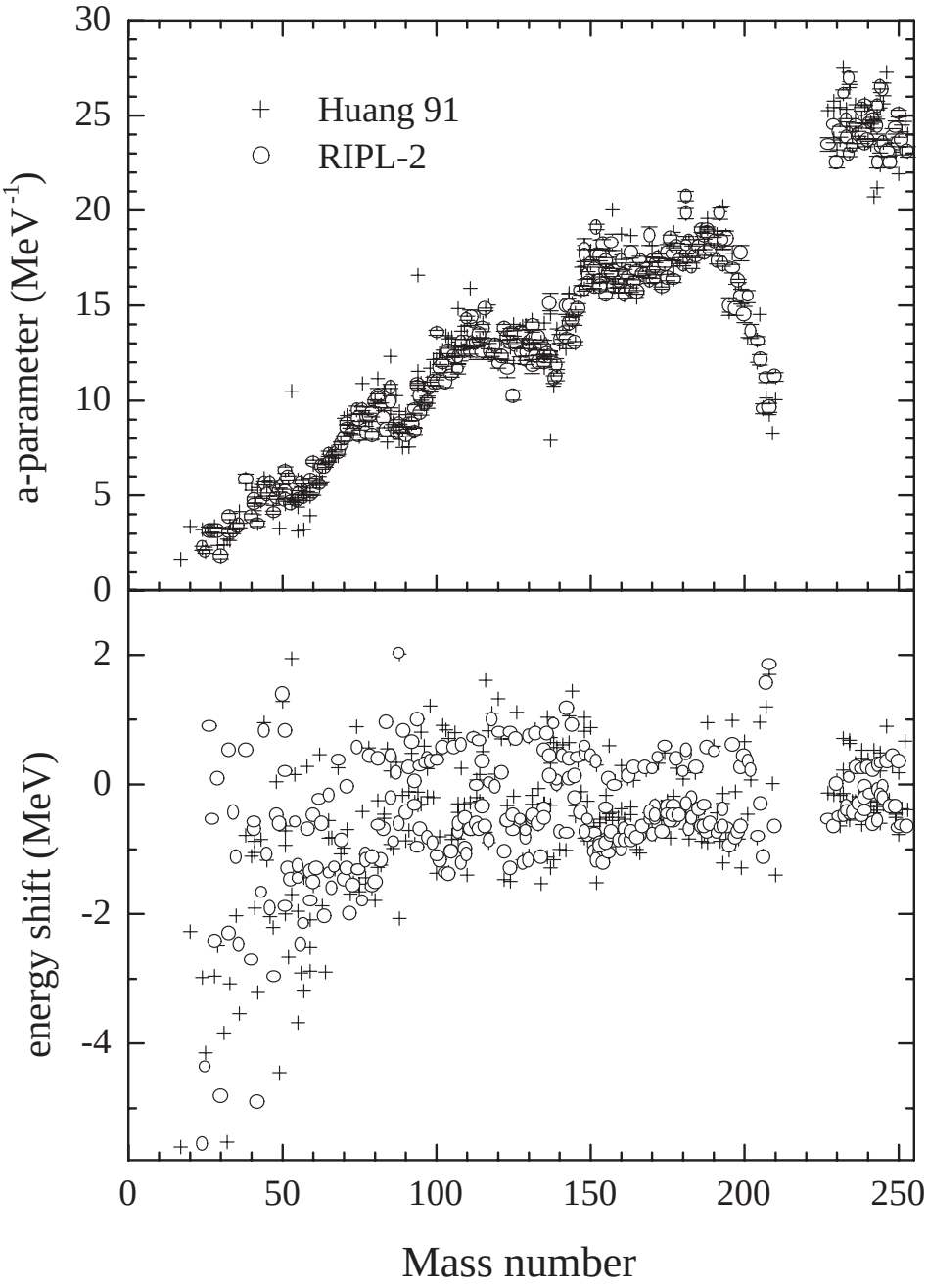

Figure 6.5: Level density parameters in the back-shifted Fermi-gas model.

available data, but because of the large uncertainties more accurate spin cutoff parameters are difficult to estimate. Accordingly, the half-rigid-body moments of inertia were used for the evaluation of the a-parameters presented in Fig. 6.5.

The complete set of level density parameters obtained for the back-shifted Fermi-gas model is given in the *level-density-bsfg.dat* file, and the format is described in the *level-density-bsfg.readme* file.

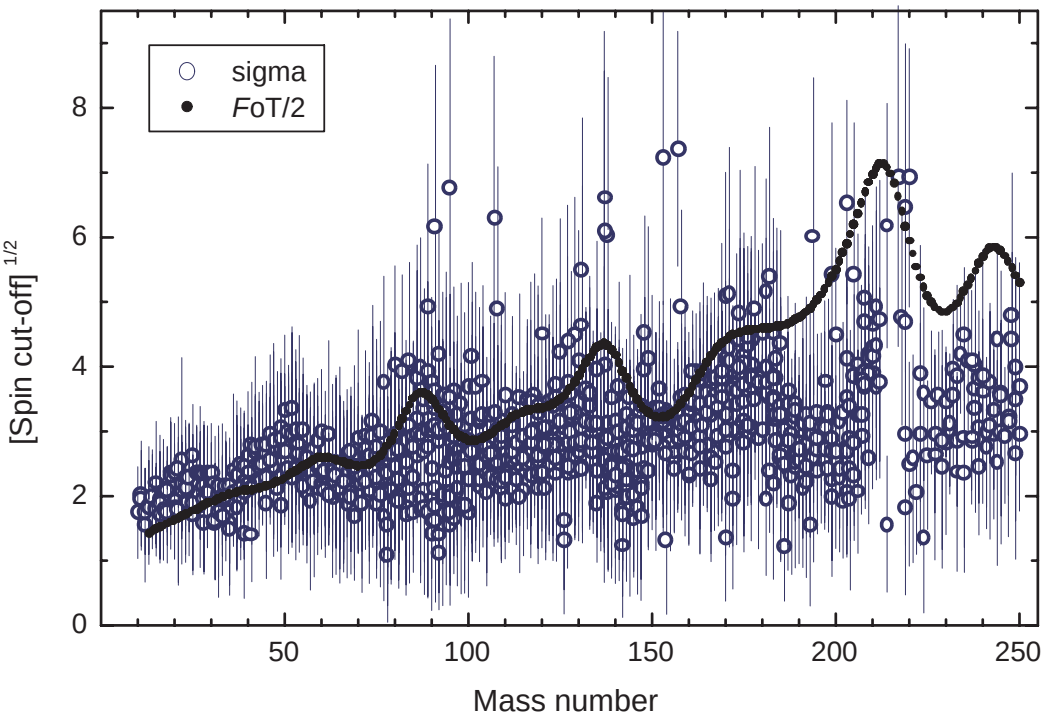

Figure 6.6: Spin cutoff parameters obtained from the analysis of low-lying levels in comparison with calculations using the half-rigid-body value of the moment of inertia.

Systematics for the level density parameters of the BSFG model were developed in Ref. [6.26] on the basis of Eq. 6.11, which differs from the above for the Gilbert-Cameron model through mainly the pairing corrections. These corrections were taken to be equal to $(\delta_Z+\delta_N)/2$ for even-even nuclei, 0 for odd nuclei, and $-(\delta_Z+\delta_N)/2$ for odd-odd nuclei. Whereas for the Möller-Nix shell corrections and the asymptotic level density parameter given by Eqs. 6.13, the following coefficients (in MeV^{-1}) were obtained:

$$\alpha = 0.1337, \qquad \beta = -0.06571, \qquad \gamma = 0.04884. \tag{6.19}$$

We performed similar analysis for the a-parameters shown in Fig. 6.5. The Myers-Swiatecki shell corrections were used, the asymptotic level density parameter was taken as Eq. 6.13, and the pairing corrections were chosen to be equal to $12/A^{1/2}$ for even-even nuclei, 0 for odd nuclei, and $-12/A^{1/2}$ for odd-odd nuclei. The following coefficients (in MeV^{-1}) were obtained:

$$\alpha = 0.0904 \pm 0.0005, \qquad \beta = 0.0373 \pm 0.0035, \qquad \gamma_0 = 0.325 \pm 0.015. \tag{6.20}$$

For the Möller-Nix shell corrections and the asymptotic level density parameter defined by Eqs. 6.15 these coefficients are

$$\alpha = 0.0883 \pm 0.012, \qquad \beta = (1.03 \pm 0.84)10^{-4}, \qquad \gamma_0 = 0.325 \pm 0.015. \tag{6.21}$$

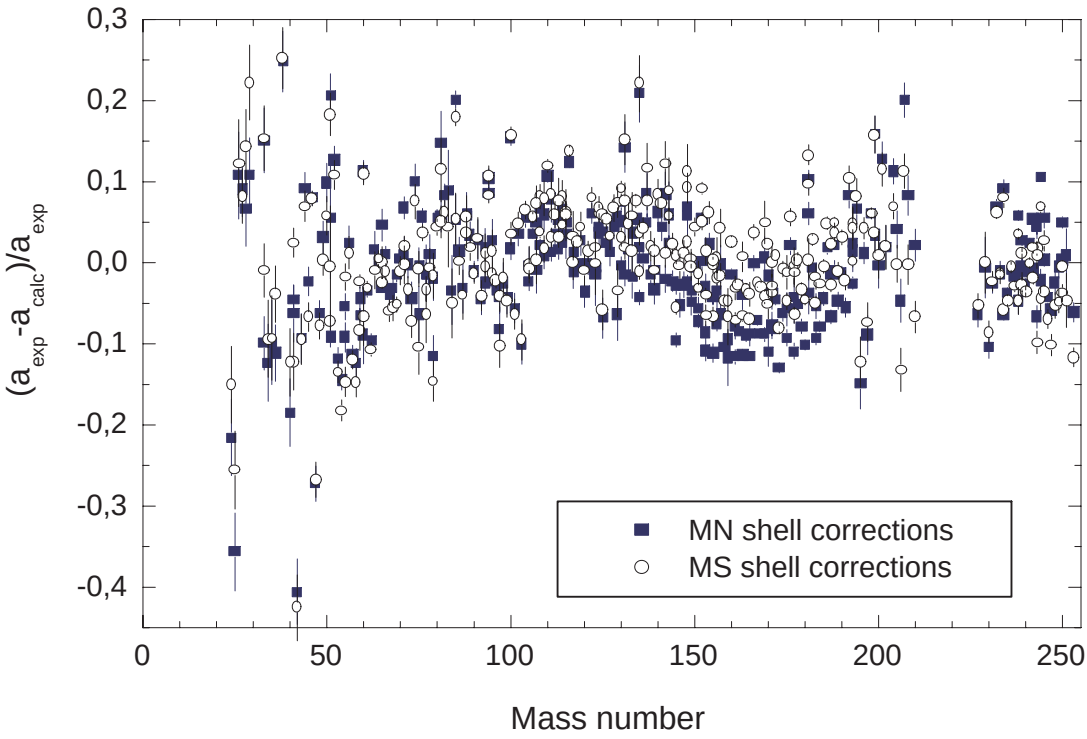

Figure 6.7: Deviations between the level density parameters derived from the resonance spacing analysis and their systematics for the BSFG model.

Deviations of the a-parameters in Fig. 6.5 from the parameters calculated on the basis of the above systematics are shown in Fig. 6.7 for both sets of shell corrections. Standard deviations are 0.085 for the systematics with the Myers-Swiatecki corrections, and 0.088 for the Möller-Nix corrections.

An alternative approach was developed for the systematics of the level density parameters by the Brussels group [6.27]. The a-parameters derived from the neutron resonance spacings were approximated by the relationship

$$a(U,Z,A) = \tilde{a}\ [1 + 2\ \gamma\ \delta\ E_0\ \mathrm{e}^{-\gamma(U-\delta)}]$$

The shell corrections were derived from the experimental (or theoretical) binding energies considered in Chapter 2 with the simple spherical liquid-drop formula

$$M_{LD} = a_v A + a_s A^{\frac{2}{3}} + (a_{sym} + a_{ss}A^{-\frac{1}{3}})AI^2 + a_c Z^2/A^{\frac{1}{3}},$$

where $I = (N-Z)/A$. An optimized fit to the 1888 experimental masses with $N, Z \geq 8$ [6.28] leads to a final rms deviation of 3 MeV for the liquid-drop parameters (all in MeV):

$$a_v = -15.6428,\ a_s = 17.5418,\ a_{sym} = 27.9418,\ a_{ss} = -25.3440,\ a_c = 0.70.$$

With pairing corrections of $\delta = 0.5, 0, -0.5$ for even-even, odd, and odd-odd nuclei, respectively, the spin cutoff parameter $\sigma^2 = 0.0194A^{5/3}\sqrt{U/a}$; the asymptotic level density

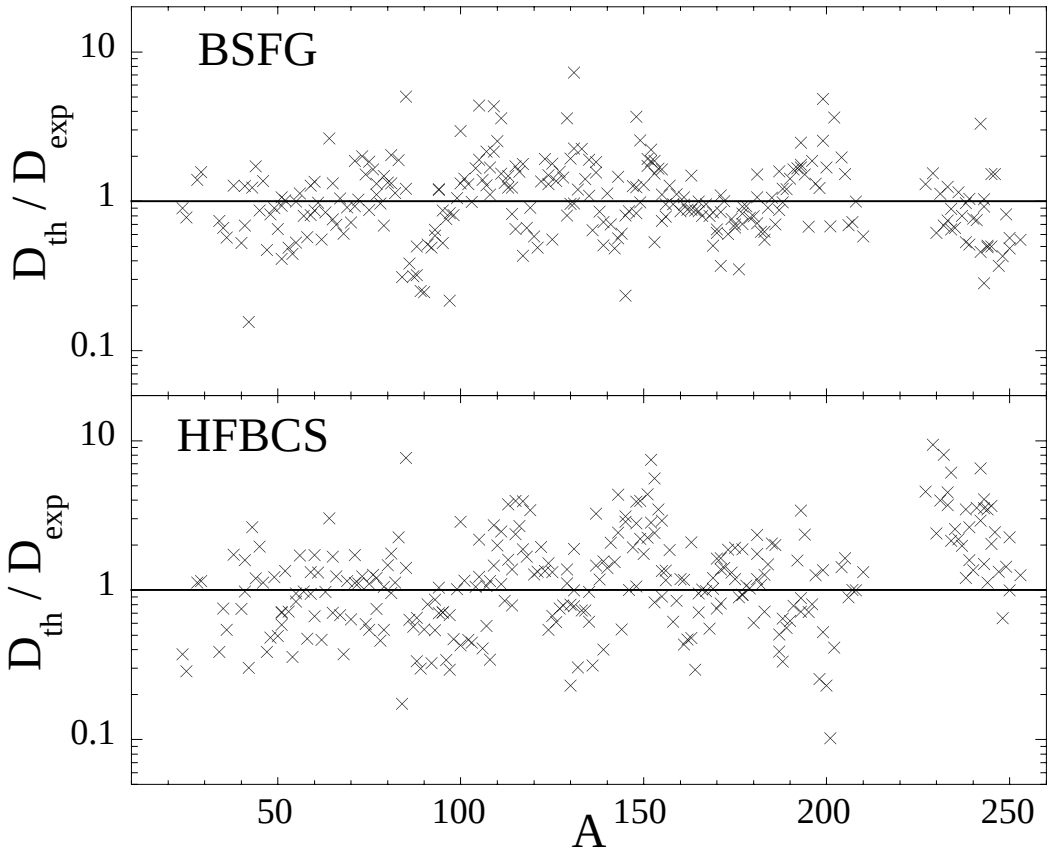

Figure 6.8: Comparison between theoretical D_{th} and experimental D_{exp} values of the s-neutron resonance spacings. The theoretical predictions are obtained with the analytical BSFG formula given in the text (upper panel) and the HFBCS-based model (lower panel).

parameters of Eqs. 6.13, can be obtained from a least-squares fit of the updated s-neutron resonance spacings D_{exp} to give the following coefficients (in MeV^{-1}):

$$\alpha = 0.1012, \qquad \beta = 0.0356, \qquad \gamma = 0.030. \tag{6.22}$$

Ratios D_{th}/D_{exp} of the theoretical and experimental resonance spacings are shown in Fig. 6.8. The root mean square deviation factor can be used to estimate the overall deviation with respect to the experimental data:

$$f_{rms} = exp\left[\frac{1}{N_e}\sum_{i=1}^{N_e}\ln^2\frac{D^i_{th}}{D^i_{exp}}\right]^{1/2},$$

where N_e is the number of nuclei considered. The present parameterization describes the experimental data with a deviation $f_{rms} = 1.78$ that is comparable with the deviation factor $f_{rms} = 1.48$ obtained for the more complex parameterization of the BSFG model parameters in Ref. [6.26]. Results of microscopic calculations of resonance spacings are also shown in Fig. 6.8 for comparison, and will be considered later.

Note that the BSFG model can diverge for the very low excitation energies for even-even and odd nuclei. So the BSFG model should be combined with the constant temperature model for excitation energies below the accepted upper boundary of low-lying levels.

Of course, the nuclear temperatures and energy shifts for such a low-energy approach will be rather different from those considered for the Gilbert-Cameron model (see above).

6.1.3 Generalized superfluid model

On the basis of all results considered above, we can conclude that the Fermi-gas and constant temperature models provide us with comparatively simple and convenient formula for parameterizing experimental data on nuclear level densities. However, these models do not give any explanation for the shifts of excitation energies and shell changes of the level density parameters. An interpretation of these effects must be obtained on the basis of more rigorous models that take into consideration shell inhomogeneities of single-particle level spectra, and the superfluid and collective effects produced by the residual interaction of nucleons. A detailed discussion of such models can be found in Ref. [6.18]. However, rigorous microscopic methods to calculate level densities are extremely laborious which limits their application to experimental data analyses. Thus, there is a need to develop a consistent phenomenological description of nuclear level densities that takes into account the basic ideas of microscopic approaches to the structure of highly excited nuclear levels, while being sufficiently simple and convenient for broad application.

The influence of the super-conductive pairing correlations on nuclear properties can be characterized by the value of the correlation functions ($\Delta_{0\tau}$), which determine directly the even-odd differences in the nuclear binding energies and the energy gap of $2\Delta_{0\tau}$ in the spectrum of quasi-particle excitations in even-even nuclei. The critical temperature t_c of the phase transition from a super-conductive (superfluid) to a normal state is also related to the correlation function

$$t_c = 0.567\Delta_0. \tag{6.23}$$

The excitation energy corresponding to the critical temperature may be expressed as:

$$U_c = \frac{\pi^2}{6} g t_c^2 + \frac{1}{4} g \Delta_0^2 - n\Delta_0, \tag{6.24}$$

where $n = 0$, 1 and 2 for even-even, odd and odd-odd nuclei, respectively.

Above the critical energy the level density and other nuclear thermodynamic functions can be described by the Fermi-gas relationship in which the effective excitation energy is defined as

$$U^* = U - E_{cond}, \tag{6.25}$$

where E_{cond} is the condensation energy that determines a reduction of the nuclear ground state energy due to the pairing correlations

$$E_{cond} = \frac{1}{4} g \Delta_0^2 - n\Delta_0. \tag{6.26}$$

Below the phase transition point (Eq. 6.23) the expressions for the thermodynamic functions of a nucleus are rather complex, and will not be considered here. Complete expressions can be found in Refs. [6.18, 6.29, 6.30], and the corresponding codes were included in the RIPL-1 files.

If coherent collective effects are included to accommodate excited level structure, the nuclear level density may be expressed as

$$\rho(U) = \rho_{qp}(U) K_{vibr}(U) K_{rot}(U), \tag{6.27}$$

where ρ_{qp} is the level density due to quasi-particle excitations only, and K_{vibr} and K_{rot} are the corresponding enhancement coefficients due to vibrational and rotational excitations, respectively.

Rotational enhancement of the level density in the adiabatic approximation depends on the nuclear shape symmetry, and can be written as [6.31]

$$K_{rot} = \begin{cases} 1 & \text{for spherical nuclei,} \\ \mathcal{I}_{\perp} t & \text{for deformed nuclei,} \end{cases} \tag{6.28}$$

where $\mathcal{I}_{\perp}$ is the moment of inertia relative to the perpendicular axis. This formula is obtained if mirror and axial symmetry of a deformed nuclei is assumed. The most stable nuclei of the rare-earth elements ($150 \leq A \leq 190$) and the actinides $A \geq 230$ have this shape. Rotational enhancement of the level density becomes greater for non-axial forms [6.31].

The vibrational enhancement coefficient is determined in the microscopic approach by the relationship

$$K_{vibr} = \prod_i \left[\frac{1 - \exp(-\omega_i^0/t)}{1 - \exp(-\omega_i/t)} \right]^{g_i}, \tag{6.29}$$

where ω_i is the energy of the vibrational excitations, ω_i^0 is the energy of the corresponding quasi-particle excitation, and g_i is the degeneracy of such excitations. The presence of quasi-particle energies in Eq. 6.29 accounts to some extent for non-adiabatic effects in excited nuclei. Due to symmetry constrains imposed on the nuclear Hamiltonian, the rotational and vibrational excitations become connected in a consistent microscopic approach [6.18]. As a result, the calculated collective enhancement coefficients are always reduced in comparison to the adiabatic estimation.

The adiabatic estimation of K_{rot} increases the nuclear level densities by a factor of 50-100 compared to calculations based on quasi-particle excitations alone. Increases of level densities due to vibrational excitations will only be appreciable for low-energy excitations with $\omega_i <$ 1-2 MeV.

Over the previous twenty years, some microscopic models have been developed to consider collective effects in highly excited nuclei. The results of all these models demonstrate the damping of level density enhancement factors with increase of excitation energy. On the basis of the level density calculations within the SU-3 model (oscillator mean field with the quadrupole-quadrupole interaction between particles), Hansen and Jensen [6.32] obtained the empirical function

$$K_{rot}(U) = \frac{K_{rot}^{adiab}(U)}{1 + \exp[(U - U_r)/d_r]}, \tag{6.30}$$

that describes the damping of rotational enhancement factors. The parameters of this formula were estimated as

$$U_r = 120 A^{1/3} \beta_2^2 \text{ MeV}, \qquad d_r = 1400 A^{-2/3} \beta_2^2 \text{ MeV}, \tag{6.31}$$

where β_2 is the quadrupole deformation parameter. Some other phenomenological descriptions for the damping enhancement factor were discussed in Refs. [6.33, 6.34, 6.35]. All such descriptions include at least one or two parameters that can fluctuate from one nucleus to another. Rather large uncertainties exist in estimates of the collective damping enhancement, and unfortunately we have no reliable experimental data that could be used for a crucial test of the various model predictions.

The vibrational enhancement of the level density can be approximated by the equation

$$K_{vibr} = \exp[\delta S - (\delta U/t)], \tag{6.32}$$

where δS and δU are changes in the entropy and excitation energy, respectively, that result from the vibrational modes. These changes are described by the Bose gas relationships:

$$\begin{aligned} \delta S &= \sum_i (2\lambda_i + 1)[(1+n_i)\ln(1+n_i) - n_i \ln n_i], \\ \delta U &= \sum_i (2\lambda_i + 1)\omega_i n_i, \end{aligned} \tag{6.33}$$

where ω_i are the energies, λ_i are the multipolarities, and n_i are the occupation numbers for vibrational excitations at a given temperature. The disappearance of collective enhancement of the level density at high temperatures can be taken into account by defining the occupation numbers in terms of the equation:

$$n_i = \frac{\exp(-\gamma_i/2\omega_i)}{\exp(\omega_i/t) - 1}, \tag{6.34}$$

where γ_i are the spreading widths of the vibrational excitations. This spreading of collective excitations in nuclei should be similar to the zero-sound damping in a Fermi liquid, and the corresponding width can be written as

$$\gamma_i = C(\omega_i^2 + 4\pi^2 t^2). \tag{6.35}$$

A value of $C = 0.0075A^{1/3}$ MeV^{-1} was obtained from the systematics of the neutron resonance densities of medium-weight nuclei [6.36]. This analysis adopted experimental values for the energies of the first 2^+ excitation, and $\omega = 50A^{-2/3}$ MeV for the octupole excitations. Due to higher energies, the influence of the latter is much weaker than for the quadrupole excitations.

The shell inhomogeneities of single-particle level spectra result in a particular form of energy dependence of the level density parameter $a(U)$: shell effects become weaker with increasing excitation energy, and at sufficiently high energies the dependence of parameter a on the mass number tends to the semi-classical value (Eq. 6.3). This important behavior of the level density parameter was used in defining the systematics of the Fermi-gas model parameters (Eq. 6.11). Similar equations for the GSM model [6.29] can be written as

$$a(U,Z,A) = \begin{cases} \tilde{a}(A)\,[1 + \delta E_0\ f(U^*)/U^*] & \text{for } U \geq U_c, \\ a_c(U_c, Z, A) & \text{for } U < U_c. \end{cases} \tag{6.36}$$

An additional shift of the excitation energies

$$U_{eff} = U^* + \delta_{shift}$$

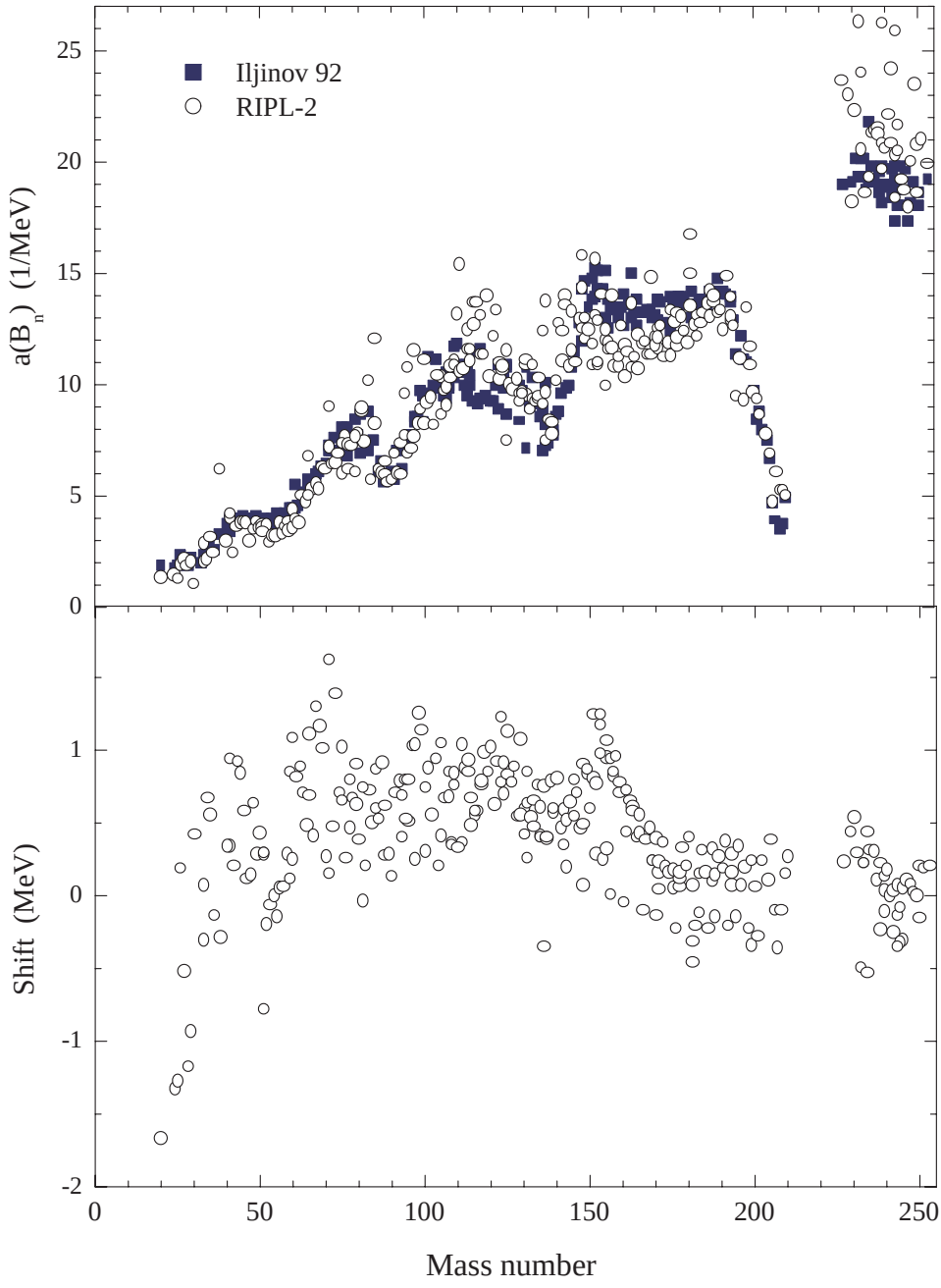

Figure 6.9: Level density parameters for the generalized superfluid model.

was introduced into Eq. 6.36 [6.35, 6.36] to take into account possible shortcomings of the global systematics of the pairing correlation functions and collective enhancement coefficients. The set of parameters $\tilde{a}$ and δ_{shift} was obtained from the simultaneous fitting of the cumulative numbers of low-lying levels and neutron resonance spacings, using the same data set as for the Gilbert-Cameron and backed-shifted Fermi-gas models. The parameters obtained are shown in Fig. 6.9, and are contained within the *level-densities-gsfm.dat* file. Results of a similar analysis performed with the Fermi-gas model that takes into account the collective enhancement of level densities are also shown for comparison

[6.11]. Collective enhancement reduces the values of the a-parameters that corresponds to the observed neutron resonance spacings, but the shell effects remain approximately the same as shown in Figs. 6.1 and 6.4 .

At first glance, the systematics of the level density parameters in terms of the Fermi-gas and GSM models appear to be equally justified, since they give almost identical descriptions of the level densities at excitation energies close to the neutron binding energy. However, these descriptions correspond to different absolute values of the level density parameters, because the inclusion of collective effects decreases the resulting a-parameters. The reduced values agree reasonably well with both the experimental data derived from the spectra of inelastically scattered neutrons with energies up to 7 MeV, and with theoretical calculations of the a-parameters for the single-particle level schemes of a Woods-Saxon potential [6.29]. This agreement is very encouraging because the evaporation spectra are most sensitive to the level density parameter. Differences between the a-parameter obtained from resonance data and from evaporation spectra cannot be explained in terms of the Fermi-gas model without accounting for the collective effects. Consideration of the level density collective enhancement is also very important for a consistent description of the observed fissile behaviour of highly-excited nuclei [6.37].

Nowadays, there is overwhelming evidence that the description of the level densities of excited nuclei should use more consistent models than those of the Fermi-gas model, albeit inevitably more complex. The success of the generalized superfluid model is attributed to the inclusion of the well-known major components of nuclear theory: pairing correlations, shell effects and collective excitations. Some complexity in the model seems to be justified by the mutual consistency of the parameters obtained from the various experimental data, and by the close relationship between the theoretical concepts used to describe the structure of low-lying nuclear levels and the statistical properties of highly excited nuclei.

Individual parameters are preferable for all practical applications. Parametric uncertainties are not important in predicting the level densities within an intermediate energy region if the experimental data for neutron resonances and low-lying levels have been chosen correctly. Analyses of the evaporation spectra of different particles are of great interest in studies of nuclear level densities. The energy dependencies of the level densities obtained from the spectrum analyses of various threshold reactions are in good agreement with the calculations based on the individual parameters of the GSM model [6.36].

However, many tasks require nuclear level density parameters for which no experimental data are available. Under such circumstances, global parameters may be used, and certain localised systematics may be proposed for these parameters that are based on extrapolations of the isotopic or isotonic changes. Experimental data on the cumulative number of low-lying levels can be fitted to one of the individual parameters, which may be advantageous in maintaining the global systematics for other parameters. We performed the analisis data shown in Fig. 6.9 in order to obtain a global systematics of the GSM parameters . Using the Myers-Swiatecki shell corrections and Eqs. 6.13 for the asymptotic and damping a-parameters, the following coefficients (in MeV^{-1}) have been obtained from a least-squares fit of the data:

$$\alpha = 0.103 \pm 0.004, \qquad \beta = -0.105 \pm 0.014, \qquad \gamma_0 = 0.375 \pm 0.015. \tag{6.37}$$

The energy shifts (in MeV) were approximated by the simple relationship:

$$\delta_{shift} = 0.617 - 0.00164\ A.$$

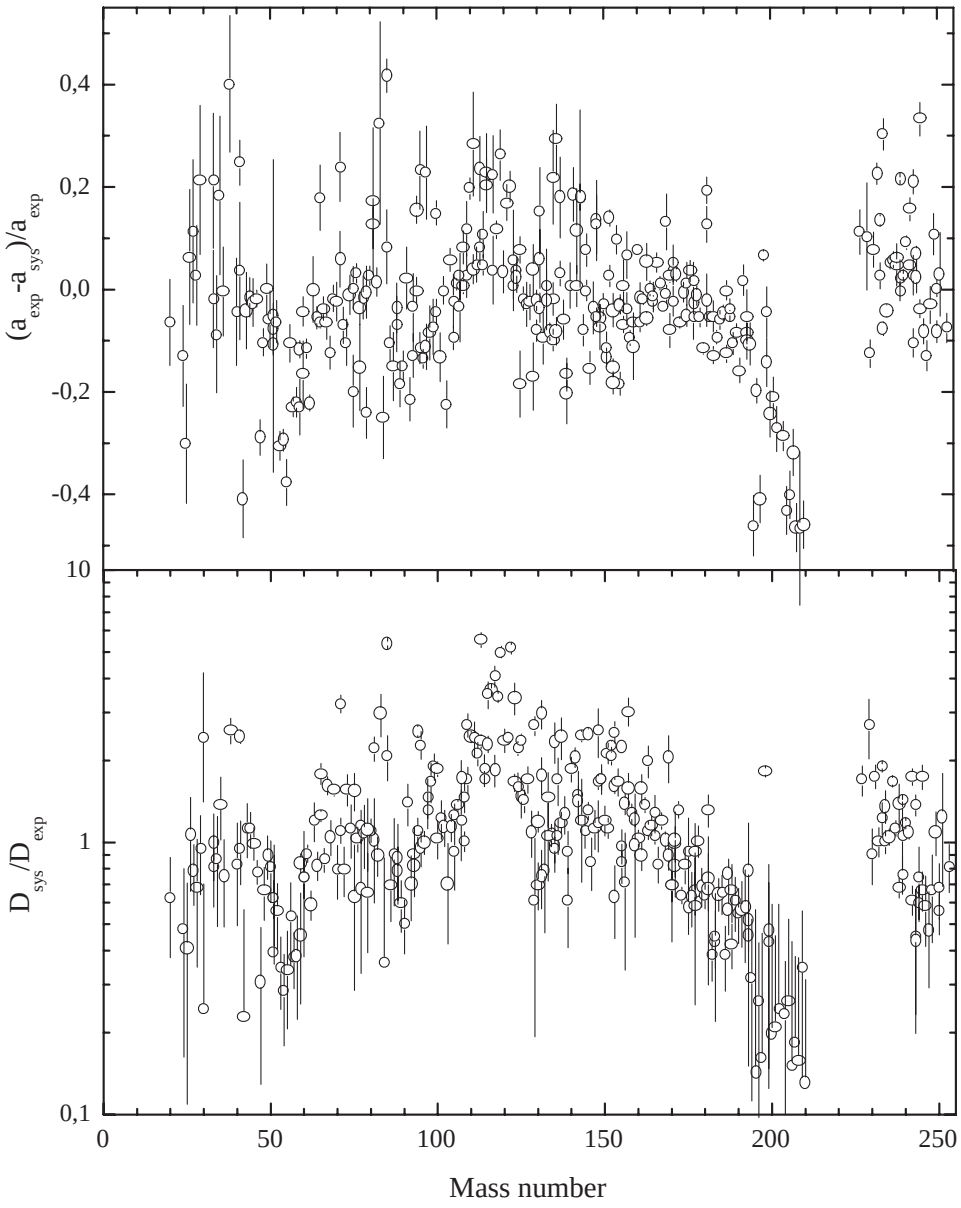

Figure 6.10: Deviations between the level density parameters derived from the resonance spacing analysis and their systematics for the GSM model.

Deviations between the a-parameters calculated on the basis of such systematics and estimated from the resonance spacing analysis (Fig. 6.9) are shown in Fig. 6.10. The standard deviation for the a-parameters is equal to 0.169, and the equivalent factor $f_{rms} = 1.98$.

Deviations for GSFM are generally not much larger than equivalent data for the Gilbert-Cameron model or BSFG. Careful analyses imply that the major deviations are related to the near-magic nuclei for which the shell effects are so strong that their consistent description is possible for only microscopic models. Some essential deviations also exist for nuclei in which the structure of the collective excitations is intermediate between

vibrational and rotational. A more accurate estimate of collective enhancements could be required for such nuclei than the separate consideration of vibrational and rotational effects used in the above analysis.

6.1.4 Microscopic Generalized Superfluid Model

A more rigorous description of the level densities and other statistical characteristics of excited nuclei can be obtained from calculations performed with realistic schemes of the single-particle levels. Such calculations are considered in detail in Ref. [6.18]. The thermodynamic functions of an excited nucleus (similar to Eq. 6.2 of the Fermi-gas model) may be written in the form

$$\begin{aligned} S &= \sum_i g_i[\beta E_i \overline{n}_i + \ln(1+\exp(-\beta E_i)], \\ U &= \frac{1}{2}\sum_i g_i[\sqrt{(\epsilon_i-\lambda)^2+\Delta_0^2} - E_i(1-2\overline{n}_i)] + \frac{\Delta_0^2-\Delta^2}{G}, \end{aligned} \tag{6.38}$$

where β $(= 1/t)$ is the inverse temperature, E_i are the energies of quasiparticle nuclear excitations, $\overline{n}_i = [1+\exp(-\beta E_i)]^{-1}$ are the occupation numbers for the corresponding single-particle levels, and g_i is the degeneracy of these levels and the sums for i runs over all single-particle levels for both protons and neutrons. The quasiparticle energies $E_i = [(\epsilon_i - \lambda_\tau)^2 + \Delta_\tau^2]^{1/2}$ are related to the single-particle energies and the correlation function Δ_τ by the equations

$$\begin{aligned} G_\tau^{-1} &= \frac{1}{4}\sum_i g_i \frac{1-2\overline{n}_i}{E_i}, \\ N_\tau &= \frac{1}{2}\sum_i g_i[1 - \frac{\epsilon_i-\lambda_\tau}{E_i}(1-2\overline{n}_i)], \end{aligned} \tag{6.39}$$

where N_τ is the number of protons or neutrons in a nucleus, λ_τ is the corresponding chemical potential, and G_τ is the pairing force constant. Eqs. 6.39 determine the proton and neutron correlation functions for the ground state of a nucleus at $t = 0$.

For given schemes of single-particle levels, Eqs. 6.38 and 6.39 permit the thermodynamic functions and the nuclear level densities to be calculated without any additional parameters. Differences between the behavior of the thermodynamic (Eqs. 6.38) and the Fermi-gas functions (Eqs. 6.2) can be traced by determining the following functions

$$\begin{aligned} a' &= S^2/4U, \qquad \overline{a} = \frac{\pi^2}{6}\beta\sum_i g_i\overline{n}_i(1-\overline{n}_i), \\ \overline{m^2} &= \frac{pi^2}{6\overline{a}}\beta\sum_i m_i^2 g_i\overline{n}_i(1-\overline{n}_i), \qquad \mathcal{I}_\parallel = \beta\sigma^2. \end{aligned} \tag{6.40}$$

Calculated level density parameters for low excitation energies reproduce rather well the shell variations of the Fermi-gas model parameters observed in experimental data [6.18]. At high excitation energies (above 50 MeV), the mass number dependence of the calculated parameters is very close to the semiclassical expression (Eq. 6.3).

Codes for microscopic calculations of the nuclear level densities are included in the RIPL-1 and RIPL-2 libraries. Collective effects are also included in these codes on the basis of the same approximations as for the phenomenological generalized superfluid model.

The single-particle level schemes of Möller *et al.* [6.24] are recommended for such calculations because they were also used to determine the recommended nuclear binding energies, shell corrections and deformations (see Chapter 2). Therefore, their application to the level densities provides the desired consistency between the ground and excited states.

An alternative description of nuclear level densities has been proposed in Ref. [6.19], based on the Extended-Thomas-Fermi plus Strutinsky-Integral model for the ground state properties (single-particle level schemes and pairing strengths). Although this approach represents the first global microscopic formula that could reasonably reproduce the experimental neutron resonance spacings, some large deviations have been found (for example, in the Sn region). These deficiencies have been removed in the new HFBCS-based model [6.38], which predicts all the experimental resonance spacings with an accuracy comparable to the equivalent data obtained by the phenomenological BSFG formula ($f_{rms} = 2.14$ for the ratios D_{th}/D_{exp}, as illustrated in Fig. 6.8). This microscopic model is based on the HFBCS ground state description [6.38] as characterized by a nucleon effective mass close to the real mass, a property of particular importance for reliable level density evaluations that provides a good description of the single-particle level density near the Fermi surface. HFBCS quantities relevant to the level density calculations can be found in the **single-particle-levels/spl-hfbcs** subdirectory, including the deformation parameters, the single-particle level schemes (energy, parity, spin), pairing strengths and the corresponding cut-off energies for both the neutron and proton systems.

The HFBCS single-particle schemes and deformations are used in addition to the renormalized pairing strength to estimate the spin-dependent level density within the statistical approach. All details of the level density calculations and predictions can be found in Ref. [6.38]. Such a model includes

- BCS pairing (constant-G approximation) with a renormalized strength and blocking effect for odd-mass and doubly odd nuclei,
- Gaussian-type spin dependence with microscopic shell and pairing effects on the spin cut-off parameter,
- collective contribution of the rotational band on top of each intrinsic state, and the disappearance of colletive enhancements at increasing excitation energies,
- deformation effects taken into account in the single-particle spectra,
- improved description of the cumulative number of nuclear levels at very low energies,
- reliable description of the level densities at high energies.

The microscopic HFBCS-based model has been renormalized to experimental data (278 neutron resonance spacings and 1210 low-lying levels) to account for the available experimental information, and can consequently be used for practical applications with a high degree of confidence. The level densities are tabulated for about 8000 nuclei with $8 \leq Z \leq 110$ lying between the proton and the neutron drip lines, and can be found in the **level-densities-hfbcs** subdirectory. Each table includes the spin-dependent level densities at energies up to $U = 150$ MeV and spin up to J = 29 (59/2) for each isotope considered. The nuclear temperature, cumulative number of levels and total level and

state densities are also included in these tables. Level densities at the inner and outer fission saddle points are estimated using the HFBCS-based model for some 2300 nuclei with $78 \leq Z \leq 120$; details of the corresponding calculations can be found in Chapter 8.

Another quantity of particular importance in reaction cross-section calculations and extracted traditionally from level density formula corresponds to the cut-off energy U_{max} above which the experimental level scheme ceases to be complete, or the number of known levels N_{max} up to which the level scheme is complete. N_{max} is usually obtained from a simple fit to the low-lying states with the constant temperature formula (see Chapter 3). However, this oversimplified model cannot reproduce any of the shell, pairing and deformation effects at low energies, except in a purely phenomenological manner by a two-parameter adjustment. N_{max} has now been determined on the basis of the microscopic HFBCS predictions [6.38]. Estimated N_{max} and U_{max} values can be found in the *nmax-umax-hfbcs.dat* file (including some 1220 nuclei for which more than 20 excited levels are known experimentally). N_{max} values obtained are substantially smaller than those derived from the constant-T evaluation presented in Chapter 3.

6.2 Partial level densities

The partial level density is used in pre-equilibrium reaction calculations to describe the statistical properties of particle-hole excitations [6.39]. Since the pioneering studies by Strutinsky [6.40], Ericson [6.41] and Blann [6.42], numerous theoretical methods have been developed to determine partial level densities (PLD), and a variety of approaches have been used in pre-equilibrium calculations. Some of these studies involve theoretical methods for incorporating physical phenomena such as shell effects and residual pairing interaction.

Despite extensive research, even the most sophisticated theoretical predictions can significantly deviate from reality. Difficulties arise in testing the validity of determining partial densities through comparison of calculated and measured pre-equilibrium spectra because of the uncertainties in our understanding of the pre-equilibrium reaction mechanisms. A useful collection of articles on PLD can be found in the conference proceedings on Nuclear Level Densities in Upton, New York in 1983 [6.43] and at Bologna in 1989 [6.44]. State-of-the-art methods to calculate PLD were recently reviewed by Běták and Hodgson [6.45].

The most widely used approach to PLD is an equidistant single-particle model using closed-form expressions, as proposed by Williams [6.46], and further refined by Dobeš and Běták [6.47], Kalbach [6.43, 6.48, 6.49, 6.50], Zhang and Yang [6.51], Baguer *et al* [6.52], Anzaldo-Meneses [6.53] and Hilaire *et al* [6.54].

Pairing effects play an important role in partial level density near the particle-hole configuration thresholds as shown by Strutinsky [6.40] and later more consistently by Ignatyuk and Sokolov [6.55] and Moretto [6.56]. Their results for pairing correction were parametrized by Fu [6.57] and Kalbach [6.49]. Numerical values of the Fu parameterization were recently refitted to the original results of Ignatyuk and Sokolov [6.55] to improve their accuracy near the thresholds [6.58].

An important modification has been made by Běták and Dobeš [6.59] to limit the holes to excitation energies less than the nuclear well depth. This approach was extended by Stankiewicz *et al* [6.60] and Obložinský [6.61] to consider binding energy restrictions. An analytical method to calculate PLD starting from an arbitrary single-particle level scheme was first proposed by Dobeš and Běták [6.47]. Chadwick and Obložinský [6.62] introduced the particle-hole state-densities with linear momentum in order to describe the linear momentum structure of the phase space of the excited particles and holes (excitons). Accuracy of the PLD formula that consider the Pauli exclusion principle was improved by Baguer *et al* [6.52]. As suggested by Běták and Dobeš [6.59], the new formulation was extended by De and Hua [6.63] to include the finite depth of the potential well and binding energy constraints. Corrections for the PLD calculation near the threshold were derived by Anzaldo-Meneses [6.53], while an extensive study of the equidistant spacing model was performed by Hilaire *et al* [6.54]. A new closed formula was proposed, which compares very well with the results of the exact calculations; however, this model is not easy to implement in routine calculations.

Since closed-form expressions for partial level densities based on equidistant levels are widely used in pre-equilibrium calculations, we provide below simple expressions for their determination as proposed by De and Hua [6.63]. Pairing correction is included following the parameterization of Fu [6.49, 6.57, 6.58]. The references cited above can also be consulted for other formulations.

6.2.1 Equidistant formula with exact Pauli correction term and binding-energy and well-depth restrictions

The density of p-particle h-hole states with residual nucleus energy U can be factorized into the energy-dependent density and spin distribution, $\rho(p,h,U,J) = \omega(p,h,U)\ R_n(J)$. Adopting the equidistant model expression for the energy dependent one-component (no neutron-proton distinction) density with finite hole-depth and binding-energy restrictions [6.63]:

$$\omega(p,h,U) = \frac{g^n}{p!h!}\sum_{i=0}^{p}\sum_{j=0}^{h}(-1)^{i+j}\binom{p}{i}\binom{h}{j}\sum_{\lambda=0}^{n-1}(E-\alpha(p,h)-iB-j\epsilon_{_F})^{n-1-\lambda}\frac{B(p,h,\lambda)}{(n-1-\lambda)!} \times\ \Theta(E-\alpha(p,h)-iB-j\epsilon_{_F}), \tag{6.41}$$

where

$$\begin{aligned} n &= p+h \\ \alpha(p,h) &= (p^2+h^2)/2g \\ B(p,h,\lambda) &= \sum_{k=0}^{\lambda} C(p,k)C(h,\lambda-k) \\ C(m,\lambda) &= \sum_{i=0}^{\lambda}\frac{b_i}{i!}(-\frac{m}{g})^i C(m-1,\lambda-i) \\ C(0,\lambda) &= \delta_{\lambda 0} \end{aligned}$$

and g is the single-particle density, B is the binding energy, $\epsilon_{_F}$ is the Fermi energy and $\alpha(p,h)$ is the Pauli energy (i.e., minimum possible $p-h$ configuration energy, if pairing

is not considered). The b_i coefficients are the Bernoulli numbers which are tabulated elsewhere ($b_0 = 1$, $b_1 = 1/2$, $b_{2k+1} = 0$ for $k \geq 1$,...). Θ-function is unity if the argument is positive, and zero otherwise. The single-particle density is often taken as $g = A/13$, which approximates to the average single-particle density near the Fermi energy. As pointed out by Kalbach [6.49], we can implement the pairing corrections by substituting the Pauli energy $\alpha(p,h)$ by the threshold energy $E_{thresh}(p,h)$ [6.49, 6.58]:

$$E_{thresh}(p,h) = \frac{g(\Delta_0^2 - \Delta^2)}{4} + p_m \left[(p_m/g)^2 + \Delta^2\right]^{1/2}$$

where $p_m = \max(p,h)$, and Δ_0 and Δ are the ground and excited state pairing gaps, respectively. The ratios of the pairing gaps were reported by Rejmund *et al* [6.58] to be:

$$\begin{aligned} (\Delta/\Delta_0) &= 0.996 - 2.36(n/n_c)^{1.57}/(E/C)^{0.76} \quad \text{if } (E/C) \geq 1.03 + 2.07(n/n_c)^{2.91} \\ &= 0 \qquad\qquad\qquad\qquad\qquad\qquad\qquad\qquad\quad \text{otherwise} \end{aligned}$$

where $C = g\Delta_0^2/4$ is the condensation energy, and $n_c = 0.791 g\Delta_0$ is the number of excited quasi-particles at the phase-transition point from the super-fluid state to the normal state.

As $B \to \infty$ and $\epsilon_{_F} \to \infty$ in Eq. (6.41), only the first term (corresponding to i = 0 and j = 0) remains on the right side, and we obtain the PLD expression derived by Baguer *et al* [6.52]. Expanding the factor $(E - \alpha(p,h) - iB - j\epsilon_{_F})^{n-1}$ by means of the binomial theorem, we can obtain the equidistant model expression for the energy-dependent one-component density with finite hole-depth and binding-energy restrictions similar to those derived by Běták and Dobeš [6.59] and Obložinsky [6.61]

$$\omega(p,h,U) = \frac{g^n}{p!h!(n-1)!} \sum_{i=0}^{p} \sum_{j=0}^{h} (-1)^{i+j} \binom{p}{i} \binom{h}{j} (E - \alpha(p,h) - iB - j\epsilon_{_F})^{n-1}$$
$$\text{x } \Theta(E - \alpha(p,h) - iB - j\epsilon_{_F}). \qquad (6.42)$$

A Gaussian spin distribution is usually adopted:

$$R_n(l) = \frac{2J+1}{2\sqrt{2\pi}\sigma_n^3} \exp\Big[-\frac{(J+1/2)^2}{2\sigma_n^2}\Big], \qquad (6.43)$$

where J is the spin and σ_n is the spin cut-off parameter (often taken as $\sigma_n^2 = 0.24nA^{2/3}$ [6.64]).

RIPL-2 includes a code written by Avrigeanu and Avrigeanu to calculate partial level densities using various models, as described in their extensive paper [6.65].

6.2.2 Microscopic theory

Most semi-empirical approaches to partial level densities are based on various simplifying approximations. Such approaches often account inadequately for shell effects, pairing effects and parity distributions. More involved microscopical methods have been developed

to address these deficiencies and calculate realistic particle-hole level densities using the single-particle level scheme of the shell model. Additionally, the BCS formalism has been included to account more properly for pairing effects. An exact method of computing partial nuclear level densities directly from a set of single-particle states has been proposed by Williams [6.66], which is based on the repetitive use of recursion relations to expand the grand partition function and does not rely on the saddle-point approximation (unlike the traditional statistical method). Far shorter computation times than the combinatorial approach (counting all possible configurations) are required. Unfortunately, this method cannot treat residual interactions in the classical form, and therefore is only useful in the non-interacting Fermi-gas model.

The advent of high speed computers has encouraged the use of calculational methods which do not depend on closed-form expressions. These studies include combinatorial approaches involving exhaustive counting of particle-hole configurations [6.67, 6.68, 6.69, 6.70, 6.71]. The combinatorial method yields an exact level density (at least within the independent particle model), but is very time consuming and can become intractable at high excitation energies or for large shell model spaces (heavy nuclei). Pairing interaction may be included by applying BCS theory [6.70], but at the expense of significantly increased computation times. Therefore, the Monte-Carlo technique as proposed by Cerf [6.72, 6.73] is normally adopted to avoid exhaustive counting of the excited levels. Monte Carlo methods provide very efficient algorithms for solving combinatorial problems (e.g., combinatorial optimization problems solved by simulated annealing). However, these methods as applied to partial level densities are still at a relatively early stage of development [6.74].

RIPL-2 includes the *microscopic.for* code developed by Capote and Pedrosa [6.75] from the ICAR code described in Ref. [6.70]. This code allows for microscopic calculations of particle-hole partial level densities (up to $3p-3h$ for even-even nuclei), which represent the dominant contribution to the pre-equilibrium component of emission spectra. Shell-model single-particle levels are required as input, and are also included in this compilation (Nix-Möller and Hartree-Fock-BCS).

6.3 Conclusions and recommendations

For any application of the statistical theory of nuclear reactions, the parameters describing the level density must be obtained from reliable experimental data. Both the cumulative numbers of low-lying levels and the average spacings of neutron resonances are normally used for this purpose. The level density parameters fitted to such data were compiled in RIPL-1 for the three models most frequently used in practical calculations: i) Gilbert-Cameron approach that combines the constant temperature model for low excitation energies and the Fermi-gas model at high energies; ii) back-shifted Fermi-gas model; iii) generalized superfluid model that considers the shell, pairing and collective effects.

During the development of RIPL-2, the previously recommended data were tested and revised on the basis of the updated evaluations of the neutron resonance spacings and the low-lying level systematics considered in Chapters 3 and 4. Revised parameter sets were obtained for all three models. Furthermore, the systematics of the level density parameters were developed for each model in terms of the shell correction approach. Such systematics are recommended for level density calculations involving nuclei that have no

experimental data on either their resonance spacings or low-energy level densities.

RIPL-2 contains large quantities of data from the microscopic calculations of nuclear level densities based on the HFBCS model. The microscopic model takes into account the shell, pairing and blocking effects, deformation effects in the single-particle spectra, collective enhancement of level densities at low excitation energies and damping at high excitations. Corresponding tables of level densities for about 8000 nuclei are provided. The codes and single-particle level schemes for the microscopic calculations of the nuclear level densities are also given.

Microscopic calculations can be useful for detailed studies of the role of partial level densities in the pre-equilibrium emission since such calculations take into account shell and pairing effects. However, the results should always be treated with caution, as the predictive capabilities of all partial level density theories are limited. For many pre-equilibrium calculations, the more phenomenological models included in Avrigeanu's code are adequate. The general formula derived by De and Hua [6.63] is recommended for use, which includes pairing corrections, binding energy and finite potential depth constraints, and a precise treatment of the Pauli exclusion principle. However, the limitations of such partial level density predictions should be kept in mind, especially considering the uncertainties in our understanding of pre-equilibrium reaction mechanisms.

6.4 Summary of codes and data files

The structure of the directory is as follows:

```
densities/
     partial/
          pld-analytical.readme
          pld-analytical.tgz
          pld-microscopic.readme
          pld-microscopic.tgz

     single-particle-levels/
          spl-frdm/
          spl-frdm.readme
          spl-hfbcs/
          spl-hfbcs.readme
          spl-retrieve.for
          spl-retrieve.readme

     total/
          level-densities-bsfg.dat
          level-densities-bsfg.readme
          level-densities-gc.dat
          level-densities-gc.readme
          level-densities-gsfm.dat
          level-densities-gsfm.readme
          level-densities-hfbcs/
          level-densities-hfbcs.readme
          level-densities-micro.readme
          level-densities-micro.tgz
          nmax-umax-hfbcs.dat
          nmax-umax-hfbcs.readme
```

```
shellcor-ms.dat
shellcor-ms.readme
```

The programs and data files included in the directory are:

pld-analytical.readme - description of *pld-analytical.tgz* file.

pld-analytical.tgz - FORTRAN code that provides a set of subroutines for calculating p-h level densities using analytical expressions for various equidistant and Fermi-gas single-particle models.

pld-microscopic.readme - description of *pld-microscopic.tgz* file

pld-microscopic.tgz - FORTRAN code for microscopic calculation of p-h state densities.

spl-frdm/zxxx.dat - single-particle levels and ground state deformations calculated within the FRDM model.

spl-frdm.readme - description of *spl-frdm/zxxx.dat* files.

spl-hfbcs/zxxx.dat - single-particle levels and ground state deformations calculated within the Hartree-Fock-BCS model.

spl-hfbcs.readme - description of *spl-hfbcs/zxxx.dat* files.

spl-retrieve.for - code for retrieving single-particle level schemes from *spl-frdm/zxxx.dat* and *spl-hfbcs/zxxx.dat* files.

spl-retrieve.readme - description of *spl-retrieve.for* file.

level-densities-bsfg.dat - level density parameters for BSFG model.

level-densities-bsfg.readme - description of *level-densities-bsfg.dat* file.

level-densities-gc.dat - level density parameters for the Gilbert-Cameron approach.

level-densities-gc.readme - description of *level-densities-gc.dat* file

level-densities-gsfm.dat - level density parameters for the Generalized Superfluid Model.

level-densities-gsfm.readme - description of *level-densities-gsfm.dat* file.

level-densities-hfbcs/zxxx.dat - tabulated nuclear level densities calculated on the basis of the statistical partition function approach, based on the realistic microscopic single-particle level schemes determined within the HF-BCS mass model.

level-densities-hfbcs.readme - description of *level-densities-hfbcs/zxxx.dat* file.

level-densities-micro.readme - description of *level-densities-micro.tgz file.*

level-densities-micro.tgz - microscopic statistical code for calculation of level densities, with phenomenological treatment of rotational and vibrational enhancements and including their temperature damping.

nmax-umax-hfbcs.dat - compilation of Nmax and Umax based on microscopic nuclear level densities.

nmax-umax-hfbcs.readme - description of *nmax-umax-hfbcs.dat* file

shellcor-ms.dat - shell corrections of Myers-Swiatecki mass formula.

shellcor-ms.readme - description of *shellcor-ms.dat* file.

REFERENCES

[6.1] BETHE, H., Rev. Mod. Phys. **9** (1937) 69.

[6.2] LANG, J.M., LE COUTEUR, K.J., Proc. Phys. Soc. **A67** (1954) 586.

[6.3] ERICSON, T., Adv. Phys. **9** (1960) 425.

[6.4] ERBA, E., FACCHINI, U., SAETTA-MENICHELLA, E., Nuovo Cim. **22** (1961) 1237.

[6.5] GILBERT, A., CAMERON, A.G.W., Can. J. Phys. **43** (1965) 1446.

[6.6] LYNN, J.E., Theory of Neutron Resonance Reactions, Clarendon Press, Oxford (1968).

[6.7] MALYSHEV, A.V., Level Density and Structure of Atomic Nuclei, Atomizdat, Moscow (1969) (in Russian).

[6.8] BABA, H., Nucl. Phys. **A159** (1970) 625 .

[6.9] DILG, W., SCHANTL, W., VONACH, H., UHL, M., Nucl. Phys. **A217** (1973) 269.

[6.10] REFFO, G.,in Nuclear Theory for Applications, IAEA-SMR-43, Trieste (1980) 205.

[6.11] ILJINOV, A.S., MEBEL, M.V., BIANCHI, N., DE SANCTIS, E., GUARALDO, C., LUCHERINI, V., MUCCIFORA, V., POLLI, E., REOLON, A.R., ROSSI, P., Nucl. Phys. **A543** (1992) 517.

[6.12] INTERNATIONAL ATOMIC ENERGY AGENCY, Handbook for Calculations of Nuclear Reaction Data - Reference Input Parameter Library, IAEA-TECDOC-1034, Vienna (1998).

[6.13] COOK, J.L., FERGUSON, H., MUSGROV, L., Aust. J. Phys. **20** (1967) 477.

[6.14] SU ZONGDI, ZHUANG YOUXIANG, WANG CUILAN, ZHOU CHUNMEI, Neutron Nuclear Reaction Theory and Application, INDC(CPR)-002, IAEA, Vienna (1985).

[6.15] LU GUOXIONG, DONG LIAOYUAN, HUANG ZHONGFU, QIU GUOCHUN, SU ZONGDI, Contribution to 3rd Research Co-ordination Meeting on RIPL, Trieste (1997).

[6.16] IGNATYUK, A.V., STAVISSKI, V.S., SHUBIN, Yu.N., Nuclear Data for Reactors, IAEA, Vienna (1970).

[6.17] RAMAMURTHY, V.S., KAPOOR, S.S., KATARIA, S.K., Phys. Rev. Lett. **25** (1970) 386.

[6.18] IGNATYUK, A.V., Statistical Properties of Excited Atomic Nuclei, Energoatomizdat, Moscow (1983) in Russian; INDC(CCP)-233, IAEA, Vienna (1985).

[6.19] GORIELY, S., Nucl. Phys. **A605**, (1996) 28.

[6.20] IGNATYUK, A.V., SMIRENKIN, G.N., TISHIN, A.S., Sov. J. Nucl. Phys. **21** (1975) 255.

[6.21] KATARIA, S.K., RAMAMURTHY, V.S., Nucl. Phys. **A349** (1980) 10.

[6.22] MENGONI, A., NAKAJIMA, Y., J. Nucl. Sci. Technol. **31** (1994) 151.

[6.23] MYERS, W.D., SWIATECKI, W.J., Ark. Fysik **36** (1967) 593.

[6.24] MÖLLER, P., NIX, J.R., MYERS, W.D., SWIATECKI, W.J., At. Data Nucl. Data Tables **59** (1995) 185.

[6.25] IGNATYUK, A.V., in Capture Gamma-Ray Spectroscopy and Related Topics, WENDER, S., (Ed.), Melville, NY, AIP 529 (2000) 481.

[6.26] RAUSCHER, T., THIELEMANN, F.K., KRATZ, K.L., Phys. Rev. **C56** (1997) 1613.

[6.27] GORIELY, S., Contribution to 3rd Research Co-ordination Meeting on RIPL-2, IAEA, Vienna (2000).

[6.28] AUDI, G., WAPSTRA, A.H., Nucl. Phys. **A595** (1995) 409.

[6.29] IGNATYUK, A.V., ISTEKOV, K.K., SMIRENKIN, G.N., Sov. J. Nucl. Phys. **29** (1979) 450.

[6.30] IGNATYUK, A.V., WEIL, J.L., RAMAN, S., KAHANE, S., Phys. Rev. **C47** (1993) 1504.

[6.31] BOHR, A., MOTTELSON, B., Nuclear Structure, Vol. 2, Benjamin Inc., New York and Amsterdam (1974).

[6.32] HANSEN, G., JENSEN, A., Nucl. Phys. **A406** (1983) 236.

[6.33] MAINO, G., MENGONI, A., VENTURA, A., Phys. Rev. **C42** (1990) 988.

[6.34] RASTOPCHIN, E.M., SVIRIN, M.N., SMIRENKIN, G.N., Sov. J. Nucl. Phys. **52** (1990) 1258.

[6.35] IGNATYUK, A.V., in Nuclear Data Evaluation Methodology, DUNFORD, C., (Ed.) World Scientific, Singapore (1992) 411.

[6.36] GRUDZEVICH, O.T., IGNATYUK, A.V., PLYASKIN, V.I., ZELENETSKY, A.V., in Proc. Nuclear Data for Science and Technology, Mito (1988).

[6.37] IGNATYUK, A.V., ISTEKOV, K.K., OKOLVICH, V.N., SMIRENKIN, G.N., in Physics and Chemistry of Fission, IAEA, Vienna, Vol. 1 (1980) 21.

[6.38] DEMETRIOU, P., GORIELY, S., Nucl. Phys. **A695** (2001) 95.

[6.39] GRIFFIN, J.J., Phys. Rev. Lett. **17** (1966) 478.

[6.40] STRUTINSKY, V.M., in Proc. Int. Conf. Nucl. Phys., Paris (1958) 617.

[6.41] ERICSON, T., Adv. Phys. **9** (1960) 425.

[6.42] BLANN, M., Phys. Rev. Lett. **21** (1968) 1357.

[6.43] Proceedings of IAEA Advisory Group Meeting on Basic and Applied Problems on Nuclear Level Densities, Upton, New York, 11-15 April 1983, BHAT, M.R. (Ed.), Brookhaven National Laboratory, BNL-NCS-51694 (1983).

[6.44] Proceedings of OECD Meeting on Nuclear Level Densities, Bologna, 15-17 Nov 1989, REFFO, G., HERMAN, M., MAINO, G., (Eds.), World Scientific, Singapore (1992).

[6.45] BĚTÁK, E., HODGSON, P., Rep. Progr. Phys. **61** (1998) 483.

[6.46] WILLIAMS Jr., F.C., Nucl. Phys. **A166** (1971) 231.

[6.47] DOBEŠ, J., BĚTÁK, E., Nucl. Phys. **A272** (1976) 353.

[6.48] KALBACH, C., Phys. Rev. **C32** (1985) 1157.

[6.49] KALBACH, C., Nucl. Sci. Eng. **95**, (1987) 70.

[6.50] KALBACH, C., Z. Phys. **A332**, (1989) 157.

[6.51] ZHANG JIN SHANG, YANG XIAN JUN, Z. Phys. **A329** (1988) 69.

[6.52] BAGUER, N., CAPOTE, R., PEDROSA, R., Z. Phys. **A334** (1989) 397.

[6.53] ANZALDO-MENSES, A., Z. Phys. **A353** (1995) 295.

[6.54] HILAIRE, S., DELAROCHE, J.P., KONING, A.J., Nucl. Phys. **A632** (1998) 417.

[6.55] IGNATYUK, A.V., SOKOLOV, Yu.V., Sov. J. Nucl. Phys. **17** (1973) 376.

[6.56] MORETTO, L.G., Nucl. Phys. **A243** (1975) 77.

[6.57] FU, C.Y., Nucl. Sci. Eng. **86** (1984) 344; Nucl. Sci. Eng. **92** (1986) 440.

[6.58] REJMUND, F., IGNATYUK, A.V., JUNGHANS, A.R., SCHMIDT, K.-H., Nucl. Phys. **A678** (2000) 215.

[6.59] BĚTÁK, E., DOBEŠ, J., Z. Phys. **A279** (1976) 319.

[6.60] STANKIEWICZ, K., MARCINKOWSKI, A., HERMAN, M., Nucl. Phys. **A435** (1985) 67.

[6.61] OBLOŽINSKÝ, P., Nucl. Phys. **A453** (1986) 127.

[6.62] CHADWICK, M.B., OBLOŽINSKÝ, P., Phys. Rev. **C44** (1991) R1740; Phys. Rev. **C46** (1992) 2028.

[6.63] MAO MING DE, GUO HUA, J. Phys. **G19** (1993) 421.

[6.64] REFFO, G., HERMAN, M., Lett. Nuovo Cimento **34** (1982) 261.

[6.65] AVRIGEANU, M., AVRIGEANU, V., Comp. Phys. Comm. **112** (1998) 191.

[6.66] WILLIAMS Jr., F.C., Nucl. Phys. **A133** (1969) 33.

[6.67] HILLMAN, M., GROOVER, J.R., Phys. Rev. **185** (1969) 1303.

[6.68] HILLMAN, M., Phys. Rev. **C9** (1974) 289.

[6.69] FORD, G.P., Nucl. Sci. Eng. **66**, (1978) 334.

[6.70] HERMAN, M., REFFO, G., Comp. Phys. Comm. **47** (1987) 103; HERMAN, M., REFFO, G., Phys. Rev. **C36** (1987) 1546; HERMAN, M., REFFO, G., REGO, R.A., Phys. Rev. **C37** (1988) 797.

[6.71] HILAIRE, S., DELAROCHE, J.P., GIROD, M., Eur. Phys. J. **A12** (2001) 169.

[6.72] CERF, N., Phys. Lett. **B268** (1991) 317.

[6.73] CERF, N., Phys. Rev. **C49** (1994) 852.

[6.74] DEAN, D.J., KOONIN, S.E., Phys. Rev. **C60** (1999) 054306.

[6.75] CAPOTE, R., PEDROSA, R., DENSIDAD code, private communication (1997).

7 GAMMA-RAY STRENGTH FUNCTIONS

Coordinators: M. Herman and V. Plujko

Summary

Methods and related parameters for modeling γ-ray cascades in highly excited nuclei have been reviewed. This assessment includes experimental radiative strength functions, Giant Resonance parameters and various means of calculating γ-ray strength functions in excited nuclei. Emphasis has been placed on the E1 γ-transitions, which tend to dominate nuclear reactions. Recent analytical expressions for dipole transition γ-ray strength functions provide reasonably reliable results over a relatively wide range of γ-ray energies (from zero to above the GDR energy). RIPL-1 data are recommended for other γ-ray multipolarities [7.1].

RIPL-2 contains tabulated dipole γ-ray strength functions and Giant Dipole Resonance parameters that result from extensive microscopic calculations and can be used directly by nuclear reaction codes.

Gamma emission is one of the most significant channels for nuclear de-excitation processes, and accompanies most nuclear reactions. Both gamma decay and photo-absorption can be described through radiative strength functions [7.2, 7.3], while electron-positron decay depends on the shape of the γ-ray strength functions [7.4, 7.5]. There are two types of radiative strength functions:

(i) 'downward' strength function ($\overleftarrow{f}$), which determines the average radiative width of the γ-decay, and

(ii) photo-excitation (upward) strength function ($\overrightarrow{f}$) related to the cross-section for γ-ray absorption.

The γ-decay strength function for a γ-ray emission of multipole type XL is defined as the average reduced partial radiation width $\epsilon_\gamma^{-(2L+1)}\langle\Gamma_{XL}(\epsilon_\gamma)\rangle$ per unit energy interval of resonances with average spacing D:

$$\overleftarrow{f}_{XL}(\epsilon_\gamma) = \epsilon_\gamma^{-(2L+1)}\langle\Gamma_{XL}(\epsilon_\gamma)\rangle/D, \tag{7.1}$$

where ϵ_γ is the γ-ray energy. The photo-excitation strength function $\overrightarrow{f}_{E\lambda}$ is determined by the average photo-absorption cross section $\langle\sigma_{XL}(\epsilon_\gamma)\rangle$ summed over all possible spins

of final states [7.3]:

$$\overrightarrow{f}_{E1}(\epsilon_\gamma) = \frac{\epsilon_\gamma^{-2L+1}}{(\pi\hbar c)^2}\frac{\langle\sigma_{XL}(\epsilon_\gamma)\rangle}{2L+1}. \tag{7.2}$$

All γ-decay strength functions depend on the temperature T_f of the final states, which is a function of the γ-ray energy in contrast to the initial state temperature T. The transmission coefficient $T_{XL}(\epsilon_\gamma)$ of the γ-ray emission is given by the relationship

$$T_{XL}(\epsilon_\gamma) = 2\pi\epsilon_\gamma^{(2L+1)}\overleftarrow{f}_{XL}(\epsilon_\gamma). \tag{7.3}$$

Therefore, γ-ray strength functions are important constituents of the compound nucleus model calculations of capture cross sections, γ-ray production spectra, isomeric state populations, and competition between γ-ray and particle emission. Relevant multipolarities in this context are $E1$, $M1$ and $E2$. The γ-ray strength functions include information on nuclear structure, and are widely used to study the mechanisms of nuclear reactions as well as nuclear structure. Widths and energies of the giant multipole resonances and nuclear deformation parameters in heated nuclei are extracted from experimental data by comparing of the shape of the experimental γ-ray strength functions with theoretical data [7.6, 7.7, 7.8, 7.9, 7.10].

Since γ-ray strengths functions are used in time-intensive calculations, simple closed-form expressions or ready-to-use tables are most convenient. Whereas the approaches based on recent theoretical achievements are useful in improving the reliability of the closed-form expressions.

Important quantities for the calculation of γ-ray strength functions are Lorentzian parameters of giant resonances, derived traditionally from the analysis of the photo-absorption cross sections for the $E1$ and $E2$ giant resonances. However, this experimental database is rather scarce and measurements have not been undertaken for many target nuclei. Therefore, several global systematic parameterizations have been derived for the multipolarities of primary importance. Finally, experimental γ-ray strength functions are extremely useful for adjusting theoretical values.

7.1 Experimental γ-ray strength functions

All experimental γ-ray strength functions have been collected together over a period of about forty years, based on measurements of partial radiative widths $\Gamma_{\gamma i}$ by means of three different types of experiment. Most of the data are derived from discrete resonance-capture measurements using the method of slow neutron time-of-flight spectrometry. Thermal neutron-capture data can be used (with some restrictions) in certain cases to derive γ-decay strength functions. Finally, another source of data is provided by photonuclear reactions. Analyses of all these experiments involves averaging over Porter-Thomas fluctuations, which governs the distribution of partial radiative widths.

The most extensive compilation of experimental γ-ray strength functions has been prepared by Kopecky, and was included in RIPL-1 [7.1]. These data were adopted for RIPL-2, reformatted, and included in the **gamma/gamma-strength-exp.dat** file. E1 and M1 strength functions (fE1 and fM1) are given for nuclei from ^{20}F up to ^{239}U, and

some of the original values were corrected (typically for non-statistical effects). Both original and recommended values are listed in units of 10^{-8} MeV^{-3}. Readers are referred to RIPL-1 documentation for more details regarding compilation and data reduction [7.1].

7.2 Standard closed-form models for E1 strength function

The Brink hypothesis is widely used to calculate the dipole γ-ray strength function [7.11, 7.12]. E1 strength in the SLO model ($\overleftarrow{f}_{E1} \equiv \overleftarrow{f}_{SLO}$) has Lorentzian shape with an energy independent width Γ_r:

$$\overleftarrow{f}_{SLO}(\epsilon_\gamma) = 8.674 \cdot 10^{-8} \sigma_r \Gamma_r \frac{\epsilon_\gamma \Gamma_r}{(\epsilon_\gamma^2 - E_r^2)^2 + (\Gamma_r \epsilon_\gamma)^2} \quad (\text{MeV}^{-3}), \tag{7.4}$$

where the Lorentzian parameters σ_r, E_r, and Γ_r are the peak cross section, energy and width of the Giant Resonance, respectively. This approach is probably the most appropriate method for describing photo-absorption data on medium-weight and heavy nuclei [7.3, 7.13, 7.14]. However, the SLO model for γ emission significantly underestimates the γ-ray spectra at low energies $\epsilon_\gamma \lesssim 1$ MeV [7.15]. A global description of the γ spectra by the Lorentzian approach can be obtained over the energy range $1 \lesssim \epsilon_\gamma \lesssim 8$ MeV when the Giant Dipole Resonance parameters are inconsistent with those derived from the photo-absorption data. Generally, SLO overestimates experimental data such as capture cross sections and the average radiative widths in heavy nuclei [7.3, 7.16, 7.17, 7.18, 7.19], and therefore improvements based on microscopic methods are needed.

The first model that gave a correct description of the $E1$ strengths at energies ϵ_γ close to zero was proposed in Ref. [7.20], followed by the development of an Enhanced Generalized Lorentzian model (EGLO) in Refs. [7.1, 7.21]. For spherical nuclei, the EGLO radiative strength function consists of two components: (i) a Lorentzian with energy- and temperature-dependent empirical width, and (ii) a term corresponding to the zero value of the γ-ray energy as defined in Ref. [7.20]. The γ-decay dipole strength within the EGLO model ($\overleftarrow{f}_{E1} \equiv \overleftarrow{f}_{EGLO}$) is defined by the equation [7.1, 7.21]:

$$\overleftarrow{f}_{EGLO}(\epsilon_\gamma) = 8.674 \cdot 10^{-8} \sigma_r \Gamma_r \left[\frac{\epsilon_\gamma \Gamma_k(\epsilon_\gamma, T_f)}{(\epsilon_\gamma^2 - E_r^2)^2 + (\epsilon_\gamma \Gamma_k(\epsilon_\gamma, T_f))^2} + 0.7 \frac{\Gamma_k(\epsilon_\gamma = 0, T_f)}{E_r^3} \right], \tag{7.5}$$

where the energy-dependent width $\Gamma_k(\epsilon_\gamma, T_f)$ is defined as proportional to the collisional damping width in the Fermi-liquid through the empirical function $\mathcal{K}(\epsilon_\gamma)$:

$$\Gamma_k(\epsilon_\gamma, T_f) = \mathcal{K}(\epsilon_\gamma) \frac{\Gamma_r}{E_r^2} \left[\epsilon_\gamma^2 + (2\pi T_f)^2 \right], \quad \mathcal{K}(\epsilon_\gamma) = \kappa + (1 - \kappa) \frac{\epsilon_\gamma - \epsilon_0}{E_r - \epsilon_0}. \tag{7.6}$$

The factor κ depends on the model adopted, and was obtained from the average resonance capture data, while $\epsilon_0 = 4.5$ MeV. If the Fermi-gas model is used, κ is given by [7.1]

$$\kappa = \begin{cases} 1, & A < 148, \\ 1 + 0.09(A - 148)^2 \exp\left(-0.18(A - 148)\right), & A \geq 148. \end{cases} \tag{7.7}$$

The EGLO model reproduces the experimental γ-ray data rather well in the mass region $A = 50 - 200$, and was recommended in RIPL-1 as the most appropriate approach to a simplified definition of the E1 γ-ray strength function [7.1]. However, the EGLO (and SLO) expressions for the γ-decay strength function in heated nuclei are parameterizations of the experimental data, and contradict recent theoretical findings:

- Shapes of the EGLO and SLO radiative strength functions are inconsistent with the general relationship between the γ-ray strength function of the heated nuclei and the imaginary part of the nuclear response function to the electromagnetic field [7.22, 7.23, 7.24, 7.27].
- Damping width of the EGLO model is proportional to the collisional component of the zero-sound damping width in the infinite Fermi-liquid in which only the collisional (two-body) relaxation is taken into account. However, the important contribution to the total width is also given by the fragmentation (one-body) width arising from the nucleon motion in a self-consistent mean field [7.25, 7.26]. This width is almost independent of the nuclear temperature and is not included in the EGLO model. On the other hand, the energy-independent width in the SLO model accounts for the fragmentation but not for collisional damping.

These shortcomings can be avoided by using new closed-form models proposed in Refs. [7.27] and [7.32].

7.3 Refined closed-form models for E1 strength function

The approach proposed in Refs. [7.27, 7.28, 7.29, 7.30, 7.31] is consistent with the detailed balance principle [7.6], and was originally referred to as the Thermodynamic Pole Approximation (renamed the Modified Lorentzian (MLO) approach because the resulting expression is a Lorentzian scaled with an enhancement factor). The energy-dependent damping width in the MLO model also includes a simplified fragmentation contribution corresponding to the 'wall approximation' for one-body dissipation. An expression for the dipole γ-ray strength function within the MLO model ($\overleftarrow{f}_{E1} \equiv \overleftarrow{f}_{MLO}$) is obtained by calculating the average radiative width of nuclei with micro-canonically distributed initial states. This function has the following form for spherical nuclei [7.28, 7.29, 7.30, 7.31]:

$$\overleftarrow{f}_{MLO}(\epsilon_\gamma) = 8.674 \cdot 10^{-8} \mathcal{L}(\epsilon_\gamma, T_f) \sigma_r \Gamma_r \frac{\epsilon_\gamma \Gamma(\epsilon_\gamma, T_f)}{(\epsilon_\gamma^2 - E_r^2)^2 + (\Gamma(\epsilon_\gamma, T_f)\epsilon_\gamma)^2} \ (MeV^{-3}), \quad (7.8)$$

$$\mathcal{L}(\epsilon_\gamma, T_f) \equiv \frac{1}{1 - \exp(-\epsilon_\gamma / T_f)}. \quad (7.9)$$

where E_r and Γ_r are the giant dipole resonance energy and width, respectively, $\Gamma(\epsilon_\gamma, T_f)$ is the strength function width (depends on the γ-ray energy and temperature T_f of the final state), and σ_r is the peak value of the photo-absorption cross section at E_r. The energies and width are expressed in units of MeV, and σ_r in mb. Note that the width Γ at energy $\epsilon_\gamma = E_r$ can be identified with the GDR width $\Gamma_r(\mathcal{T})$ in the heated nucleus of temperature $\mathcal{T}$: $\Gamma_r(\mathcal{T}) = \Gamma(\epsilon_\gamma = E_r, \mathcal{T})$.

The scaling factor $\mathcal{L}(\epsilon_\gamma, T_f)$ in Eq. 7.8 determines the enhancement of the radiative strength function in a heated nucleus as compared to a cold nucleus. This quantity can be interpreted as the average number of 1p-1h states excited by an electromagnetic field with frequency $\omega = \epsilon_\gamma/\hbar$, and is only important for low-energy radiations[1]. However, $\mathcal{L}$ is essential for the consistency of Eqs. 7.1 and 7.8 with respect to the detailed balance principle in constant temperature systems (see Refs. [7.22, 7.23, 7.24, 7.27]).

The Lorentzian term appears in Eq. 7.8 as the imaginary part of the nuclear linear response function to the electric dipole field. This shape is predicted by the extended hydrodynamic model of Steinwedel-Jensen (ESJ) [7.30, 7.36] for heated nuclei, with friction between the proton and neutron fluids, and also by a semi-classical Landau-Vlasov equation with a memory-dependent collision term if the γ-transition strength is concentrated near the giant resonance [7.31]. The Lorentzian shape stems from the random-phase approximation in cold nuclei [7.37].

Different semi-empirical expressions for the damping width Γ were previously used in the MLO approach, but the resulting radiative strength functions were close to each other [7.31]. Therefore, we present here only the simplest expression corresponding to the ESJ model to approximate the independent sources of dissipation [7.31, 7.38, 7.39]; the width is taken as the sum of a collisional damping width (Γ_C) and a term (Γ_F) that simulates the fragmentation component of the width:

$$\Gamma(\epsilon_\gamma, \mathcal{T}) = \Gamma_C(\epsilon_\gamma, \mathcal{T}) + \Gamma_F(\epsilon_\gamma). \tag{7.10}$$

Component Γ_C is inversely proportional to the collision relaxation time τ in the isovector channel at dipole distortion of the Fermi surface [7.38, 7.39, 7.40], and depends linearly on the γ-ray energy within the doorway state relaxation mechanism of heated nuclei:

$$\Gamma_C = \Gamma_{C,\ d} \equiv \frac{\hbar}{\tau(\epsilon_\gamma, \mathcal{T})} = C_{coll} E_r \left(\epsilon_\gamma + U\right), \tag{7.11}$$

where U is the thermal excitation energy; $U = a\mathcal{T}^2$ within the Fermi-gas model, and $a = \pi^2 g/6$, with g representing the single nucleon state density at the Fermi surface. Linear energy dependence of the collisional damping width in Eq. 7.11 results from the inverse proportionality of the effective mean square matrix element (for transitions between the incoherent particle-hole states) to the excitation energy [7.40, 7.41]. The linear energy dependence of the collisional width was also obtained by means of the test particle approach, when nucleon collisions were considered as s-wave scattering between pseudoparticles [7.42, 7.43].

The parameter C_{coll} in Eq. 7.11 is determined from the in-medium cross section $\sigma(np)$ of neutron-proton scattering near the Fermi surface:

[1] $\mathcal{L}$ also appears in the Fermi-liquid approach with explicit allowance for single-particle occupation numbers of compound nuclear states (in Ref. [7.33], see Eq.(22) for the strength function at $\epsilon_\gamma \ll E_r$). An extension of this method to γ-ray energies near GDR resonances slightly violates the detailed balance principle [7.34, 7.35].

$$C_{coll} = \frac{1}{4\pi^2}\frac{16m}{9\hbar^2}\sigma(np) = c \cdot F,\ c = \frac{1}{4\pi^2}\frac{16m}{9\hbar^2}\sigma_f(np) = 0.542 \cdot 10^{-3},\ F = \sigma(np)/\sigma_f(np), \tag{7.12}$$

in which the in-medium cross section $\sigma(np)$ is assumed to be proportional (factor F) to the value of the free space cross section $\sigma_f(np) = 5\ fm^2$ near the Fermi surface. This relationship for C_{call} ensures agreement between the relaxation time given by Eq. 7.11 and that calculated from the collisional integral within the Fermi-liquid approach at $\epsilon_\gamma = E_r$ and $\mathcal{T} = 0$.

Γ_F in Eq. 7.10 is proportional to the wall formula Γ_w [7.44] with a scaling factor k_s:

$$\Gamma_F(\epsilon_\gamma) = k_s(\epsilon_\gamma)\Gamma_w,\ \ \Gamma_w = \frac{3\hbar v_F}{4R_0} = 36.43 \cdot A^{-1/3}\ (MeV) \tag{7.13}$$

at Fermi-energy $\epsilon_F = mv_F^2/2 = 37$ MeV. For simplicity, the energy-dependent power approximation is adopted for the factor k_s :

$$k_s(\epsilon_\gamma) = \begin{cases} k_r + (k_0 - k_r)|(\epsilon_\gamma - E_r)/E_r|^{n_s}, & \epsilon_\gamma < 2E_r, \\ k_0, & \epsilon_\gamma \geq 2E_r, \end{cases} \tag{7.14}$$

where the quantities $k_0 \equiv k_s(\epsilon_\gamma = 0)$ and $k_r \equiv k_s(\epsilon_\gamma = E_r)$ determine the contribution of the "wall" component to the width at zero and GDR energies, respectively. The value of k_r is obtained from fitting the GDR width Γ_r at zero temperature to Eqs. 7.10 - 7.14, with $\epsilon_\gamma = E_r$. Values for $k_0 = 0.3$, $n_s = 1$, and $F = 1.0$ were found by fitting the predictions of the MLO model to the experimental γ-decay strengths.

Another approach to determining the E1 γ-ray strength is the Generalized Fermi Liquid (GFL) model proposed in Ref. [7.32]. The general shape of the dipole strength function is similar to that obtained by applying the Fermi-liquid theory to finite systems [7.20], but with an energy-dependent width which includes fragmentation damping from the dipole-quadrupole interaction. The GFL dipole strength function in spherical nuclei $\overleftarrow{f}_{E1} \equiv \overleftarrow{f}_{GFL}$ is defined by the equation:

$$\begin{aligned} \overleftarrow{f}_{GFL}(\epsilon_\gamma) &= 8.674 \cdot 10^{-8}\sigma_r\Gamma_r\frac{\mathcal{K}_{GFL}\epsilon_\gamma\Gamma_m(\epsilon_\gamma, T_f)}{(\epsilon_\gamma^2 - E_r^2)^2 + \mathcal{K}_{GFL}(\Gamma_m(\epsilon_\gamma, T_f)\epsilon_\gamma)^2}\ (MeV^{-3}), \\ \mathcal{K}_{GFL} &= \sqrt{E_r/E_0} = (1 + F_1'/3)^{1/2}/(1 + F_0')^{1/2} = 0.63, \end{aligned} \tag{7.15}$$

where F_0' and F_1' are the Landau parameters of the quasi-particle interaction in the isovector channel of the Fermi system ($F_0' = 1.49$ and $F_1' = -0.04$) according to Ref. [7.32], and E_0 is an average energy for one-particle one-hole states forming GDR. Eq. 7.15 is an extension of the original expression [7.32], in which the term $\mathcal{K}_{GFL}(\Gamma_m\epsilon_\gamma)^2$ has been added to the denominator to avoid singularity of the GFL approach near the GDR energy. The factor $\mathcal{K}_{GFL}$ is included to preserve the standard relationship between the strength function at the GDR energy and peak value σ_r of the photo-absorption cross section.

Similarly to Eq. 7.10, the width Γ_m in Eq. 7.15 is taken to be the sum of a collisional damping width (Γ_C) and a term (Γ_{dq}) that simulates the fragmentation width:

$$\Gamma_m(\epsilon_\gamma, \mathcal{T}) = \Gamma_C(\epsilon_\gamma, \mathcal{T}) + \Gamma_{dq}(\epsilon_\gamma), \quad \Gamma_C = \Gamma_{C,\ f} \equiv C_f \left(\epsilon_\gamma^2 + 4\pi^2\mathcal{T}^2\right). \tag{7.16}$$

The collisional component corresponds to the damping width in the infinite Fermi-liquid model, and Γ_{dq} results from spreading the giant dipole resonance over surface quadrupole vibrations as a consequence of the dipole-quadrupole interaction:

$$\Gamma_{dq}(\epsilon_\gamma) = C_{dq}\epsilon_\gamma \mid \bar{\beta}_2 \mid \sqrt{1 + \frac{E_2}{\epsilon_\gamma}} = C_{dq}\sqrt{\epsilon_\gamma^2\bar{\beta}_2^2 + \epsilon_\gamma s_2}, \quad s_2 = E_2\bar{\beta}_2^2. \tag{7.17}$$

$C_{dq} = (5\ln 2/\pi)^{1/2} = 1.05$, E_2 is the energy of the first excited vibrational 2^+ state (in MeV), and $\bar{\beta}_2$ is the effective deformation parameter characterizing the nuclear stiffness with respect to surface vibrations. The latter is determined from the reduced electric photo-absorption rate $B(E2)\uparrow \equiv B(E2, 0^+ \rightarrow 2^+)$ for the transition between the ground state and 2^+ state [7.45, 7.46]:

$$\bar{\beta}_2^2 \equiv \frac{5}{2}\frac{E_2}{C_2} = B(E2)\uparrow /(\frac{3}{4\pi}eR_0^2)^2, \tag{7.18}$$

where C_2 is the stiffness factor of the restoring force, $R_0 = r_0A^{1/3}$ is the radius of a spherical nucleus of equal volume, and e is the elementary charge. Note that Eq. 7.17 coincides with the expression for the GDR damping width in Ref. [7.47] after substituting the γ-ray energy ϵ_γ with the GDR energy E_r.

C_f in Eq. 7.16 represents the collisional damping component in the GFL model, and is determined by defining the total GFL damping width at the GDR energy in cold nuclei to be equal to the width Γ_r ($\Gamma_m(\epsilon_\gamma = E_r, \mathcal{T} = 0) = \Gamma_r$). Note that C_f within the Fermi-liquid approach [7.40, 7.48, 7.49] is determined from the in-medium cross section $\sigma(np)$ of the neutron-proton scattering near the Fermi surface, and is equal to C_{coll} as determined by Eq. 7.12.

Finally, we consider a hybrid formula for the E1-strength function proposed in Ref. [7.50]. The general form of this hybrid approach coincides with Eq. 7.4 when $\Gamma_h(\epsilon_\gamma)\Gamma_r$ is adopted in the numerator and the denominator instead of Γ_r^2. The energy-dependent width $\Gamma_h(\epsilon_\gamma)$

$$\Gamma_h(\epsilon_\gamma) = \mathcal{K}_{GFL}\Gamma_r\frac{\epsilon_\gamma^2 + 4\pi^2T_f^2}{\epsilon_\gamma E_r} \tag{7.19}$$

is infinite at zero energy ($\epsilon_\gamma \rightarrow 0$) in heated nuclei, while the damping width Γ_h at zero temperature depends linearly on the γ-ray energy as does the collisional width Γ_C in Eq. 7.11.

The expressions discussed above have to be generalized for the calculation of $E1$ strength functions in deformed nuclei, which are usually considered axially symmetric with the radius defined by

$$
\begin{aligned}
R(\theta) &= R_0^{'}\left(1+\alpha_2 P_2(\cos\theta)\right) = R_0^{'}\left(1+\beta_2 Y_{20}\right), \\
R_0^{'} &= R_0/\lambda, \quad \lambda^3 = 1+\frac{3}{5}\alpha_2^2+\frac{2}{35}\alpha_2^3,
\end{aligned}
\tag{7.20}
$$

where $R_0^{'}$ is the radius of a spherical nucleus of equal volume, $P_2(\cos\theta)$ is the Legendre polynomial, and $Y_{20} = (5/4\pi)^{1/2}P_2$ is the spherical harmonic. Both α_2 and $\beta_2 = (4\pi/5)^{1/2}\alpha_2$ are quadrupole deformation parameters chosen to reproduce the ground-state quadrupole nuclear moments Q. The $E1$ strength function in deformed nuclei is defined as the sum of two components, each with the corresponding energy $E_{r,j}$, damping width $\Gamma_{r,j}$ and peak value for the photo-absorption cross-section $\sigma_{r,j}$. Parameters $E_{r,j}$, $\Gamma_{r,j}$ and $\sigma_{r,1}$ $(j = 1, 2)$ correspond to collective vibrations along $(j = 1)$ and perpendicular to $(j = 2)$ the axis of symmetry.

The fragmentation damping widths $\Gamma_{F,1}$, $\Gamma_{F,2}$ of the collective vibrations along two principal axes of a spheroid are assumed in MLO to be proportional to the dipole widths ($\Gamma_{s,1}$ and $\Gamma_{s,2}$) of the surface dissipative model [7.59]:

$$
\Gamma_{F,\,j}(\epsilon_\gamma) = k_s(\epsilon_\gamma)\Gamma_{s,\,j}, \quad \Gamma_{s,1} = \Gamma_w/a_0^\delta, \quad \Gamma_{s,2} = \Gamma_w/b_0^\delta, \quad \delta = 1.6,
\tag{7.21}
$$

where a_0 and b_0 are relative semi-axes of a spheroid

$$
a_0 \equiv R(\theta=0)/R_0 = (1+\alpha_2)/\lambda, \quad b_0 \equiv R(\theta=\pi/2)/R_0 = (1-0.5\alpha_2)/\lambda.
\tag{7.22}
$$

The parameters k_r (Eq. 7.14) and C_f (Eq. 7.16) appear in expressions that define the damping widths for MLO and GFL in deformed nuclei, and are determined by fitting theoretical damping widths $\Gamma_{r,j}$ of the normal modes of the giant dipole resonance in cold nuclei to the corresponding experimental values. C_f can become negative, leading to negative values for the in-medium cross sections $\sigma(np)$ if the same relationship between C_f and $\sigma(np)$ as in spherical nuclei is used for deformed nuclei (see Eq. 7.12, with $C_{coll} = C_f$).

7.4 Comparison of closed-form expressions with experimental data

Variations in the dipole γ-decay strength functions ($\overleftarrow{f}_{E1}$) with mass number are shown in Fig. 7.1 for 50 nuclei included in the **gamma/gamma-strength-exp.dat** file of RIPL-2. The back-shifted Fermi-gas model (BSFG) was used to define the thermal excitation energy $U_f = U - U_S - \epsilon_\gamma$ of the final state in terms of the temperature T_f [7.60]; this approach relates the temperatures T and T_f to each another and to the thermal excitation energy U of the initial state, with $T_f = (1+\sqrt{1+4a(aT^2-T-\epsilon_\gamma)})/2a$ and $T = (1+\sqrt{1+4a(U-U_S)})/2a$ in which U_S is the energy shift parameter and a is the level density parameter. Values for the level density parameters a and energy shifts U_S were taken from the **beijing_bs1.dat** file of RIPL-1 [7.1] with rigid-body moments of inertia, or from global

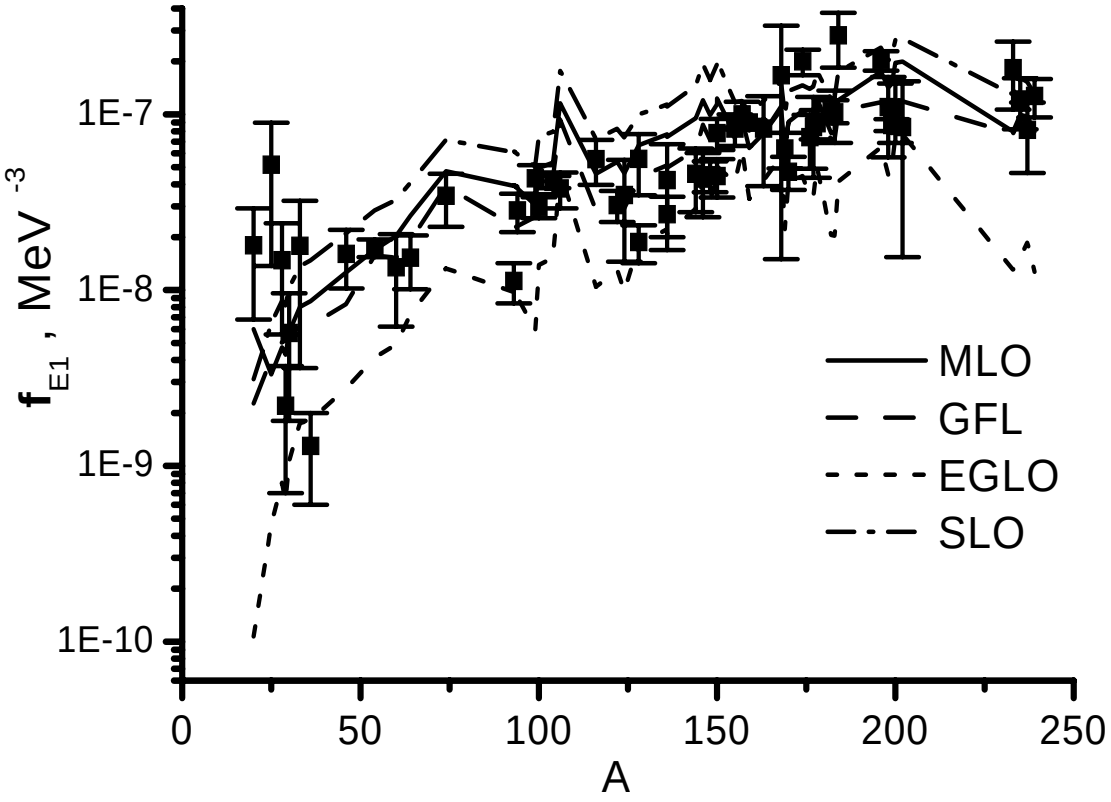

Figure 7.1: $E1$ γ-decay strength functions plotted against mass number.

systematics [7.61] when no experimental data were available. Quadrupole deformation parameters β_2 were calculated from the ground-state deformation parameters given in the **masses/mass-frdm95.dat** file and using Eqs. 7.28 and 7.27. Nuclei with $\beta_2 \leq 0.01$ were considered to be spherical. The effective quadrupole deformation parameters $\bar{\beta}_2$ and energies E_2 of the first 2^+ state for even-even nuclei in the GFL model were taken from *raman_tableI.txt* of Ref. [7.45]. When experimental data were unavailable for even-even nuclei and for all odd and odd-odd nuclei, $|\bar{\beta}_2|$ were used for $\bar{\beta}_2$ and global parameterization was adopted for s_2 [7.45]

$$s_2 \equiv E_2 \bar{\beta}_2^2 = 217.16/A^2. \tag{7.23}$$

The results shown in Fig. 7.1 were calculated for γ-ray energies that correspond to the mean energy $\bar{\epsilon}_\gamma$ of E1 transitions in the **gamma/gamma-strength-exp.dat** file. These plots show that the GFL, MLO and EGLO models describe the experimental γ-decay data with $\epsilon_\gamma \approx B_n$ better than the SLO model. GFL and MLO calculations are in very close agreement and reproduce the experimental data for heavy nuclei ($A \gtrsim 150$) better than the other two models. Fig. 7.2 shows calculated γ-decay strengths ($\overleftarrow{f}_{E1}$) for ^{90}Zr; experimental data are taken from Ref. [7.62] and the GFL, MLO and EGLO data are calculated for the experimental energies U and ϵ_γ. The MLO and SLO models for ^{90}Zr describe the experimental data better than GFL and EGLO, and the MLO representation is closer to the experimental data than that of the SLO model.

Fig. 7.3 shows the calculated strength functions ($\overleftarrow{f}_{E1}$) for ^{144}Nd, with the initial ex-

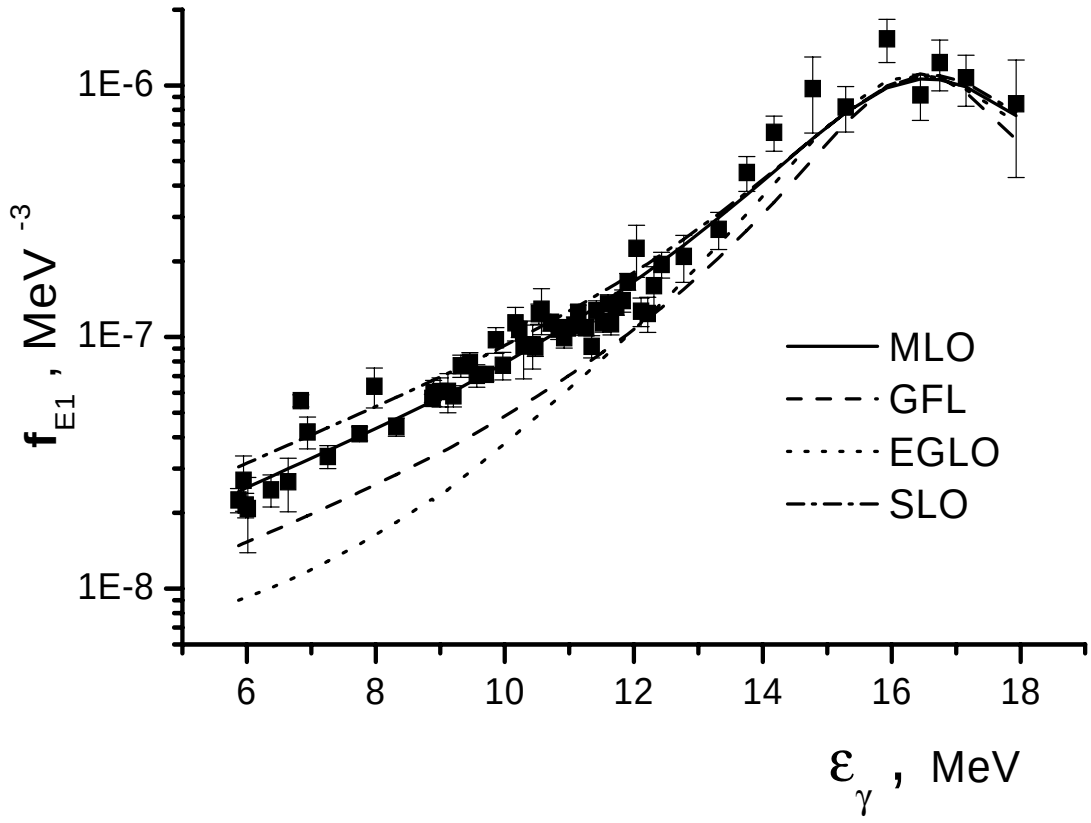

Figure 7.2: $E1$ gamma-decay strength function plotted against energy ϵ_γ for ^{90}Zr.

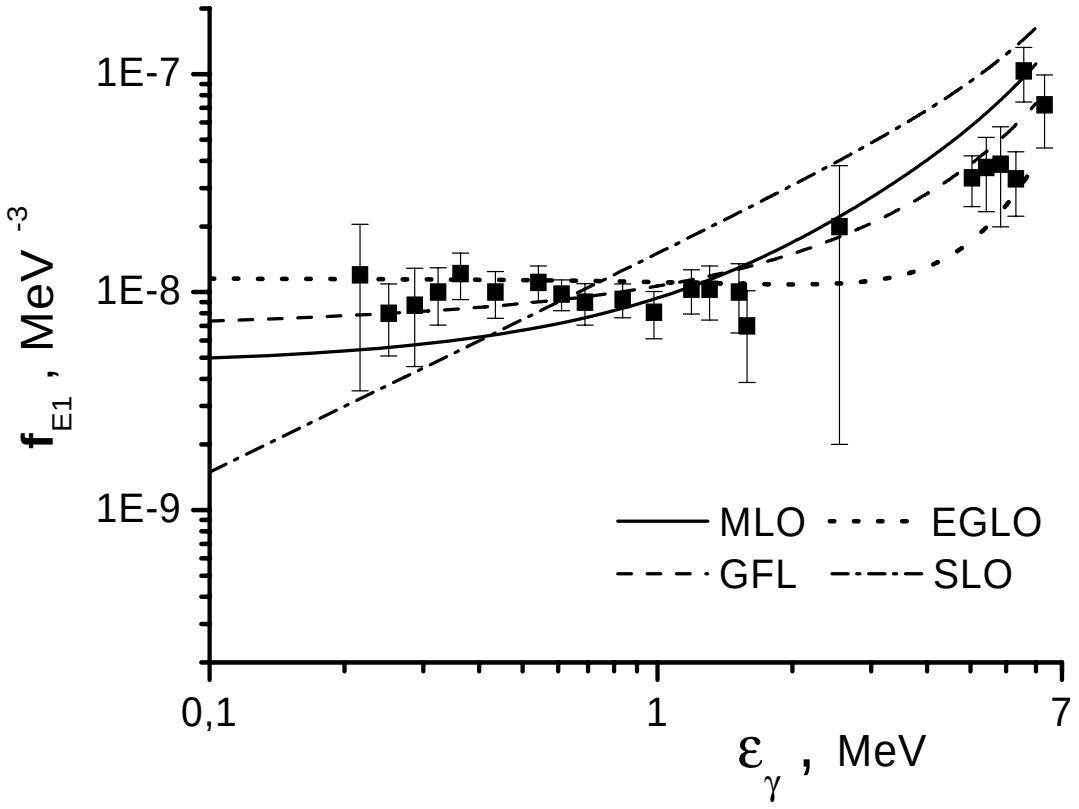

Figure 7.3: $E1$ gamma-decay strength function of ^{144}Nd for $U = B_n$.

citation energy U equal to the neutron binding energy $B_n(\approx 7.8$ MeV). The experimental data are taken from Ref. [7.15]. EGLO, GFL and MLO results are characterized by a non-zero limit and temperature dependence at low γ-ray energies. All three models are in reasonable agreement for $\epsilon_\gamma \lesssim 3$ MeV, and describe the experimental data much better than the SLO model (which predicts a vanishing strength function at zero γ-ray energy). However, GFL, MLO and SLO results at $\epsilon_\gamma \gtrsim 5$ MeV are closer to the experimental data than the values calculated by the EGLO method.

The photo-excitation strength function is expressed in the same form (7.2) as the γ-decay strength function, but with the temperature of the initial state (T) instead of the final state temperature (T_f). $E1$ photo-excitation strength functions calculated by the MLO and SLO models are in good agreement for warm and cold nuclei over a wide range of gamma-ray energies near the GDR peak energy.

7.5 Microscopic approach to E1 strength function

The Lorentzian or previously described closed-form expressions for the γ-ray strength suffer from various shortcomings:

(i) unable to predict the enhancement of the E1 strength at energies below the neutron separation energy as demonstrated by nuclear resonance fluorescence experiments - this departure from a Lorentzian profile may occur in various ways, such as a pygmy E1 resonance [7.51] which is observed in fp-shell nuclei and heavy spherical nuclei near closed shells (Zr, Mo, Ba, Ce, Sn and Pb);

(ii) even if a Lorentzian function provides a suitable representation of the E1 strength, the location of the maximum and width remain to be predicted from some underlying model for each nucleus, as described in the previous sections - this approach clearly lacks reliability when dealing with exotic nuclei.

Therefore, microscopic models have been developed with the aims of providing predictive power and reasonably reliable E1 strength functions. Attempts in this direction have been specifically conducted within the quasi-particle random-phase-approximation (QRPA) [7.52].

The spherical QRPA model includes a realistic Skyrme interaction, and has been used recently for large-scale derivations of the E1 strength function [7.53, 7.54]. This global calculation predicts GDR in close agreement with experimental data, i.e., rms deviation of the predictions from measurements of 84 nuclides is only about 300 keV. The final E1 strength functions obtained by folding the QRPA strengths with a Lorentzian function also reproduce satisfactorily the photo-absorption as well as the average resonance capture data at low energies [7.53]. These aforementioned QRPA calculations have been performed for all $8 \leq Z \leq 110$ nuclei lying between the two drip lines. QRPA distributions in the neutron-deficient region, as well as along the valley of β-stability, are very close to a Lorentzian profile in the MLO model. Significant departures from Lorentzian are found for neutron-rich nuclei with large asymmetry coefficients $I = (N - Z)/A = (A - 2Z)/A$, as shown in Fig. 7.4 for the E1 photo-excitation strength function ($f_\gamma(E1)$) in units of

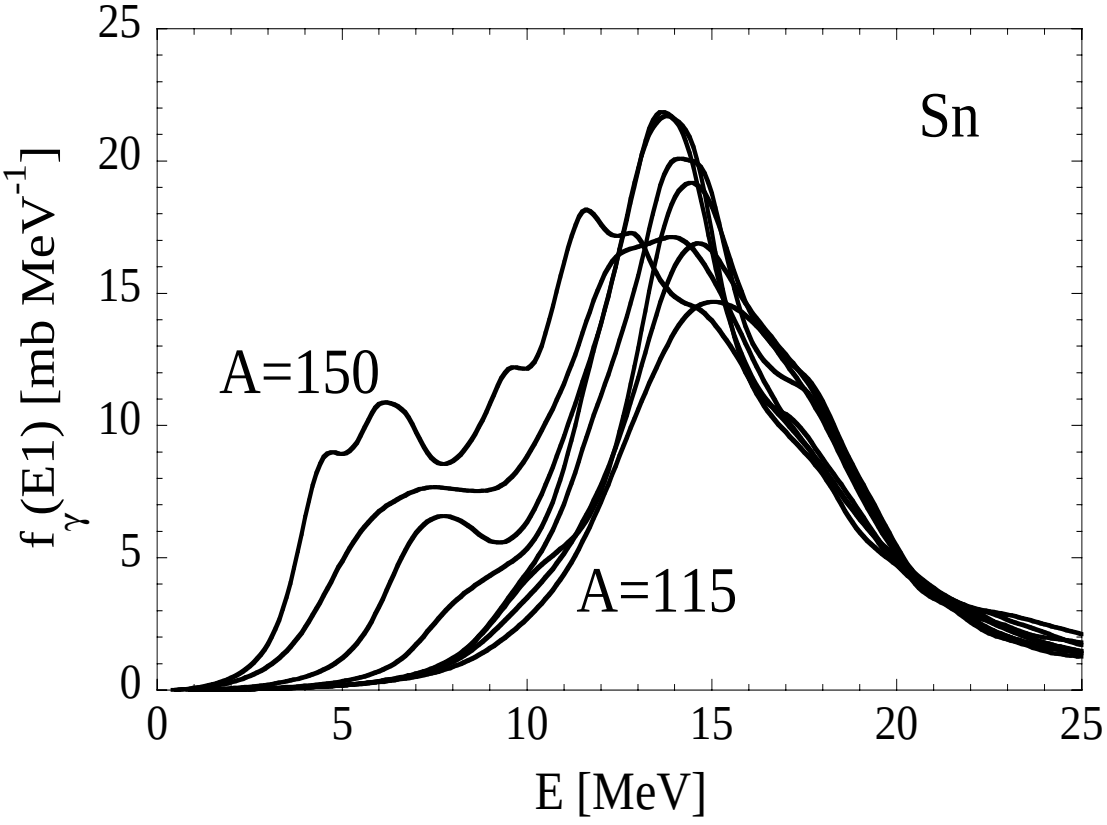

Figure 7.4: E1 strength function $f_\gamma(E1)$ for the Sn isotopic chain as predicted by QRPA with the SLy4 Skyrme force; only isotopes between A=115 (I= 0.13) and A=150 (I= 0.33) are displayed in steps of ΔA=5.

$mb \cdot MeV^{-1}$:

$$f_\gamma(E1) \equiv \frac{\langle \sigma_{E1} \rangle (mb)}{\epsilon_\gamma (MeV)} = 3(\pi\hbar c)^2 \ \overrightarrow{f}_{E1}(\epsilon_\gamma) \equiv 1.15 \cdot 10^6 \ \overrightarrow{f}_{E1}\,(MeV^{-3}). \tag{7.24}$$

RPA-like calculations [7.52, 7.54, 7.55, 7.56] as well as the semiclassical second RPA model [7.57] show that neutron excess affects the spreading of the isovector dipole strength, as well as the centroid of the strength function. The energy shift is found to be larger than predicted by the usual $A^{-1/6}$ or $A^{-1/3}$ dependence given by the phenomenological liquid-drop approximations [7.44]. Some extra strength is also predicted to be located at sub-GDR energies, and to increase with neutron excess (Fig. 7.4). Even if this behaviour represents only a few percent of the total E1 strength, an increase by up to an order of magnitude of the radiative capture cross section can occur for some exotic neutron-rich nuclei [7.53].

Microscopic predictions of the E1-strength functions determined by the QRPA model and based on the SLy4 Skyrme force are included in RIPL-2 for 3317 nuclei, with $8 \leq Z \leq 84$ lying between the proton and neutron driplines. The QRPA equations were solved in the configuration space so as to exhaust the energy-weighted sum rule, and all calculations were performed within the spherical approximation. A folding procedure was applied to the QRPA strength distribution in order to take the damping of the collective motion into account. A phenomenological splitting of the QRPA resonance strength was performed

within the same folding procedure for the deformed nuclei. All modelling details and a comparison with experimental data can be found in Ref. [7.53]. The E1 strength has been tabulated on an energy grid of 0.1 MeV between 0 and 30 MeV, and these data can be found in a series of **gamma/gamma-strength-micro/zxxx.dat** files.

Another semi-microscopic approach was recently proposed in Ref. [7.58], based on the continuum-RPA description of particle-hole states and a phenomenological description of quasi-particle damping. This model takes into account nucleon pairing and describes rather well the low-energy part of the radiative dipole strengths. Similarly to the QRPA method, this approach does not use a thermodynamic description of the ensemble of initial highly-excited states.

7.6 Giant dipole resonance parameters

The parameters for giant resonances with E1, M1 and E2 multipolarities were collected in RIPL-1 [7.1] and have also been adopted for RIPL-2. Compilation of the Giant Dipole Resonance parameters is contained in the **gamma/gdr-parameters-exp.dat** file. An extended database of the photo-nuclear reaction parameters $E_{r,j}$, $\sigma_{r,j}$ can be found in *Atlas of Giant Dipole Resonances* [7.63], although this publication does not contain explicit information on the damping width components $\Gamma_{r,j}$ in deformed nuclei but provides only full-width at half-maximum of the largest peak in the photo-absorption cross section. Therefore, these data can not be directly used in radiative strength or reaction calculations.

Unknown GDR parameters can be estimated from various systematics, which are reliable for nuclei near to the beta-stability line with $A \gtrsim 40$. The global systematics for dipole isovector giant resonance parameters can be based on the interpolation of experimental data, and are defined below (see also Refs. [7.13, 7.14, 7.65], and RIPL-1 for references):

Spherical nuclei

$$\begin{aligned} E_r &\equiv E_0 = 31.2\ A^{-1/3} + 20.6\ A^{-1/6} \quad MeV, \\ \Gamma_r &= 0.026\ E_r^{1.91} \quad MeV, \\ \sigma_r &\equiv \sigma_0 = 1.2 \times 120\ NZ\ /\ (A\pi\Gamma_r), \quad mb \end{aligned} \tag{7.25}$$

The factor of 1.2 in the expression for σ_r is the value of the experimental energy-weighted sum in units of the classical dipole Thomas-Reiche-Kuhn sum rule $\sigma_{TRK} = 60(NZ/A)$ $(MeV \cdot mb)$.

$$\begin{aligned} E_{r,1} &= E_{r,2}/\left[0.911\frac{a_0}{b_0}+0.089\right], \quad E_{r,2}=E_0\frac{1}{b_0}\left[1-1.51\cdot 10^{-2}\cdot(a_0^2-b_0^2)\right], \\ \Gamma_{r,1} &= 0.026E_{r,1}^{1.91}, \qquad\qquad \Gamma_{r,2}=0.026E_{r,2}^{1.91}, \\ \sigma_{r,1} &= \sigma_0/3, \qquad\qquad \sigma_{r,2}=2\sigma_0/3, \end{aligned} \tag{7.26}$$

where indexes 1 and 2 correspond respectively to the collective motion along and perpendicular to the axis of symmetry with relative semi-axes of a spheroid $a_0 = (1+\alpha_2)/\lambda$, $b_0 = (1-0.5\alpha_2)/\lambda$ (see Eqs. 7.20 and 7.22).

The energy expressions in Eq. 7.26 were derived from the hydrodynamic model of Steinwedel-Jensen [7.64] (Fig. 2 and Eq. 9), and for small deformations $E_{r,1} \simeq E_0/(1+\alpha_2)$ and $E_{r,2} \simeq E_0/(1-0.5\alpha_2)$ as reported in RIPL-1[2] [7.1]. Effective quadrupole deformation parameters α_2 or β_2 of the equivalent spheroid (Eq. 7.20) were determined from the ground-state deformation parameters $\beta_n \equiv \alpha_n\sqrt{(2n+1)/4\pi}$, with the nuclear radius expansion expressed in spherical harmonics. β_n parameters were calculated in Ref. [7.66], and are listed in the **masses/mass-frdm95.dat** file. The nuclear quadrupole moment $Q^{'}$ was calculated in units of $(3/4\pi)ZeR_0^2$ for every nucleus by the equation (see also Eqs.1.22 and 6.19 in Ref. [7.67]):

$$Q^{'} = \bar{\alpha}_2 + \frac{4}{7}\bar{\alpha}_2^2 - \frac{1}{7}\bar{\alpha}_2^3 - \frac{94}{231}\bar{\alpha}_2^4 + \frac{8}{7}\bar{\alpha}_2\bar{\alpha}_4 + \frac{72}{77}\bar{\alpha}_2^2\bar{\alpha}_4 + \frac{200}{693}\bar{\alpha}_4^2, \tag{7.27}$$

where $\bar{\alpha}_n \equiv \beta_n/\sqrt{(2n+1)/4\pi}$, with the ground-state deformation parameters β_n taken from Ref. [7.66]. The quadrupole deformation α_2 of an effective spheroidal nucleus was then determined from the calculated quadrupole moment $Q^{'}$ by solving the equation:

$$\alpha_2 + \frac{4}{7}\alpha_2^2 - \frac{1}{7}\alpha_2^3 - \frac{94}{231}\alpha_2^4 = Q^{'}, \tag{7.28}$$

where only terms up to the fourth order in α_2 from the general expression for $Q^{'}$ are retained. Effective quadrupole deformation parameters α_2 have been determined this way for 8979 nuclei in the **masses/mass-frdm95.dat** file, and are tabulated in the **deflib.dat** file contained in the **gamma/gamma-strength-analytic.tgz** archive.

Nuclei at high excitation energy and with high angular momentum can be created in heavy-ion reactions. Static deformation is damped with increasing excitation energy, and the nuclei become spherical. On the other hand, rotation leads to dynamic deformation, and calculation of the γ emission in such cases should use a spheroidal shape approximation [7.8, 7.9, 7.68, 7.69]. Simple expressions were proposed in Ref. [7.70], based on the liquid-drop model [7.71] with a rigid-body estimate for the nuclear moment of inertia and a dynamic quadrupole deformation parameter for the rotating nuclei as a function of angular momentum and mass number A. The oblate nucleus at slow rotation transits

[2] β was used in RIPL-1 instead of α_2.

sharply to prolate shape when the frequency increases. General expressions are of the form:

$$\beta_2 = \beta_2 (I, A) = E_S (I) (a_1 + a_2 E_S (I)) / (1 + a_3 E_S (I))^2 \tag{7.29}$$

with

$$a_i = b_i + c_i (A + d_i)^2 , \tag{7.30}$$

where $E_S (I) = E^0_{rot} I (I + 1) = 34.5 A^{-5/3} I (I + 1)$ MeV is the rotation energy of the equivalent spherical nucleus with spin I. Slowly rotating spheroidal nuclei have an oblate shape, which changes to prolate shape at a critical angular momentum I_{cr}. Coefficients b_i, c_i and d_i in Eq. 7.30 have the following values in the case of oblate nuclei (slow rotation):

$$\begin{array}{lll} b_1 = -7.46 \cdot 10^{-3}, & c_1 = -1.94 \cdot 10^{-7}, & d_1 = -107.1; \\ b_2 = -4.20 \cdot 10^{-5}, & c_2 = -4.25 \cdot 10^{-9}, & d_2 = -93.90; \\ b_3 = \ 5.70 \cdot 10^{-3}, & c_3 \ = \ 2.44 \cdot 10^{-7}, & d_3 = -73.51. \end{array} \tag{7.31}$$

Coefficients b_i, c_i and d_i for prolate nuclei (fast rotation) are:

$$\begin{array}{lll} b_1 = -6.36 \cdot 10^{-3}, & c_1 = -6.33 \cdot 10^{-7}, & d_1 = -48.3; \\ b_2 = \ 1.02 \cdot 10^{-3}, & c_2 \ = \ 1.42 \cdot 10^{-7}, & d_2 = -95.9; \\ b_3 = \ 0.02, & c_3 \ = \ 8.59 \cdot 10^{-7}, & d_3 = -74.1. \end{array} \tag{7.32}$$

The dependence of the critical spin I_{cr} on mass number A and proton number Z is given by the formula:

$$I_{cr} = I_{cr} (A, Z) = q_1 + q_2 Z^2 , \tag{7.33}$$

where

$$q_i = \tilde{q}_{i,1} + \tilde{q}_{i,2} \cdot A + \tilde{q}_{i,3} \cdot A^2 , \tag{7.34}$$

and

$$\begin{array}{lll} \tilde{q}_{1,1} = \ 55.10, & \tilde{q}_{1,2} = \ -0.063, & \tilde{q}_{1,3} = \ 5.120 \cdot 10^{-3}; \\ \tilde{q}_{2,1} = -0.013, & \tilde{q}_{2,2} = 2.840 \cdot 10^{-6}, & \tilde{q}_{2,3} = -2.570 \cdot 10^{-7}. \end{array} \tag{7.35}$$

The dynamical deformation parameter at slow rotation (Eqs. 7.29 - 7.31) is practically identical to the value obtained analytically in Refs. [7.46, 7.69, 7.72]:

$$\beta_2 \simeq -\sqrt{5\pi/4} \times 2.1 A^{-7/3} I(I+1)/(1 - 0.0205 Z^2/A). \tag{7.36}$$

Macroscopic models describing the the relative motion of protons against neutrons have also been successful in reproducing experimental GDR energies and widths [7.44,

7.79]. An effect often neglected by systematics concerns the experimentally-observed shell-dependence of the GDR width, that can be explained by considering the coupling between dipole oscillations and quadrupole surface vibrations [7.77]. RIPL-2 provides improved predictions of the GDR energies and widths for about 6000 nuclei from $14 \leq Z \leq 110$ lying between the proton and the neutron driplines. GDR is represented in the Goldhaber-Teller model [7.78], where the proton sphere vibrates against the neutron sphere. The dynamics of the oscillation is assumed to be dominated by the np-interaction as described in Ref. [7.79], with a renormalized strength $K = 1360A^{-1/6}$ MeV fm^3 derived from a least-squares fit to the experimental GDR energies [7.50]. Both the nucleon density distribution and ground-state deformation are taken from the Extended Thomas-Fermi plus Strutinsky Integral (ETFSI) compilation [7.80, 7.81]. The expression for the shell-dependent GDR width is taken from Ref. [7.77] using the newly-determined GDR energies and the ETFSI shell corrections. Comparisons between predicted and experimental GDR energies and widths are shown in Fig. 7.5; more details can be found in Ref. [7.50]. GDR in deformed nuclei splitinto two peaks for oscillations parallel and perpendicular to the axis of rotational symmetry. All GDR energies and widths are tabulated in the **gamma/gdr-parameters-theor.dat** file.

7.7 M1 and E2 transitions

The GFL and MLO models can also be used to estimate the M1 strength $\overleftarrow{f}_{M1}(\epsilon_\gamma)$ over a broad range of γ-ray energies when either experimental data or systematics for the ratio $\mathcal{R} = \overleftarrow{f}_{E1}(B_n)/\overleftarrow{f}_{M1}(B_n)$ at neutron binding energy B_n are known. Then, the M1 strength function can be calculated from the following relationship:

$$\overleftarrow{f}_{M1}(\epsilon_\gamma) = \frac{\overleftarrow{f}_{E1}(B_n)}{\mathcal{R}} \frac{\phi_{M1}(\epsilon_\gamma)}{\phi_{M1}(B_n)}, \tag{7.37}$$

where $\phi_{M1}(\epsilon_\gamma)$ describes the shape of the dipole magnetic radiative strength function, and the dipole electric radiative strength $\overleftarrow{f}_{E1}(B_n)$ is calculated using one of the models discussed. Experimental values of the ratio $\mathcal{R}$ can be extracted for some nuclei from the **gamma/gamma-strength-exp.dat** file. Global parameterization of the $\mathcal{R}$ is given by [7.1]:

$$\mathcal{R} = \frac{\overleftarrow{f}_{E1}(B_n)}{\overleftarrow{f}_{M1}(B_n)} = 0.0588 \cdot A^{0.878}, \quad B_n \approx 7\ MeV. \tag{7.38}$$

Two models are in common use for the function ϕ_{M1}:

(i) $\phi_{M1}(\epsilon_\gamma) = const$ according to the single-particle model, and

(ii) $\phi_{M1}(\epsilon_\gamma)$ from the SLO model (Eq. 7.4) and corresponding to the spin-flip giant resonance mode [7.46], with the following global parameterization for the energy and damping width [7.1]:

$E_r = 41 \cdot A^{-1/3}\ MeV$, $\Gamma_r = 4\ MeV$.

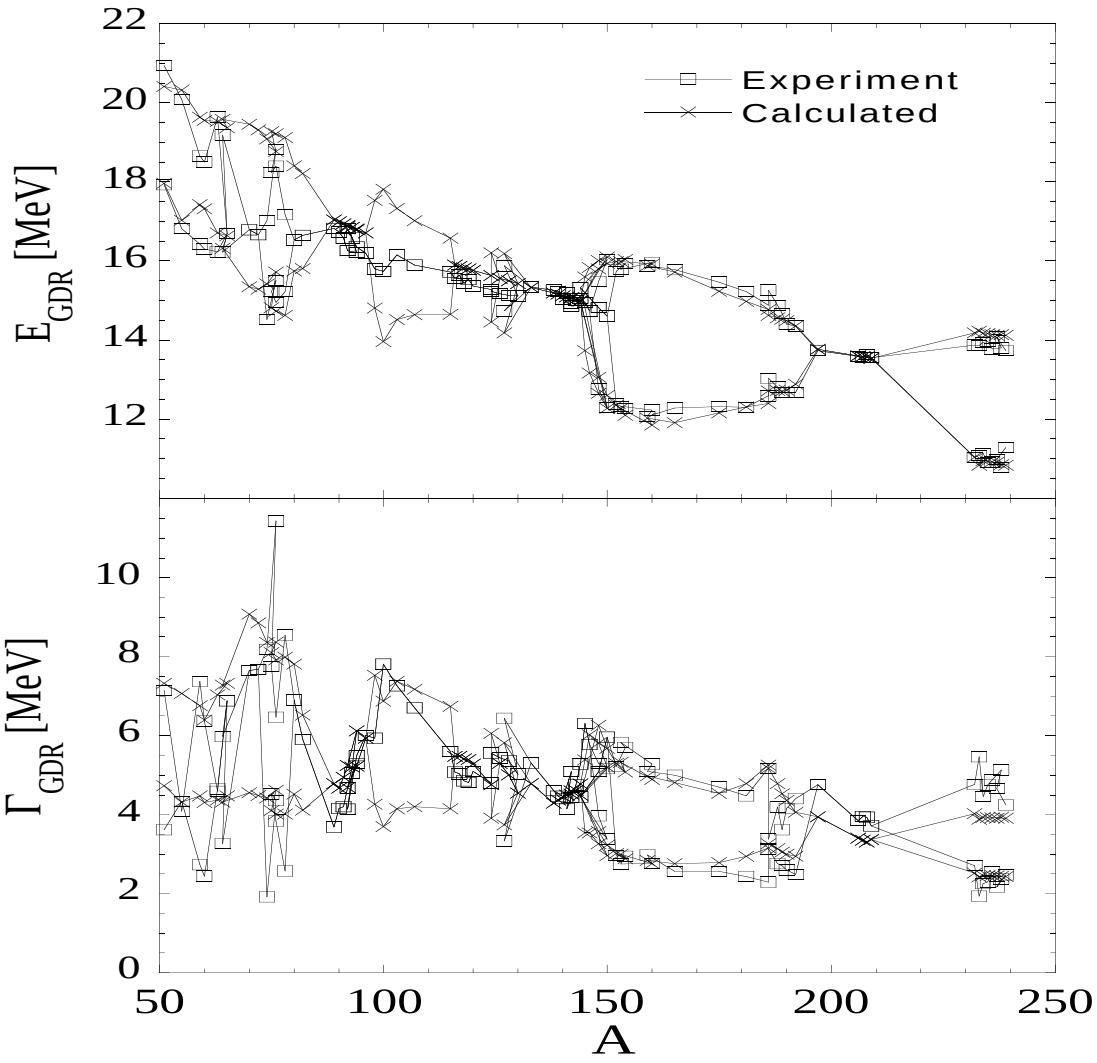

Figure 7.5: Comparison of experimental data with GDR energies and widths given in the **gdr-parameters-theor.dat** file.

E2 radiation is linked to the excitation of the giant quadrupole isoscalar resonances, and a Lorentzian is recommended to describe the E2 strength. The single-particle model with energy-independent strengths is recommended for the $M2$-, $E3$- and $M3$-radiations [7.73].

Note that the sum of the experimental γ-decay strength functions for the E1+M1 transitions in the energy interval up to B_n has been determined recently in Refs. [7.74, 7.75, 7.76] from the analysis of two-step γ-cascades after thermal neutron capture in the following nuclei: ^{40}K, ^{80}Br, ^{114}Cd, $^{124,125}Te$, ^{128}I, $^{137,138,139}Ba$, ^{140}La, ^{146}Nd, ^{150}Sm, $^{156,157}Cd$, ^{160}Tb, ^{164}Dy, ^{166}Ho, ^{168}Er, ^{170}Tm, ^{174}Yb, $^{176,177}Lu$, ^{181}Hf, ^{182}Ta, ^{183}W, $^{188,190,191,193}Os$, ^{192}Ir, ^{196}Pt, ^{198}Au and ^{200}Hg.

Experimental dipole radiative strengths for nuclei with $50 \lesssim A \lesssim 90$ and $6 \lesssim \epsilon_\gamma \lesssim 10$ MeV have been determined by studying the γ emission in (p,γ)-reactions (see Refs. [7.34, 7.35], and references therein).

7.8 Conclusions and recommendations

Numerical studies indicate that the calculations of the γ-decay strength functions within the EGLO, GFL and MLO models give similar results at low γ-ray energies ($\epsilon_\gamma \lesssim 3\ MeV$). These three models describe the experimental data much better than the SLO model at these low energies, and also define a non-zero and temperature-dependent limit for the vanishing γ-ray energy. Results from the GFL, MLO and SLO models at $\epsilon_\gamma \gtrsim 5\ MeV$ are closer to the experimental data than those obtained from EGLO. The $E1$ photo-excitation strength functions for cold nuclei calculated with the MLO and SLO model agree over a reasonably large range of γ-ray energies around the GDR peak.

The overall comparison between the EGLO, GFL, MLO and SLO models and experimental data showed that MLO and GFL provide the most reliable methods for determining the E1 γ-ray strength functions over a relatively wide energy interval ranging from zero to above the GDR peak. GFL and MLO are not time consuming calculational routes and are recommended for general use; both of them can be used to predict the statistical dipole γ-ray emission and extract the GDR parameters from the experimental data for heated nuclei. We note that the GFL model is not consistent with the detailed balance principle in systems with constant temperature, and the collisional components of the GFL damping width can become negative in some deformed nuclei.

A code has been developed as part of the RIPL-2 project to predict E1 strength functions by means of the MLO, GFL, EGLO and SLO models, and is included in the **gamma/gamma-strength-analytic.tgz** file.

Large-scale QRPA calculations of the E1 strength have been undertaken in Ref. [7.53], and are tabulated in the **gamma/gamma-strength-micro/zxxx.dat** files that give the same degree of accuracy as the MLO model in the energy range from 4 to 8 MeV for nuclei close to the stability line. However, QRPA calculations reveal broadening of the GDR shape when moving away from the stability line. This effect stems from the microscopic treatment and can not be accounted for by using experimental GDR shapes, which were measured for stable nuclei only. Thus, the use of the QRPA results can also be recommended for calculations on nuclei far from the stability line.

7.9 Summary of codes and data files

The programs and data files included in the directory are:

gamma-strength-analytic.readme - description of FORTRAN code for analytical calculation of the E1 strength function in terms of SLO, EGLO, MLO and GFL models.

gamma-strength-analytic.tgz - source of FORTRAN code for analytical calculation of the E1 strength function in terms of SLO, EGLO, MLO and GFL models.

gamma-strength-exp.dat - compilations of experimental E1 and M1 strength functions.

gamma-strength-exp.readme - description of *gamma-strength-exp.dat* file.

gamma-strength-micro/ - E1 strength functions determined within QRPA model.

gamma-strength-micro.readme - description of *gamma-strength-micro* file.

gdr-parameters-exp.dat - compilation of experimental giant dipole resonance parameters.

gdr-parameters-exp.readme - description of *gdr-parameters-exp.dat* file.

gdr-parameters-theor.dat - theoretical predictions of the giant dipole resonance energies and widths for about 6000 nuclei.

gdr-parameters-theor.readme - description of *gdr-parameters-theor.dat* file.

REFERENCES

[7.1] KOPECKY, J., "Gamma-Ray Strength Functions", Handbook for calculations of nuclear reaction data - Reference input parameter library, IAEA-TECDOC-1034, Vienna (1998) 97; directory GAMMA on the Web site http://www-nds.iaea.org/ripl/.

[7.2] BARTHOLOMEW, G.A., EARLE, E.D., FERGUSSON, A.J., KNOWLES, J.W., LONE, M.A., Adv. Nucl. Phys. **7** (1973) 229.

[7.3] LONE, M.A., "Neutron induced reactions", Proc. 4th. Int. Symp., Smolenice, Czechoslovakia, 1985, KRISTIAK, J., BETAK, E., REIDEL, D., (Eds.), Publ. Comp. Dordrecht, Holland (1986) 238.

[7.4] MONTOYA, C.P., SCHADMAND, S., DIOSZEGI, I., HOFMAN, D.J., ZHANG, P.H., PAUL, P., Z. Phys. **A340** (1991) 371.

[7.5] SCHADMAND, S., VARMA, R., BANERJEE, S.R., BACK, B.B., HOFMAN, D.J., MONTOYA, C.P., PAUL, P., J. Phys. **G21** (1995) 821.

[7.6] SNOVER, K., Ann. Rev. Nucl. Part. Sci. **36(1)** (1986) 545.

[7.7] GAARDHOJE, J.J., Ann. Rev. Nucl. Part. Sci. **42** (1992) 483.

[7.8] BROGLIA, R.A., BORTIGNON, P.F., BRACCO, A., Prog. Part. Nucl. Phys. **28** (1992) 517.

[7.9] PIERROUTSAKOU, D., AUGER, F., ALAMANOS, N., GOMES, P.R.S., SIDA, J.L., GILLIBERT, A., FRASCARIA, N., LHENRY, I., ROYNETTE, J.C., SUOMIJÄRVI, T., Nucl. Phys. **A600** (1996) 131.

[7.10] MATTIUZZI, M., BRACO, A. CAMERA, F., ORMAND, W.E., GAARDHØJE, J.J., MAJ, A., MILLION, B., PIGNANELLI, M., TVETER, T., Nucl. Phys. **A612** (1997) 262.

[7.11] BRINK, D.M., PhD Thesis, University of Oxford (1955) 101.

[7.12] AXEL, P., Phys. Rev. **126** (1962) 671.

[7.13] BERMAN, B.L., FULTZ, S.C., Rev. Mod. Phys. **47** (1975) 713.

[7.14] DIETRICH, S.S., BERMAN, B.L., At. Data Nucl. Data Tables **38** (1988) 199.

[7.15] POPOV, Yu.P., "Neutron induced reactions", Proc. Europhys. Topical Conf., Smolenice, 1982, Physics and Applications, Vol. 10, OBLOZINSKY, P. (Ed.) (1982) 121.

[7.16] MCCULLAGH, C.M., STELTS, M., CHRIEN, R.E., Phys. Rev. **C23** (1981) 1394.

[7.17] KOPECKY, J., UHL, M., Phys. Rev. **C41** (1990) 1941.

[7.18] BEČVÁŘ, F., CEJNAR, P., CHRIEN, R.E., KOPECKY, J., Phys. Rev. **C46** (1992) 1276.

[7.19] COCEVA, C., Nuovo Cim. **107A** (1994) 85.

[7.20] KADMENSKIJ, S.G., MARKUSHEV, V.P., FURMAN, V.I., Yad. Fiz. **37** (1983) 277; Sov. J. Nucl. Phys. **37** (1983) 165.

[7.21] KOPECKY, J., UHL, M., CHRIEN, R.E., Phys. Rev. **C47** (1993) 312.

[7.22] RING, P., ROBLEDO, L.M., EGIDO, J.L., FABER, M., Nucl. Phys. **A419** (1984) 261.

[7.23] EGIDO, J.L., WEIDENMUELLER, H., Phys.Rev. **C39** (1989) 2398.

[7.24] EGIDO, J.L., RING, P., J. Phys. **G19(1)** (1993) 1.

[7.25] SPETH, J., VAN DE WOUDE, A., Rep. Prog. Phys. **44** (1981) 719.

[7.26] BERTSCH, G.F., BROGLIA, R.A., Oscillations in Finite Quantum Systems, Cambridge University Press, New York (1994).

[7.27] PLUJKO, V.A., Yad. Fiz. **52** (1990) 1004; Sov. J. Nucl. Phys. **52** (1990) 639.

[7.28] PLUJKO, V.A., Nucl. Phys. **A649** (1999) 209c.

[7.29] PLUJKO, V.A., Acta Phys. Pol. **B31** (2000) 435.

[7.30] PLUJKO, V.A., in Proc. 9th Int. Conf. Nucl. Reaction Mechanisms, Varenna, Italy, June 2000, GADIOLI, E. (Ed.) Suppl. N. 115 (2000) 113.

[7.31] PLUJKO, V.A., EZHOV, S.N., KAVATSYUK, M.O., GREBENUYK, A.A., YERMOLENKO, R.V., in Proc. Int. Conf. Nuclear Data for Science and Technology, Oct. 2001, Tsukuba, Ibaraki, Japan. J. Nucl. Sci. Technol., Supp. 2 (August 2002) 811.

[7.32] MUGHAGHAB, S.F., DUNFORD, C.L., Phys. Lett. **B487** (2000) 155.

[7.33] SIROTKIN, V.K., Yad. Fiz. **43** (1986) 570.

[7.34] NEMSHKALO, B.A., SIROTKIN, V.K., SHEBEKO, K.B., Yad. Fiz. **55** (1992) 123.

[7.35] FEDORETS, I.D., Yad. Fiz. **64** (2001) 51.

[7.36] EISENBERG, J.M., GREINER, W., Nuclear Theory, Vol. 1, Nuclear Models, Collective and Single-Particle Phenomena, North-Holland, Amsterdam (1987) Chapter 14, 3-5.

[7.37] DOVER, C.B., LEMMER, R.H., HAHNE, F.J.W., Ann. Phys. **70** (1972) 458.

[7.38] KOLOMIETZ, V.M., PLUJKO, V.A., SHLOMO, S., Phys. Rev. **C54** (1996) 3014.

[7.39] PLUJKO, V.A., Acta Phys. Pol. **B30** (1999) 1383.

[7.40] PLUJKO, V.A., GORBACHENKO, O.M., KAVATSYUK, M.O., Acta Phys. Slov. **51** (2001) 231; PLUJKO, V.A., EZHOV, S.N., GORBACHENKO, O.M., KAVATSYUK, M.O., J. Phys.: Condensed Matter **14** (2002) 9473.

[7.41] OBLOŽINSKÝ, P., Phys. Phys. **C35** (1987) 407.

[7.42] BONASERA, A., BURGIO, G.F., DI TORO, M., Phys. Lett. **B221** (1989) 233.

[7.43] SMERZI, A., BONASERA, A., DI TORO, M., Phys. Rev. **C44** (1991) R1713.

[7.44] MYERS, W.D., SWIATECKI, W.J., KODAMA, T., EL-JAICK, L.J., HILF, E.R., Phys. Rev. **C15** (1977) 2032.

[7.45] RAMAN, S., NESTOR, C.W., Jr., TIKKANEN, P., At. Data Nucl. Data Tables **78** (2001) 1.

[7.46] BOHR, A.G., MOTTELSON, B.R., in Nuclear Structure, Vol. II, Benjamin London (1975) 636.

[7.47] LE TOURNEUX, J., Mat. Fys. Medd. Dan. Vid. Selsk. **34** (1965) 1.

[7.48] AYIK, S., BOILEY, D., Phys. Lett. **B276** (1992) 263; *ibid*, **B284** (1992) 482E.

[7.49] KOLOMIETZ, V.M., PLUJKO, V.A., SHLOMO, S., Phys. Rev. **C52** (1995) 2480.

[7.50] GORIELY, S., Phys. Lett. **B436** (1998) 10.

[7.51] GOVAERT, K., BAUWENS, F., BRYSSINCK, J., DE FRENNE, D., JACOBS, E., MONDELAERS, W., GOVOR, L., PONOMAREV, V.Yu., Phys. Rev. **C57** (1998) 2229.

[7.52] CATARA, F., LANZA, E.G., NAGARAJAN, M.A., VITTURI, A., Nucl. Phys. **A624** (1997) 449.

[7.53] GORIELY, S., KHAN, E., Nucl. Phys. **A706** (2002) 217.

[7.54] KHAN, E., SUOMIJÄRVI, T., BLUMENFELD, Y., NGUYEN VAN GIAI, ALAMANOS, N., AUGER, F., BAUGE, E., BEAUMEL, D., DELAROCHE, J.P., DELBOURGO-SALVADOR, P., DROUART, A., FORTIER, S., FRASCARIA, N., GILLIBERT, A., GIROD, M., JOUANNE, C., KEMPER, K.W., LAGOYANNIS, A., LAPOUX, V., LÉPINE-SZILY, A., LHENRY, I., LIBERT, J., MARÉCHAL, F., MAISON, J.M., MUSUMARRA, A., OTTINI-HUSTACHE, S., PIATTELLI, P., PITA, S., POLLACCO, E.C., ROUSSEL-CHOMAZ, P., SANTONOCITO, D., SAUVESTRE, J.E., SCARPACI, J.A., ZERGUERRAS, T., Nucl. Phys. **A694** (2001) 103.

[7.55] HAMOMOTO, I., SAGAWA, H., ZHANG, X.Z., Phys. Rev. **C55** (1997) 2361; *ibid*, **C57** (1998) R1064.

[7.56] VRETENAR, D., PAAR, N., RING, P., LALAZISIS, G.A., Nucl. Phys. **A692** (2001) 449.

[7.57] PLUJKO, V.A., KAVATSYUK, M.O., KAVATSYUK, O.O., Proc. 11th Int. Symp. Capture Gamma-Ray Spectr. and Related Topics (CGS 11), Pruhonice near Prague, Czech Republic, Sept. 2002, KVASIL, J., CEJNAR, P., KRTICKA, M. (Eds.), World Scientific, Singapore (2003) 793.

[7.58] RODIN, V.A., URIN, M.G., Physics of Elementary Particle and Atomic Nuclei (Fyzika elementarnich chastitz i atomnogo yadra), Dubna, **31** (2000) 976.

[7.59] BUSH, B., ALHASSID, Y., Nucl. Phys. **A531** (1991) 27.

[7.60] DILG, W., SCHANTL, W., VONACH, H., UHL, M., Nucl. Phys. **A217** (1973) 269.

[7.61] VON EGIDY, T., SCHMIDT, H.H., BEHKAMI, A.N., Nucl. Phys. **A481** (1988) 189.

[7.62] SZEFLIŃSKI, Z., SZEFLIŃSKA, G., WILHELMI, Z., RZĄCA-URBAN, T., KLAPDOR, H.V., ANDERSON, E., GROTZ, K., METZINGER, J., Phys. Lett. **B126** (1983) 159.

[7.63] INTERNATIONAL ATOMIC ENERGY AGENCY, Handbook on photonuclear data for applications. Cross-sections and spectra. Final report of a co-ordinated research project 1996-1999. IAEA-TECDOC-1178, Vienna (2000).

[7.64] DANOS, M., Nucl. Phys. **5** (1958) 23.

[7.65] CARLOS, P., BERGERE, R., BEIL, H., LEPRETRE, A., VEYSSIERE, A., Nucl. Phys. **A219** (1974) 61.

[7.66] MOLLER, P., NIX, J.R., MYERS, W.D., SWIATECKI, W.J., At. Nucl. Data Tables **59** (1995) 185.

[7.67] HASSE, R.W., MYERS, W.D., Geometrical Relationships of Macroscopic Nuclear Physics, Springer-Verlag, Berlin, Heidelberg, New York (1988)

[7.68] BLANN, M., Phys. Rev. **C21** (1980) 1770.

[7.69] BORTIGNON, P.F., BROGLIA, R.A., BRACCO, A., CASSING, W., DØSSING, T., ORMAND, W.E., Nucl.Phys. **A495** (1989) 155c.

[7.70] GORBACHENKO, O.M., PLUJKO, V.A., Visnik Kyivskogo Universitetu, seria fis.-mat. nauk N**1** (2001) 434; Abstracts 51th Conf. Nucl. Spectr. Nucl. Structure, September 2001, Sarov, Russia, VNIIEPH, P.130(304).

[7.71] BERINGER, R., KNOX, W.J., Phys. Rev. **121** (1961) 1195.

[7.72] VIGDOR, S.E., KARWOWSKI, H.J., Phys. Rev. **C24** (1982) 1068.

[7.73] BLATT, M., WEISSKOPF, V.F., Theoretical Nuclear Physics, John Wiley, New York (1952) 647.

[7.74] VASILIEVA, E.V., SUKHOVOJ, A.M., KHITROV, V.A., Preprint P3-99-203, JINR, Dubna (1999).

[7.75] VASILIEVA, E.V., SUKHOVOJ, A.M., KHITROV, V.A., Physics of Elementary Particle and Atomic Nuclei (Fyzika elementarnich chastitz i atomnogo yadra), Dubna, **31** (2000) 350.

[7.76] VASILIEVA, E.V., SUKHOVOJ, A.M., KHITROV, V.A., Yad. Fiz. **64** (2001) 3.

[7.77] THIELEMANN, F.K., ARNOULD, M., Proc. Conf. Nuclear Data for Science and Technology, BOCKHOFF, K. (Ed.), Reidel, Dordrecht (1983) 762.

[7.78] GOLDHABER, M., TELLER, E., Phys. Rev. **74** (1948) 1046.

[7.79] VAN ISACKER, P., NAGARAJAN, M.A., WARNER, D.D., Phys. Rev. **C45** (1992) R13.

[7.80] GORIELY, S., in Proc. 10th Int. Symp. Capture Gamma-Ray Spectroscopy and Related Topics, WENDER, S. (Ed.), AIP Conf. Proc. 529 (2002) 28.7

[7.81] ABOUSSIR, Y., PEARSON, J.M., DUTTA, A.K., TONDEUR, F., At. Data Nucl. Data Tables **61** (1995) 127.

8 NUCLEAR FISSION

Coordinators: S. Goriely and A. Ignatyuk

Summary

A set of fission barriers and the corresponding nuclear level densities have been generated for various applications. Accurate level densities are prescribed within GSM for reactor physics studies. Since fission level densities and barrier parameters are strongly interdependent, the corresponding set of parameters for both the inner and outer fission barriers has also been provided. Some specific applications, such as accelerator-driven systems and stellar nucleosynthesis, require a knowledge of large numbers of fission barriers and level densities to estimate spontaneous as well as neutron-induced or β-delayed fission probabilities. Hence, the present compilation includes fission barriers for some 2301 nuclei with $78 \leq Z \leq 120$ derived by means of the ETFSI method, and the corresponding level densities at both saddle-point deformations predicted by the microscopic model based on HFBCS single-particle properties.

The main concepts of nuclear fission theory are based essentially on the liquid-drop model [8.1, 8.2]. According to this model, competition between the surface tension forces of a nuclear liquid drop and the Coulomb repulsion forces related to the nuclear charge leads to the formation of an energy barrier which prevents spontaneous decay of the nucleus. The penetrability of the barrier determines the half-life for spontaneous fission. In the liquid-drop model, the height of the fission barrier for heavy nuclei decreases rapidly with increase of Z^2/A, and should disappear when $(Z^2/A)_{cr} = 46 - 48$. The decrease in height results in an exponential increase in barrier penetrability. These barrier changes exhibit good agreement with the behavior of the spontaneous fission lifetimes of the actinide nuclei, ranging from the long-lived isotopes of uranium to the artificially synthesized short-lived isotopes of fermium and mendelevium [8.3, 8.4, 8.5, 8.6]. The height of the barrier is a key ingredient for a description of fission cross sections measured in different nuclear reactions.

Early studies show that despite some successful results the liquid-drop model cannot explain the major peculiarity of spontaneous and low-energy fission of the actinides, namely the asymmetric mass distribution of fission fragments [8.7], implying that shell effects have a strong influence on fission fragment formation. Initially, fission mass-asymmetry was explained in terms of some modifications of the liquid-drop model predictions for configurations close to the scission point (point where the fissioning nucleus breaks into two fragments). However, new phenomena were discovered in the 1960s that required more radical changes in the fission model in order to be explained, particularly

the spontaneously-fissioning Am isomers [8.8] and the intermediate resonance structures observed in the neutron-induced fission cross sections [8.9, 8.10] that cannot be explained by adopting the traditional formula for fission barrier penetrability.

Calculations of nuclear deformation energies based on the shell correction method [8.11, 8.12] played a crucial role in explaining the above phenomena. The fission barriers calculated for the actinides consisted of a two-hump curve with a rather deep potential well between the humps. This two-hump shape also identified the spontaneously-fissioning isomers as the lowest states of a fissioning nucleus in the second potential well, and the intermediate resonances as excited states of a nucleus in this well [8.13, 8.14].

Our present knowledge of the fission barriers can be represented in terms of three groups:

(i) results of broad scale investigations of fission cross sections for pre-actinides that undergo different charged-particle induced reactions to give the main experimental information on the droplet properties of nuclei - interest in such data has increased dramatically over the previous decade due to extensive discussions of accelerator-driven power systems for the transmutation of nuclear waste;

(ii) two-humped barriers of actinides studied with a high accuracy that undergo neutron-induced reactions of significant importance in reactor physics - investigations of the fission barriers at low energies were extended for many actinides to the high energies of charged-particle induced reactions in order to study the changes of fission barriers with increased excitation;

(iii) barriers required to explain the existence of long-lived superheavy elements with $Z > 102$ due only to the shell effects in fission barriers - our knowledge and understanding of superheavy nuclei are still very scanty, and there are extremely large uncertainties associated with the quantification of their fission barriers (see Ref. [8.15] for a good review of superheavy nuclei).

Our studies concentrate on the first two groups of data, which are connected with the basic tasks of the RIPL project. Another field that requires extensive data on fission barriers is astrophysics which encompasses stellar nucleosynthesis and the rapid neutron-capture process. Microscopic calculations of the fission barriers associated with this phenomenon will be discussed in the final part of the chapter.

8.1 Fission barriers and level densities for pre-actinides

As with any other decay width, the fission width (Γ_f) for an excited nucleus is determined by the product of the excited level spacing (D_c) and the sum of the transmission coefficients over all channels leading to fission:

$$\Gamma_f(U_c) = \frac{D_c(U_c)}{2\pi} \sum T_{fi} \ . \tag{8.1}$$

Based on the principles of the liquid-drop model, the intermediate saddle configuration at the top of a fission barrier is of vital importance in the determination of fission probability.

A significant amount of the initial excitation energy at the saddle point is concentrated in the fission degree of freedom, which imposes significant limitations on the excitations of other degrees of freedom. Therefore, only the transitional states in the saddle point are usually considered as the fission channels [8.16]. The spectrum of such channels should be similar to the observed level spectra of the heavy deformed nuclei, taking into account possible changes in the symmetry and deformation of transitional states. All limitations connected with the conservation laws for energy, angular momentum and parity should also be taken into consideration in Eq. (8.1).

Most measurements of the fission cross sections for pre-actinides were performed at energies above the fission barriers. Fission widths for such energies can be written in the form:

$$\Gamma_f(U_c) = \frac{1}{2\pi\rho_c(U_c)} \int_0^{U_c - B_f} \rho_f(U_c - B_f - E)dE \ , \tag{8.2}$$

where ρ_c and ρ_f are the level densities for the equilibrium compound and saddle configurations, respectively, and B_f is the fission barrier height [8.1]. Eq. (8.2) shows the strong interdependence of the barrier parameters and the level densities. Approximations used in the level density description of the fission cross-section analyses have been discussed by many authors [8.17, 8.18, 8.19, 8.20, 8.21], and the corresponding uncertainties of the models applied should always be kept in mind when comparing the fission barriers derived from available experimental data.

The most complete compilations of the experimental fission barriers are given in Refs. [8.22, 8.23, 8.24], where comprehensive sets of references can be found. A large amount of data has accumulated on the fission barriers for light charged-particle induced reactions. Many measurements of the fission cross sections were also performed for the heavy-ion induced reactions [8.25]. However, because of the rather complex models involved in the analysis of heavy-ion reactions, the uncertainties in the estimated fission barriers are usually found to be much larger than for light charged-particle reactions.

Generally, fission barriers are approximated by the equation:

$$B_f = B_{ld} - \delta E_0 + \delta E_f, \tag{8.3}$$

where B_{ld} is the liquid-drop component of the fission barrier, δE_0 is the ground state shell correction, and δE_f is the corresponding shell correction for the saddle configuration of the fissioning nucleus. Usually, one assumes that the shell effects vanish for the strongly-deformed saddle configurations of pre-actinides, and the ground-state shell corrections are equal to the microscopic corrections in the nuclear masses as considered in Chapter 2. Differences between the various estimates of the fission barriers relate mainly to the liquid-drop component of the fission barrier.

Various versions of the liquid-drop model have been developed [8.26, 8.27, 8.28, 8.29], that differ as a consequence of the choice of model parameters and the additional components connected with the diffuse-surface, curvature and proximity effects. Rather simple equations for the liquid-drop barriers were proposed recently on the basis of the Thomas-Fermi model [8.30]. Measured barriers for about 120 nuclei were fitted by the formula:

$$B_f(Z, N) = S(Z, N)F(X), \tag{8.4}$$

where $S = A^{2/3}(1-kI^2)$ is proportional to the nuclear surface energy with $I = (N-Z)/A$, and the surface symmetry coefficient k is defined as $k = 1.9 + (Z - 80)/75$. The fission parameter (X) is proportional to the ratio of the Coulomb and surface energies, and can be defined as

$$X = Z^2/A(1 - kI^2). \tag{8.5}$$

Function F is cubic, and joined smoothly to a straight line at $X = X_1$:

$$F(X) = \begin{cases} 0.000199748(X_0 - X)^3 & \text{for } \mathrm{X}_1 \leq \mathrm{X} \leq \mathrm{X}_0, \\ 0.595553 - 0.124136(X - X_1) & \text{for } 30 \leq \mathrm{X} \leq \mathrm{X}_1, \end{cases} \tag{8.6}$$

with $X_0 = 48.5428$ and $X_1 = 34.15$.

Available experimental data on the fission barriers for pre-actinides are compared in Fig. 8.1 [8.23, 8.24] with the estimations derived from Eq. (8.4). The FRDM shell corrections (see Chapter 2) were used to transform the experimental fission barriers to liquid-drop barriers. A good description of the experimental barriers led us to recommend Eq. (8.4) as probably the best approximation of the liquid-drop fission barriers in the region of $X \geq 30$. Lighter nuclei have a dumb-bell shape at the saddle point, and the calculations based on the Yukawa-plus-exponential double-folded approximation for nuclear energies may be preferable [8.29]. The corresponding code for such calculations is included in RIPL-2, and the experimental fission barriers compiled in Ref. [8.24] for near-magic nuclei with strong shell effects are given in the **fission-barriers-exp.dat** file together with the barriers for actinides (as discussed later). All models considered in Chapter 6 can be used to calculate the fission widths (Eq. 8.1). However, in order to maintain consistency, the same model should be used for the fission and particle widths that defined the dominant channels of a compound nucleus decay. The shell, pairing and collective effects are essentially different for the ground and saddle states, and these differences should certainly be taken into account in calculations of nuclear fission.

Shell effects can apparently be neglected for the saddle level densities, but they are important for the neutron widths of near-magic nuclei shown in Fig. 8.1. The energy dependence of the a-parameters given by Eqs. (6.11) and (6.36) is extremely important for such nuclei, as confirmed by many results of fission cross section analyses [8.20, 8.23, 8.31].

Pairing effects are implicitly associated with the energy dependence of the effective moment of inertia, which determines the angular distributions of the fission fragments [8.32]. Analysis of the corresponding experimental data has shown that the correlation parameter for the saddle point (Δ_f) should always be specified as about 15% larger than for the ground states [8.33]. The relationship $\Delta_f = 14/A^{1/2}$ can be used as a reasonable approximation for the pairing parameter within the saddle point.

Collective enhancement of nuclear level densities is clearly displayed when undertaking a systematic analysis of the fission cross sections for spherical and deformed nuclei [8.19, 8.21, 8.34]. A consistent description of the shell, pairing and collective effects can only be achieved by means of the generalized superfluid model (GSFM). GSFM parameters can be derived on the basis of the systematics considered in Chapter 6, with corresponding modifications to the pairing, asymptotic level density parameters and moments of inertia of the saddle states.

Differences between the asymptotic level density parameters for the fission and neutron channels are affected by the surface component for the density of single-particle states.

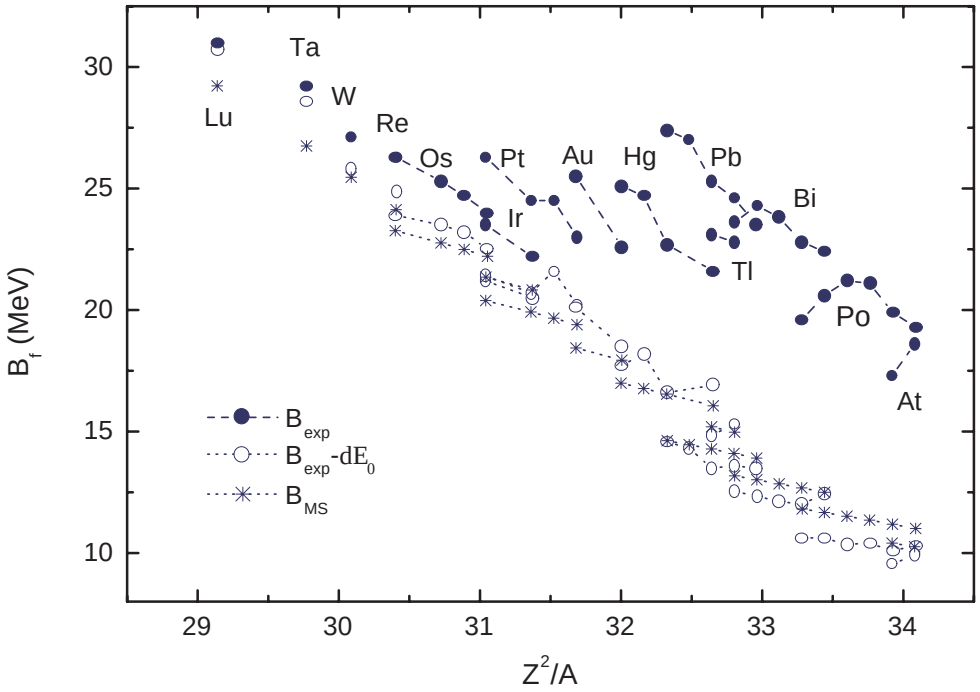

Figure 8.1: Fission barriers of pre-actinides and their liquid-drop components in comparison with liquid-drop model estimates [8.30]

Adopting the semi-classical approach, the level density parameter can be expressed in the form [8.20, 8.35, 8.36]

$$\tilde{a} = c_v A + c_s B_s A^{2/3} + c_c B_c A^{1/3}, \tag{8.7}$$

where c_i are the coefficients for the volume, surface and curvature components, and B_i are the corresponding functions that describe the relative increase of the surface or curvature under deformation of a nucleus. The dumb-bell saddle shapes of pre-actinides correspond to $B_s = 2^{1/3}$, which leads to the ratio $a_f/a_n > 1$ used in all analyses of fission cross sections. However, there are large uncertainties associated with estimates of the coefficient ratio c_s/c_v [8.20, 8.35, 8.36]. Evaluations of the ratio $c_s/c_v = 1.30$ based on microscopic calculations involving the single-particle level schemes of the Wood-Saxon potential [8.20], or $c_s/c_v = 1.53$ derived from phenomenological systematics of the neutron resonance densities seem to be the most reasonable approaches. Both methods give an a_f/a_n ratio of between 1.05 and 1.07 which is supported by the direct results of fission cross section analyses [8.23].

8.2 Fission barriers and level densities for actinides

Highly accurate evaluations are required for the neutron-induced fission cross sections of the main fissile and fertile nuclei. The fission barriers and corresponding level densities are key ingredients of such evaluations. Full-scale Hauser-Feshbach theory, the coupled-

channel optical model and double-humped fission barrier parameterization are normally used in such calculations, supported by numerous experimental data that demonstrate the importance of the shell, pairing and collective effects at both the equilibrium and saddle nuclear states.

Eq. (8.1) is adopted for the fission width, but the transmission coefficients should be estimated in accordance with the two-humped structure of fission barriers for which penetrabilities vary with energy in a much more complicated manner than for a one-hump barrier [8.13, 8.14]. The quasi-stationary states of the nucleus in the well between the humps have a strong modulating effect on the penetrability of the two-humped barrier [8.13, 8.37]. These modulations are manifested in the sub-barrier fission cross-sections as intermediate structures, examples of which are the resonances observed in the ^{230}Th(n, f) reaction at neutron energies of about 700 keV [8.9] and the structure displayed in the neutron-induced fission cross-sections of ^{240}Pu [8.10]. More comprehensive discussions of the experimental data on intermediate structures in actinide fission cross sections can be found in Refs. [8.13, 8.38].

The transmission coefficient for the deep second well can be averaged over the intermediate structures, and written in the form:

$$< T(E) >= \frac{T_A T_B}{T_A + T_B + T_\gamma} \tag{8.8}$$

where T_A and T_B are the penetrability of the humps A and B respectively, and T_γ is the probability for gamma decay in the second well. The transition through the two-humped barrier is determined by the probability of sequential transitions through each of the humps. If $T_\gamma << (T_A + T_B)$, the probability of the transition through the asymmetric two-hump barrier is the same as that for the one-hump barrier and equivalent to the higher hump.

Penetrabilities for each hump can be approximated by the well-known formula for the penetrability of a parabolic barrier:

$$T_i(E) = \left\{1 + exp\left[\frac{2\pi}{\omega_i}(E_i - E)\right]\right\}^{-1}, \tag{8.9}$$

where E_i is the energy of the transition state and ω_i is the curvature close to the top of the corresponding barrier. As a consequence of the exponential growth of penetrability (which is much stronger than the decrease in level spacing), the average fission width (Eq. 8.1) for the two-humped barrier increases exponentially with increasing excitation energy in an approximately similar manner to one higher hump. At energies above that of the barrier, the penetrability does not prevent nuclear transitions to open fission channels, and the fission width increases because of the growth in the number of open channels, which is much weaker than the sub-barrier increase of the fission width. This change in the growth rate of fission widths is usually adopted in experimental data analyses as a direct method for the estimation of fission barrier heights.

The quantum structure of the fission channels at the top of each barrier is extremely important in the formulation of accurate descriptions of the fission cross sections at the sub-barrier and near-barrier energies. Such structure depends strongly on the symmetry of nuclear deformations at the corresponding saddle states. Shell model calculations

have been undertaken, supported by the results of fission fragment angular distribution analyses. The fissioning nucleus has been calculated to possess axial asymmetric shape at the inner saddle A, and axial-symmetric and mirror-asymmetric shape at the outer saddle B. Mirror-asymmetric even-even nuclei have ground-state rotational band levels with $K^\pi = 0^+$, $J = 0, 2, 4...$ - that unify with the octupole band levels $K^\pi = 0^-$, $J = 1, 3, 5...$ in the common rotational band (which includes levels with all possible values of angular momentum and parity). Additional unification arises for axial asymmetric shapes and levels of the γ-vibrational band with $K^\pi = 2^+$, $J = 2, 4...$ The quantum number of the corresponding rotational bands for odd and odd-odd nuclei should be estimated in accordance with the angular momentum addition rules for unpaired particles and the corresponding rotational bands. As the result, the fission cross section analysis involves a much more complex structure of saddle transient states than the well-studied collective-level sequences of the deformed rare-earth nuclei and actinides.

The saddle shape symmetry should be taken into consideration when evaluating the collective enhancement of the level densities. Thus, for axial-symmetric, mirror-asymmetric shapes, the rotational enhancement must be increased by a factor of two relative to the estimates given in Chapter 6 (Eq. 6.28). The rotational enhancement must be even larger for γ-asymmetric shapes:

$$K_{rot} = 2\sqrt{2\pi}\,\{\mathcal{I}_x\mathcal{I}_y\mathcal{I}_z\}^{1/2}\,t^{3/2}, \tag{8.10}$$

where $\mathcal{I}_i$ is the moment of inertia relative to the corresponding axis, and t is the nuclear temperature for transient states. Obviously, the moment of inertia should also be calculated for deformations corresponding to the saddle states.

The pairing effects at transient states are displayed most clearly in the energy dependence of the parameter K_0^2, which determines the angular distribution of the fission fragments [8.32]. This parameter is proportional to the effective moment of inertia of transient states, and is similar to the spin cutoff parameter in the level density formula (Eq. 6.1). The correlation function (Δ_f) obtained from the analysis of the fission fragment angular distributions for even-even plutonium isotopes can be approximated by the relationship $\Delta_f = 14/A^{1/2}$ MeV [8.39], and such an estimation of the pairing for the saddle states is very close to the results obtained for the pre-actinides [8.33].

As a consequence of the essential role of the shell, pairing and collective effects, a consistent description of the experimental data for the fission cross sections of actinides can be obtained through the generalized superfluid model (GSFM). Data for the light charged-particle induced reactions have been analyzed for a large group of nuclei in Ref. [8.40] and for neutron-induced reactions in Refs. [8.41, 8.42, 8.43]. The neutron cross sections have been measured to a high degree of accuracy, and therefore their analyses are usually considered as the most reliable estimates of the fission barriers and fission level densities. Shell corrections were derived (in MeV) from an analysis of the fission cross sections in the first plateau region (2 - 5 MeV over the fission barrier) [8.41], using the phenomenological version of GSFM (see Chapter 6):

$$\delta E_0^A = \begin{cases} 2.6 & \text{for Z} \leq 97, \\ 2.6 - 0.1(Z - 97) & \text{for Z} > 97, \end{cases}$$

$$\delta E_0^B = \begin{cases} 0.6 + 0.1(Z - 97) + 0.04(N - 143) & \text{for Z} < 97, \\ 0.6 + 0.04(N - 143) & \text{for Z} \geq 97 \end{cases} \tag{8.11}$$

Pairing parameters were assigned $\Delta_f^A = \Delta_f^B = \Delta_0 + 0.2$ MeV, where Δ_0 is the pairing for the ground states (neutron channels). The perpendicular moments of inertia for the level density calculations were chosen to be equal to $100\hbar^2/MeV$ for the inner saddle, $200\hbar^2/MeV$ for the outer saddle, and approximately $75\hbar^2/MeV$ for the ground states [8.42].

Note that the matching of the discrete saddle states with the level density parameters used at high energies can be important for the consistent description of the fission cross sections at the near-barrier energies. Thus, the GSFM parameters for the fission channels should be estimated by adopting schemes for the saddle states of each hump; frequently, the constant temperature model is applied instead of adjusting such parameters. The temperatures are usually taken to be the same as for the neutron channels (see Chapter 6), and the energy shifts are only adjusted to the adopted saddle state schemes.

Another important effect at the near-barrier energies is the step-like behavior of the level density near the thresholds of one- and two-quasi-particle excitations. Such step-like structures are observed directly in the low-energy variations of the parameter K_0^2 determined from the fission fragment angular distribution [8.39], and can be explained within the framework of GSFM [8.44]. The well-known structure in the neutron-induced fission cross sections of ^{235}U around 1 MeV can be considered as evidence of step-like changes of the fission level density at the two-quasi-particle excitation threshold [8.42]. An analysis of the irregularities in the neutron-induced fission cross sections of other nuclei is presented in Ref. [8.45]; the partial level density formula considered in Chapter 6 can be applied to such irregularities, and possible simplifications were discussed.

Fission barrier parameters have been estimated from modeling analyses of the available experimental data for the neutron-induced fission cross sections of the uranium, neptunium, plutonium, americium and curium isotopes [8.43, 8.46, 8.47]. Barrier parameters for Th and Pa nuclei were also obtained by adopting essentially the same approach [8.48, 8.49, 8.50]; however, these specific data were less accurately estimated due to the more complex structure of the fission barriers in light actinides as compared to transuranium nuclei. The inner and outer fission barrier heights are shown in Fig. 8.2. Corresponding data were included in the RIPL-1 files, and have been combined with the recommended barriers for pre-actinides in the **fisbar-experimental.dat** file of RIPL-2. A comparison between these data and the fission barriers evaluated in Ref. [8.24] shows that there is good agreement for the outer barriers of the uranium, plutonium and americium isotopes. Some disagreements exist for the inner barrier heights, although the general isotopic dependences are very similar; furthermore, significant discrepancies occur in the case of the outer barriers of the curium isotopes.

Barrier curvature parameters are usually evaluated with relatively large uncertainties from analyses of the sub-barrier behavior of fission cross sections [8.38, 8.45]. The following parameters can be recommended as optimal (in MeV): $\hbar_A = 0.9 - 1.0, 0.8$ and 0.60, and $\hbar_B = 0.6, 0.5$ and 0.4 for the even-even, odd and odd-odd nuclei, respectively. Even-odd differences in the curvature parameters are dependent on the superconductive pairing correlations and their impact on the stiffness and reduced mass parameters of the fissioning nucleus at the saddle.

Pairing parameters for the fission channels are given in the recommended data files, together with the corresponding fission barriers. These data are shown in Fig. 8.3 in com-

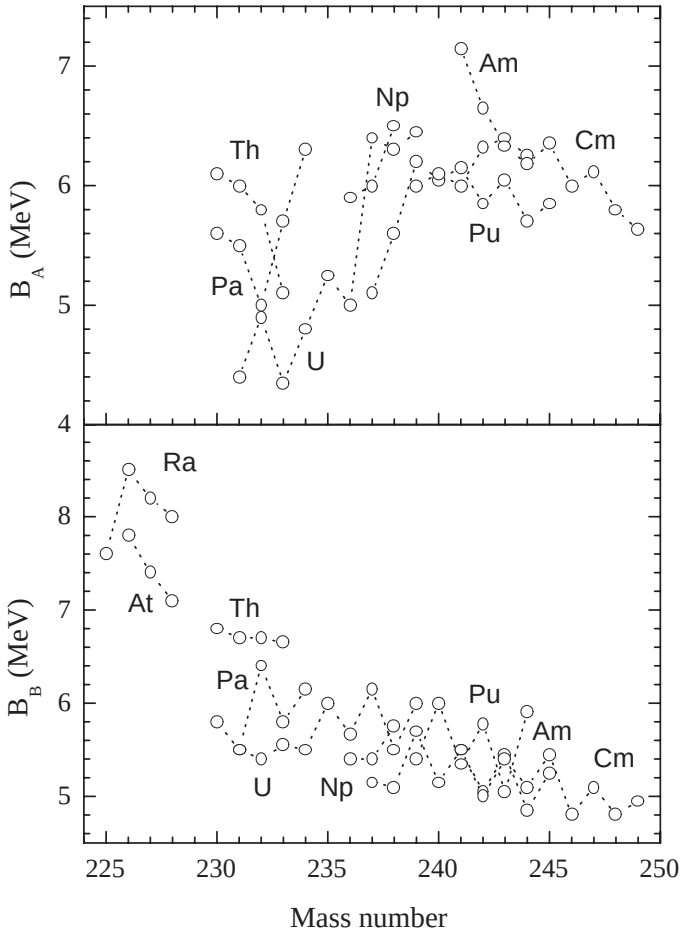

Figure 8.2: Inner (A) and outer (B) fission barriers derived from the analysis of neutron-induced fission cross sections [8.46, 8.47, 8.48, 8.49, 8.50].

parison with the simple approximations used in the systematics of the pairing parameters for the equilibrium and saddle states. An increase of the pairing at the saddle point is confirmed by all results of the fission cross section analysis, but the difference between Δ_f and Δ_0 seems to fluctuate strongly. Variations of Δ_f have an important effect on the fission barrier values extracted from the cross-section analysis. Despite such well-defined variations, the uncertainties in the fission barrier parameters are difficultly to estimate accurately. For even-even nuclei in which the sub-barrier and over-barrier cross sections are analyzed simultaneously, the uncertainties in the higher-hump estimates are about 0.2 MeV; these uncertainties are even larger for the lower hump with values of about 0.5 MeV. Approximately the same uncertainties should be adopted for the fission barriers of odd and odd-odd nuclei for which the over-barrier cross sections can be analyzed. Finally, the uncertainties of the outer barriers of the curium isotopes are probably ever larger.

Many of the above results were obtained from analyses of the fission cross sections at excitations lower than 15 - 20 MeV above the fission barrier. According to the general concepts of the shell correction method, the two-humped structure of any fission barrier should disappear at higher excitation, and liquid-drop fission barriers with asymptotic level density parameters should be used to describe both the fission cross section and

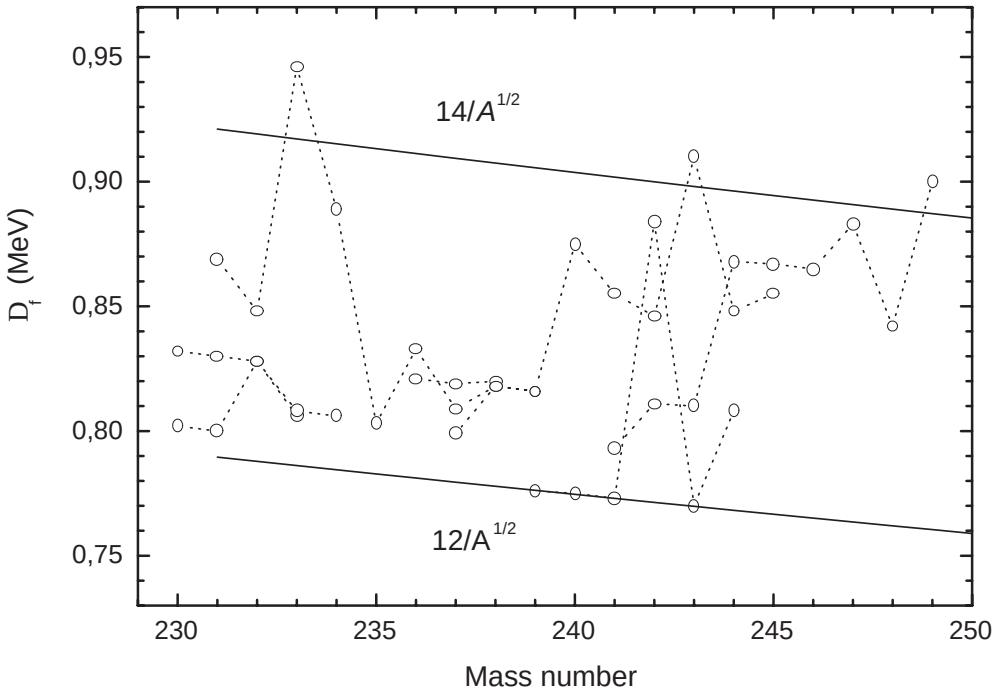

Figure 8.3: Pairing parameters Δ_f derived from an analysis of neutron-induced fission cross sections; solid lines correspond to the average pairing parameters used for the level densities at equilibrium deformations (lower line) and recommended for the saddle states (upper line).

all competitive reaction cross sections at excitation energies above 30 - 50 MeV. This prediction would appear to be supported by the available experimental data [8.31, 8.34], although there are difficulties separating unambiguously the first-step fission of an initial nucleus from the multi-chance fission of daughter nuclei that arises after the emission of one or more neutrons. So, we have only theoretical estimates of excitations at which the transition from shell to liquid-drop model behavior should occur, and lack a satisfactory understanding of what approximations should be applied to define the fission barriers and fission level densities in the transitional energies.

8.3 Large-scale microscopic calculations of fission barriers and level densities

The origin of approximately half the stable nuclides heavier than iron that are observed in nature has been explained in terms of stellar nucleosynthesis through the rapid neutron-capture process (or r-process) [8.51]. These complex fundamental studies require a large number of estimated fission data. Although the exact astrophysical site at which the r-process develops still represents one of the major puzzles in nucleosynthesis theory, the r-process is believed to take place in environments characterized by high neutron densities ($N_n \gtrsim 10^{20}$ cm^{-3}), such that successive neutron captures can proceed into neutron-rich

regions some considerable distance from the valley of β-stability. This process produces nuclei with decreasing neutron binding energies, and consequently faster (γ, n) photodisintegration that competes with the slowing-down (n, γ) reactions at high temperatures ($T \gtrsim 10^9$ K). With timescales usually thought to be much longer than the characteristic timescale of (n, γ) and (γ, n) reactions, β-decay drives the material to higher Z elements. Depending on the strength of the neutron flux as well as the duration of the neutron irradiation, nuclei up to the super-heavy mass region can be produced in timescales of the order of a second. So far, no astrophysical model is able to provide any reliable predictions of the thermodynamic conditions under which the r-process can take place. Fission processes are important in describing the nuclear mechanisms taking place during the r-process:

(i) if matter reaches the super-heavy neutron-rich region during the neutron irradiation, fission could recycle the nuclear flow and affect the nucleosynthesis of the bulk of the r-process nuclei;

(ii) all nuclei produced during the r-process irradiation with $A \gtrsim 208$ are neutron-rich heavy progenitors of the r-abundance peak in the Pb region - their production ratio depends on the fission probabilities, so that a correct treatment of the fission processes is needed to predict the production of Pb and Bi during and after neutron irradiation;

(iii) r-process nucleosynthesis creates long-lived ^{232}Th, ^{235}U and ^{238}U that are used as cosmochronometers to estimate the upper age limit of the Galaxy [8.52].

An accurate knowledge of the astrophysics, as well as the nuclear properties affecting the progenitors of these chronometers (particularly the fission probabilities of their progenitors) is a fundamental pre-requisite for a reliable age estimate.

Changes in the abundance of the heavy nuclei as a result of the high neutron fluxes and temperatures encountered during the r-process nucleosynthesis can only be satisfactorily calculated by using a network of nuclear reactions that includes all of the necessary neutron capture, photodisintegration, β-decay, α-decay, β-delayed particle and fission processes. The fission processes include spontaneous, β-delayed and neutron-induced fission for which the probabilities must be estimated for some 2000 nuclei with $80 \lesssim Z \lesssim 110$ located mainly in the neutron-rich region. Therefore, we have compiled fission-barrier data for some 2301 nuclei with $78 \leq Z \leq 120$ as derived using the ETFSI method, and the corresponding level densities at both saddle point deformations predicted by the microscopic model (more details are given below).

8.3.1 Fission barriers

Data file **fisbar-etfsi.dat** contains predictions of the fission barriers and saddle point deformations as obtained from the Extended Thomas-Fermi plus Strutinsky Integral (ETFSI) model [8.53, 8.54]. ETFSI is a semi-classical approximation to the Hartree-Fock method in which the shell corrections are calculated with the "integral" version of the Strutinsky theorem; BCS corrections are also added with a delta-pairing force. The fission barriers are derived with the SkSC4 Skyrme force on which the ETFSI-1 mass

formula is based. Experimental primary barriers can be reproduced [8.24] within plus or minus 1.5 MeV (except for elements with $Z < 87$ which have barriers above 10 MeV). Fig. 8.4 shows the relative accuracy $(B_{exp} - B_{th})/B_{exp}$ of this global prediction for the primary barriers, i.e., the highest barrier (see Ref. [8.53] for more details). These predictions are accurate to within ± 40%, which is an excellent result in view of the global character of the model based on a Skyrme force fitted exclusively in terms of nuclear masses.

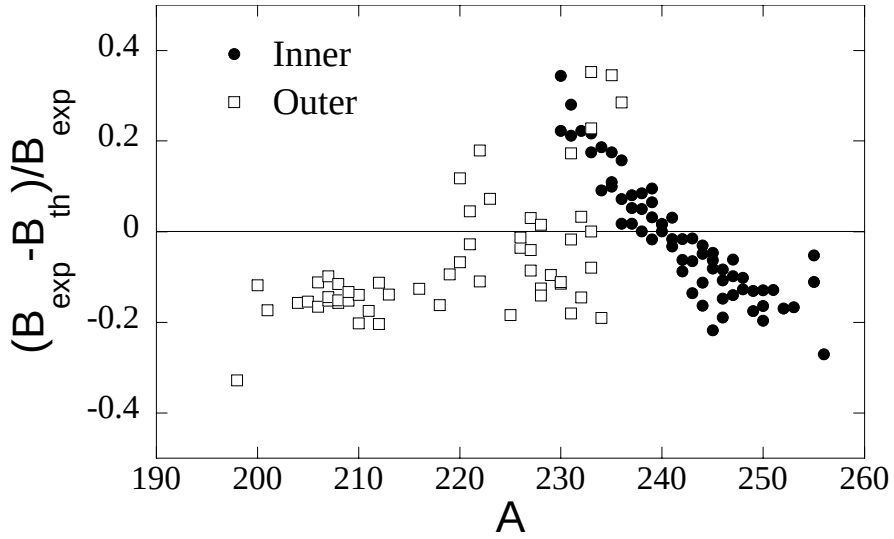

Figure 8.4: Relative errors $(B_{exp} - B_{th})/B_{exp}$ in the primary (i.e., highest) barriers calculated by ETFSI.

The ETFSI compilation includes 2301 nuclei with $78 \leq Z \leq 120$, and their masses range from slightly neutron-deficient to extremely neutron-rich nuclei (close to or at the calculated neutron drip line) up to $A = 318$. These data contain the nuclei considered in Ref. [8.53] for which experimental barriers are known, and a slightly extended version of the set published in Ref. [8.54]. Experimental fission barriers are also included that were compiled in Ref. [8.53] and originated mainly from Ref. [8.24].

A maximum of two barriers are given for each nucleus (inner and outer), corresponding to the highest saddle points among the "slightly" and "strongly" deformed. Those two groups of saddle points correspond to well-separated values of the elongation parameter c (c_{in} and c_{out} (see below)); $c_{in} < 1.6$ and $c_{out} > 1.6$ for many nuclei, although $1.5 < c_{out} < 1.6$ in some cases.

As well as the calculated inner and outer barriers, the deformation parameters at the corresponding saddle points are included in the RIPL-2 database. The nuclear shapes are limited to axially symmetrical deformations that are described in terms of Brack parameterization (c, h, α), where c is the elongation parameter ($c < 1, = 1$ and > 1 for oblate, spherical and prolate shapes, respectively), h is associated with the "necking" of the nuclear surface (shapes corresponding to different regions of the (c, h) plane are described in Ref. [8.53]), and α quantifies left-right asymmetry ($\alpha = 0$ for symmetric shapes). Asymmetry parameters a_{in} and a_{out} listed in RIPL-2 do not refer to α, but to $\tilde{\alpha}$ as defined in Ref. [8.53] to be $\alpha\ c^3$; the mass ratio of the two fission fragments is roughly given by $(1 + 3/8\ \tilde{\alpha})/(1 - 3/8\ \tilde{\alpha})$. All calculated fission barriers have deformation parameters within the domain: $1.00 < c < 2.36$, $-0.26 < h < 0.22$ and $0 \leq \tilde{\alpha} < 0.75$.

8.3.2 Fission level densities

Level densities need to be provided for all the nuclei of interest. As already stressed, shell, pairing and deformation effects are essential input in the provision of a reliable estimate of the level densities at the fission saddle points. Furthermore, the most appropriate model that includes all these effects in a consistent form is the microscopic model based on the partition function method, as described in Chapter 6 [8.55]. This model is based on HFBCS single-particle properties, and predicts all the experimental s-wave resonance spacings with accuracies comparable to those obtained by the phenomenological BSFG formula. HFBCS is characterized by a nucleon effective mass close to the real mass [8.56], which is a particularly important parameter for reliable evaluations of level densities (provides a good description of the single-particle level density near the Fermi surface). When extrapolating level densities to exotic neutron-rich super-heavy nuclei, a microscopic approach might also be more stable than a phenomenological model.

The level density model includes:

- BCS pairing (in the constant-G approximation) with a renormalized strength and blocking effect for odd-mass and doubly-odd nuclei;
- Gaussian-type spin dependence, with microscopic shell and pairing effects that impact on the spin cut-off parameter;
- deformation effects that modify the single-particle spectra and the collective contribution of the rotational bands on top of each intrinsic state;
- an improved description at very-low energies [8.55].

The single-particle level scheme is consistently calculated for each saddle point by the deformed HFBCS model, based on the MSk7 Skyrme force [8.56] and constrained on the saddle-point quadrupole, octupole and hexadecapole moments. Identical pairing strengths (within the constant-G approximation) are used in these calculations and to determine the level density of the ground-state equilibrium deformation. However, no consideration is given to the possibility of a damping of the collective effects at increasing excitation energies.

The level densities are separately given the inner (**levden-hfbcs-inner** subdirectory) and outer (**levden-hfbcs-outer** subdirectory) saddle points as tabulations covering 2300 nuclei, with $78 \leq Z \leq 120$ included in the ETFSI compilation of fission barriers. Each table includes the spin-dependent level densities for energies up to $U = 150$ MeV and spin up to $J = 29$ (59/2). The nuclear temperature, cumulative number of levels, and total level and state densities are also included in the tables. Ground-state level densities are available in table format [8.55], and have been included in the RIPL-2 compilation (see Chapter 6). Note that the level density for left-right asymmetric fission barriers should be increased by a factor of 2 (this correction is not included in the tables).

Predicted fission level densities can be quantified in terms of the a_f/a ratio (i.e., a-parameter at the saddle point (a_f) corresponding to the (inner or outer) fission barrier expressed as a fraction of the equilibrium ground-state configuration (a)). Two examples

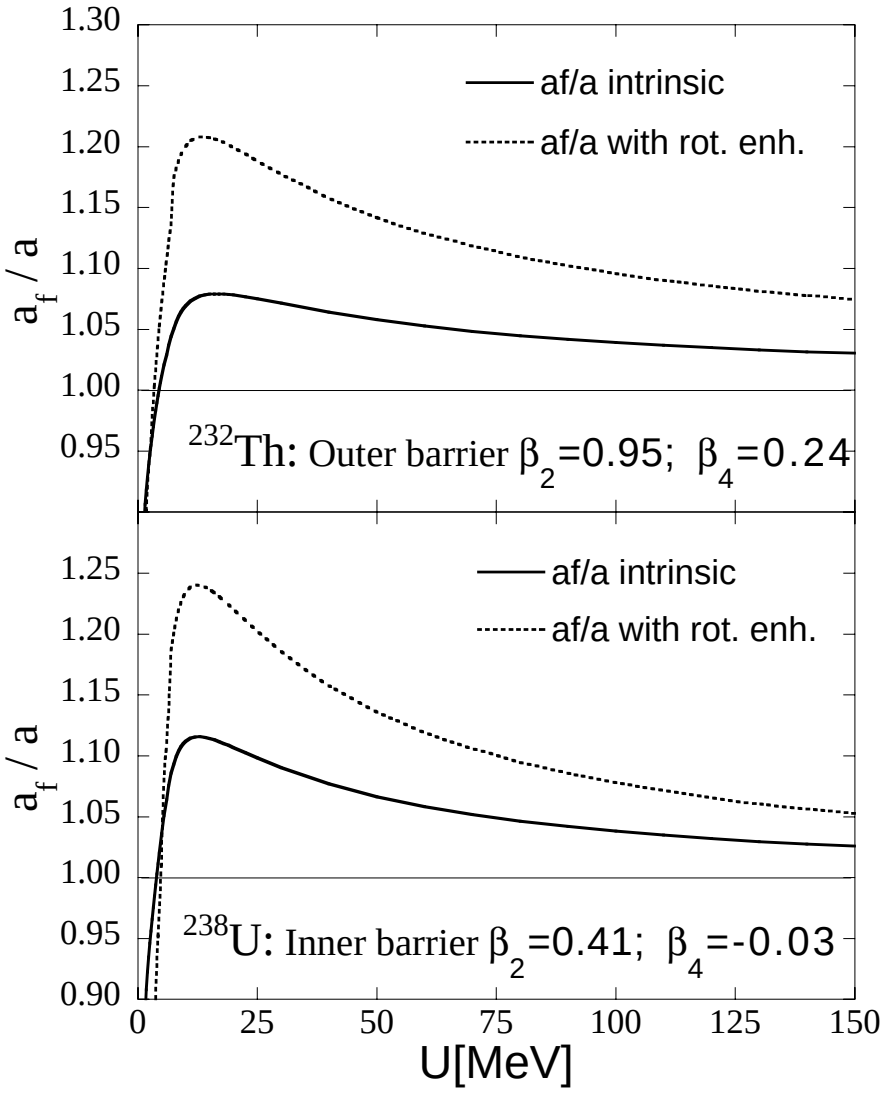

Figure 8.5: a_f/a ratios with and without (i.e., intrinsic) rotational enhancement as a function of the excitation energy for ^{232}Th and ^{238}U predicted by the HFBCS-based nuclear level density.

are shown in Fig. 8.5: two estimates of a_f/a ratio for ^{232}Th outer and ^{238}U inner barriers. Saddle-point deformations correspond to the values determined by the ETFSI model. First estimate corresponds to the intrinsic a_f/a ratio, i.e., entropy S_f/S ratio ($a = U/t^2$ differs from $a = S/2t$ in the microscopic approach, and consequently the entropy ratio must be considered to estimate the traditional a-ratio used in practical applications). Second estimate gives the equivalent a-ratio when the rotational enhancement factor is implicitly included in the a-parameter:

$$\rho(U) = \frac{\sqrt{\pi}}{12\ a^{1/4}\ U^{5/4}} \exp(2\sqrt{a\ U}) \tag{8.12}$$

where $\rho(U)$ correspond to the general formula (Eq. 6.1) in which the total microscopic level density with the collective contribution of the rotational bands was adopted.

The level densities have not been extensively tested on fission cross sections. However, a preliminary analysis of neutron-induced fission at low energies shows that a systematic increase of level densities is required to reproduce the experimental cross section

if use is made of the RIPL-2 recommended fission barriers (as given in the **fisbar-experimental.dat** file and described in the previous section). This increase can be obtained by a shift of approximately 1 MeV in the energy scale provided in the level density tables.

8.4 Conclusions and recommendations

Fission barriers and fission level densities are key ingredients of the statistical description of the fission cross sections induced by different incident particles. The fission barrier parameters derived from analyses of the available experimental data have been compiled for both pre-actinides and actinides. Two groups of fissioning nuclei can be formulated that differ essentially in their barrier properties:

(i) fission barriers close to the liquid-drop model predictions with the ground-state shell corrections for the pre-actinides, and

(ii) two-humped barriers with strong shell effects in the ground-state, and both humps for actinides.

The fission density models used for nuclear data evaluations should include in a consistent manner all variations of the shell, pairing and collective effects related to the fission barrier structures. A phenomenological or microscopic version of the generalized superfluid model appears to be the most suitable for such tasks, coupled with significant changes to the level density parameters of the fission channels as recommended above.

The RIPL-2 files include a large amount of data produced from microscopic calculations of the fission barriers (based on the ETFSI) and fission level densities (based on the HFBCS single-particle level schemes). The microscopic model takes into account the shell, pairing and blocking effects, the deformation effects in the single-particle spectra, and the collective enhancement of level densities at low excitation energies and their disappearance at high excitations. Corresponding tables of the level densities for about 2301 nuclei with $87 \leq Z \leq 120$ are provided in RIPL-2.

8.5 Summary of codes and data files

The structure of the corresponding RIPL-2 directory is as follows:

```
fission/
        fisbar-experimental.dat
        fisbar-experimental.readme
        fisbar-etfsi.dat
        fisbar-etfsi.readme
        fisbar-liquiddrop.for
        fisbar-liquiddrop.readme
        levden-hfbcs.readme
        levden-hfbcs-inner/Zxxx.dat
        levden-hfbcs-outer/Zxxx.dat
```

Programs and data files included in the directory are:

fisbar-experimental.dat - fission barrier parameters derived from the analysis of experimental data available for pre-actinides and actinides.

fisbar-experimental.readme - description of *fisbar-experimental.dat* file.

fisbar-etfsi.dat - fission barriers for 2301 nuclei with $78 \leq Z \leq 120$ calculated by means of the Extended Thomas-Fermi plus Strutinsky Integral (ETFSI) method.

fisbar-etfsi.readme - description of *fisbar-liquiddrop.for* file.

fisbar-liquiddrop.for - FORTRAN code for the liquid-drop model calculations of the fission barriers and the moment of inertia of fissioning nuclei.

fisbar-liquiddrop.readme - description of *fisbar-liquiddrop.for* file.

levden-hfbcs.readme - description of *levden-hfbcs-inner/Zxxx.dat* and *levden-hfbcs-outer/Zxxx.dat* files.

levden-hfbcs-inner/Zxxx.dat, levden-hfbcs-outer/Zxxx.dat - level densities calculated for the inner and outer fission barriers, respectively, based on the microscopic approach HFBCS single-particle level schemes.

REFERENCES

[8.1] BOHR, N., WHEELER, J.A., Phys. Rev. **56** (1939) 426.

[8.2] FRENKEL, Ya.I., JETP **9** (1939) 641.

[8.3] GHIORSO, A., HARVEY, B.G., CHOPPIN, G.R., THOMPSON, S.G., SEABORG, G.T., Phys. Rev. **98** (1955) 1518;
GHIORSO, A., THOMPSON, S.G., HIGGINS, G.H., SEABORG, G.T., STUDIER, M.H., FIELDS, P.R., FRIED, S.M., DIAMOND, H., MECH, J.F., PYLE, G.L., HUIZENGA, J.R., HIRSCH, A., MANNING, W.M., BROWNE, C.I., SMITH, H.L., SPENCE, R.W., Phys. Rev. **99** (1955) 1048.

[8.4] FLEROV, G.N., 2nd Conf. Peaceful Uses of Atomic Energy, United Nations, Geneva, **14** (1958) 151.

[8.5] FLEROV, G.N., TER-AKOPIAN, G.M., Sov. Part. Nucl. **46** (1983) 817.

[8.6] SEABORG, G.T., LOVELAND, W.D., Elements beyond Uranium, Wiley, New York (1990).

[8.7] VANDENBOSH, R., HUIZENGA, J.R., Nuclear Fission, Academic Press, New York (1973).

[8.8] POLIKANOV, S.M., et al., JETP **42** (1962) 1464.

[8.9] VOROTNIKOV, P.E., DUBROVINA, S.M., OTROSHCHENKO, G.A., SHIGIN, V.A., Sov. J. Nucl. Phys. **5** (1967) 207.

[8.10] MIGNEKO, E., THEOBALD, J.P., Nucl. Phys. **A112** (1968) 603.

[8.11] STRUTINSKY, V.M., Sov. J. Nucl. Phys. **3** (1966) 449; *ibid.*, Nucl. Phys. **A95** (1967) 420.

[8.12] STRUTINSKY, V.M., Nucl. Phys. **A122** (1968) 1.

[8.13] LYNN, J.E., Theory of Neutron Resonance Reactions, Clarendon Press, Oxford (1968).

[8.14] BJORNHOLN, S., STRUTINSKY, V.M., Nucl. Phys. **A136** (1969) 1.

[8.15] HOFMANN, S., MUNZENBERG, G., Rev. Mod. Phys. **72** (2000) 733.

[8.16] BOHR, A., 1st Conf. Peaceful Uses of Atomic Energy, Geneva, 1955, United Nations, NY, **2** (1955) 151.

[8.17] THOMPSON, S.G., Arkiv Fysik **36** (1967) 267.

[8.18] MORETTO, L.G., Physics and Chemistry of Fission, IAEA, Vienna, Vol. 1 (1974) 329.

[8.19] FREIESLEBEN, H., BRITT, H.C., HUZENGA, J.R., Physics and Chemistry of Fission, IAEA, Vienna, Vol. 1 (1974) 421.

[8.20] IGNATYUK, A.V., ITKIS, M.G., OKOLOVICH, V.N., SMIRENKIN, G.N., TISHIN, A.S., Sov. J. Nucl. Phys. **21** (1976) 612.

[8.21] IGNATYUK, A.V., ISTEKOV, K.K., SMIRENKIN, G.N., Sov. J. Nucl. Phys. **30** (1979) 1205.

[8.22] DAHLINGER, M., VERMEULEN, D., SCHMIDT, K.H., Nucl. Phys. **A376** (1982) 94.

[8.23] IGNATYUK, A.V., et al., Sov. Part. Nucl. **16** (1985) 709.

[8.24] SMIRENKIN, G.N., INDC(CCP)-359, IAEA, Vienna (1993).

[8.25] OGANESSIAN, Yu.Tc., LAZAREV, Yu.A., Treatise on Heavy-Ion Science, BROMLEY, D. (Ed.), Vol. 4 (1987) 3.

[8.26] COHEN, S., SWIATECKI, W.J., Ann. Phys. **22** (1963) 406.

[8.27] HASSE, R.W., Ann. Phys. **68** (1971) 377.

[8.28] KRAPPE, H.J., NIX, J.R., SIERK, A.J., Phys. Rev. **C20** (1979) 992.

[8.29] SIERK, A.J., Phys. Rev. **C33** (1986) 2039.

[8.30] MYERS, W.D., SWIATECKI, W.J., Phys. Rev. **C60** (1999) 014606.

[8.31] VIGDOR, S.E., KARWOWSKI, H.J., JACOBS, W.W., KAILAS, S., SINGH, P.P., SOGA, F. THROWE, T.G., Phys. Rev. **C26** (1982) 1035.

[8.32] HALPERN, I., STRUTINSKY, V.M., 2nd Conf. Peaceful Uses of Atomic Energy, United Nations, Geneva **15** (1958) 408.

[8.33] IGNATYUK, A.V., ISTEKOV, K.K., SMIRENKIN, G.N., Sov. J. Nucl. Phys. **36** (1982) 54.

[8.34] JUNGHANS, A.R., DE JONG, M., CLERC, H-G., IGNATYUK, A.V., KUDYAEV, G.A., SCHMIDT, K-H., Nucl. Phys. **A629** (1998) 635.

[8.35] TOKE, J., SWIATECKI, W.J., Nucl. Phys. **A372** (1981) 141.

[8.36] REISDORF, W., Z. Phys. **A300** (1981) 227.

[8.37] GAĬ, E.V., IGNATYUK, A.V., RABOTNOV, N.S., SMIRENKIN, G.N., Sov. J. Nucl. Phys. **10** (1970) 311.

[8.38] BJORNHOLN, S., LYNN, J.R., Rev. Mod. Phys. **52** (1980) 725.

[8.39] SHPAK, D.L., OSTAPENKO, Yu.B., SMIRENKIN, G.N., Sov. J. Nucl. Phys. **13** (1971) 950.

[8.40] GAVRON, A., BRITT, H.C., KONECNY, E., WEBER, J., WILHELMY, J.B., Phys. Rev. **C13** (1976) 2374;
GAVRON, A., BRITT, H.C., GOLDSTONE, P.D., SCHOENMACKERS, R., WEBER, J., WILHELMY, J.B., Phys. Rev. **C15** (1977) 2238.

[8.41] KUPRIYANOV, V.M., SMIRENKIN, G.N., FURSOV, B.I., Sov. J. Nucl. Phys. **39** (1984) 281.

[8.42] IGNATYUK, A.V., MASLOV, V.M., Sov. J. Nucl. Phys. **54** (1991) 647.

[8.43] MASLOV, V.M., KIKUCHI, Y., Nucl. Sci. Eng. **124** (1996) 492.

[8.44] IGNATYUK, A.V., SOKOLOV, Yu.V., Sov. J. Nucl. Phys. **19** (1974) 1229.

[8.45] MASLOV, V.M., Z. Phys. **A347** (1994) 211.

[8.46] MASLOV, V.M., SUKHOVITSKIJ, E.Sh., PORODZINSKIJ, Yu.V., KLEPATSKIJ, A.B., MOROGOVSKIJ, G.B., INDC(BLR)-4, INDC(BLR)-5, IAEA, Vienna (1996).

[8.47] MASLOV, V.M., SUKHOVITSKIJ, E.Sh., PORODZINSKIJ, Yu.V., MOROGOVSKIJ, G.B., INDC(BLR)-7, INDC(BLR)-9, INDC(BLR)-10, IAEA, Vienna (1997).

[8.48] MASLOV, V.M., Ann. Nucl. Energy **19** (1992) 181.

[8.49] MASLOV, V.M., Yadernye Konstanty **1** (1992) 80.

[8.50] MASLOV, V.M., Yadernye Konstanty **4** (1987) 19.

[8.51] ARNOULD, M., TAKAHASHI, K., Rep. Prog. Phys. **62** (1999) 393.

[8.52] GORIELY, S., ARNOULD, M., Astron. Astrophys. **379** (2001) 1113.

[8.53] MAMDOUH, A., PEARSON, J.M., RAYET, M., TONDEUR, F., Nucl. Phys. **A644** (1998) 389.

[8.54] MAMDOUH, A., PEARSON, J.M., RAYET, M., TONDEUR, F., Nucl. Phys. **A679** (2001) 337.

[8.55] DEMETRIOU, P., GORIELY, S., Nucl. Phys. **A695** (2001) 95.

[8.56] GORIELY, S., TONDEUR, F., PEARSON, J.M., At. Data Nucl. Data Tables **77** (2001) 311.

List of participants

T. Belgya:	Institute of Isotope and Surface Chemistry Chemical Research Centre, Budapest, Hungary
O. Bersillon:	Centre d'Etudes Nucleaires de Bruyeres-le-Chatel, Bruyeres-le-Chatel, France
R. Capote Noy:	Centro de Estudios Aplicados al Desarrollo Nuclear, Havana, Cuba
T. Fukahori:	Japan Atomic Energy Research Institute Tokai-mura, Naka-gun, Japan
Ge Zhigang:	China Institute of Atomic Energy, Beijing, PR China
S. Goriely:	Universite Libre de Bruxelles, Brussels, Belgium
M. Herman:	Scientific Secretary (from March 2000), International Atomic Energy Agency, Vienna, Austria
A.V. Ignatyuk:	Institute of Physics and Power Engineering, Obninsk, Russian Federation
S. Kailas:	Bhabha Atomic Research Centre, Bombay, India
A.J. Koning:	Fuels Actinides and Isotopes NRG Nuclear Research and Consultance Group, Petten, The Netherlands
P. Obložinský:	Brookhaven National Laboratory, Upton, USA (Scientific Secretary until March 2000, International Atomic Energy Agency, Vienna, Austria)
V. Plujko:	Taras Shevchenko National University, Kiev, Ukraine
P.G. Young:	Chairman, Los Alamos National Laboratory, Los Alamos, USA

ERRATA

The RIPL potentials 9101 (Huizenga Igo), 9401(Nolte) and 9600(Avrigeanu) for alpha-induced reactions were corrected in the RIPL-2 database on 10 September 2004. Their imaginary part was defined as a surface potential, when it should be volume potential.